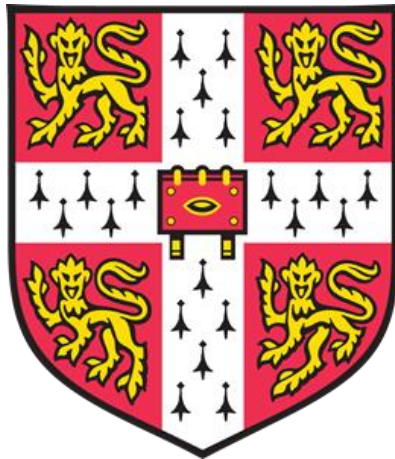# MODIFYING CHONDROITIN SULFATION ENHANCES RETINAL GANGLION CELL AXON REGENERATION

Craig Steven Pearson

Gonville and Caius College

and

The John van Geest Centre for Brain Repair

Department of Clinical Neurosciences

May 2018

This dissertation is submitted for the degree of Doctor of Philosophy.

Modifying Chondroitin Sulfation Enhances Retinal Ganglion Cell Axon Regeneration

Craig Pearson

Abstract

The failure of mammalian CNS neurons to regenerate their axons derives from a combination of intrinsic deficits and extrinsic obstacles. Following injury, chondroitin sulfate proteoglycans (CSPGs) accumulate within the glial scar that forms at the lesion site in response to the insult. CSPGs inhibit axonal growth and regeneration, an action mediated by their sulfated glycosaminoglycan (GAG) chains, especially those with 4-sulfated (4S) sugars. Arylsulfatase B (ARSB) selectively cleaves 4S groups from the non-reducing ends of GAG chains without disrupting other, potentially growth-permissive motifs. In this thesis, "Modifying Chondroitin Sulfation Enhances Retinal Ganglion Cell Axon Regeneration," I, Craig Pearson, seek to determine the time course and spatial distribution of CSPG accumulation in the glial scar following acute injury, and then to demonstrate that ARSB is effective in reducing the inhibitory actions of CSPGs. I examine the effects of ARSB in an *in vitro* model of the glial scar and *in vivo*, using optic nerve crush (ONC) in adult mice. ARSB is clinically approved for replacement therapy in patients with mucopolysaccharidosis VI and therefore represents an attractive candidate for translation to the human CNS. My findings illustrate the importance of CSPGs as a barrier to axon extension following injury, and show compelling evidence that selective modification of the sulfation pattern on GAG chains results in significant enhancement of RGC axonal regeneration. Finally, I combine ARSB treatment with a host of intrinsic pro-regenerative stimuli and show robust, long-distance regeneration of RGC axons through the optic chiasm and into the optic tract. Taken together, the results of this thesis argue for the therapeutic potential of modifying the extracellular matrix to promote regeneration of axons in the CNS.

PREFACE

This dissertation is the result of my own work and includes nothing which is the outcome of work done in collaboration except as declared in the Preface and specified in the text.

It is not substantially the same as any that I have submitted, or, is being concurrently submitted for a degree or diploma or other qualification at the University of Cambridge or any other University or similar institution except as declared in the Preface and specified in the text. I further state that no substantial part of my dissertation has already been submitted, or, is being concurrently submitted for any such degree, diploma or other qualification at the University of Cambridge or any other University or similar institution except as declared in the Preface and specified in the text

It does not exceed the prescribed word limit for the relevant Degree Committee.

ABSTRACT

The failure of mammalian CNS neurons to regenerate their axons derives from a combination of intrinsic deficits and extrinsic obstacles. Following injury, chondroitin sulfate proteoglycans (CSPGs) accumulate within the glial scar that forms at the lesion site in response to the insult. CSPGs inhibit axonal growth and regeneration, an action mediated by their sulfated glycosaminoglycan (GAG) chains, especially those with 4-sulfated (4S) sugars. Arylsulfatase B (ARSB) selectively cleaves 4S groups from the non-reducing ends of GAG chains without disrupting other, potentially growth-permissive motifs. In this thesis, "Modifying Chondroitin Sulfation Enhances Retinal Ganglion Cell Axon Regeneration," I, Craig Pearson, seek to determine the time course and spatial distribution of CSPG accumulation in the glial scar following acute injury, and then to demonstrate that ARSB is effective in reducing the inhibitory actions of CSPGs. I examine the effects of ARSB in an *in vitro* model of the glial scar and *in vivo*, using optic nerve crush (ONC) in adult mice. ARSB is clinically approved for replacement therapy in patients with mucopolysaccharidosis VI and therefore represents an attractive candidate for translation to the human CNS. My findings illustrate the importance of CSPGs as a barrier to axon extension following injury, and show compelling evidence that selective modification of the sulfation pattern on GAG chains results in significant enhancement of RGC axonal regeneration. Finally, I combine ARSB treatment with a host of intrinsic pro-regenerative stimuli and show robust, long-distance regeneration of RGC axons through the optic chiasm and into the optic tract. Taken together, the results of this thesis argue for the therapeutic potential of modifying the extracellular matrix to promote regeneration of axons in the CNS.

ACKNOWLEDGEMENTS

I don't remember any of the wishes I've made over birthday cakes. I toss coins into fountains and watch meteors skim the edge of the atmosphere, and then, as soon as the moment passes, I forget whatever it was I wanted. These wishes are fleeting, not fixed. So when, on a recent visit to Tokyo, I came across hundreds of prayer tablets hanging in neat rows around a camphor tree at the Meiji Jingu shrine, I was captivated. I spent an hour reading them. What struck me was the language—how people ask for the things they want most deeply. It felt like hearing someone's whispered thoughts the moment before the candles are blown out.

The prayers were all personal, and, at first glance, rather generic. Everyone wanted love, health, and happiness; nobody asked the gods to end climate change or resolve international conflicts. But between the lines, they bristled with unexpected details. One person wrote: "I wish my vitiligo would slowly disappear." Another, in a brisk scrawl: "I wish to grow old with Linda. I wish for Philip to one day get his vision back." *Slowly. One day*. Here, I thought, are people who don't want to ask for too much. They're hopeful, but patient. They're willing to wait.

As someone whose research explores how we might someday regenerate cells in the visual system to restore people's sight, I read that second wish with a pang. I thought about the work that comprises my doctoral dissertation and asked myself: have my efforts brought that "one day" any closer? It's impossible to know.

This thesis represents the work of four years, and in a way, it is also the fulfillment of a wish. Shortly after I moved to Washington, DC, for the second half of my PhD, a lab colleague took us to a New Year festival hosted by the local Japanese cultural society. We played traditional games and ate food while taiko drummers performed on the main stage. I noticed next to the stage a large round doll with a bushy beard and blank white eyes. When I asked what it represented, Sayuri told me it was a daruma, a totem that reminds you of a commitment you've made. You color in his left eye when you set the goal and fill in the right eye once you've achieved it. I bought a miniature daruma for a few dollars. Later, at my desk in the lab, I drew in the left eye.

My goal was straightforward: to publish my research in a reputable scientific journal. Anything more ambitious—curing blindness, changing lives—would have felt absurd. When I bought my daruma doll, I'd already spent more than two years learning techniques and acquiring preliminary data for a set of experiments that might, if successful, move the needle

of knowledge by a fraction of a degree. The progress of science often feels geologically slow. Setting and celebrating achievable goals along the way makes it possible to keep going. And yet, behind all that, there are people like Phillip, whoever he is, living out there in the wider world, aware—perhaps acutely, perhaps only vaguely—that people like me are working to develop technologies that might change the way they see. Something tells me he wouldn't be particularly concerned with which journal my work gets published in.

In May, I attended the annual meeting of the Association for Research in Vision and Ophthalmology to present my findings. In addition to meeting fellow researchers and physicians, I spoke with several patients living with eye disease and low vision. "Keep doing what you're doing," some of them told me. Also: "Work harder." A week later I was in Tokyo, exchanging revisions of a paper with my supervisor twelve time zones away. We had calls in the morning and evening, and in between, I wandered museums taking notes on my phone and walked through parks eavesdropping on conversations I couldn't understand. A few hours before my flight home, I stopped by the Meiji Jingu shrine and read the wishes at the camphor tree. Not long after I landed, I got an email that our paper had been accepted.

At my desk, I filled in the right eye of the daruma doll and thought. *There,* I thought. *Your sight has been restored. Now what?*

At the New Year, daruma dolls are burned alongside prayer tablets and other talismans in a ceremonial fire, whether or not the goal they carry has been met. It's a cleansing and a renewal. I've been thinking about this recently, about what I'll wish for if I happen to pick up another daruma doll, or the next time I pass a fountain or see a shooting star. I understand, now, the value of thinking on a different scale. I can imagine coloring in an eye and setting the daruma on my desk, as before. And maybe next year I'll throw it into the fire unfulfilled—and again the next year, and the next, and the next. Somehow, this doesn't feel like failure.

equally meaningful clinical work; Herb's example has shown me how to build a successful and enduring career by asking the right questions and maintaining a passion for the scientific endeavor. In addition to their mentorship, I would also like to thank my co-supervisor Prof James Fawcett, who graciously accepted me into his group meetings and has provided innumerable suggestions, resources, and connections, all of which I have done my best to utilize. Each of these mentors has inspired me beyond what words can express. I am lucky to have had them at this foundational stage of my education.

I am grateful to Dr. Amanda Barber for her influence and support. From day one of my PhD, she has been a beacon whose example I have done my best to follow. Her insight has shaped not only how I approached the challenges of a PhD, but also how I think about science and the scientific endeavor at the most fundamental level. In so many respects, I look up to her as a model and feel lucky to also call her a friend. Our many conversations have made a lasting impression on me, and I hope we will continue to exchange ideas as our careers move forward.

I wish to thank Dr. Hiro Katagiri for his seemingly endless depths of experience and advice. He has taught me more than I can express, from the finest details of experimental techniques, to the art of crafting a cover letter, to considering research problems from multiple angles, to asking tough questions and designing experiments to yield meaningful answers. I can't possibly count the ways in which his influence has shaped my thinking, and he has done all of this with a positive attitude and work ethic that I will carry forever as an example of science done right.

I owe a great debt to my friends and colleagues at the Brain Repair Centre, where I learned the skills and techniques necessary to undertake this project, and collected the data that would form the foundation of my PhD research: Dr. Andy Osborne, a generous model of hard work and dedication who was always happy to answer questions and refuel my enthusiasm for my work; Raquel Gomez-Conceicao, a fantastic partner who never hesitated to step in and help when I needed it most; Dr. Alessia Tassoni, a true ray of sunshine who helped me set up my animal work and taught me many of my most-used techniques, Dr. Rachel Chong, who sat down to boost my confidence when I really needed it; Dr. Joshua Cave, who worked alongside me with enthusiasm and diligence for my final summer in Cambridge. I am deeply grateful for the guidance and mentoring of Dr. Jessica Kwok, who gave me valuable practical advice and kindly showed me how to improve just about every aspect of my experimental methods; Dr. Patrice Smith, who enthusiastically trained me on surgical and dissection techniques and was a source of joyful encouragement during my first

year; Dr. Richard Eva, who enabled me to contribute to exciting projects that broadened the breadth and scope of my scientific education; and Dr. Ruma Raha-Chowdhury, who took time to teach, advise, and encourage me during the early years of my PhD. I also want to acknowledge all my friends in the BRC After Hours Club, whose companionship and commiseration made it possible for me to push myself to work harder, smarter, and—when necessary—to take a break: Bart Nieuwenhuis, Veselina Petrova, Heleen van't Spijlker, Alejandro Carnicier, Dr. Menghon Cheah, Nataly Martynyuk, Astrid Wendler, Nina Kouli, Dr. Damiano Barone, Dr. Laetitia Schwab, Nalini Tata, and all of my other classmates and friends: thank you for your inspiration.

Equally, I wish to thank everyone at the National Heart, Lung, and Blood Institute who enabled me to work at a level of productivity I didn't imagine was possible: Dr. Panpan Yu, a brilliant scientist who gave me essential training early in my studies; Dr. Caitlin Mencio, a sharp mind and wonderful personality who made it a joy to come into the lab every day; Dr. Sharada Tilve, whose outstanding advice and example I will take with me far beyond my PhD; Chinyere Agbaegbu, who never failed to make me laugh, and at the same time lent an ear when things went south; Andrea Solano, always enthusiastic and profoundly dedicated; Juan Carlos Cespedes, a model of how to succeed with a smile on your face; Ashlea Morgan and Hannah Batchelor, two exceptional post-bacs who kept me in the loop even when we were separated by an ocean and two digital screens: thank you for your advice, input, and encouragement. Their presence has been instrumental in my development as a scientist, and I can't wait to see what all of them do next. Elsewhere at NHLBI, I want to thank Dr. Rod Levine, Dr. Randy Clevenger, Karen Keeran, Dr. Christian Combs, Dr. Daniela Malide, Dr. Zuxi Yu, and Dr. Wai Wong, for their assistance with experiments, their encouraging mentorship, and their models of how to undertake ambitious research with passion and grace. I feel immensely lucky to have trained in such a stimulating and friendly environment.

Finally, I wish to thank the people outside of my two labs who have nonetheless provided vital support intellectually and emotionally: Dr. Melissa Baumann, Dr. Natalie Phillips, Joana Petrescu, Alyssa Bilinski, Dan Cotfas, Irene Falk, Katherine McDaniel, and, most importantly of all, my wonderful family. Mom, Dad, and James, without you, none of this would have been possible. Thank you.

TABLE OF CONTENTS

FIGURES AND TABLES

Chapter 1

Chapter 2

Chapter 3

Chapter 4

Chapter 5

Chapter 6

LIST OF PUBLICATIONS

C. Pearson, C. Mencio, A. C. Barber, K. R. Martin, and H. M. Geller. Identification of a critical sulfation in chondroitin that inhibits axonal regeneration. *eLife* 2018;7:e37139.

C. Pearson. A therapeutic link between astrogliosis and remyelination in a mouse model of multiple sclerosis. *The Journal of Neuroscience* 2018; 38(1): 29-31.

P. Yu, C. Pearson, and H. M. Geller. Flexible roles for proteoglycan sulfation and receptor signaling. *Trends in Neurosciences* 2017; 17: 30211-4.

C. Pearson and K. R. Martin. Cell based therapies for glaucoma. *Advances in Clinical Neuroscience and Rehabilitation* 2015; 15(6): 13-14.

C. Pearson and K. R. Martin. Stem cell approaches to glaucoma, from aqueous outflow modulation to retinal neuroprotection. *Progress in Brain Research* 2015; 220: 241-256.

LIST OF CONFERENCES

C. Pearson, K. Martin, and H. Geller. Arylsulfatase B modifies chondroitin sulfation and enhances retinal ganglion cell axon regeneration. Association for Research in Vision and Ophthalmology (ARVO) annual meeting. Honolulu, Hawaii. Poster. May 2018. *(Fully funded by travel grants from Fight for Sight and the Biomedical Research Alliance.)*

C. Pearson, K. Martin, and H. Geller. Modifying chondroitin sulfation enhances retinal ganglion cell axon regeneration in the mouse optic nerve. Optic Nerve Meeting. Obergurgl, Austria. Oral Presentation. December 2017. *(Fully funded by travel grants from the Isabelle Bouhon Travel Fund and Gonville and Caius College)*

C. Pearson, K. Martin, and H. Geller. Modifying chondroitin sulfation enhances retinal ganglion cell axon regeneration in the mouse optic nerve. Society for Neuroscience (SfN) annual meeting. Washington, DC. Poster. November 2017.

C. Pearson, K. Martin, and H. Geller. Modifying chondroitin sulfate proteoglycans enhances retinal ganglion cell axon regeneration in the mouse optic nerve. Association for Research in Vision and Ophthalmology (ARVO) annual meeting. Baltimore, Maryland. Poster. May 2017. *(Fully funded by travel grant from the Guarantors of Brain)*

C. Pearson, K. Martin, and H. Geller. Optic Nerve Crush: Molecular Responses to Acute Injury in the Visual System. Optic Nerve Meeting. Obergurgl, Austria. Oral Presentation. December 2015. *(Fully funded by travel grant from Gonville and Caius College)*

C. Pearson, K. Martin, and H. Geller. Characterization of the Injury Response to an Optic Nerve Crush in the Mouse. International Symposium for Neural Regeneration. Asilomar, California. Poster. November 2015. *(Fully funded by travel grants from Marshall Aid Commemoration Commission and International Symposium for Neural Regeneration)*

C. Pearson, A. Barber, K. Martin, and H. Geller. Distribution of Chondroitin Sulfate Proteoglycans After Acute Optic Nerve Injury. British Neuroscience Association: Festival of Neuroscience. Edinburgh, Scotland. Poster. April 2015. *(Fully funded by competitive travel grant from the E.G. Fearnside Fund)*

C. Pearson, A. Barber, K. Martin, and H. Geller. Distribution of Chondroitin Sulfate Proteoglycans After Acute Optic Nerve Injury. Cambridge Neurological Society Symposium. Cambridge, UK. Poster. March 2015. *(Awarded first prize for best research pitch)*

CHAPTER 1: INTRODUCTION

1.1 | OVERVIEW

The sense of sight enables people to perceive and respond to their surroundings, and is profoundly connected to many aspects of the human experience. Conditions that affect the visual system are a major global health concern, afflicting hundreds of millions of people worldwide. Degenerative diseases of the retina and optic nerve that lead to permanent visual impairment or blindness can severely reduce quality of life and have an enormous economic and emotional impact on patients, their caregivers, and society at large. Vision loss often occurs after retinal ganglion cell (RGC) axons, which connect the eye to the brain via the optic nerve, are damaged. Currently, no therapies exist that effectively promote regeneration of RGC axons to reconnect with their targets in the brain and restore vision. RGCs fail to regrow after injury for two primary reasons: 1) they lack the intrinsic growth factors necessary for regeneration, and 2) the extracellular environment in the optic nerve impedes axon regrowth. Previous work has shown that axon regeneration can be stimulated by altering the intrinsic growth state of RGCs, but few studies have adequately addressed the inhibitory factors in the optic nerve environment. A key aspect of this extracellular environment is the glial scar, which forms when astrocytes become reactive after injury and also includes activated microglia, macrophages, and extracellular matrix (ECM) molecules such as chondroitin sulfate proteoglycans (CSPGs). CSPGs are inhibitors of neuron growth that serve important roles as repulsive guidance cues during development and restrict plasticity in the brain during adulthood. CSPGs are also expressed following injury to central nervous system tissue, and in this context, they act as a barrier to regenerating axons. Removing or modifying CSPGs has the potential to reduce this inhibition and enable more robust axon regeneration following injury. The aims of this PhD were to investigate the cellular and molecular responses to optic nerve injury with a specific focus on CSPGs, and to develop an enzyme-based therapy that targets CSPGs to enhance RGC axon regeneration in the presence of an intrinsic growth-promoting stimulus. Answering these questions will enable future therapies to overcome both intrinsic and extrinsic barriers to axon growth in the optic nerve, paving the way for translatable treatments with the potential to regenerate the optic pathway and restore vision.

1.2 | ANATOMY OF THE VISUAL SYSTEM

The visual system evolved to enable organisms to detect and respond to their environment. This intricate apparatus transforms patterns of light into information encoded in neural circuits. The anatomy of the mammalian visual system has several common features: the eye, which captures and focuses light via the lens; the retina, where energy from photons is converted into neural signals and which performs early-level processing of such visual features as orientation and movement; the optic pathway, which consists of nerve fibers that organize and transmit information from the retina; and the brain, where visual information is processed and perception is produced. The structure of these systems naturally underpins their functions, and an understanding of visual system anatomy is therefore vital to studies of disease, injury, and repair.

1.2.1 | Retina

The retina is a thin sheet of transparent neural tissue that lines the back of the eye. It consists of three primary cell layers (**Figure 1.1**): the outer nuclear layer (ONL), which contains light-sensing photoreceptors; the inner nuclear layer (INL), which contains bipolar, amacrine, and horizontal cells, and the ganglion cell layer (GCL), which contains RGCs. The cornea and lens focus light onto the retina, where photons pass through the GCL and INL before arriving at the ONL. Photoreceptors contain proteins called opsins, which are bound to the photosensitive molecule 11-*cis*-retinal. When a photon encounters this complex, its energy causes the double bond in 11-*cis*-retinal to isomerize, producing all-*trans*-retinal. This induces a conformational shift in the opsin protein, which leads to a cascade of second messenger signals that ultimately causes the photoreceptor to hyperpolarize, a process termed phototransduction. This series of events enables photoreceptors to respond to individual photons, making them highly sensitive detectors of light. The shift from a steady state of depolarization, in which photoreceptors produce what is called "dark current," to a hyperpolarized state, transforms light into a neural code, which is passed from photoreceptors to bipolar cells and subsequently to RGCs. Information is integrated as it passes from one cell layer to the next, with multiple photoreceptors often converging on a single bipolar cell, and likewise multiple bipolar cells signaling to a single RGC. Information can be further modified by interneurons called horizontal cells whose processes extend into the outer plexiform layer

(OPL) between photoreceptors and bipolar cells, and by neurons called amacrine cells that extend into the inner plexiform layer (IPL) between bipolar cells and RGCs, as well as by glial cells such as Muller glia, which span the entire retina. Ultimately, the flow of information from the incident photon to the RGC enables the retina to encode a remarkably complex set of features in an extremely short amount of time. Numerous subtypes of specialized RGCs have evolved to convey information about these sets of features to the brain, where it undergoes further processing so that the organism can respond appropriately to a dynamic environment.
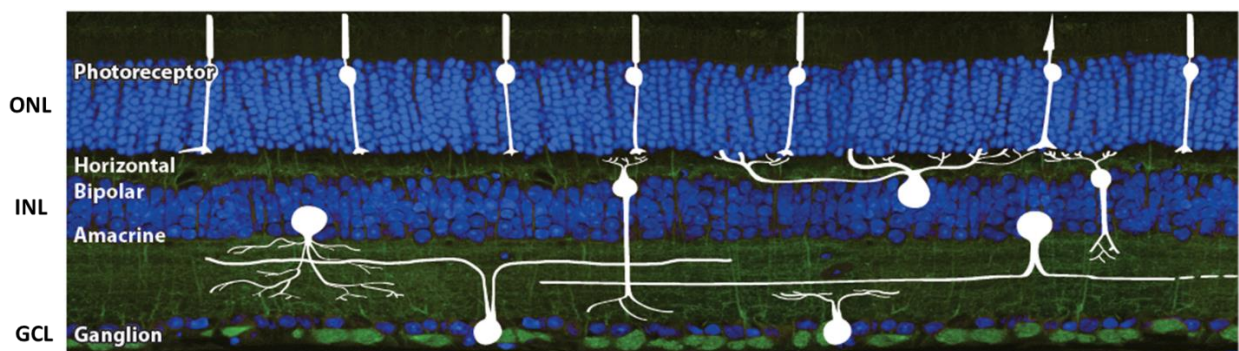
Figure 1.1. Neural cell types in the retina. The retina contains five neuronal cell types. The outer nuclear layer (ONL) is composed of light-sensitive photoreceptors. The inner nuclear layer (INL) contains bipolar cells that connect photoreceptors with the retinal ganglion cells (RGCs) of the ganglion cell layer (GCL). Also located in the INL are horizontal cells and amacrine cells, which modulate signal transmission through the other layers. RGC axons project from the retina through the optic disc and into the optic nerve. Figure adapted from Sanes & Masland 2015.

Our understanding of RGC subtypes has seen dramatic progress in recent years, with more than 30 subtypes identified (Sanes & Masland 2015). Many tools have emerged for classifying and labeling these distinct subpopulations so they can be more comprehensively studied. RGCs are primarily classified by four criteria: morphology, gene expression, spacing in the retina, and physiological properties (**Figure 1.2**) (Sanes & Masland 2015). They can also be understood by their function. For instance RGCs that respond to a stimulus moving in a particular direction are termed directionally selective (dsRGCs); another subtype are α-RGCs, which have larger somas and branching dendrites; some RGCs contain the pigment melanopsin, making them intrinsically photosensitive (ipRGCs); others respond most strongly to light-dark edges (local edge detectors, or LEDs); each of these subtypes can be further subdivided based on the four features described above (Sanes & Masland 2015).

Naturally, the fact that RGCs respond preferentially to different types of stimuli affects their projections to the brain. Different RGC subtypes send their axons to different central targets for processing (Dhande et al. 2015). In recent years, unique genetic markers for different RGC subtypes have been identified, making it possible to isolate and examine these cells with greater scrutiny (Dhande et al. 2015).
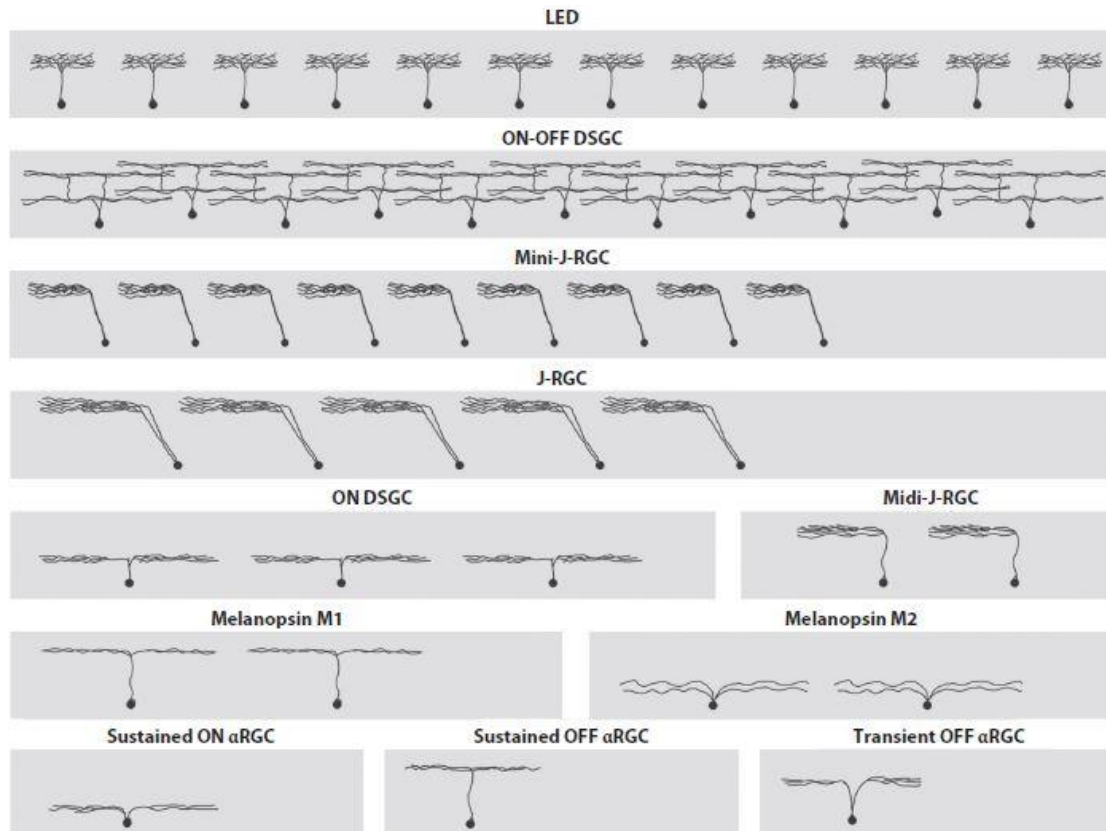
Figure 1.2. RGC subtypes shown in lateral cross-section. RGC subtypes can be classified by their differing morphologies. The number of each cell type shown above approximately matches their frequency in the mouse retina. Abbreviations: DSGC, directionally selective ganglion cell; J-RGC, junctional adhesion molecule B–positive RGC; LED, local edge detector; RGC, retinal ganglion cell. Figure adapted from Sanes & Masland 2015.

1.2.2 | Optic pathway

RGCs send their axons toward the central retina, where they pass through the optic disc and enter the optic nerve (**Figure 1.3**). The transitional region between the retina and optic nerve is called the optic nerve head (ONH), and its anatomy differs widely, even among mammals. In humans, a network of collagen fibers forms the lamina cribrosa, a dense matrix

that also contains astrocytic processes and forms a series of canals roughly 40-220 μm in diameter, through which RGC axons project (Elkington et al. 1990). The lamina cribrosa is of particular interest in the study of glaucoma, where deformation and displacement of the lamina cribrosa, often associated with elevated intraocular pressure (IOP), exerts a physical stress on the RGC axons and potentially contributes to their progressive degeneration. While other primates such as monkeys also possess the lamina cribrosa, it is absent in mice and rats, who instead have a glia lamina composed of optic nerve head astrocytes, which serves a similar function.
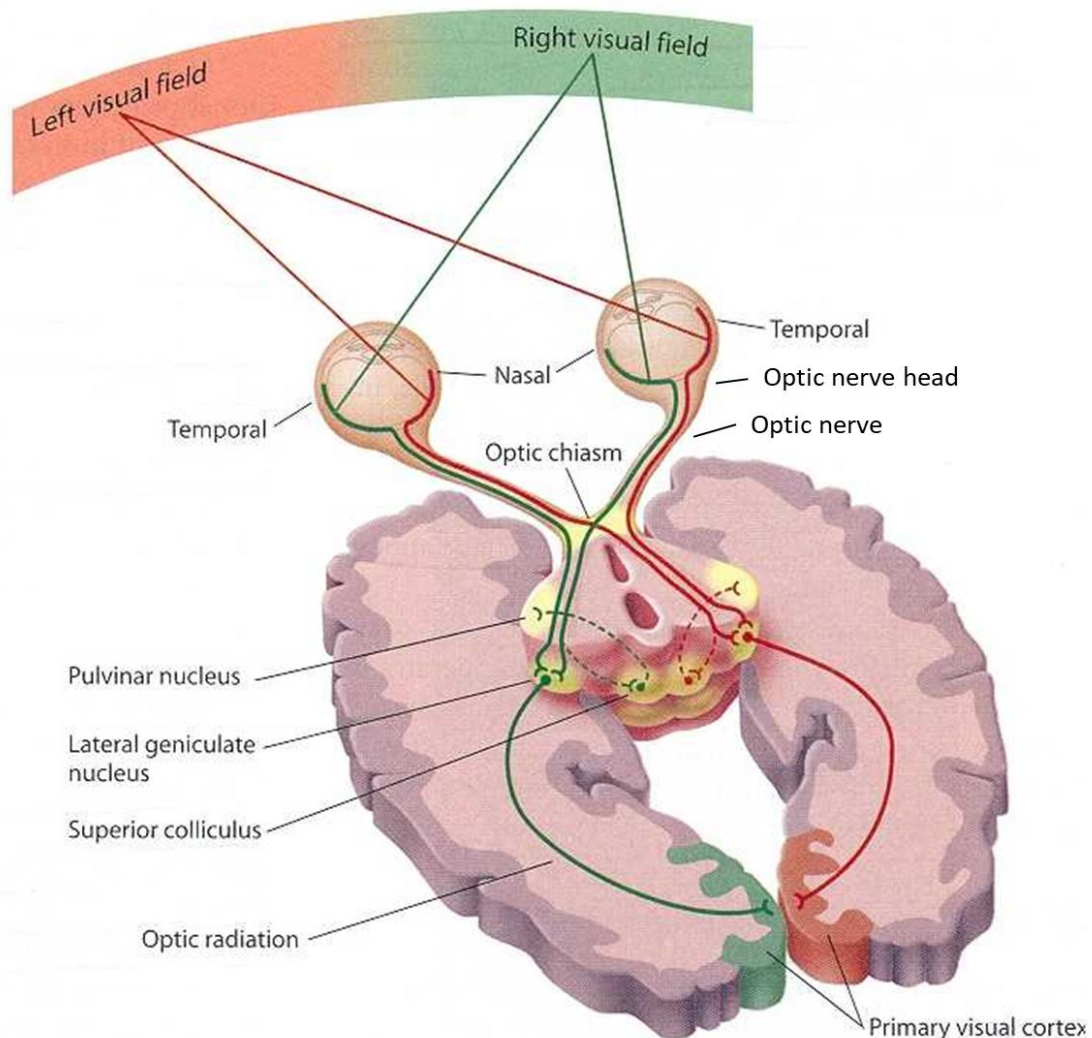
Figure 1.3. Anatomy of the visual pathway in humans. RGCs respond to information from the left and right visual fields according to their location in the retina. RGCs send their axons to the central retina, where they pass through the optic disc to form the optic nerve. The two nerves cross at the optic chiasm, where RGC axons decussate and project into the brain. Figure adapted from California State University Sacramento.

The optic nerve is considered part of the central nervous system (CNS). RGC axons are myelinated, except for a brief region at the optic nerve head, by oligodendrocytes, as opposed to the Schwann cells that myelinate peripheral nerve axons. RGC axons project in parallel through the optic nerves until they reach the optic chiasm. In binocular animals, visual information from the two hemifields is processed separately, on opposing side of the brain. Therefore, RGCs whose receptive fields encode information from the right visual hemifield project to the left hemisphere of the brain, and vice versa (**Figure 1.3**). To accomplish this patterning, axons must decussate at the optic chiasm according to their origins in the retina. In highly binocular animals, such as humans, about 60% of RGCs cross at the chiasm; in species where the eyes are positioned at the sides of the head, such as mice, about 95-97% cross (Petros et al. 2008). Axons then travel through the optic tracts and enter the brain.

The RGC axons are the only neuronal tissue in the optic nerves; however, many glial cell types are also present. In addition to oligodendrocytes, astrocyte processes are found throughout the optic pathway, as are resident microglia. These cells perform an array of structural and maintenance functions, and become reactive after injury and undergo progressive changes over the course of neurodegenerative diseases. The optic nerve is surrounded by meninges, including the three layers of the dura, arachnoid, and pia mater. The meninges contain fibroblasts which, like astrocytes and microglia, respond to acute injury by forming a scar to limit the spread of inflammatory damage. The optic pathway forms early in development, with RGC axons fully extended prior to birth, and remains relatively unchanged in adulthood. As mentioned above, mammalian RGC axons damaged by injury or degeneration do not naturally regenerate.

1.2.3 | Brain targets

Visual information arrives at the brain via synapses formed by RGC axons at several key target regions. At least 46 discrete targets have been proposed as part of the retinofugal pathway (Morin & Studholme 2014). These can be grouped under broad categories, such as visual circuits that govern general physiology, circuits that drive reflexive behaviors, and circuits that encode higher order visual features and contribute to conscious perception (Dhande et al. 2015). It is worth noting that different target regions receive axons from

different, often overlapping groups of RGC subtypes, indicating specialized networks for processing information from discrete types of stimuli (**Figure 1.4**).
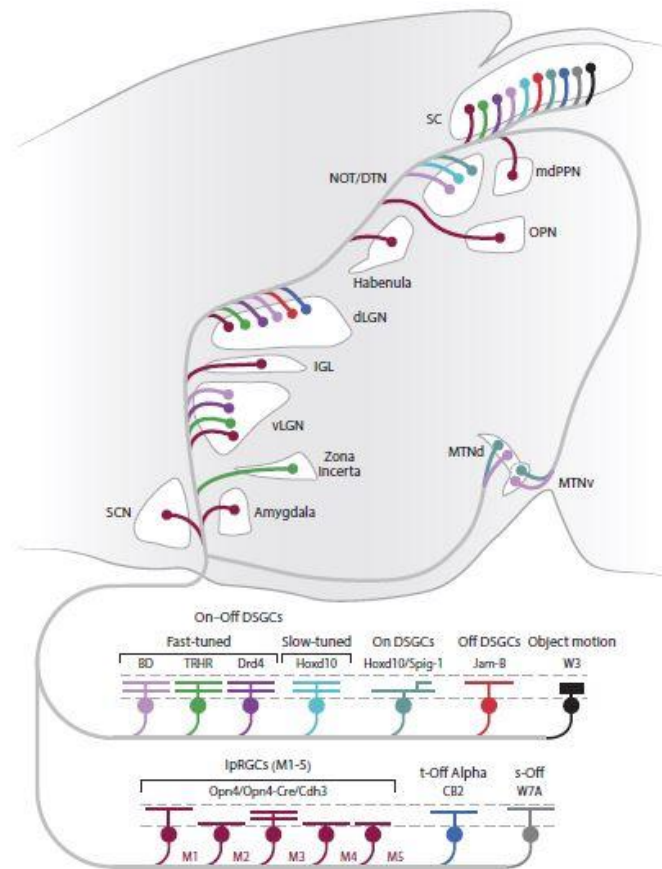
Figure 1.4. Different RGC subtypes project to distinct target regions in the brain. Retinal neurons facilitate a variety of functions, ranging from the maintenance of an organism's physiological state to the conscious perception of visual features in the environment. These functions require different sets of encoded information, which is transmitted by different RGC subtypes. Abbreviations: dLGN, dorsal lateral geniculate nucleus; DSGCs, direction-selective ganglion cells; IGL, intergeniculate leaflet; ipRGCs, intrinsically photosensitive retinal ganglion cells; mdPPN, medial division of the posterior pretectal nucleus; MTNd, dorsal medial terminal nucleus; MTNv, ventral medial terminal nucleus; NOT/DTN, nucleus of the optic tract/dorsal terminal nucleus; OPN, olivary pretectal nucleus; SC, superior colliculus; SCN, suprachiasmatic nucleus; s-Off, Off-sustained; t-Off, Off-transient; vLGN, ventral lateral geniculate nucleus. Figure adapted from Dhande et al. 2015.

The majority of retinofugal axons project to the dorsal lateral geniculate nucleus (dLGN) and superior colliculus (SC). The LGN integrates sensory information and relays it along what is termed the optic radiation to the primary visual cortex, where higher order processing occurs. Inputs to the LGN are organized retinotopically, which means that the spatial relationships of RGC cell bodies in the retina are preserved. The structure of the

dLGN varies widely across species, with primates exhibiting a six-layered structure that provides for a preliminary segregation of inputs, whereas rodents do not exhibit the same degree of lamination (Reese 1988). The LGN also receives input from visual cortex along the corticogeniculate pathway, creating a feedback loop. The SC, known as the tectum in non-mammals, also exhibits retinotopy and is considered an important map of visual space. It facilitates the organism's responses to orientation and body position. The SC also initiates motor commands that control the orientation of the gaze, and has been implicated in functions including tracking of moving stimuli, pursuit, and attention, as well as defense mechanisms such as the freezing and looming responses. Its relative size is much smaller in mammals than in other species, corresponding to larger regions associated with visual cortex.

The earliest visual target reached by RGC axons is the suprachiasmatic nucleus (SCN), which controls circadian rhythm. It is located directly above the optic chiasm, and receives input from melanopsin-containing ipRGCs. It has been proposed that light-sensing RGCs drive photoentrainment and facilitate the setting of the biological clock (Berson et al. 2002; Foster et al. 1991). While this appears to be true, it has been demonstrated that circadian rhythm is not abolished even in melanopsin knockout mice, suggesting that ipRGCs do not signal exclusively through their intrinsically photosensitive properties, but also receive inputs from photoreceptors in the "traditional" sense (Dhande et al. 2015). Knocking out ipRGCs entirely leads to a complete loss of photoentrainment, indicating that these cells are essential to the process (Hatori et al. 2008; Göz et al. 2008; Güler et al. 2008). The SCN is also innervated by pathways arising in the thalamus, suggesting indirect mechanisms of entrainment. The dLGN, ventral LGN (vLGN), and intergeniculate leaflet (IGL) are the main retinorecipient regions of the thalamus. Studies have shown that the vLGN and IGL are vital for the process whereby daily exposure to light entrains diurnal behaviors.

An essential adaptive function of the visual system is its ability to accommodate a wide range of luminance levels, from bright sunlight to the darkness of night. One element of this accommodation arises from adjusting the aperture of the pupil, thereby reducing the amount of light that enters the eye. The automatic process by which the pupil dilates and contracts is known as the pupillary light reflex (PLR). The PLR is controlled by both ipRGCs and photoreceptors. ipRGCs project to the olivary pretectal nucleus (OPN), which resides between the dLGN and the SC. Elevation of light levels stimulates contraction of the pupil via connections through the OPN, and low light levels lead to pupil dilation, enabling the visual system to respond dynamically to varying light levels.

Another important set of reflexes in the visual system facilitate small changes in head and eye position that serve to stabilize the image on the retina by accommodating for movement or changes in body, head, or eye position. The optokinetic reflex (OKR) and vestibuloocular reflex (VOR) work together to make fast, image-stabilizing compensatory movements that streamline the intake of visual information. It appears that dsRGCs are the primary drivers of these reflex circuits, responding rapidly to changes in the orientation and motion of visual stimuli. Brain regions essential to these reflexes include the nucleus of the optic tract and the dorsal, medial, and lateral terminal nuclei, which receive their primary inputs from dsRGCs.

Once RGC axons reach these central targets, they must form functional synapses. Significant effort has been dedicated toward understanding how these connections are formed, and emerging work suggests that a high degree of complexity governs these synaptic contacts. For instance, connections between RGCs and thalamocortical cells (TCs) have been observed to consist of mixed synapses with multiple RGC types and morphologically diverse TCs, with no apparent set of rules dictating which cells were found together (Morgan et al. 2016). It has been demonstrated that axons form early, weak synapses upon first encountering their targets during development, and that these connections are refined and strengthened based on visual experience, until the conclusion of a critical period after which plasticity sharply declines and networks become stabilized. The incredible complexity seen in the wiring of RGCs to their central targets has led to questions of whether regenerated axons could ever come close to restoring functional, healthy vision. Evidence suggests that regenerated RGCs do form functional synapses (Bei et al. 2016), but how these connections contribute to visual perception remains unknown. These topics are addressed in greater detail in later sections.

1.3 | VISUAL PATHWAY DEVELOPMENT

The optic pathway arises from the mesoderm and ectoderm. Early in embryonic development, two optic vesicles develop on either side of the forebrain. Each optic vesicle subsequently forms an optic cup, with the inner layer of the optic cup eventually maturing into the retina, and the outer layer maturing into the retinal pigment epithelium. The neuronal population of the retina arises from multipotent retinal progenitor cells, which differentiate

into different retinal neurons according to a precise ordering mechanism (Reese 2011). The fate of retinal progenitor cells depends on intrinsic cell-autonomous mechanisms as well as environmental signals, including paracrine signaling from nearby developing cells. Subsets of retinal precursor cells produce key transcription factors at different periods of development, which can dictate cell fate (**Figure 1.5**). For instance, RGC differentiation is associated with early expression of the *Math5* gene, and knockout of Math5 reduces the population of RGCs in the retina (Brown et al. 2001). However, this gene alone is not responsible for RGC differentiation, as Math5-expressing progenitor cells can also form other retinal neuronal cells, including horizontal cells, amacrine cells, and photoreceptors. Members of the *Brn3* family have been associated with generating RGCs during development (Badea et al. 2009). As RGC nuclei migrate to their final position in the retina, they extend small projections called radial processes, which will eventually become their axons (McLoon & Barnes 1989). RGCs ultimately migrate to form an evenly-spaced mosaic, comprised of distributions of different subtypes. As ongoing studies continue to investigate the subtle differences between RGC subtypes, our understanding of this patterning will continue to expand.
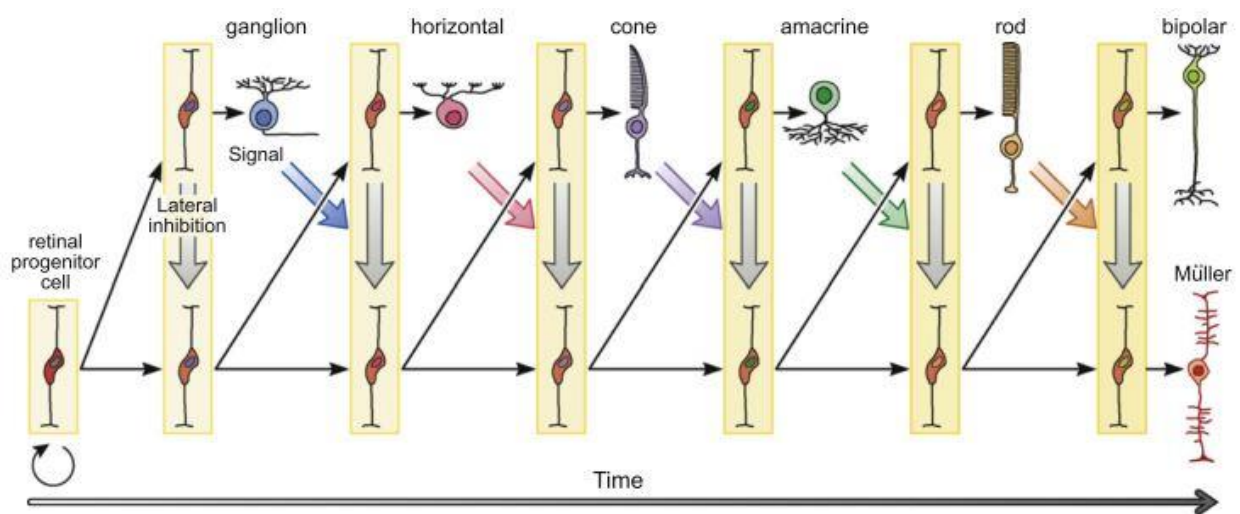
Figure 1.5. Differentiation of retinal progenitor cells in to retinal neurons. Different retinal neurons arise from retinal progenitor cells in a specific order over the course of development, influenced by both intrinsic and extrinsic factors. Figure adapted from (Reese 2011).

Developing RGC axons grow from the basal surface of the cell and extend into the optic fiber layer, where they project toward the optic disc in the central retina. The generation

and early extension of axons is influenced by both intrinsic factors, including integrins and cadherins, and extracellular factors in the neuroepithelium (Erskine & Herrera 2007). The directional growth of axons from the peripheral retina to the optic disc is guided, in part, by gradients of CSPGs, which inhibit neurite extension and thereby serve as a repulsive cue directing axons toward the central retina and optic nerve head (Brittis et al. 1992). The presence of Slit family proteins in the inner nuclear layer and their receptor Robo2 expressed on RGCs also contributes to the guidance of developing RGC axons (Erskine & Herrera 2007). At the optic disc, the expression of netrin-1 by glial cells signals RGC axons to the exit the eye (Deiner et al. 1997). It should be noted that different RGC axons arise and extend at different times, with the earliest, termed "pioneer axons," helping establish mature axon tracts (Brittis & Silver 1995). Axons that arise later in development fasciculate around these pioneer axons with the aid of cell-surface molecules. After exiting the eye, RGC axons populate the optic stalk, through which they extend toward the brain. Numerous tightly-regulated signaling molecules prevent axons from undertaking aberrant paths, including the inhibitory Sema5A, which constrains axons within the developing optic pathway (Oster 2003).

When growing axons enter the ventral diencephalon, they decussate, forming the optic chiasm. Much energy has been dedicated to understanding the mechanisms of RGC axon decussation at the developing optic chiasm, as it is an incredibly complex phenomenon and has provided many instructive insights regarding axon guidance and spatiotemporal signaling. In its simplest form, the process of axon crossing can be considered to have three key stages (**Figure 1.6**) (Petros et al. 2008). In the early phase, RGC pioneer axons, which predominantly arise from the dorsocentral retina, enter the diencephalon and form two projections, one of which extends ipsilaterally and the other contralaterally. During the peak phase, axons from the ventrotemporal retina arrive at the midline and are repelled, entering the ipsilateral optic tract, whereas all other axons cross at the midline, entering the contralateral optic tract. Again, the extent to which axons arising from the ventrotemporal retina are repelled at the midline is dependent on the degree of binocularity of the animal. Finally, in the late phase, the late-arriving RGCs encounter the optic chiasm, and most project contralaterally.
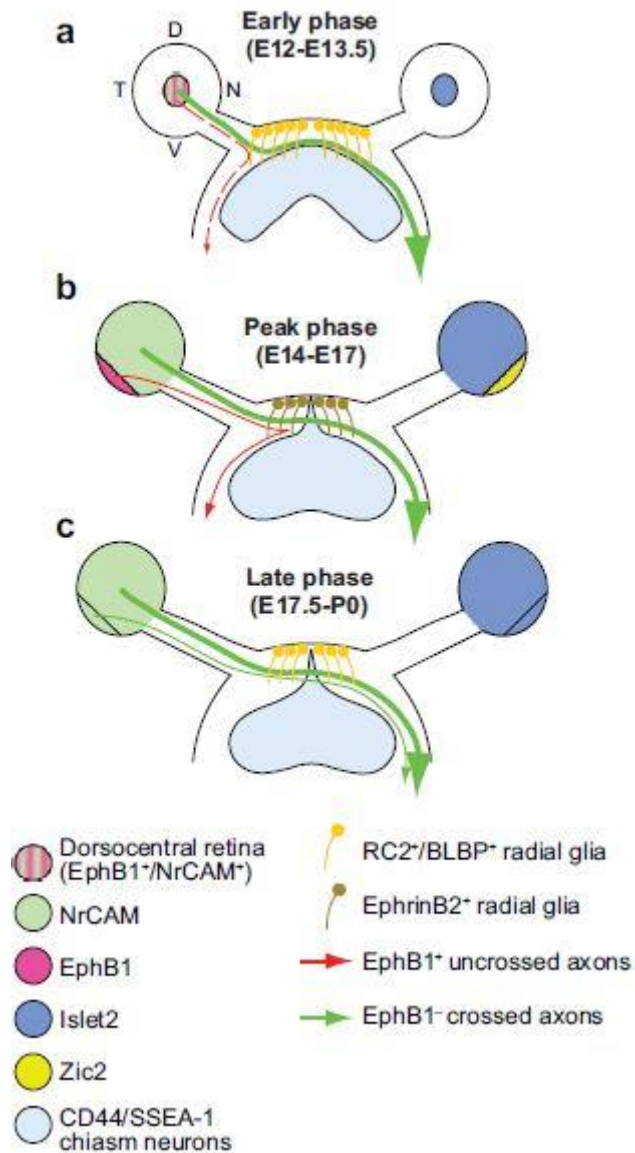
Figure 1.6. RGC axons decussate at the optic chiasm. RGC axons from different regions of the retina (D: dorsal, V: ventral, T: temporal, N: nasal) enter the chiasm at different times. Their crossing behavior is controlled by a variety of glial cells and associated signaling molecules. In the early and late phases, radial glia express RC2 and BLBP, whereas during the peak phase they predominantly express EphrinB2. The presence of EphB1 receptors on axons is partially responsible for whether they cross upon encountering EphrinB2 at the midline, with EphB1$^+$ cells turning back from the midline while EphB1$^-$ cells cross the midline. Other important factors in optic chiasm development include NrCAM, which is essential for axon crossing, and CSPGs, which prevent axons from extending outside the optic pathway. Abbreviations: EphB1, Ephrin type-B receptor 1; NrCAM, Neuronal cell adhesion molecule; Islet2, Isl2 insulin related protein 2; Zic2, Zinc finger protein 2; BLBP, Brain lipid-binding protein; SSEA-1, Stage-specific embryonic antigen 1. Figure adapted from (Petros et al. 2008).

The midline of the developing optic chiasm is defined by radial glial cells (Marcus & Mason 1995). Once axons cross at the optic chiasm, they navigate through the diencephalon and along the telencephalon, with their paths constrained by inhibitory factors including CSPGs that limit aberrant growth into inappropriate regions. RGC axon fasciculation, mediated by integrins and cadherins, also reduces aberrant off-target navigation. It is worth noting the highly regulated spatiotemporal expression of extracellular guidance cues during development (**Figure 1.6**). Studies of optic nerve regeneration in adult animals have shown that successful navigation of regenerating RGC axons at the optic chiasm is rare, with many axons failing to cross appropriately into the contralateral optic tract (Luo et al. 2013; Pernet & Schwab 2014; Bray et al. 2017). The behavior of axons at key decision points in the optic pathway suggests that new environments strongly influence growth cone dynamics: when they reach the optic nerve head, the optic chiasm, and their terminal targets in the brain, RGC growth cones undergo cyclic expansion, pausing, and retraction (Holt 1989; Bovolenta & Mason 1987; Mason & Wang 1997). Therefore, expanding our understanding of the mechanisms responsible for decussation of developing RGC axons may contribute to new insights for facilitating regeneration after injury. These questions are addressed in more detail in Chapters 5 and 6.

After crossing at the optic chiasm and navigating through the optic tract, RGC axons must find their targets in the LGN and SC and form functional synapses. Crucially, the retinotopic map must be preserved at these target regions. As a general rule, axons arising from RGCs in the nasal retina project to the posterior areas of their targets, whereas those arising from the temporal retina project to anterior areas (Erskine & Herrera 2007). Dorsal and ventral RGCs are mapped to dorsal and ventral areas of targets, respectively. This mapping requires EphA/ephrinA signaling, with EphrinAs exhibiting a gradient in the LGN, and mice lacking EphrinA showing a loss of retinotopy (Erskine & Herrera 2007). Neural activity in the retina appears to influence the action of EphrinA, and the importance of "retinal waves" of spontaneous electrical activity during development has been extensively studied (Wong 1999). This suggests a role for visual activity in determining retinotopy, which adds to the evidence that early visual experience is necessary for higher-order visual functioning. Once RGC axons have terminated at the proper target region, they form synapses with neurons in these regions. Following closure of the critical period, these synapses are highly stable, with limited plasticity. Signals from RGCs are integrated in the thalamus and travel onward to the visual cortex for higher order processing.

1.4 | OPTIC NERVE DAMAGE

1.4.1 | Progressive neurodegeneration

The most common form of optic nerve damage in humans is glaucoma. Glaucomatous optic neuropathies are a group of diseases characterized by changes in the structure of the optic nerve head and the progressive loss of RGCs. Glaucoma is the leading cause of irreversible blindness worldwide; its global prevalence is estimated to exceed 100 million people by 2040 (Tham et al. 2014). The main modifiable risk factor for glaucoma is elevated intraocular pressure (IOP), although not all glaucoma cases are associated with high IOP (Weinreb et al. 2014). Other risk factors include age and ethnic origin (Vidal-Sanz et al. 2012). Elevated IOP is linked with dysfunction of the trabecular meshwork (TM) and increased resistance to outflow of aqueous from the anterior chamber of the eye. Aqueous humor drains from the eye via the TM, located in the angle between the iris and the cornea (**Figure 1.7**). The balance between aqueous production and outflow determines IOP (Goel 2010). It is believed that the TM and Schlemm's canal senses IOP fluctuation via mechanical signals and respond by altering their resistance to fluid flow (Acott et al. 2014; Acott & Kelley 2008; Keller et al. 2009; Titze et al. 2003). At least two mechanisms have been shown to contribute to this modulation of resistance: secretion of enzymes and extracellular matrix, and phagocytosis of debris, pigment, and other materials in the aqueous humor (Zhang et al. 2007; Buller et al. 1990). Dysfunction of the aqueous outflow pathway often arises from decreased cellularity in the TM (Liton et al. 2005), which leads to excessive resistance, high IOP, and ultimately a heightened risk of developing glaucoma (Alvarado et al. 1981; Grierson & Howes 1987).
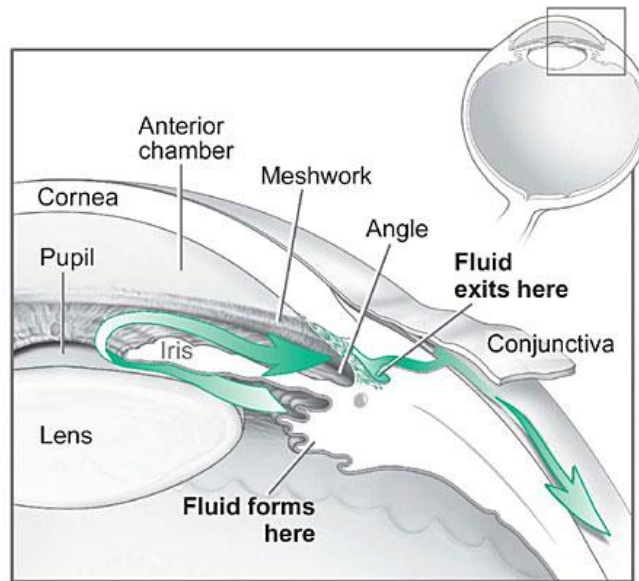
Figure 1.7. The aqueous outflow pathway is dysfunctional or damaged in glaucoma. In the healthy eye, aqueous humor flows into the anterior chamber and exits through the trabecular meshwork. Occlusion of this pathway leads to elevated intraocular pressure and is a primary risk factor for glaucoma. Figure adapted from the National Eye Institute (nei.nih.gov).

The biomechanical and physiological causes of optic nerve damage are not entirely understood. This is partly because anatomical differences between species make modelling glaucoma in animals difficult. For instance, the human optic nerve head possesses a lamina cribrosa, whereas mice and rats have a glia lamina. However, in both humans and rodents, it has been suggested that elevated IOP injures RGC axons at the optic nerve head via mechanical deformation of the lamina cribrosa or glia lamina (**Figure 1.8**). Further, studies have shown that astrocytes in the optic nerve head become reactive in response to glaucoma, indicating that the mechanical strain may stimulate changes in cell reactivity (Wang et al. 2017). Others have demonstrated that elevated IOP is associated with a loss of retrograde axonal transport in rodents (Vidal-Sanz et al. 2012). The failure of axonal transport and passive diffusion in RGCs suggests that there are likely metabolic causes underlying the progressive degeneration observed in glaucoma. Following extended periods of high IOP, RGC axons, dendrites, and soma undergo Wallerian degeneration, a well-known feature of many neurodegenerative diseases. Expression of the Wld^S gene, which slows Wallerian degeneration, delayed axonal degeneration in a rat model of glaucoma (Beirowski et al. 2008). Wallerian degeneration is irreversible, meaning that subsequent loss of vision is also irreversible if axons are unable to regenerate.
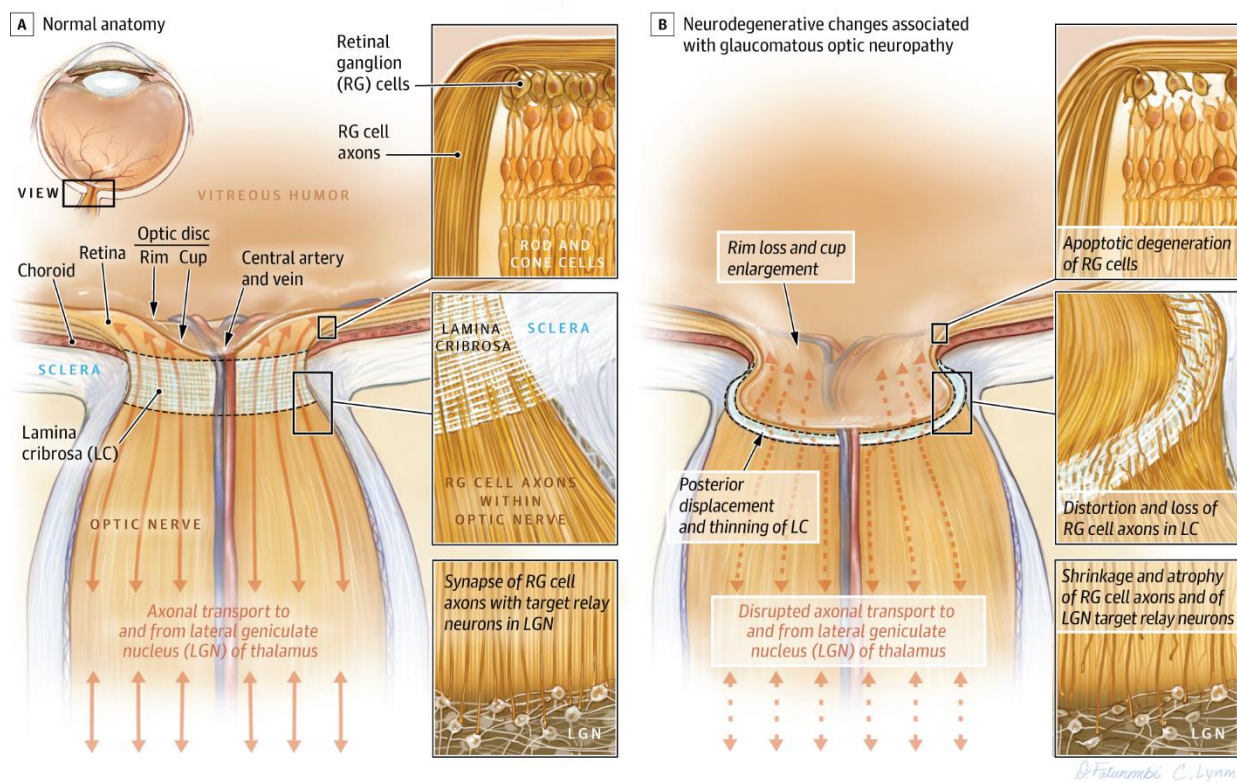
Figure 1.8. Elevated intraocular pressure leads to RGC damage and degeneration.
Accumulation of aqueous humor in the anterior chamber contributes to high intraocular
pressure. High IOP causes mechanical strain at the optic nerve head, where, in humans, the
lamina cribrosa deforms and distorts the axons of RGCs. Additionally, disruptions of axonal
transport contribute to metabolic dysfunction of RGCs. These stressors cause degeneration of
axons and atrophy of cell soma, and ultimately cell death. Figure adapted from (Weinreb et
al. 2014).

Current therapeutic approaches for human glaucoma patients consist mainly of self-
administered eye drops, surgery, or laser treatment to enhance aqueous outflow and lower
IOP. However, in many cases IOP reduction does not successfully prevent the degeneration
of RGCs, and poor patient adherence to prescribed treatment regimes can render them
ineffective. Furthermore, symptomatic reduction in vision typically arises only late in the
disease, after significant damage has been incurred. Thus, there is an urgent need for
treatments which not only lower IOP and protect RGCs from dying, but also promote the
growth of implanted or regenerated RGC axons through the optic nerve to restore functional
vision.

Degeneration of optic nerve axons is also associated with multiple sclerosis (MS). MS is an inflammatory disease characterized by multiple focal regions of demyelination and axonal damage in the brain, spinal cord, and optic nerve known as plaques (Compston & Coles 2008). While demyelinated axons in MS plaques may spontaneously remyelinate in the relapsing-remitting phase of the disease, the failure of remyelination in the progressive phase yields extensive neurodegeneration, leading to severe dysfunction and disability (Franklin 2002). Human patients with MS commonly exhibit atrophy of the nerve fiber layer and ganglion cell layer in the retina. A related condition, neuromyelitis optica, involves inflammation and demyelination of the optic nerve and spinal cord, and produces some similar symptoms in the retina. Optic nerve damage and loss of RGCs in the retina have also been observed in Alzheimer's disease (Sadun & Bassi 1990).

1.4.2 | Acute trauma

While less common than degenerative diseases such as glaucoma, traumatic injury to the optic nerve can also cause optic neuropathy, leading to loss of vision. The optic nerve may be injured by direct contact of an object, such as a bullet, knife, or fragments of broken orbital bone, as well as indirectly, following compressive injuries to the head. Tumors in and around the optic nerve can also compress and damage RGC axons. Indirect optic nerve damage can be caused by obstructing blood flow to the tissue, or, conversely, from hemorrhaging following a head injury. Extreme torsional rotation of the eye can strain and damage the nerve. In many cases, optic nerve atrophy is not apparent until weeks following the initial insult. The conditions can be unilateral, affecting one eye, or bilateral, affecting both eyes. Vision loss sustained in these conditions is typically irrecoverable, especially after direct injury of axon tracts. Treatments such as surgical decompression of the nerve and administering steroids have proved beneficial in some cases. However, a comprehensive study asserted that outcomes for patients treated with surgery or steroids were no better than those who received no treatment (Levin et al. 1999). Risk factors for traumatic optic neuropathies are not easily identified, although the same study reported that 85% of victims are male, and the average age was 34 (Levin et al. 1999). While the prevalence of traumatic optic neuropathies is far lower than that of degenerative diseases, many experimental models of optic nerve regeneration in animals rely on crush or transection of RGC axons, because the

injury is highly replicable and regenerating axons can be easily visualized and reliably quantified.

1.5 | AXON REGENERATION IN THE CNS

1.5.1 | Overview of nerve regeneration

The nervous system is essential for animal life, controlling the acquisition of information from the surrounding world and the conversion of that information into neural signals, and then processing those signals to determine the organism's reactions and physiological state. Damage to the nervous system can lead to severe dysfunction across virtually all aspects of life. Millions of people each year suffer from traumatic brain injury, stroke, spinal cord injury, and other conditions affecting the CNS. In humans, as in other mammals, neurons in the CNS fail to regenerate their axons following injury or degeneration. This creates an urgent need for the discovery of therapies that protect nerve cells against damage and promote and sustain the regeneration of neural tracts and circuits.

The field of neuroregeneration research is informed by the successful regeneration of mammalian PNS neurons and non-mammalian CNS neurons. In these neurons, the Wallerian degeneration that follows injury is often succeeded by extension of axons and subsequent reinnervation of targets. These events do not occur in the mammalian CNS. The evolutionary basis for mammals' loss of regenerative capacity remains unknown; one hypothesis is that the risks of partial regeneration or miswiring of regenerated circuits outweigh the potential benefits. It is known that poorly or improperly regenerated peripheral neurons can occasionally lead to neuropathies and neuropathic pain, lending credence to this theory. Conversely, it has been suggested that sustaining a CNS injury makes animals so vulnerable to attack or starvation that there is no chance of recovery, and therefore no selective pressure to maintain regenerative ability. While the origins of the differences between PNS and CNS, and between mammals and non-mammals, are not entirely clear, much can be learned from studying the regenerative competence of these systems (**Figure 1.9**). For instance, studies have compared the genetic profiles of non-mammalian CNS neurons with their mammalian counterparts to identify target genes for intervention. And autologous mammalian peripheral nerve grafts have been implanted at sites of CNS lesions, leading to measurable improvements in regeneration. While such experiments are limited in their ability to predict

successful translational therapies, they nonetheless provide valuable insight into the mechanisms and dynamics of neuroregeneration.
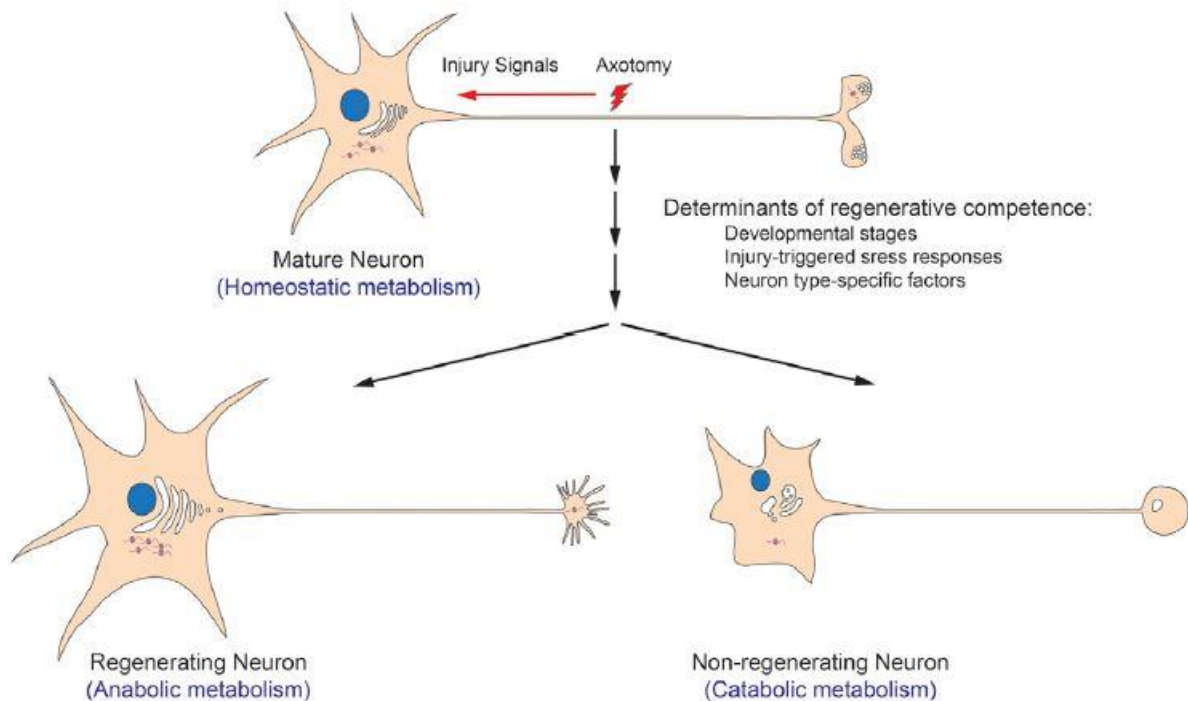
Figure 1.9. Neurons exhibit differing degrees of regenerative competence. Key factors that determine a cell's regenerative competence include its developmental stage, the presence of intrinsic and extrinsic growth-promoting and growth-inhibiting factors, and neuron-specific gene expression. Generally, mammalian CNS neurons fail to regenerate whereas non-mammalian neurons and mammalian PNS neurons are regeneration competent. Figure adapted from (He & Jin 2016).

Evidence that RGCs and other CNS neurons have a capacity for regeneration after injury was demonstrated as early as the 1980s, when Albert Aguayo and others showed that CNS axons will grow through a peripheral nerve graft following injury (**Figure 1.10**) (So & Aguayo 1985; Vidal-Sanz et al. 1987; Richardson et al. 1980; David & Aguayo 1981). This suggested that, when the extracellular environment was made more amenable to axonal growth, regeneration of injured CNS tracts was possible. Because nerve grafting poses substantial technical challenges and high levels of variability, this technique is rarely used in current studies. However, in the decades since Aguayo's findings were first reported, a broad spectrum of approaches have been utilized to stimulate RGC axon regeneration after optic nerve injury. Most of these address the cells' intrinsic state. Intrinsic approaches encompass breeding of transgenic animals or virally mediated gene therapy, including methods such as

cre-lox recombination or emerging technologies such as CRISPR-Cas9. Approaches that modify the environment are far less common, possibly due to the difficulty of directly targeting the optic nerve with therapeutic agents. These challenges are discussed below, and addressed directly in Chapter 3.
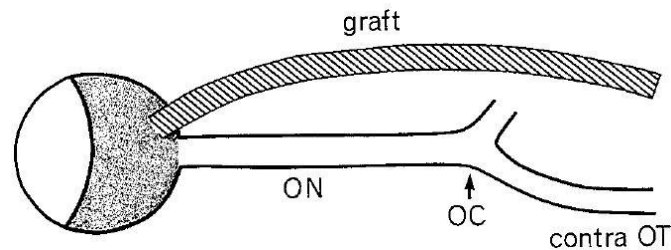
Figure 1.10. Injured RGC axons extend into a peripheral nerve graft. Implanting a segment of peripheral nerve at the site of a puncture lesion in the retina enables injured RGC axons to extend from the retina into the graft. This evidence showed that CNS axons, including RGCs, are capable of regeneration given a permissive microenvironment. Abbreviations: ON, optic nerve; OC, optic chiasm; OT, optic tract. Figure adapted from (So & Aguayo 1985).

1.5.2 | Intrinsic and extrinsic obstacles to regeneration

To achieve robust regeneration of CNS axons, two primary obstacles must be overcome: neurons' intrinsic failure to assume an active growth state, and a growth-inhibitory environment that prohibits the extension of new axons. Over the past decades, it has become apparent that therapies must address both intrinsic and extrinsic factors to facilitate axon growth, navigation and reinnervation of synaptic targets.

Intrinsic

CNS neurons' failure to regenerate is due in part to changes in gene expression between development and adulthood. Genetic programs active during the initial embryonic growth phase include axon associated genes that promote extension and formation of early nerve tracts. After this critical period of development, expression of growth-related genes is largely reduced. For instance, the growth rate of mammalian embryonic RGCs declines steeply after birth, with little to no spontaneous axon growth observed in adult systems

(Goldberg, Espinosa, et al. 2002). Reactivating developmental growth states by identifying key genetic pathways and manipulating specific gene expression has been demonstrated as a viable strategy for stimulating regeneration after injury. One common target of CNS regeneration therapies is the phosphatase and tensin homolog (PTEN) gene. PTEN is an upstream inhibitor of mammalian target of rapamycin (mTOR), the hub of a signaling pathway that controls cell growth and protein synthesis as well as metabolism (Lipton & Sahin 2014). PTEN, by acting through the phosphoinositide 3-kinase (PI3K)-AKT-mTOR pathway, plays a central role in cell survival and proliferation (M. S. Song et al. 2012). Knocking down or suppressing PTEN activates this pathway, thereby promoting cell growth programs. Deletion of PTEN in a transgenic floxed mouse line led to enhanced survival and robust regeneration of RGC axons after optic nerve injury (Park et al. 2008). Suppression of PTEN expression using a short hairpin RNA improved regeneration of corticospinal tract neurons in mice after spinal cord injury (Zukor et al. 2013). Manipulating the expression of PTEN or other genes involved in signaling pathways that control cell growth and proliferation is thus a promising step toward resolving the intrinsic inability of CNS neurons to regenerate axon tracts after injury.

Intrinsic control of axon regeneration has been reviewed extensively (**Figure 1.11**) (He & Jin 2016; Liu et al. 2011; Fischer & Leibinger 2012). Many relevant factors have been proposed and demonstrated. Neurons may lack sufficient neurotrophic factors in the adult CNS, limiting the much-needed support for undertaking new axon growth. It is known that inflammation stimulates regeneration in mature CNS neurons, and therefore it is possible to target elements of the inflammatory or immune response to promote regrowth of axons following damage or degeneration (Benowitz & Popovich 2011). Embryonic axon growth often relies on specific patterns of electrical stimulation, suggesting that coordinated neuronal activity may promote more effective axon growth and navigation (Goldberg, Espinosa, et al. 2002). Successful therapeutic regeneration stimuli will likely combine multiple intrinsic approaches. In Chapter 5, I demonstrate the effectiveness of several intrinsic approaches and further discuss their respective merits and challenges.

Figure 1.11. Intrinsic factors affecting CNS axon regeneration. The intrinsic failure of CNS neurons to regenerate their axons derives from both loss of intrinsic growth ability and the presence of extrinsic growth-inhibiting factors. Intrinsic regenerative ability can be enhanced by several methods, ranging from addition of growth factors and signaling molecules to genetic modulation of key cell proliferation pathways. Figure adapted from (He & Jin 2016).

Extrinsic

The ECM in the CNS occupies the spaces between neurons and glial cells and is composed primarily of proteins secreted by these cells. It performs active supportive functions which go beyond simply providing a structural framework for CNS cells. During development, the ECM plays a key role in directing the growth of new axon tracts via spatially and temporally controlled patterning of molecular guidance cues (**Figure 1.12**). These patterns are themselves mediated by tightly regulated gene expression in neurons and

glia. In adulthood, the ECM forms structures such as the perineuronal nets (PNNs), which include CSPGs, hyaluronan, link proteins and tenascin-R (Kwok et al. 2010; Köppe et al. 1997) and surround neuronal cell bodies, stabilizing the synaptic connections between linked neurons (Pyka et al. 2011). The ECM undergoes substantial changes after CNS injury, primarily as a result of glial cells entering a reactive state and mobilizing to form a glial scar (**Figure 1.12**).

Nervous system environments / Inhibitory effects

a Developing nervous system

–
Robust axon growth and pathfinding

Embryonic axons
(Trks, DCC, Ephs, ROBOs, neuropilins/plexins, etc.)

Trophic and guidance molecules
(Neurotrophins, netrins, ephrins, SLITs, semaphorins, etc.)

b Mature CNS

Target

+
Limited plasticity and collateral sprouting

Intact adult axons
(NgR complex, EphA4, plexin B1, etc.)

Oligodendrocytes
(Nogo-A, MAG, OMgp, ephrin B3, Sema4D, etc.)

Astrocytes
(CSPGs)

c Injured CNS

+++
Impaired axon regeneration with limited compensatory sprouting and plasticity

Injured axons with dystrophic growth cones
(NgR complex, EphA4, plexin B1, etc.)

Oligodendrocytes and myelin debris
(Nogo-A, MAG, OMgp, ephrin B3, Sema4D, etc.)

Reactive astrocytes and glial scar
(Injury-induced ↑CSPGs)

Figure 1.12. The CNS microenvironment changes during development and after injury. The mammalian CNS possesses a growth-promoting environment early in development, but upon maturation of nervous circuits and tracts, the growth-promoting factors are scarce and the environment is less permissive. Following injury, the presence of myelin debris, oligodendrocytes, reactive astrocytes, and other components of the glial scar prevent axons from extending through the lesioned area. Figure adapted from (Yiu & He 2006).

The glial scar forms as a response to CNS tissue damage. Many definitions and interpretations of the "glial scar" have been put forward, and many elements of the scar's role with respect to injury and repair remain under debate. Here, we define the glial scar as a part of the local immune response following CNS injury, wherein glial cells and several other non-neuronal cells such as pericytes and meningeal cells at the lesion site become hypertrophic or reactive (Faulkner 2004; Silver et al. 2015). Reactive astrocytes can be detected by an increase in the cells' expression of glial fibrillary acid protein (GFAP), and this technique is often used to visualize the glial scar using immunohistochemistry (Bignami & Dahl 1974). The consequences of glial scarring are manifold, and considerable disagreement remains regarding how damaged neurons interact with the cells and matrix proteins that make up the scar. It has been demonstrated that the glial scar acts to repair the blood-brain barrier (BBB) and sequester inflammation at the lesion site, thereby limiting damage to nearby cells (Faulkner 2004). Indeed, the degree of scarring appears linked to the level of BBB disruption and the influx of non-CNS components, including activated macrophages, into the lesion site (Preston et al. 2001). This suggests that the glial scar plays an important role in reducing the scope of tissue damage after CNS injury. However, the scar is also a potential physical and chemical barrier to the regeneration of axons. Acute injuries produce a core of reactive astrocytes, oligodendrocyte precursor cells (OPCs), microglia, fibroblasts, and activated macrophages (**Figure 1.13**) (Soderblom et al. 2013; Sabelstrom et al. 2013; Barnabé-Heider et al. 2010; Busch et al. 2010; Horn et al. 2008; Meletis et al. 2008). When newly regenerating axons encounter this barrier, their active growth cones become dystrophic, forming the endbulbs first described by Ramon y Cajal. These endbulb structures signify the terminus of the regeneration path, as few if any axons successfully penetrate the scar. In addition to the scar itself, the area distal to the lesion where axons have degenerated is also highly inhibitory to growth. This is in large part due to the presence of myelin debris, which inhibits growing axons. Similarly, the presence of myelin-forming oligodendrocytes is deleterious to axon regeneration, mediated in large part by Nogo family proteins, which are expressed on oligodendrocytes.

a Microlesion
- Blood–brain barrier is minimally disrupted
- Astrocytes maintain normal alignment, but produce CSPGs and KSPGs along the injury tract
- Axons cannot regenerate beyond the lesion
- Macrophages invade the lesion site

b Contusive lesion
- Blood–brain barrier is disrupted, but meninges are intact
- Cavitation occurs at the lesion epicentre
- Astrocyte alignment is altered at the lesion site
- Astrocytes produce CSPGs and KSPGs in a gradient increasing from the penumbra towards the centre of the lesion
- No fibroblast invasion of lesion core and therefore no fibroblast-expressed inhibitors are present (see below)
- Macrophages invade the lesion and its core
- Dystrophic axons approach the lesion before growth ceases

Astrocyte | Dystrophic axon | Fibroblast | Macrophage | Altered ECM of injury site | Cavitation | Reactive astrocyte

c Large stab lesion
- Blood–brain barrier is disrupted
- Cavitation occurs at the lesion centre
- Astrocyte alignment is altered at the lesion site
- Astrocytes produce CSPG and KSPG in a gradient increasing towards the lesion
- TGF, ephrin-B2 and Slit protein expression increases in reactive astrocytes adjacent to fibroblasts
- Fibroblasts invade the lesion and express SEMA3 and the EPHB2 receptor
- Macrophages invade the lesion and release inflammatory cytokines
- Dystrophic neurons are highly repelled by the lesion core and express neuropilin 1

Figure 1.13. Formation of the glial scar following different types of injury. Examples from the spinal cord show different types of CNS injury and the resulting morphologies and composition of the glial scar Reactive astrocytes and fibroblasts cluster around the lesioned area, preventing axons from extending beyond the lesion. Figure adapted from (Silver & Miller 2004).

Within the glial scar, changes in the deposition of ECM molecules perform a central role in creating a growth-inhibitory CNS microenvironment (**Figure 1.14**). For injuries wherein the dura mater is spared, changes in ECM components are driven primarily by reactive astrocytes, which express heightened levels of tenascin-C and CSPGs (Burnside &

44

Bradbury 2014; Silver & Miller 2004). After injury, the accumulation of CSPGs in and around the glial scar contributes to the overall inhibitory effect of the local microenvironment toward new axons. As such, CSPGs have been widely studied in the context of injury and regeneration, and removing them from the ECM or modifying their post-translational structure to reduce their inhibitory influence can facilitate the growth of regenerating axons. Characterizing the accumulation of CSPGs within the glial scar and subsequently modifying their inhibitory structures to facilitate axonal regeneration is the primary focus of this thesis.
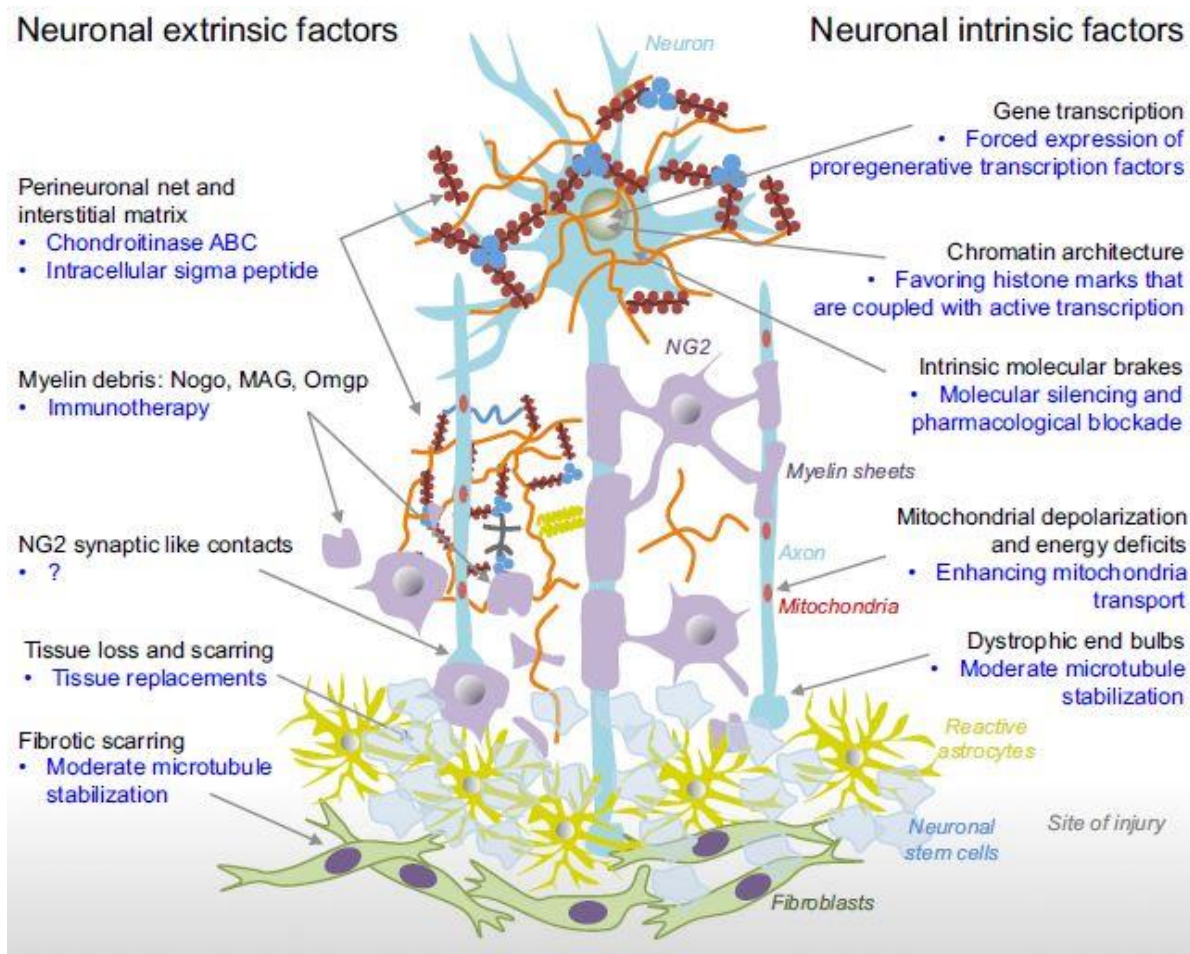
Figure 1.14. Comparison of extrinsic and intrinsic factors. Extrinsic factors that limit axon regeneration include the CSPG family proteins, the presence of myelin debris from degenerating axons, the presence of NG2 which appears to entrap axons, loss of tissue, and astrocytic and fibrotic scarring. Figure adapted from (Tedeschi & Bradke 2017).

1.6 | THE GLIAL SCAR AND CSPGS

Proteoglycans are composed of a protein core covalently joined to one or more glycosaminoglycan (GAG) chains. These linear, unbranched chains are assembled from repeating disaccharide units, the composition of which determines the GAG's classification as chondroitin sulfate (CS), heparan sulfate (HS), keratan sulfate (KS), or dermatan sulfate (DS) (**Figure 1.15**). CSPGs are the most abundant proteoglycans in the mammalian CNS and can be inhibitory or permissive to neurons depending on their structural features, enabling these dynamic proteins to play flexible roles in axon growth and guidance during development, at synapses, and after injury.
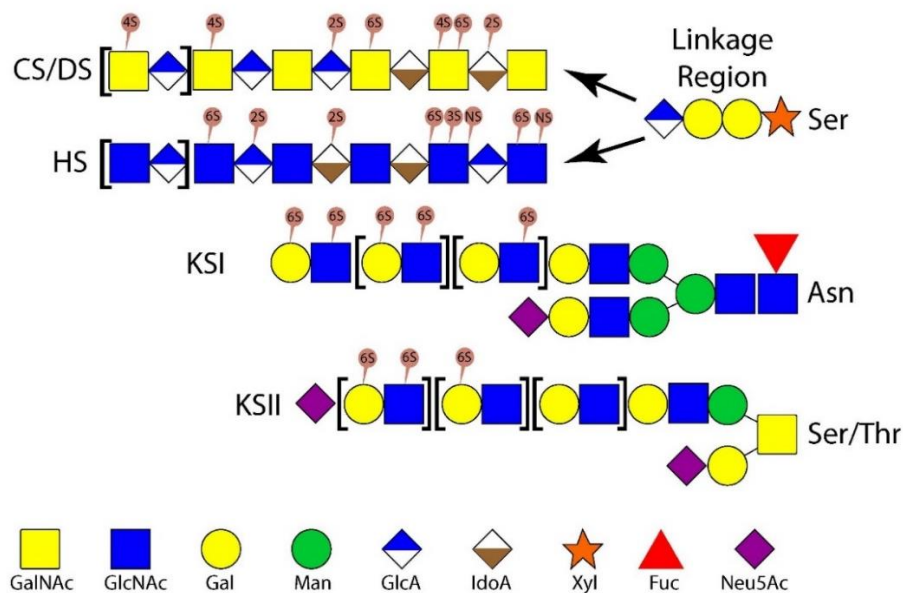
Figure 1.15. Structural diversity and classification of proteoglycans. A series of cooperative enzymes add sugars to the growing GAG chain. Up to 100 residues may be added. Sulfotransferase enzymes then add sulfate groups to a number of possible positions on the sugar rings. Epimerases can convert glucuronic acid to iduronic acid. Because the processes of chain extension and sulfation are not template driven, proteoglycans possess an incredible structural diversity. Sulfation does follow a set of common patterns, leading to several distinct classifications of the sulfation code. Abbreviations: CS, chondroitin sulfate; DS, dermatan sulfate; HS, heparan sulfate; Ser, serine; Asn, asparagine; Thr, threonine; GalNAc, N-acetyl-galactosamine, GlcNAc, N-Acetylglucosamine; Gal, galactose; Man, mannose; GlcA, glucuronic acid; IdoA, iduronic acid; Xyl, xylose; Fuc, fucose; Neu5Ac, N-Acetylneuraminic acid. Figure adapted from (Yu et al. 2017).

1.6.1 | CSPG structure and classification

The CSPG family comprises a diverse array of molecules that share several common structural elements (**Figure 1.16**). The lectican group encompasses molecules formed from a core protein to which are bound several CS-GAG chains composed of repeating disaccharide units made of N-acetyl-galactosamine (GalNAc) and glucuronic acid (GlcA) (**Figure 1.17**) (Siebert et al. 2014). Molecules in the lectican family, which include aggrecan, versican, neurocan and brevican, differ in the number of GAG chains attached to their core protein: aggrecan can have hundreds of GAG chains bound to a single core protein, whereas neurocan and brevican may have only a few, or none at all. Outside of the lectican family, phosphacan is a proteoglycan formed as a splice variant of receptor-type protein tyrosine phosphatase (RPTP), which contains binding regions for CS-GAG attachment. Chondroitin sulfate proteoglycan 4 (CSPG4, also known as neuron-glial antigen 2 or NG2) is a transmembrane protein expressed by OPCs, activated microglia, and macrophages, and contains relatively little sequence homology to other CSPGs.
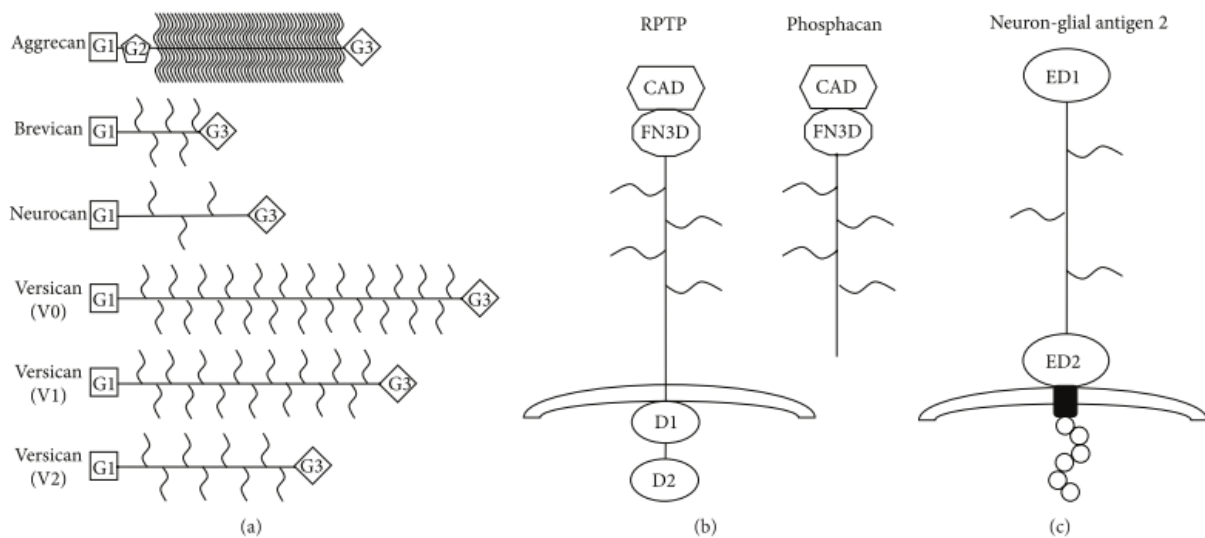
Figure 1.16. Types of CSPGs. The lectican family of CSPGs differ in the number of GAG chains attached to their core protein, and non-lectican CSPGs include phosphacan, an RPTP splice variant, and NG2, a transmembrane protein found in OPCs and immune cells. Figure adapted from (Siebert et al. 2014).

CSPGs differ in the post-translational modifications that influence their respective functions in the CNS. For example, the number of GAG chains attached to the core protein, and the length of the core protein itself, are key determinants of the molecules' biological activity. Experiments using chondroitinase ABC (ChABC) have demonstrated that the GAG chains, as opposed to the core protein, mediate the inhibitory effect of CSPGs on neurite growth. ChABC is a bacterial enzyme, produced by *Proteus vulgaris*, that removes disaccharide units from the terminal nonreducing end of the GAG chain (Habuchi 1967), effectively stripping the GAG chains from the CS core protein. Treating glial scar explants with ChABC rendered them permissive to neurite growth (Mckeon 1995). Administration of therapeutic ChABC doses in rats resulted in significant regeneration of cerebrospinal tract axons after spinal cord injury (Bradbury et al. 2002). Removal of CS GAGs appears to contribute to a more growth-permissive microenvironment and facilitate regeneration of damaged CNS axons. Precisely which features of GAG chains mediate this effect are not fully understood. A likely candidate is the "sulfation code," the pattern of sulfate groups post-translationally added to the carbons of GAG sugars.
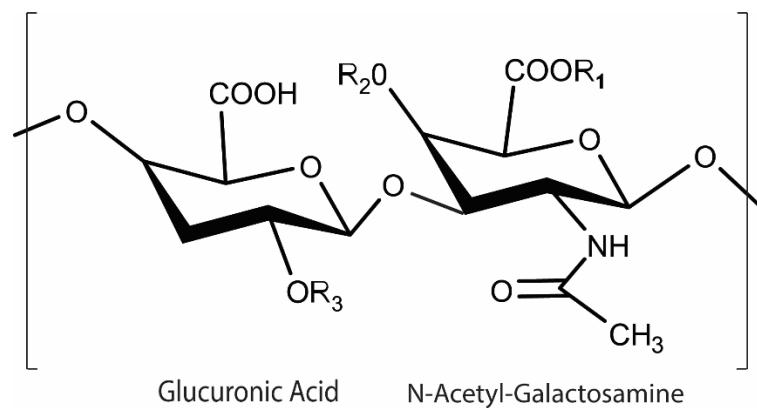
Figure 1.17. Structure of chondroitin disaccharide. Chondroitin GAG chains consist of repeating disaccharide units. Each disaccharide contains a glucuronic acid and an *N*-acetyl-galactosamine. Sulfation groups can be added at several positions on these rings by sulfotransferase enzymes, leading to a diverse set of possible patterns. Figure adapted from (Yu et al. 2017).

1.6.2 | CSPG sulfation

The sulfation code has been observed to play an influential role in determining the biological actions of CSPGs. The addition of sulfate groups to the disaccharide units of CS GAG chains is performed by sulfotransferase enzymes. Sulfate can be added at carbon 4 (4S) or carbon 6 (6S) of the GalNAc unit, or carbon 2 (2S) of the GlcA unit. Combinations of these patterns result in several variants of sulfated GAG chains on individual proteins (**Table 1.1**), and different variants exert different effects on neuronal growth. 4S has been found to be highly inhibitory toward axon growth *in vitro* (Wang et al. 2009), whereas 6S has been shown to be both inhibitory and permissive to axon growth in different experiments (Lin et al. 2011; Properzi et al. 2005). Modifying sulfation directly thus offers a targeted approach to reducing CSPG-mediated inhibition of regenerating axons *in vivo*.

Sulfation	Position	Unit Name
No sulfation	0S	CS-O
Chondroitin-4-*O*-sulfate	4S (R2)	CS-A
Chondroitin-6-*O*-sulfate	6S (R3)	CS-C
Chondroitin-2,4-*O*-sulfate	2S, 4S (R1, R2)	CS-B
Chondroitin-2,6-*O*-sulfate	2S, 6S (R1, R3)	CS-D
Chondroitin-4,6-*O*-sulfate	4S, 6S (R2, R3)	CS-E
Chondroitin-2,4,6-*O*-sulfate	2S, 4S, 6S (R1, R2, R3)	CS-T

Table 1.1. Nomenclature of chondroitin sulfate disaccharides. Several naming systems are used to distinguish CS GAGs with different sulfation code. Table adapted from (Yu et al. 2017).

Because of the lack of genetic knockout models, our knowledge of CS GAG chain function in the mammalian nervous system derives primarily from studies of the effects of GAG chains on neurite formation and neuronal polarization in culture (Miller & Hsieh-Wilson 2015). Following the demonstration that GAG chains inhibit dorsal root ganglion neurites in culture (Carbonetto et al. 1983), many groups have used *in vitro* assays to evaluate how GAG chains with differing sulfate composition influence neurite growth. Unfortunately, it has not been possible to achieve a consistent standard for GAG composition in such

experiments. Efforts to synthesize CS GAG chains are still in their infancy, meaning that virtually all data have been collected using tissue-derived GAG chains whose composition varies depending on the source of the tissue; even GAGs from the same tissue exhibit batch-to-batch variation (Rapp et al. 2005). Therefore, results of experiments studying GAG chain sulfation yield a wide range of results and interpretations, depending upon both the cell type used and the composition of the GAG chains.

Because of these drawbacks, the overall picture of the role of GAG sulfation gleaned from *in vitro* experiments is somewhat confusing. For instance, one study showed that rat cerebral cortical neurons were inhibited by CS-C but not CS-A (Butterfield et al. 2010), and another that they were inhibited by CS-E (Karumbaiah et al. 2011). Chick dorsal root ganglion (DRG) neurons, on the other hand, were inhibited by CS-E (Brown et al. 2012), but not CS-A or CS-C, while another study showed that CS-C as well as DS were both inhibitory to chick DRGs (Verna et al. 1989). Our group has shown that CS-A, but not CS-C, is inhibitory to mouse cerebellar granule cell neurites, and that this inhibition is dependent on 4S (Wang et al. 2008). The role of 4S appears to be outsized in mediating the inhibitory actions of CS: an antibody against 4S improves neurite outgrowth on aggrecan (Yang et al. 2017) and selective removal of 4S specifically at the non-reducing end of GAG chains is sufficient to reduce CS-mediated inhibition of rat hippocampal neuron growth (Zhang et al. 2014). For chick retinal neurites, CS-C, -D or -E, but not CS-A, were observed to be inhibitory (Shimbo et al. 2013), while chick trigeminal neurites were inhibited by CS-A, CS-C and dermatan sulfate (DS) (Schwend et al. 2012). In contrast, rat hippocampal neurite outgrowth was generally promoted by CS-D and CS-E as well as several different oversulfated DS saccharides (Clement et al. 1998; Clement et al. 1999; Bao et al. 2004; Hikino et al. 2003). The Hsieh-Wilson lab has produced GAG mimetics with pure sulfation patterns. And yet, even among these purified samples, the results are inconsistent, with CS-E mimetics both inhibiting (Rawat et al. 2008) and promoting (Tully et al. 2004) hippocampal neurite outgrowth.

There are several possible explanations for the heterogeneous responses to CS GAG chains in culture. One is that each laboratory uses its own strategy for creating substrates, as well as its own tissue source and culture conditions: some studies compare growth on poly-amino acids with growth on CS GAGs, while others evaluate GAG actions on neurons plated on laminin or fibronectin, both of which depend on integrin receptor activation for their growth-promoting activity. Different types of neurons may express specific complements of receptors for the growth promoting substrate or for CS GAG chains, and they may also

produce distinct types of ECM molecules that interact with GAGs, altering the outcome. Some of these effects are due to direct interactions with the neurons, while others, especially using the more highly-sulfated GAGs, may be through GAG chain interactions with growth factors such as pleiotrophin and contactin-1, which promote growth (Hashiguchi et al. 2010; Mikami et al. 2009), and semaphorins, which inhibit growth (Dick et al. 2013). Furthermore, methods of measuring effects may fail to detect subtle differences: while both CS-D and CS-E each promoted the outgrowth of embryonic mouse hippocampal neurites, there were differences in the morphology of the cells on the different GAGs (Hikino et al. 2003). The future availability of defined CS GAG chains along with more consistent experimental protocols and molecular probes for different classes of neurons may help resolve these inconsistencies.

The critical role of CS sulfation is also supported by *in vivo* evidence. For instance, the sulfate composition of CS GAG chains has been shown to change with age. In the mouse cerebellum, the percentage of CS-A units rises from 50% at birth to 85% in the young adult, with a corresponding decrease in CS-C units from 35% to 5%, and O units from 9% to 3% (Ishii & Maeda 2008b). siRNA-mediated knockdown of sulfotransferases reduced cortical neuronal migration, indicating that sulfation is essential to this developmental process (Ishii & Maeda 2008a). Other experiments using knockout animals suggest that 6S on CS-C may promote growth (Lin et al. 2011), and that an age-associated increase in the ratio of 4S GAG to 6S GAG in perineuronal nets may decrease synaptic plasticity (Foscarin et al. 2017). This is supported by the observation that overexpression of chondroitin 6-O-sulfotransferase-1, which decreases the ratio of 4S to 6S in perineuronal nets, increases seizure susceptibility (Yutsudo & Kitagawa 2015). These studies emphasize the urgent need for genetic manipulation of other chondroitin sulfotransferases to illuminate their biological functions and generate a clearer picture of the role sulfation plays in development and aging.

1.6.3 | CSPG signaling

Signaling pathways downstream of CSPG binding to neuronal receptors have been widely studied. The diversity of species, neuronal subtypes, and culture conditions used make these findings difficult to compare directly. However, several important pathways have emerged as important to CSPG signaling, and these are briefly noted below.

Rho/ROCK

The Rho GTPase family (Cdc42, Rac1, and RhoA (Jain et al. 2004)) and their downstream effector ROCK are activated by aggrecan, impeding neurite outgrowth and inducing growth cone collapse (Chan et al. 2008). Pharmacologically suppressing ROCK enhances axon growth on aggrecan substrates (Borisoff et al. 2003). Likewise, directly inhibiting Rho reverses CSPG-mediated inhibition (Monnier et al. 2003). Inhibiting Rho GTPase family members Cdc42 and Rac1 also overcomes CSPG-dependent inhibition of axon growth (Jain et al. 2004).

Cytoskeleton

ROCK pathway activation acts through downstream effectors related to cytoskeletal dynamics, including cofilin, which disassembles actin filaments (Gopalakrishnan et al. 2008). Inhibition of nonmuscle myosin II causes actin and microtubule reorganization, which accelerates axon extension and enables axons to cross boundaries with inhibitory CSPG substrates (Yu et al. 2012; Hur et al. 2011). When actin filament formation was inhibited in DRGs *in vitro*, microtubule realignment upon contact with a CSPG boundary was limited and growth cone turning prevented (Challacombe et al. 1996). Suppressing microtubule dynamics produced a similar effect, with limited growth cone turning at a CSPG boundary (Challacombe et al. 1996).

PI3K-Akt-mTOR

Activation of this cell cycle regulatory pathway overcomes CSPG inhibition of axon extension (Silver & Silver 2014). The CSPG-binding receptors PTPσ and LAR share common signaling pathways, including RhoA, Akt and Erk (Ohtake et al. 2016). An antagonist of the PI3K-Akt-mTOR pathway, GSK-3β, is activated by CSPGs, and its inactivation leads to neurite growth *in vitro* and axon sprouting and functional recovery *in vivo* (Dill et al. 2008).

EGFR

Suppressing EGFR's kinase function enhances regeneration of neurons (Koprivica et al. 2005). Downstream of EGFR, MAPK signaling mediates CSPG inhibition of neurite growth from cerebellar granule neurons (Kaneko et al. 2007). Blocking EGFR promotes growth and migration of human neural precursor cells (Novozhilova et al. 2015). Survival of neural stem cells is promoted by CSPGs acting through EGFR pathways as well as JAK/STAT3 and PI3K/Akt (Tham et al. 2010).

Integrins

Young embryonic neurons can adapt to inhibitory environments, growing more readily than mature neurons across CSPG surfaces; this may be due to upregulation of integrin (Lemons et al. 2005). In hostile growth conditions, young neurons express integrin family receptors (Condic 2001), whereas adult neurons lack the growth-promoting α9 integrin subunit (Andrews et al. 2009). Induced expression of alpha-integrins in adult neurons enhances growth and regeneration of axons (Condic 2001; Andrews et al. 2009; Cheah et al. 2016). Aggrecan and Nogo-A both inactivate integrins. Aggrecan decreases levels of phosphorylated FAK and pSrc without directly affecting surface integrins. Activating integrins directly reverses the inhibitory effects (Tan et al. 2011). In melanoma cells, CSPGs bind alpha-4-beta-1 integrin to inhibit cell adhesion, mediated by a CS-GAG binding site on alpha-4 integrin (Iida et al. 1998). Neuronal precursor cells respond to cleavage of CSPGs by ChABC with enhanced proliferation, differentiation, and migration, mediated by integrin signaling (Gu et al. 2009).

Calcium

Intracellular calcium regulates growth cone dynamics during axon extension (Gomez & Spitzer 2000). In culture, neurons encountering a CSPG substrate display a rise in intracellular calcium, dependent on influx through non-voltage-gated calcium channels (Snow et al. 1994). However, growth cone avoidance of CSPG surfaces occurs regardless of a transient rise in intracellular calcium, suggesting that this behavior is not dependent on elevated intracellular calcium (Snow et al. 1994). The transient calcium influx provoked by CSPGs is similar to that elicited by AMPA and kainate, and antagonizing AMPA and kainate

receptors blocked CSPG-mediated calcium influx (Maroto et al. 2013). This suggests that CSPGs activate AMPA and kainate receptors to elevate intracellular calcium.

PKC

Blocking PKC activity reduces inhibition from CSPGs, and inhibiting PKC *in vivo* led to enhanced axon regeneration after spinal cord injury in rats (Sivasankaran et al. 2004). Downregulating or inhibiting PKC *in vitro* increased neurite crossing on non-permissive astrocytes, suggesting that astrocyte-derived matrix molecules such as CSPGs signal through PKC to influence neurite growth (Powell et al. 2001).

Local protein synthesis

Depletion of intra-axonal RhoA synthesis enhanced growth of neurons in CSPG-rich media (Walker et al. 2012). Increased protein translation was confirmed by an increase in phosphorylated 4E-BP1 levels (Walker et al. 2012). Sema3A, a negative guidance cue, also stimulates local translation of RhoA mRNA in axons (Wu et al. 2005).

1.6.4 | CSPGs in the healthy CNS

The CNS is particularly rich in proteoglycans, which are distributed widely throughout the brain, spinal cord, and optic nerves (Novak & Kaye 2000). CSPGs are the most abundant proteoglycans in the mammalian CNS. Historically, CSPGs and other ECM components were primarily thought to play a structural role, filling the gaps between cells and supporting complex neuronal structures. CSPGs are now known to perform a diversity of additional functions in the CNS. These include growth factor regulation, as the GAG chains of CSPGs are known to bind both growth promoting factors (Deepa et al. 2002; Deepa et al. 2004) and growth inhibiting factors (Kantor et al. 2004). By binding growth-related factors, CSPGs facilitate ligand-receptor signaling, localize key molecules to sites of growth during development, and build reservoirs of growth-related molecules that can later be mobilized when needed (Galtrey & Fawcett 2007). They can also function as receptors that modulate cell signaling (Oohira et al. 2000). CSPGs play wide-ranging roles in nervous system development. They are present at early sites of cell proliferation in the brain and spinal cord

(Engel et al. 1996). Because their GAG chains generally inhibit axonal growth, CSPGs often function as repulsive guidance cues. The axon guidance function of CSPGs is particularly well studied in the visual system, as described below. Another critical domain for CSPGs in the CNS is neural plasticity, implicating CSPGs in learning and memory. The composition and sulfation code of CSPGs in the CNS changes with age, which supports the notion that CSPGs are dynamic molecules whose diverse roles change flexibly over time and in different regions of the CNS, making them an object of interest and extensive study.

1.6.5 | CSPGs after CNS injury

CNS injuries induce reactive gliosis, as described above. CSPGs are synthesized by multiple cell types in this response, including astrocytes, which when reactive produce brevican, neurocan, and phosphacan (Jones et al. 2003), as well as microglia and oligodendrocyte precursor cells (OPCs), which are known to produce NG2 and versican (Asher et al. 2002). The precise temporal and spatial expression of CSPGs in the glial scar varies among different core proteins (Siebert et al. 2014). For instance, following spinal cord injury, aggrecan expression is reduced (Lemons et al. 2001), and phosphacan is transiently reduced before increasing (Morgenstern et al. 2002). In addition to changes in core proteins, the abundance of differentially sulfated GAG chains may also change following CNS injury. It has been shown that 4S GAGs are strongly upregulated at the lesion site following brain injury (Yi et al. 2012). The dynamic regulation of CSPG deposition and changes in sulfation has yet to be fully characterized, and subtle differences exist in different systems, species, and types of injury.

The time course of CSPG expression in chronic neurodegenerative diseases is more difficult to study than controlled acute injuries, particularly in human patients where tissue is generally available only in the late phase of the disease. Evidence suggests that Alzheimer's disease progression includes reactive gliosis, implying that CSPGs are upregulated in affected CNS tissue (McGeer & McGeer 1995). CSPGs have also been detected in the white matter of MS patients (Sobel & Ahmed 2001). Changes in CSPG expression have been linked to seizures in a rat model of epilepsy (Okamoto et al. 2003), and to plasticity in brain areas damaged by stroke (Galtrey & Fawcett 2007). Treating lesioned areas with ChABC often improves axonal sprouting and plasticity, although the extent to which such therapies

promote functional recovery, and their viability as clinical treatments in humans, remains a topic of debate (Zhao & Fawcett 2013; Burnside & Bradbury 2014; Bradbury & Carter 2011).

1.6.6 | CSPGs in the visual system

CSPGs in the visual system direct the patterning of RGCs in the developing retina and facilitate the extension and navigation of their axons and, in adulthood, stabilize their connections with visual targets in the brain. Understanding the factors responsible for the expression, distribution, and behavior of CSPGs is vital for studies of visual system development, damage, and repair.

CSPGs in visual system development

In the visual system, CSPGs are predominantly found in nerve fiber layers. These include the optic nerve, the interphotoreceptor matrix (IPM), and the surface of retinal pigment epithelium (RPE) cells (Varner et al. 1987). Early histological studies identified neurocan and versican as the dominant proteoglycans in the developing retina of multiple species (Li et al. 2000; Zako et al. 1997; Inatani, Tanihara, Oohira, et al. 1999). In the chick retina, CSPGs were found in the optic fiber layer, corresponding to the onset and cessation of RGC growth (Ring et al. 1995). Specifically, neurocan was identified in chick retina as early as embryonic day 7 (Li et al. 2000). Another study found neurocan and versican throughout the embryonic chick retina, whereas aggrecan and brevican were not detected (Zako et al. 1997). In rats, neurocan localizes to the inner retinal layers at birth (Inatani, Tanihara, Oohira, et al. 1999), and can be found in the IPL and OPL at postnatal stage P7-P14, after which its reactivity steadily declines. Neurocan inhibits the growth of rat RGCs in culture (Inatani et al. 2001). Both 6S and 4S GAGs were observed in association with RGC axons in the developing chick visual system (McAdams & McLoon 1995). While CSPG-mediated inhibition of neurons is generally attributed to the GAG chains, digestion of the GAG chains with ChABC failed to abolish neurocan's inhibition of neurite growth, suggesting that the core protein may be intrinsically inhibitory (Inatani et al. 2001). Various CSPGs have also been identified in bovine eyes, where an unidentified proteoglycan was found in the outer

plexiform layer and associated with horizontal cells (Williams et al. 1998). CSPGs have been identified within the developing macaque retina (Peterson et al. 1995) and in the human retina and vitreous (Azuma et al. 1998).

The presence of axon-inhibiting CSPGs during development appears essential for the functional organization of retinal neurons. Early *in vitro* studies showed that RGC growth cones extend filopodia that repeatedly sample and respond to their extracellular environment, and that CSPG expression in the retina moves from the center to the periphery, maintaining a gradient that coincides with the edge of the developing axons (Snow et al. 1991). In a time-lapse video-microscopy study, CSPG immunoreactivity was observed to recede in a wavelike motion toward the retinal periphery (Brittis & Silver 1995). This phenomenon was confirmed by another study showing the shift of CSPG expression from the central retina toward the periphery (K.-Y. Chung et al. 2000). RGCs near the edge of this receding wave send out minor processes, termed probing processes, which respond to the gradient of CSPG expression by extending toward regions of lower CSPG concentration, i.e. the central retina. The probing processes develop growth cones, enabling the axons to navigate toward the optic fissure to form the developing optic nerve. These early pioneer axons facilitate the subsequent guidance of later axons along the same path (Brittis & Silver 1995). Digesting CS GAG chains with ChABC leads to aberrant growth of RGC axons toward the retinal periphery, indicating that CSPGs are required to direct axonal growth toward the optic nerve head (Brittis et al. 1992).

In binocular animals, optic nerve fibers decussate at the optic chiasm. The boundary-forming properties of CSPGs are critical for this process. When RGC axons first enter the chiasm, CSPG levels are low in the optic fiber layer but robust in the caudal parts of the ventral diencephalon (K. Y. Chung et al. 2000). Where axons cross the midline toward the optic tract, CSPGs were observed at the site where ventral axons are sorted from dorsal axons (K. Y. Chung et al. 2000). Removal of GAG chains from embryonic brains by intraventricular injection of ChABC caused enlargement of the anterior optic tract, suggesting that CSPGs define the optic tract's anterior boundary (Ichijo & Kawabata 2001). Studies using ChABC indicate that CSPGs may also be essential for establishing age-related axon order in the mouse optic tract (Leung et al. 2003). Whereas slices from E14 mouse embryo brains typically show an increase in CSPG immunoreactivity in the optic tract that corresponds with an accumulation of phalloidin-stained axonal growth cones in the superficial optic fiber layer, slices treated with ChABC abolished this pattern, suggesting that

the organization of the developing axons had been disrupted in the absence of CS GAGs (Leung et al. 2003).

RGC axons project to visual targets in the brain to form synapses, and CSPGs prevent these axons from aberrant innervation of non-target regions. Early work suggested that CSPGs in the mouse neocortex can differentially promote or inhibit axonal extension, and proposed a role for CSPGs in segregating afferent and efferent axon tracts (Bicknese et al. 1994). Addition of CSPG to cultured rat thalamic neurons reduced cell adhesion and promoted axonal growth, an outcome that was not replicated in rat hippocampal neurons, implying a cell-type-specific effect (Fernaud-Espinosa et al. 1994). Experiments in which embryonic thalamic neurons were plated on *ex vivo* mouse forebrain slices showed that the cortical plate repels neurites, whereas the intermediate zone and subplate facilitate neurite growth, and that these opposing effects were both blunted by ChABC treatment (Emerling & Lander 1996). This suggested that different CSPGs, or perhaps different CS-binding molecules, direct cortical development in a regional manner. While comprehensive characterization of the cortex ECM has yet to be undertaken, many cortical CSPGs have been characterized. Neurocan and phosphacan in the cortical subplate were identified as permissive substrates for thalamocortical axons (Fukuda et al. 1997). Conversely, in a study of rat embryo explants, enriched levels of neurocan in the hypothalamus and epithalamus appeared to repel axons, enabling axons to extend toward their proper targets in the thalamus (Tuttle et al. 1998). Understanding the precise nature of CSPG-directed axon guidance will require a more thorough understanding of which core proteins, GAG chains, sulfation patterns, and CS-affiliated molecules are expressed both temporally and regionally in the thalamus and cortex.

CSPGs are upregulated following injuries to the visual system

While CSPG deposition following acute damage to the brain and spinal cord has been thoroughly characterized, few studies have examined the distribution and temporal progression of CSPG expression in the visual system. It has been observed that cultured RGCs exhibit reduced neurite outgrowth on *ex vivo* substrates derived from gliotic tissue. Treating these substrates with ChABC enhanced axonal extension, implicating the CSPGs as critical components of inhibition of neurite growth by the glial scar (Mckeon 1995). CSPG accumulation has been observed 24 hours (Sellés-Navarro et al. 2001) and 3 days

(Sengottuvel et al. 2011) after optic nerve injury in rats, and after 24 hours in mice (Brown et al. 2012). The presence of axon growth-inhibiting CSPGs in the injured optic nerve can be inferred by the findings of studies that do not directly measure their expression. For instance, when RhoA, a downstream effector of CSPGs, was inactivated by viral-mediated expression of C3 ribosyltransferase in RGCs, axon regeneration in the optic nerve was enhanced (Fischer et al. 2004). Intravitreal injection of a Rho antagonist (C3-07) promoted RGC axon regeneration after microcrush lesion in rats (Bertrand et al. 2005), and inhibition of Rho kinase (ROCK) likewise enhanced RGC axon regeneration after optic nerve crush (ONC) (Lingor et al. 2007). Similar results were found in cats after inhibiting ROCK with Y-39983 (Sagawa et al. 2007). The ROCK inhibitor Y-27632 also enhanced RGC survival and axon regeneration after rat ONC (Tan et al. 2012). Mice lacking the CSPG receptor RPTPσ exhibited enhanced RGC axon regeneration after ONC, an effect that was mediated by MAPK and Akt kinase activity (Sapieha et al. 2005).

While the glial scar inhibits axonal extension, it is possible to partially overcome this obstacle with the application of robust pro-regenerative stimuli, as has been demonstrated repeatedly (Park et al. 2008; de Lima et al. 2012; Lim et al. 2016). There is evidence that stimulating RGC regeneration, for instance with the implantation of a peripheral nerve graft, may reduce scar formation via the upregulation of matrix metalloproteases (MMPs), which degrade CSPGs (Ahmed et al. 2005). Similarly, peripheral nerve graft implantation following ONC attenuated the expression of RPTPα and LAR, two putative CSPG receptors, in comparison to ONC-only controls, indicating that regenerating axons may be less sensitive to CSPGs (Lorber et al. 2004). However, the scar remains a substantial barrier even in the presence of pro-regenerative stimuli. Three-dimensional reconstructions of individual RGC axons have illustrated that stimulated axons exhibit aberrant, circuitous growth on the proximal side of the glial scar, indicating an inability to effectively penetrate this region (Bray et al. 2017).

Unlike mammals, invertebrates successfully regenerate their CNS tracts following injury. The mechanisms underlying this difference have been extensively studied, and continue to be a topic of interest in neural regeneration research. In goldfish, whose optic nerve regenerates after an ONC injury, CSPG immunoreactivity is observed within the first three weeks following injury, corresponding with the period during which RGC axons extend and reestablish their connections with central targets (Battisti et al. 1992). By six weeks, CSPG levels return to baseline. Interestingly, the upregulated CSPG in the optic nerve is spatially organized, associating with regenerating axons in columns (Battisti et al. 1992). This seems

to suggest a growth-promoting role for CSPGs, an observation supported by evidence that RGCs in goldfish retinal explants exhibit enhanced axonal outgrowth following the addition of exogenous 4S GAGs (Challacombe & Elam 1997). More research is required to determine the potential differences in gene expression within goldfish RGCs that enable them to associate with CSPGs and successfully regenerate after optic nerve injury.

CSPGs are also upregulated following retinal damage. While neurocan expression is low in the mature retina, transient ischemia significantly enhances neurocan mRNA levels in rat retinas, suggesting that neurocan plays a role in the retina's response to injury (Inatani et al. 2000). In a related study, decorin was found to be upregulated in the inner retinal layers following ischemia (Inatani, Tanihara, Honjo, et al. 1999). Enhanced CSPG deposition in the retina has also been observed in several murine models of inherited photoreceptor degeneration, in conjunction with astrogliosis (Barber et al. 2013).

CSPGs are implicated in degenerative and demyelinating disease

Traumatic injury to the visual system is less common than neurodegenerative diseases such as glaucoma and multiple sclerosis, which can cause permanent visual impairment and blindness. The accumulation of CSPGs has been observed in the optic nerve head of rats subjected to elevated IOP for prolonged periods (Johnson et al. 1996). In 8-month-old DBA/2J mice, which naturally develop a glaucoma-like phenotype within their first year of life, a significant upregulation of both GFAP-expressing astrocytes and CSPGs was observed in the endfeet of Muller glia in the inner nuclear layer of the retina (Inman et al. 2011). These findings potentially link CSPG accumulation with the loss of axon density in glaucoma. Conversely, administering the disaccharide (DS) product of ChABC digestion (CSPG-DS) appears to have neuroprotective effects: intravenous injection of CSPG-DS in rats with chronic and acute elevations of IOP protected RGCs from cell death (Bakalash et al. 2007). The same group also observed neuroprotective effects of CSPG-DS in rodent models of inflammation-associated degeneration (Rolls et al. 2006) and spinal cord injury (Rolls et al. 2008). As noted previously, unlike humans, rodents do not have a lamina cribrosa; therefore, certain aspects of glaucomatous optic nerve damage are difficult to model in mice and rats. However, the accumulation of CSPGs has been confirmed in studies of monkeys with laser-induced glaucoma, where CSPGs were found in the lamina cribrosa (Fukuchi et al. 1994). In the eyes of human glaucoma patients, CSPGs have been detected in the optic nerve head

(Tezel et al. 1999), juxtacanalicular tissue (Knepper et al. 1996), and in the stroma beneath the corneal epithelium and endothelium (Uusitalo 1994). Curiously, mRNA for two CSPGs (CSPG4 and aggrecan) was found to be downregulated in a microarray of optic nerve head astrocytes from human glaucoma patients (Rosario Hernandez et al. 2002). However, this may be a side effect of elevated protein levels stimulating a self-regulating negative feedback mechanism (Inman et al. 2011).

CSPGs also appear at the site of demyelinated lesions in rodent models of multiple sclerosis. Much of this evidence arises from studies of the spinal cord, where axon regeneration and remyelination are enhanced by therapies that block the synthesis of CSPGs (Keough et al. 2016), pharmacologically reduce CSPG levels (Feliu et al. 2017), digest GAG chains with ChABC (Bartus et al. 2014), or disrupt the interactions between CSPGs and their receptors (Lang et al. 2014). In studies of optic nerve regeneration, one key concern is that regenerating axons are not myelinated, and therefore may fail to efficiently convey action potentials to the brain (Bei et al. 2016). CSPGs inhibit OPC growth and differentiation *in vitro*, and this inhibition is reversed by treatment with ChABC (Siebert & Osterhout 2011; Pendleton et al. 2013; Lau et al. 2012). Treating OPCs with the Rho inhibitor Y-27632 produced the same effect (Siebert & Osterhout 2011). Therefore, elevated CSPG expression in demyelinated areas of the optic nerve are likely to impede the remyelination process, limiting the potential for recovery of visual function. It is worth noting that myelin itself, and the myelin debris released into the optic nerve after injury, also inhibits axonal growth. One study identified the CSPGs brevican and versican V2 on differentiated oligodendrocytes, and showed that inhibiting CSPG synthesis with xylosides prevented oligodendrocytes from stimulating the collapse of axonal growth cones, providing a possible mechanism by which myelin inhibits axonal growth (Niederöst et al. 1999).

1.7 | TARGETING CSPGS *IN VIVO*

Given the growth-inhibitory properties of CSPGs, targeted removal or modification of GAG chains has the potential to improve axon regeneration, remyelination, and functional recovery after injury or degeneration of visual pathways. Several *in vivo* approaches have been developed to reduce CSPG-mediated inhibition of axons, including treatment with CSPG-targeting enzymes, disruption of CSPG synthesis with xylosides, and interference with CSPG receptor binding and downstream signaling.

1.7.1 | Enzymatic modification

ChABC has been extensively studied as a potential therapy for reducing CSPG inhibition of axonal regeneration. Enzymatic digestion of GAG chains using ChABC renders CSPGs permissive to neurite extension in culture and enhances axon regeneration after spinal cord injury in rodents (Bradbury et al. 2002). Typically, ChABC is delivered by direct application, either by injection (Bradbury & Carter 2011) or implantation of an enzyme-carrying scaffold (Lemons et al. 1999; Hyatt et al. 2010). It is also possible to engineer astrocytes to express ChABC under an astrocyte-specific promoter (Cafferty et al. 2007). Despite many promising findings that ChABC promotes axonal regeneration and, in the case of spinal cord injury, some recovery of motor function, there are several drawbacks to using this enzyme therapeutically. Robust long-distance regeneration remains rare, and the maintenance of regenerated connections over extended periods remains to be reliably demonstrated. Further, the thermal stability of ChABC is questionable, as the enzyme loses its activity fairly quickly under physiological conditions (Tester et al. 2007). The enzyme's bacterial origins also make it more difficult to envision clinical trials in human beings.

Many recent efforts have substantially improved the stability and delivery of ChABC. For instance, production of a humanized enzyme from mammalian cells has been engineered (Muir et al. 2010). A thermostabilized ChABC was shown to maintain its activity for up to 4 weeks *in vitro* at 37°C, which led to long-term suppression of GAG levels (Lee et al. 2010). Incorporating the ChABC gene into a viral vector enabled active secretion of ChABC from infected cells (Zhao et al. 2011). More recently, a dual vector system was used to create a doxycycline inducible "switch" whereby the ChABC gene activation could be temporally controlled (Burnside et al. 2018). Collectively, these and other efforts have led to greater stability and improved delivery of ChABC.

Another enzyme that modifies GAG chains is arylsulfatase B (ARSB). ARSB isolated from human cartilage was shown to have a molecular weight of 51 kDa and K_m of 2.6 mM for the substrate 4-nitrocatechol sulfate (Gold et al. 1976). The primary function of ARSB is to cleave sulfate groups from GalNAc at the C4 position at the non-reducing ends of CS and DS GAG chains, thereby enabling breakdown of complex polysaccharides (Litjens & Hopwood 2001). This process occurs intracellularly, in the lysosome, rather than in the extracellular matrix, although ARSB has also been localized to the ECM in some mammalian

cells (Mitsunaga-Nakatsubo et al. 2009). The optimal pH of the ARSB reaction is at about 5, although the enzyme remains effective at neutral pH (Roy 1987). While the active site of ARSB has been identified (**Figure 1.18**), the subsequent steps in GAG degradation and signaling cascade(s) activated by removal of 4S from the non-reducing end of CS or DS are not fully understood (Cammisa et al. 2013).
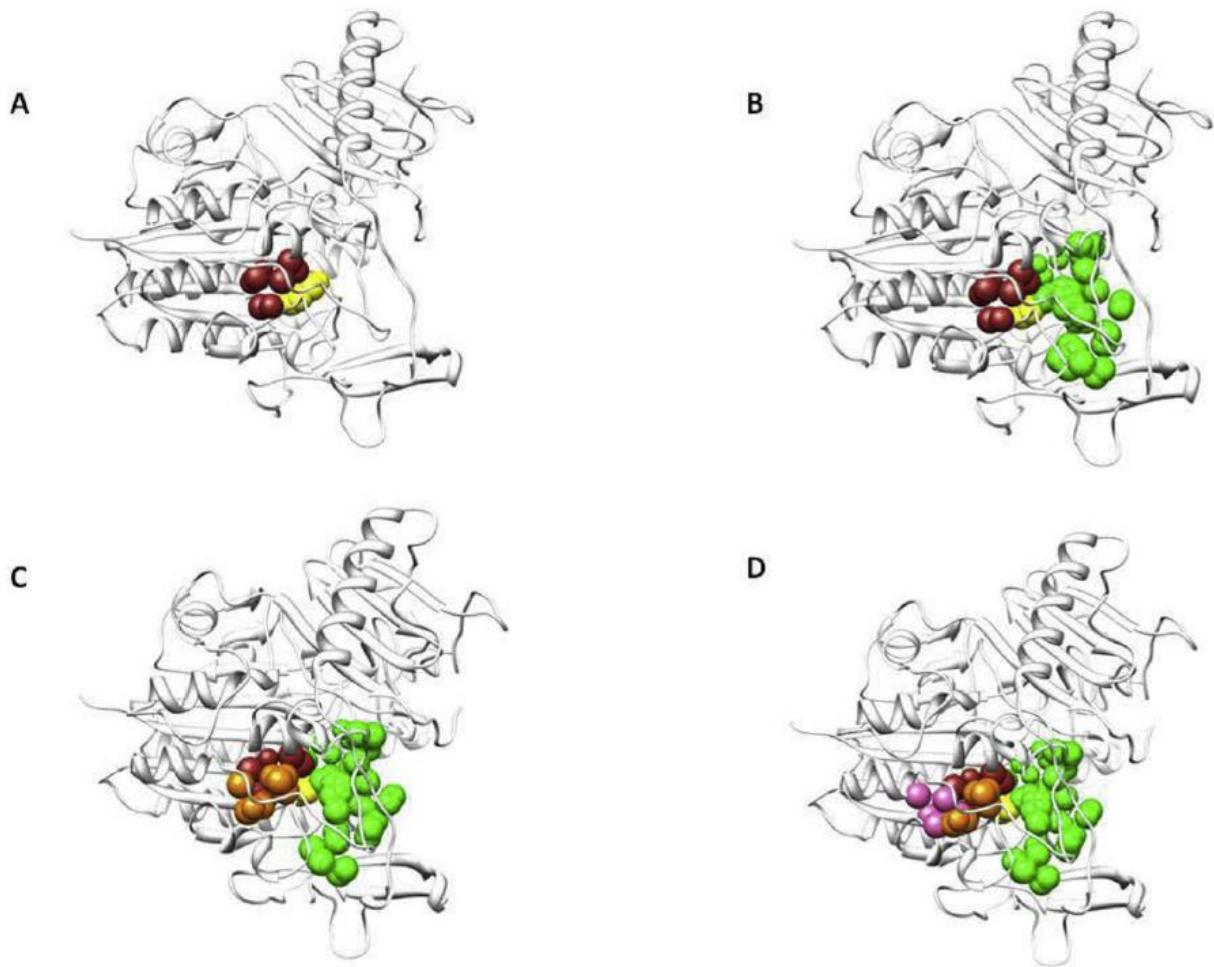
Figure 1.18. Structure and active site of ARSB. ARSB structure depicted as a ribbon. (A) The active site residue K145 (yellow) has a conserved binding pocket (brown). (B) Adjoining pockets (green) are shown in order of decreasing conservation, with (C) further pockets (orange) and (D) the least conserved pockets (pink). Figure adapted from (Cammisa et al. 2013).

Mutations of the ARSB enzyme in humans cause failure of polysaccharide degradation in the lysosome and lead to the accumulation of polysaccharides in the cartilage and other tissue (Litjens & Hopwood 2001). This condition is known as

mucopolysaccharidosis type VI (MPS VI, also known as Maroteaux-Lamy syndrome). The link between ARSB and MPS VI was shown by culturing fibroblasts from the skin of MPS VI patients and characterizing the dermatan sulfate that accumulated in these cultures, which was primarily N-galactosamine-4-sulfate (O'Brien et al. 1974). The observation that cells from MPS VI patients exhibited markedly reduced (15%) enzymatic activity of ARSB confirmed that severe dysfunction of this enzyme was linked to the accumulation of polysaccharides that underlies the primary symptoms of the disease (Shapira et al. 1975). MPS VI is now treated clinically by enzyme therapy with recombinant human ARSB. While ARSB has been used experimentally in mice with spinal cord injury (Yoo et al. 2013), it remains relatively understudied in comparison with ChABC.

1.7.2 | Xylosides

CSPGs can also be targeted *in vivo* by blocking their synthesis with xylosides, which inhibit the assembly of GAG chains by interfering with the addition of disaccharide units to the core protein. CSPGs produced in the presence of xylosides therefore lack GAG chains, and are thus far less inhibitory to neurons. Xyloside administration in the subacute phase following spinal cord injury enhanced axon regeneration and motor recovery in mice (Rolls et al. 2008). In a model of demyelination, application of xylosides reduced the total demyelinated area in comparison with controls, and also enhanced the number of mature oligodendrocytes found in the plaque (Lau et al. 2012). Application of xylosides in the visual system has been limited, but one study in micropigs observed that intravitreal injection of p-nitrophenyl-0-D-xylopyranoside disrupted the IPM and caused degeneration of photoreceptor outer segments, eventually leading to retinal detachment (Lazarus & Hageman 1992). The injections were administered to adult (4-6 months) animals, indicating that continued CSPG production may be required to maintain retinal integrity. Because xylosides are often delivered systemically, targeting specific areas of CNS lesions is generally not possible, making xylosides unlikely to translate to human clinical therapies.

1.7.3 | Interfering with receptors and signaling pathways

Another strategy for overcoming CSPG-mediated axon inhibition is interfering with signaling pathways downstream of CSPGs. The neuronal receptors for CSPGs have not been

comprehensively characterized, but it has been proposed that CSPG inhibition is mediated by receptors in the leucocyte common antigen-related phosphatase (LAR) family, the receptor RPTPσ, or the nogo-receptors NgR1 and NgR3 (Shen et al. 2009; Dickendesher et al. 2012; Fisher et al. 2011). Despite the debate surrounding the identities of putative CSPG receptors, many aspects of the downstream signaling pathways activated in the presence of CSPGs are known (Yu et al. 2017). Interfering with signaling pathways could prevent CSPG-induced signals from effecting gene expression or silencing, thereby avoiding the dystrophic response within the neuron, or even reconfigure the cytoskeletal rearrangements associated with impaired axon growth (Yu et al. 2012). In the visual system, interventions that inactivate the Rho/ROCK pathway have been shown to enhance RGC axon regeneration after ONC (Fischer et al. 2004; Lingor et al. 2007). Similarly, pharmacological inhibition of EGFR, another downstream effector of CSPGs, promotes regeneration of RGC axons (Koprivica et al. 2005). The degree of redundancy among these pathways is unclear, and it remains to be studied whether inactivating multiple pathways might have an additive effect.

EXPERIMENTAL AIMS

Restoration of vision by regenerating RGC axons is likely to require clinical therapies that address both intrinsic and extrinsic mechanisms of regeneration failure. Because the cell bodies of RGCs are easily accessible by injections into the eye, efforts to regenerate RGC axons have primarily focused on developing therapies that modify the intrinsic state of RGCs. While some studies have examined the formation and composition of the glial scar that forms in the optic nerve after acute injury, a comprehensive investigation of CSPGs has not been attempted, and the sulfation dependence of these proteins has not been addressed. The objectives of this PhD thesis were to devise a simple, reliable technique for administering therapeutic substances to the lesioned optic nerve, to elucidate the dynamics of sulfated CSPG accumulation in the glial scar, and to selectively target inhibitory CSPGs to facilitate regeneration of injured RGC axons.

Chapter 3 describes the development of a protocol for targeting the extracellular matrix in the lesioned optic nerve, with the following specific experimental aims:

1. To detail a step-by-step protocol for generating a controlled optic nerve lesion in mice, implanting a sterile gelfoam sponge at the lesion site, and analyzing the tissue to determine the effects of the intervention on RGC survival and axon regeneration.

2. To use two enzymes, ChABC and ARSB, to modify CSPGs in the lesioned optic nerve. The activity and stability of both enzymes will be assessed, first *in vitro* and then *in vivo*, with implanted scaffolds recovered over several days and assayed for the persistence of active enzyme. The penetration of active enzymes into the axon fibers of the optic nerve will be evaluated by detecting the byproducts of ChABC digestion, so-called "stubs," by immunohistochemistry and Western blot.

In Chapter 4, the expression of CSPGs by glial cells at the site of an optic nerve lesion is analyzed in two different models of CNS injury, and the ability of ARSB to selectively target 4S GAGs and enhance RGC axon regeneration is evaluated, with the following specific experimental aims:

1. To demonstrate the effects of CSPGs on neurite growth *in vitro*, and the ability of ARSB to reverse their inhibitory properties.

2. To analyze the time course, spatial distribution, and composition of CSPGs deposited in the glial scar following acute injuries to the optic nerve and spinal cord in mice and rats. Immunohistochemistry and Western blot analysis will be used to characterize changes in astrocyte reactivity and microglial activation, and to observe the production of CSPGs, particularly the 4S motif.

3. To determine whether using ARSB to modify CSPG sulfation at the non-reducing ends of GAG chains enhances the ability of RGCs to regenerate their axons following an acute injury. Mice will be treated with implanted ARSB or ChABC scaffolds following ONC, and RGC regeneration will be stimulated by ocular inflammation from an intravitreal injection of Zymosan. The regeneration of RGC axons will be assessed at multiple time points to determine the extent and duration of the effect. Treated optic nerve tissue will be further analyzed to determine whether ARSB and ChABC modify the glial component of the glial scar, and differences between ARSB and ChABC, which have different mechanisms, will be assessed.

Chapter 5 describes the effects of several therapies that stimulate RGC axon regeneration by modifying intrinsic growth pathways, and then combines these interventions with ARSB treatment to stimulate robust long-distance regeneration, with the following experimental aims:

1. To demonstrate the effects on RGC survival and axon regeneration of (i) inflammatory stimulation, (ii) enhancing endogenous electrical activity, and (iii) stimulating the mTOR pathway.

2. To combine these therapies with ARSB treatment of the lesioned optic nerve and examine long-distance axonal regeneration through the optic chiasm, including an assessment of RGC navigation and pathfinding in distal regions of the optic pathway, and to comment on the viability of combinatorial therapies for translation to human clinical trials.

LIST OF ABBREVIATIONS

4S	4-sulfation
6S	6-sulfation
AAV	adeno-associated virus
ARSB	arylsulfatase B
cAMP	cyclic adenosine monophosphate
CGN	cerebellar granule neuron
ChABC	chondroitinase ABC
CM	conditioned medium
CNO	clozapine-N-oxide
CNS	central nervous system
CS	chondroitin sulfate
CS-GAG	chondroitin sulfate glycosaminoglycan
CSPG	chondroitin sulfate proteoglycan
CTβ	choleratoxin β
dpc	days post crush
DRG	dorsal root ganglion
DS	disaccharide
E	embryonic day
ECM	extracellular matrix
GAG	glycosaminoglycan
GalNAc	*N*-Acetylgalactosamine
GAP-43	growth-associated protein 43
GCL	ganglion cell layer
GFAP	glial fibrillary acidic protein
HS	heparan sulfate
Iba1	ionized calcium-binding adapter molecule 1
INL	inner nuclear layer
IOP	intraocular pressure
IPL	inner plexiform layer
KS	keratan sulfate
LGN	lateral geniculate nucleus
MMP	matrix metalloproteinase

MPS VI	Mucopolysaccharidosis type VI
NG2	neural/glial antigen 2
Ocm	oncomodulin
ONC	optic nerve crush
ONL	outer nuclear layer
OPC	oligodendrocyte precursor cell
OPL	outer plexiform layer
PBS	phosphate buffered saline
PI3K	phosphoinositide 3-kinase
PNN	perineuronal net
PNS	peripheral nervous system
PTEN	phosphatase and tensin homolog
RGC	retinal ganglion cell
RPE	retinal pigment epithelium
RPTP	receptor-type protein tyrosine phosphatase
TGFβ	transforming growth factor β
TM	trabecular meshwork
WFA	*Wisteria floribunda* agglutinin

CHAPTER 2: METHODS

2.1 | ANIMALS

All experiments and procedures were performed in accordance with protocols approved by the Institutional Animal Care and Use Committee (IACUC) at the National Institutes of Health and the United Kingdom Animal (Scientific Procedure) Act of 1986. Female C57Bl/6 mice aged 6-8 weeks (Charles River) and female Sprague-Dawley rats weighing 250-275 g were housed in a pathogen free facility with free access to food and a standard 12 h light/dark cycle. Sample sizes were determined by statistical power calculations from pilot experiments and the results of previous studies, as described below. Animals were randomly allocated into experimental groups. Animals were removed from the study if bleeding occurred during the optic nerve crush or scaffold implantation surgery.

2.2 | CELL CULTURE

Cell culture experiments were performed by Dr. Caitlin Mencio. Primary hippocampal neuron cultures were prepared from embryonic (e17-18) C57Bl/6 mouse brains. Hippocampi were dissected and dissociated into single cell suspensions. Dissociated cells were seeded onto coverslips coated with poly-L-lysine and cultured in 500 µL Neurobasal medium containing B27 supplement and 24 mM KCl. After allowing 2 h for neuronal attachment, 500 µL of Neurobasal medium containing B27 supplement and 24 mM KCl that had been incubated for 4 h with no treatment, 10 µg/ml CSPG (for final concentration of 5 µg/ml), or CSPG (10 µg/ml) + ARSB (2 µg/ml) (final concentrations 5 µg/ml and 1 µg/ml, respectively) was added. Cells were incubated for 48 h at 37°C and 5% CO_2 atmosphere and then fixed and stained for DAPI and βIII-tubulin.

Primary cortical astrocyte cultures were prepared from neonatal (1-3 days) C57Bl/6 mouse brains as described previously (Wang et al. 2008). Cerebral cortices were dissected and dissociated into single cell suspension. Dissociated cells were seeded into T-75 flasks and grown in Dulbecco's Modified Eagle's Medium (DMEM) supplemented with 10% fetal bovine serum (FBS) at 37°C and 5% CO_2 atmosphere until cells grew to confluence (10-14 days). Flasks were shaken for 20 hours (120 rpm, 37°C) to detach microglia,

oligodendrocytes, and neurons from the more adherent astrocytes. After shaking, the medium was replaced. Media replacement was repeated 24 hours after the shaking period.

To harvest conditioned media from reactive astrocytes, purified astrocytes were plated into T-75 flasks in serum-containing medium. After reaching confluence, astrocytes were incubated with serum-free media overnight and treated with TGF-β (10 ng/mL), ARSB (1 ng/mL), TGF-β and ARSB, or neither (untreated controls), for 7 days. After harvesting, conditioned media was centrifuged at 800 rpm for 5 min to remove debris before being split into three aliquots of 2 mL each. Aliquots were treated with no enzyme, ARSB (1 µg/mL), or ChABC (1 µL/mL) for 4 h prior to addition to neuronal cultures.

Cerebellar granule neurons (CGNs) were isolated as previously described (Wang et al. 2008). Dissociated CGNs were cultured in 500 µL Neurobasal medium containing B27 supplement and 24 mM KCl and plated on poly-L-lysine-coated coverslips in 24-well plates. After allowing 2 h for neuronal attachment, 500 µL of treated conditioned medium was applied to each well in triplicate. Cells were incubated for 24 h and then fixed and stained for DAPI and βIII-tubulin. In co-culture experiments, dissociated CGNs were plated at a density of 5×10^4 cells/well onto a confluent monolayer of astrocytes in 24-well plates that had been treated for 7 d with ARSB (1 ng/mL), TGF-β (10 ng/mL) or TGF-β and ARSB.

2.3 | NEURITE OUTGROWTH ANALYSIS

Neurite outgrowth analysis was performed by Dr. Caitlin Mencio. After fixation and staining, at least 60 images were taken across two coverslips per condition. Files were analyzed by an experimenter blinded to the experimental conditions. Neurons were measured if they were isolated from other neurons and had distinct nuclei and at least one neurite longer than the diameter of the cell body. The longest neurite was measured for each neuron and at least 60 neurons were measured for each condition. Each experiment was performed in triplicate.

2.4 | GENOTYPING

2.4.1 | DNA extraction

Ear clips were obtained from transgenic and wildtype mice and flash frozen in liquid nitrogen. 50 µL alkaline lysis buffer (200 mg NaOH, 14.88 mg EDTA, 200 mL H_2O) was

added to the tubes, which were then heated at 95 °C for 1 h. 50 µL of neutralization buffer (1.3 g Tris-HCl, 200 mL H_2O) was then added, and samples were frozen at -20 °C.

2.4.2 | PCR

Primers were designed to bracket a sequence from the mutant p110α gene. PCR was then performed according to previously established methods. Briefly, a reaction mixture was prepared (12.5 µL GoTaq Hot Start Green Master Mix 2X, 0.5 µL upstream primer, 0.5 µL downstream primer, 6.5 µL nuclease-free water, and 5.0 µL DNA template). PCR was performed according to the protocol detailed in **Table 2.1**.

Table 2.1. PCR protocol.

Step	Conditions	Duration
1	94 °C	2 min
2	94 °C	30 s
3	65 – 55 °C (-0.5 °C/cycle)	90 s
4	72 °C	90 s
	repeat steps 2-4	*20 cycles*
5	94 °C	30 s
6	55 °C	90 s
7	72 °C	90 s
	repeat steps 5-7	*20 cycles*
8	72 °C	5 min
9	4 °C	hold

PCR products (10 µL per sample) were separated in a 1% agarose gel immersed in 1X TBE buffer and 0.01% ethidium bromide. Electrophoresis was performed at 100 V for 35 min. Bands were imaged under UV light and images were analyzed using ImageJ.

2.5 | ENZYME ACTIVITY ASSAYS

Activity of ChABC and ARSB was assessed immediately before surgery. ChABC (Amsbio 100332-1A) was reconstituted at 50 U/mL in a solution containing 100 mM Tris(hydroxymethyl)aminomethane hydrochloride (Tris-HCl) and 0.1% BSA. ChABC activity was measured by spectrophotometrically detecting the production of disaccharides

cleaved from the glycosaminoglycan chains of CSPGs, as has been previously described (Suzuki et al. 1968). The active production of these cleaved disaccharides can be measured by monitoring an increase in absorbance at 232 nm. Approximately 1 µL ChABC was added to 99 µL of CS-A (Sigma, 500 µg/mL in 1X PBS). Using an Ultrospec 3100pro spectrophotometer in kinetics mode, absorbance was measured at 232 nm every 15 s for 5 min. The enzyme was deemed active if an absorbance of at least 1.0 AU was reached within 5 min.

ARSB (Naglazyme®) was obtained in acidic PBS (pH 5.5) from Biomarin (San Rafael, CA). ARSB activity was measured by detecting the cleavage of a sulfate group from p-nitrocatechol sulfate (PNCS), which yields a product with an absorbance peak at 510 nm (Porter et al. 1969; Knaust et al. 1998). 1 µL of 1 µg/µL ARSB was added to 1 mL of assay buffer containing 50 mM 2-(N-morpholino)ethanesulfonic acid (MES) at pH 6.5. A stock solution of 100 mM 4-PNCS was diluted to 2 mM in 50 mM MES buffer. In a 96-well microplate, 75 µL of diluted ARSB was combined with 75 µL of 2 mM 4-PNCS substrate. As a negative control, 75 µL of MES buffer without ARSB was combined with 75 µL of 2 mM 4-PNCS. The plate was incubated at 37°C for 1 h. The reaction was then quenched by adding 150 µL of 0.2 N NaOH to each well. Absorbance was measured at 510 nm.

To measure enzyme activity at time points after *in vivo* implantation, scaffolds were recovered from freshly dissected optic nerves and placed in 1.5 mL Eppendorf tubes and stored on ice. For scaffolds loaded with ChABC, 2 µL of fresh enzyme buffer solution (100 mM Tris-HCl, 0.1% BSA) was added to the bottom of the tube, and the scaffold was immersed in this solution. After approximately 1 h on ice, 1 µL of the enzyme buffer was removed and added to the CS-A substrate in the spectrophotometer, and A_{232} was measured over 5 min as described above. For scaffolds loaded with ARSB, 250 µL of MES buffer was added to the tube containing the recovered scaffold. After approximately 1 h, three aliquots of 75 µL were removed from this solution and each combined with 75 µL 4-PNCS in a 96-well microplate. Samples were incubated at 37°C for 24 h, after which the reaction was quenched by adding 150 µL of 0.2 N NaOH. Absorbance was measured at 510 nm. In both cases, recovered scaffolds loaded with enzyme buffer served as controls.

2.6 | PREPARATION OF ZYMOSAN/CPT-cAMP AND ENZYME SCAFFOLDS

In accordance with established protocols (Yin et al. 2003; de Lima et al. 2012), Zymosan A (Sigma Z4250) was suspended in sterile PBS at a concentration of 12.5 µg/µL,

incubated at 37°C for 10 min, and vortexed. Lyophilized CPT-cAMP (Sigma C3912) was dissolved to achieve a final concentration of 50 mM CPT-cAMP. Aliquots were stored at 4°C for up to two weeks. Sterile gelfoam sponges were cut to roughly 2 mm^3 and placed to soak in a sterile tube containing 5 μL of either ChABC, ARSB, or the control buffer. Tubes were stored on ice for up to 4 h before surgical implantation.

2.7 | OPTIC NERVE CRUSH AND IMPLANTATION OF ENZYME SCAFFOLDS

Optic nerve crush was performed as described previously (Park et al. 2008). The optic nerve was exposed intraorbitally, and curved forceps were inserted beneath the external ocular muscle, avoiding the ophthalmic artery and retrobulbar sinus. The nerve was crushed approximately 1 mm behind the eye for 10 s. Immediately after the crush, eyes were monitored fundoscopically for signs of ischemia, and mice were observed for bleeding in the hours following surgery. Mice received a subcutaneous injection of 1 mg/kg buprenorphrine as an analgesic and topical application of ophthalmic ointment to prevent corneal drying.

For implantation of enzyme scaffolds, the optic nerve was exposed by gently reopening the conjunctiva and inserting curved forceps behind the eye. Carefully avoiding the ophthalmic artery and retrobulbar sinus, the enzyme- or buffer-soaked gelfoam scaffold was placed in direct contact with the optic nerve at the site of the crush lesion, approximately 1 mm behind the eye. Retinal blood flow was assessed fundoscopically, and mice received a subcutaneous injection of 1 mg/kg buprenorphrine and topical application of ophthalmic ointment.

2.8 | INTRAVITREAL INJECTION

2.8.1 | Zymosan, CPT-cAMP, and PBS

Intravitreal injections of Zymosan or a PBS control were administered immediately following implantation of the gelfoam scaffold. 2 μL of the injecting solution was drawn into a sterile 5 μL Hamilton syringe with a 33-gauge removable needle. In the case of Zymosan injections, the syringe was inspected to ensure that the needle was not blocked by Zymosan particles. The solution was then slowly injected through the superior nasal sclera at a 45° angle, avoiding the lens, external ocular muscle, and blood vessels. A sterile 33-gauge needle

was used to puncture the cornea and drain the anterior chamber before removing the injecting needle, to reduce intraocular pressure and prevent reflux of the injected solution. Different needles were used for Zymosan and PBS injections to prevent contamination, and the syringe was rinsed thoroughly with ethanol followed by sterile PBS between injections.

2.8.2 | Viruses

The viruses used for *in vivo* studies are listed in **Table 2.2**, including the titer and source. The commercially developed AAV2-hM3Dq virus map can be found in **Figure 2.1**.

Table 2.2. Viruses used for *in vivo* studies.

Virus	Titer	Source
AAV2-hM3Dq	3.48×10^{12} GC/mL	Addgene 50474-AAV2
AAV2-shPTEN	6.52×10^{12} GC/mL	Dr. Amanda Barber
AAV2-cre	1.0×10^{13} GC/mL	Dr. Patrice Smith
AAV2-eGFP	1.0×10^{13} GC/mL	Dr. Patrice Smith
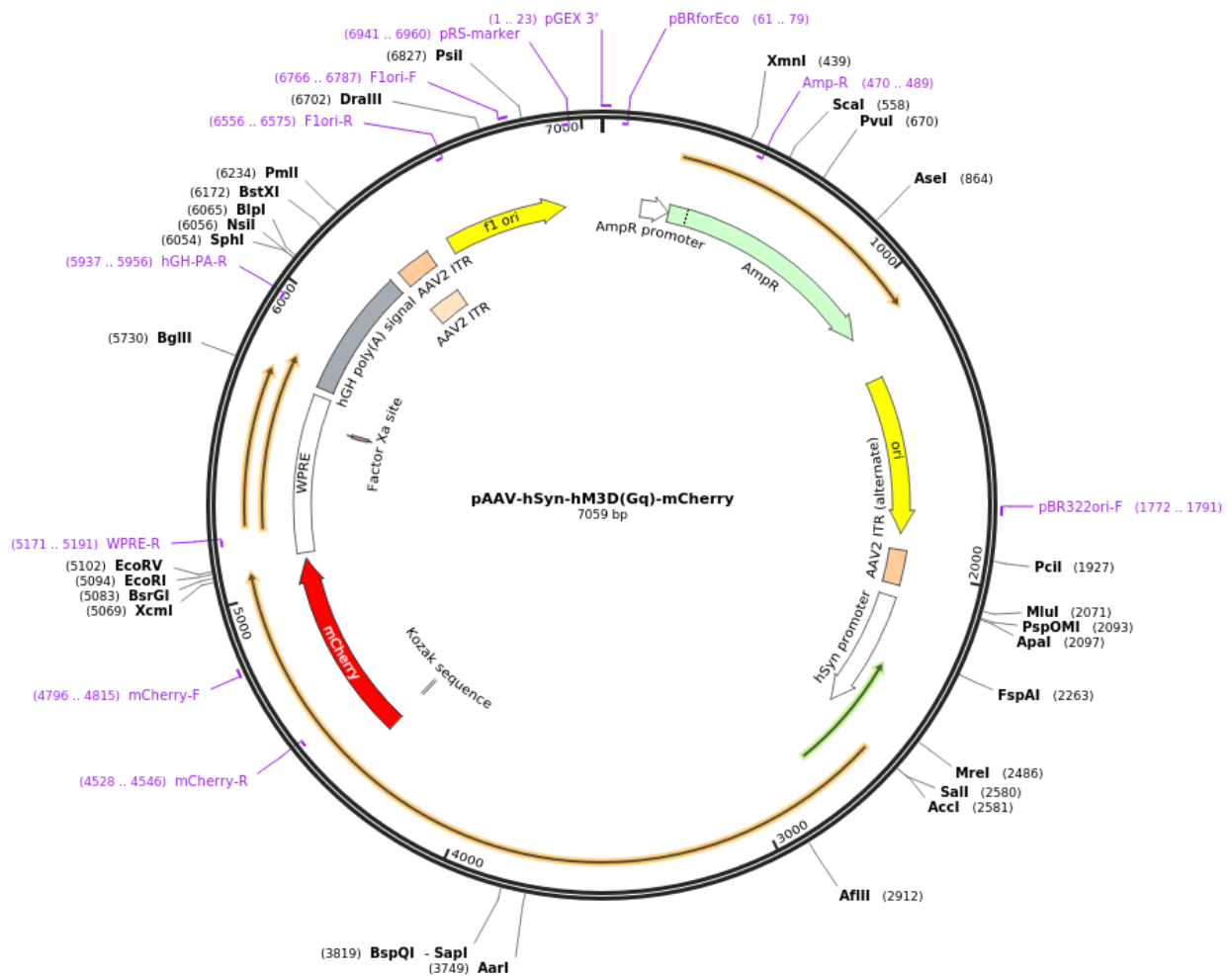
Figure 2.1. Vector map of AAV2-hM3Dq. Image shows map of AAV2-hSyn-hM3Dq-mCherry virus used for *in vivo* studies. Image from Addgene.

Intravitreal injections of viruses were administered 14 d prior to ONC. 1.5 µL of the injecting solution was injected, as described above. Different needles were used for different viruses to prevent contamination, and syringes were rinsed with ethanol followed by sterile PBS between injections.

2.8.3 | CTβ

Intravitreal injections of 1.0 µg/µL CTβ (Sigma) were administered 2 d prior to perfusion harvest. 2 µL of the solution was injected, as described above. The syringe was rinsed with ethanol followed by sterile PBS between injections.

2.9 | DORSAL COLUMN CRUSH

Dorsal column crush was performed as described previously (Cheah et al. 2016). Animals were shaved, and an incision was made above the dorsal spinal column. Vertebrae were exposed by pulling away skin and muscle and holding the tissue apart with sterile retractors. The T10 vertebral bone was removed by laminectomy. The spinal cord was exposed and the meninges carefully removed. The dorsal column was then crushed with jeweller's forceps for 10 s. The muscle and skin were sutured, and animals received a subcutaneous injection of 1 mg/kg buprenorphrine. Animals were carefully monitored for signs of infection in the days following surgery, and their mobility and bladder function were assessed daily.

2.10 | WESTERN BLOT

2.10.1 | Sample preparation

Mice were anesthetized using 1-2% isoflurane and exsanguinated, followed by cervical dislocation. Optic nerves were severed between the globe and the optic and cut into four equally sized segments of approximately 1.0-1.5 mm each. Nerve segments were immediately placed in sterile 1.5 mL Eppendorf tubes containing cold 40 µL lysis buffer (cOmplete Lysis-M, EDTA-free, Roche). Tissue was mechanically homogenized using a sterile pestle and centrifuged to separate dissolved protein from insoluble components. Protein concentration in the supernatant was determined using the BCA assay (ThermoFisher). Samples were frozen and stored at -80°C.

2.10.2 | Immunoblotting

Proteins were separated by SDS-PAGE under reducing conditions and transferred to a 0.45 µm PVDF membrane. Membranes were blocked with PBS containing 0.2% Tween-20 and 5% skim milk for 1 h at room temperature. To detect ChABC-digested CSPGs, membranes were incubated with the primary mouse monoclonal antibody BE-123 (Millipore MAB2030) diluted in an immunoenhancing reagent (Can Get Signal, Toyobo) and 5% skim milk for 2 h at 4°C, then washed and incubated with an HRP-conjugated anti-mouse IgG

secondary antibody for 30 min at room temperature. Signals were visualized with myECL^TH Imager (ThermoFisher).

2.11 | ENZYME TREATMENT OF BRAIN SECTIONS

Free-floating 30 µm sections of mouse brain were incubated with either ChABC (Sigma C3667, $\geq$ 20 µg/mL), ARSB (pH 5.5, Biomarin, 1 mg/mL), or a control buffer (50 mM Tris, 60 mM sodium acetate, and 0.02% BSA, pH 8.0) in individual wells of a 24-well plate. ChABC and ARSB were assayed to confirm activity before being added to the wells. Brain sections were incubated with enzyme and control solutions at 37°C for 8 h. To confirm that ARSB was active during the 8 h incubation period, three additional control groups were used: brain sections incubated with ARSB and 4-PNCS (1 mM), sections incubated with control buffer and 4-PNCS, and empty wells incubated with control buffer and 4-PNCS only. After the incubation, three aliquots of 70 µL were removed from each well and combined with 70 µL of 0.2 N NaOH. Absorbance was measured at 510 nm.

2.12 | IMMUNOHISTOCHEMISTRY

2.12.1 | Tissue preparation

Optic pathway tissue

Mice were anesthetized using 1-2% isoflurane and transcardially perfused with PBS followed by 4% paraformaldehyde (PFA). Optic nerves or whole optic pathway tissue were dissected, laid flat on 13 mm filter paper (Millipore AABG01300), and immersed in 4% PFA. The tissue was post-fixed overnight, then immersed in 30% sucrose for at least 24 h for cryoprotection. Tissue was embedded in Tissue-Tek OCT and snap-frozen for cryosectioning. 14 µm longitudinal sections were obtained on charged Superfrost microscope slides using a Leica CM3050 cryostat. Slides were dried and stored at -80°C.

Retinas

Whole eyes were dissected from perfused mice and placed in 4% PFA for 2 h. The solution was then replaced with 1X PBS. Whole mount retinas were prepared by removing

the cornea and lens, making four exterior cuts at half the radius of the retina, and gently peeling away the sclera to isolate the intact retina. Any vitreous body still attached to the retina was carefully removed, and the retina was placed in 1X PBS and stored at 4 °C.

Brain tissue

For analysis of perineuronal nets, fresh brain tissue was dissected from a C57Bl/6 mouse and immediately immersed in 4% PFA. Tissue was post-fixed for 24 h, cryoprotected in 30% sucrose for 24 h, embedded in Tissue-Tek OCT, and snap-frozen for sectioning.

Spinal cord

Following perfusion with 4% PFA, the spinal column was isolated and the vertebral bones removed. Intact spinal cord tissue was dissected and post-fixed in 4% PFA overnight. Tissue was cryoprotected in 30% sucrose for 24 h, embedded in Tissue-Tek OCT, and snap-frozen for sectioning.

2.12.2 | Immunostaining

Optic pathway and spinal cord

For antibodies detecting CSPGs and glial cell activation (**Table 2.3**), slides with optic nerve or spinal cord sections were incubated for 1 h in blocking solution (PBS containing 3% goat serum and 0.2% Triton X-100), then incubated overnight at 4°C in primary antibodies diluted in the blocking solution. Slides were washed three times for 5 min with PBS, incubated for 2 h with secondary antibodies, washed, and mounted onto glass coverslips with Fluoromount medium (Sigma).

The GAP-43 antibody was incubated as previously described (Leon et al. 2000). Briefly, slides were rinsed in TBS (50 mM Tris buffer containing 8.766 g/L NaCl) and then washed with methanol for 10 min. Slides were blocked in TBS containing 10% donkey serum for 1 h. The GAP-43 antibody was diluted 1:50,000 in a solution of TBS_2T (50 mM Tris buffer, 17.532 g/L NaCl, and 0.1 % Tween) containing 5% donkey serum and 2% BSA. Slides were incubated with primary antibody overnight on a rocking platform. Slides were

then washed with TBS$_2$T for 1 h, with TBS$_2$T plus 5% donkey serum and 2% BSA for 1 h, and with TBS$_2$T for 1 h, all on a rocking platform. The secondary antibody was diluted 1:1,000 in TBS$_2$T plus 5% donkey serum and 2% BSA. Slides were incubated with the secondary antibody solution for 2 h, followed by 30 min washes with TBS$_2$T, TBS$_2$T, and TBS. Slides were mounted using Fluormount and glass cover slips, and stored at 4°C for imaging.

Retina

Free-floating whole mount retinas were washed twice in 1X PBS with 0.5% TritonX-100 for 5 min. All washing steps were performed on a rocking plate at slow speed. Retinas stained with Brn3a were frozen at -80 °C for 8 min to permeabilize the plasma membrane, then thawed and washed three times with PBS/0.5% Triton for 5 min, followed by blocking with PBS, 2% BSA, 2% Trion, and 10% donkey serum for 1 h at room temperature. Retinas stained with RBPMS moved directly from the initial washing step to blocking with PBS, 2% BSA, 2% Triton, and 10% goat serum. Retinas were incubated with primary antibodies overnight at 4 °C, washed with PBS/2% Triton for 5 min, then washed three times with PBS/0.5% Triton for 30 min each. Retinas were incubated with secondary antibodies for 2 h at room temperature, washed five times with PBS for 30 min each, then mounted with the ganglion cell layer facing up on a glass superfrost slide using Fluoromount mounting medium. Slides were stored at 4 °C.

Brain

For detection of perineuronal nets, free-floating brain sections were washed with 1 mL of PBS containing 0.02% Triton-X100 three times for 30 min. Sections were incubated with 250 µL biotinylated Wisteria floribunda agglutinin (WFA) overnight at 4°C on a rocking platform. Sections were then washed with 1 mL PBS/0.02% Triton three times for 5 min, incubated with 250 µL TRITC-conjugated streptavidin for 1 h at room temperature, washed with 1 mL PBS three times for 5 min, stained with DAPI, and mounted using Fluormount and glass cover slips. Slides were stored at 4°C prior to imaging.

2.12.3 | Antibodies

Table 2.3. List of antibodies.

Primary antibodies	Dilution	Source
GAP-43 (sheep)	1:50,000	Gift of Larry Benowitz lab
GAP-43 (rabbit)	1:500	Abcam (ab7462)
CS-56 (mouse)	1:500	Sigma (C8035)
2H6 (mouse)	1:500	Amsbio (370710-IEC)
BE-123 (mouse)	1:500	EMD Millipore (MAB2030)
Iba1 (rabbit)	1:500	Wako (019-19747)
GFAP (rabbit)	1:500	Dako (Z0334)
GFAP (chicken)	1:500	Abcam (ab4674)
β-III-tubulin (mouse)	1:1,000	Sigma (T-8660)
RBPMS (rabbit)	1:500	Phosphosolutions (1830)
Brn3a (goat)	1:200	Santa Cruz (31984)
6x His tag (rabbit)	1:500	Abcam (ab137839)
Secondary antibodies		
donkey anti-sheep, Alexa Fluor 488	1:1,000	Invitrogen (A-21099)
donkey anti-sheep, Alexa Fluor 568	1:1,000	Invitrogen (A-11015)
donkey anti-goat, Alexa Fluor 568	1:1,000	Thermo Fisher (A-11057)
goat anti-rabbit, Oregon Green 488	1:1,000	Thermo Fisher (O-6381)
goat anti-rabbit, Alexa Fluor 633	1:1,000	Thermo Fisher (A-21070)
goat anti-chicken, Alexa Fluor 488	1:1,000	Thermo Fisher (A-11039)
goat anti-mouse, Alexa Fluor 568	1:1,000	Thermo Fisher (A-11004)
goat anti-mouse IgM mu chain, Dylight 650	1:500	Abcam (ab98749)
Perineuronal net detection		
biotin-conjugated Wisteria floribunda	1:500	Sigma (L1516)
agglutinin	1:1,000	Jackson (016-020-08)
TRITC-conjugated streptavidin		

2.12.4 | Microscopy and Image Processing

Tissue was imaged using a Zeiss 780 confocal microscope with 20X, 40X, and 63X objectives. Z-stacks were maximally projected onto a single plane using Zeiss image processing software. For images used in fluorescence quantification, image capture settings were held constant, and samples from within each group were imaged at the same time. Fluorescence intensity was measured using ImageJ, with identical settings for all samples within each analysis.

2.13 | QUANTIFICATION OF RGC SURVIVAL AND AXON REGENERATION

2.13.1 | RGC survival

At least eight 20X images of each whole mount retina were taken, one from the central retina of each quadrant and one from the peripheral retina of each quadrant. The number of Brn3a$^+$ or RBPMS$^+$ cells was counted manually for each image and averaged, then compared against the contralateral control retina. All imaging and cell counting was performed by an observer blinded to the experimental conditions.

2.13.2 | Axon regeneration

Axons were counted from deconvoluted confocal images (maximum intensity projections of at least 10 z-stack slices of 0.87 µm each). In ImageJ, vertical lines were drawn through each nerve section at 0.25 mm intervals starting from the lesion site, and the number of GAP-43$^+$ axons crossing each line was manually counted. Four sections were counted for each nerve. The number of regenerating axons per nerve was then calculated at each distance using a previously developed formula (Lim et al. 2016; Bei et al. 2016), with the total number of axons equal to πr^2 (r being the maximum recorded radius of the optic nerve section) times the average number of counted axons, divided by the thickness of the section (14 µm).

$$\sum axons = \frac{\pi r^2 n}{t}$$

Axon counting was verified by a separate observer blind to the experimental conditions. For quantification of longest axon, the same images were used. GAP-43$^+$ axons were identified, and the length of the longest detectable axon was measured from the lesion site using ImageJ.

2.14 | STATISTICS

Sample size for axon regeneration experiments was determined based on preliminary data from a pilot experiment. The number of regenerating axons counted at 0.50 mm distal from the lesion site was obtained from groups of mice treated with either Zymosan + ARSB (n = 4) or Zymosan + Buffer (n = 5). The control group had a mean of 104±53 axons at 0.50 mm, while the ARSB-treated group had a mean of 260±84 axons. Based on these numbers, we assumed a standard deviation of 75, to be equal for each group, and estimated using a two-sided two sample *t*-test that n = 9 mice per group would be required to achieve 80% power (at the 0.025 level) to compare ARSB treatment to a buffer control.

All statistical tests were performed using GraphPad Prism 7.0 (GraphPad Software, La Jolla, CA). Axon regeneration was assessed using two-way ANOVA and Bonferroni post-hoc analysis. Asterisks indicate significance levels as specified in the corresponding figure legends.

CHAPTER 3: TARGETING THE EXTRACELLULAR MATRIX IN THE LESIONED OPTIC NERVE

3.1 | INTRODUCTION

The visual system is a valuable model for studying mechanisms of CNS regeneration due to its accessibility: neurons in the retina are easily targeted by intravitreal injection of therapeutic agents. However, in order to modify the extracellular environment through which regenerating axons are growing, the optic nerve must be accessed directly. The optic nerve lies beneath the ophthalmic artery and external ocular muscles, and can only be accessed by delicate microsurgery. Methods of direct injection of therapeutic compounds into the optic nerve have been reported in rats (Raykova et al. 2015; D'Onofrio et al. 2011), but there appear to be no published protocols for injection into the mouse optic nerve. This represents a significant difference between the optic nerve and the spinal cord or brain, which, with stereotaxic surgery, are commonly exposed for direct injection of therapeutic agents. It is possible, however, that the environment of the mouse optic nerve can be modified by diffusion of substances through the meninges, an imperfect yet, as I show below, effective route for delivering enzymes or small molecules into the axon fibers. In this chapter, I present a detailed protocol for targeting the extracellular matrix of the mouse optic nerve by soaking sterile gelfoam scaffolds in a solution containing an active therapeutic enzyme, such as ChABC or ARSB. Following the protocol, I show data from my optimization of this technique, demonstrating that implanted enzymes retain their activity *in vivo* and successfully modify optic nerve CSPGs. Further, I share useful data regarding the protein yield of small segments of dissected optic nerve for Western blot or other quantitative analyses not specifically outlined in my protocol.

3.1.1 | Advantages of studying CNS regeneration in the visual system

Studying CNS injury and repair in the visual system has numerous advantages. The retina and optic nerve are considered part of the CNS and share many important properties with the brain and spinal cord, notably the failure of their axons to regenerate after injury. The eye itself is far more surgically accessible than the brain or spinal cord, shortening procedure times and reducing the risk of pain and complications in animal subjects. The

positioning of the ganglion cells within the vitreous-facing layer of the retina makes them receptive to substances injected into the posterior chamber of the eye, such as viruses carrying modified genes, neurotrophic factors, stem cells, and small molecules. The neuronal component of the optic nerve consists of only one cell type, the RGC, and axons extend unidirectionally over a well-defined path. RGC subtypes are well characterized, with emerging research adding to the growing library of subtype-specific genetic and morphological markers. The retina can be visualized through the transparent cornea, and repair can be assessed by dissecting retinal and optic nerve tissue and labeling surviving RGCs or regenerating axons. Because RGC soma are all located within a single retinal layer, the entire population can be examined in individual preparations, such as the retinal whole mount. The optic nerve itself can be studied histologically. Dyes are easily injected into the vitreous humor, where they have direct access to RGCs. Dyed RGCs enable the visualization of axon tracts, traveling either anterograde (injected in the vitreous humor) or retrograde (injected at the sites of synapses with visual targets in the brain). Synapse formation and stability at brain targets can be observed histologically with immunohistochemistry and electron microscopy. Additionally, a multitude of tests—ranging from electroretinography, in which a flash of light triggers responses from the entire population of retinal neurons, which can be measured with specific signals associated with unique cell populations, to behavioral measurements, such as the optokinetic reflex, direct and consensual pupil response, visual cliff, and looming response—can collectively assess incremental changes in visual function.

By utilizing the eye's physical accessibility and the diverse array of techniques for imaging and functional assessment, it is possible to evaluate changes in several domains relating to CNS regeneration. These include cell survival in the retina, the degeneration and regeneration of RGC axons in the optic nerve, and synaptogenesis and reinnervation of visual targets in the brain. While caution should be exercised in applying findings from the optic nerve to other CNS tissues, such as the brain and spinal cord, studying regeneration of RGCs in the visual system remains integral to studies of CNS regeneration as a whole.

3.1.2 | Models of optic nerve injury

Regeneration studies in the optic nerve are conducted in many species. CNS axons of non-mammals, such as fish or amphibians, regenerate spontaneously, and substantial foundational work has been performed in these systems. However, translation to human

conditions relies on studies in mammals, whose axons do not spontaneously regenerate. Rat and mouse models share several key similarities with human systems, and experiments can be performed over a relatively long time course. However, even between rodent species there exist appreciable differences in genetics and physiology. Mice are more commonly used for genetic manipulations, as myriad transgenic lines exist, with more becoming available at a steady pace, and genome maps are more detailed. Rats, on the other hand, are physically larger and therefore more amenable to the delicate surgeries required to induce optic nerve injury and subsequently to study extracted tissue. It is important to acknowledge differences between published literature examining regeneration in mice and rats, as treatments successful in one model will not necessarily translate to another, let alone to human patients.

As in human patients, experimental injuries used in studies of animal subjects can be roughly divided into acute insult and progressive degenerations. The former encompasses natural injuries such as head trauma or stroke as well as experimentally induced optic nerve crush or microcrush lesions, and the latter is best illustrated in the optic nerve by experimentally induced glaucoma. The nature of the injury profoundly affects the cellular and molecular responses, and must be selected carefully based on the objectives of the study being performed.

For glaucoma studies in particular, anatomical differences between rodents and humans must be acknowledged, including the absence of the lamina cribrosa in mice and rats and the difficulty of assessing the progression of the disease over time. While elevating IOP in animals has proven challenging, several rodent models of glaucoma have been developed, with varying degrees of success. Many rely on laser-induced occlusion of drainage pathways in the eye (Levkovitch-Verbin et al. 2002), causing aqueous build-up and elevated IOP. An advantage of laser occlusion is its thoroughness, producing reliable and well-controlled increases in IOP when performed correctly. However, it also causes inflammation around the sites of laser damage. Other techniques for blocking aqueous drainage include injecting beads or gels into the anterior chamber and directing them toward the angle. While less controlled than the laser occlusion model, these methods do not cause as much inflammation and are likely more similar to the physiological conditions in glaucoma. IOP can also be elevated by cauterizing the episcleral vein (Garcia-Valenzuela et al. 1995) or directly injecting saline into the aqueous humor pathway (Morrison et al. 1997). Additionally, a genetically inbred strain of DBA/2J mice was discovered to develop abnormally elevated IOP as the mice age, eventually mimicking the glaucomatous RGC loss seen in other models. It is crucial to

acknowledge that this wide array of injury and degeneration models will lead to differing results from therapeutic interventions to induce axon regeneration, with advantages and disadvantages inherent to each.

Other models of optic nerve injury include the induction of transient ischemia in the retina by temporarily elevating IOP (Sellés-Navarro et al. 1996) or by ligating the ophthalmic vessels to restrict the retinal blood supply (Lafuente et al. 2002). However, by far the most common method used in regeneration studies is optic nerve crush (ONC).

3.1.3 | Optic nerve crush

ONC directly injures RGC axons in the optic nerve and has been widely adopted for regeneration studies. ONC leads to the degeneration of disconnected axons and dieback to the site of the lesion, as well as the progressive death of RGCs in the retina over a relatively short timescale. While the direct clinical relevance of this type of injury is limited, its reliability and the ease of visualizing regenerating axons make ONC an attractive model for studying the effects of interventions both intrinsic (targeting RGCs in the retina) and extrinsic (modifying the extracellular environment of the optic nerve). Despite its ubiquity, the ONC model remains a topic of debate, in large part due the difficulty of distinguishing spared from regenerating axons (Fischer et al. 2017). Small differences in experimental technique—such as the type of forceps used, duration of crush, the distance of the lesion behind the eye, and so on—can yield important differences in effect. This has contributed to controversy around studies in which significant regeneration is observed (Pernet & Schwab 2014).

In this chapter, I describe the intravitreal injection of an adeno-associated virus (AAV) targeting RGCs in the mouse retina. AAV serotype 2 (AAV2) reliably infects RGCs (Buch et al. 2008), and its efficiency is easily measured by extracting treated, uninjured retinas and comparing fluorescently tagged proteins synthesized by the genes carried in the virus with immunostaining for RGC markers such as RBPMS (Kwong et al. 2010). Typically, genes delivered by AAV2 are fully expressed within 2 weeks after injection (Buch et al. 2008). At this time, RGC axons are injured with optic nerve crush, which requires a straightforward surgery wherein curved forceps are inserted behind the eye and the optic nerve is compressed or "crushed" at a distance of 1 mm. The extracellular environment at the lesion is then targeted by implanting a sterile gelfoam scaffold carrying a therapeutic enzyme

in direct contact with the optic nerve. Two days before tissue collection, the retrograde axon tracer choleratoxin β (CTβ) is injected intravitreally to visualize regenerating axons. At the 2-week post crush time point, the retinas and optic nerves are dissected. I describe a technique whereby the optic pathway, including the optic nerve head, optic chiasm, and proximal portion of the optic tract, can be dissected whole and intact for analysis of axons regenerating over long distances. Given the recent improvements in stimulating high levels of RGC axon growth, this strategy is critical for assessing the navigation of regenerating axons, particularly their ability to cross properly at the optic chiasm, a site where many axons make aberrant projections and fail to follow the paths defined during visual system development (Pernet & Schwab 2014; Pernet et al. 2013; Luo et al. 2013). I describe in detail methods for visualizing and quantifying the number of surviving RGCs in the retina and the number of regenerating axons in the optic nerve. My methods synthesize commonly used strategies that have been adapted by multiple established laboratories but, to my knowledge, not yet collected into a comprehensive step-by-step guide. This protocol details the basic components of experimental injury and basic treatments, but it can be flexibly adapted for myriad interventions and experiment designs. The total time required for one cohort of mice is less than 5 weeks, and the techniques can be easily learned and integrated into any laboratory setup or surgical facility.

3.2 | MATERIALS

REAGENTS

I have listed the reagents and equipment used in our laboratory, but similar commercially available alternatives can be easily substituted as appropriate.

ANIMALS

- Adult female C57Bl/6J mice (6-8 weeks old). Animal use should abide by the relevant authorities' guidelines, and appropriate approval from the institutional animal use committee must be obtained. Controls for sex and age are essential. Use animals of identical sex and age.

GENERAL REAGENTS

- Tetracaine hydrochloride eye drops (0.5% (wt/vol); Bausch & Lomb, cat. no. 24208-920-64)
- Tropicamide eye drops (1.0%, Sandoz, cat. no. 61314-355-02)
- Ketamine hydrochloride (10 ml of 100 mg/mL solution for injection; Pfizer)
- Xylazine (Rompun) (2% (wt/vol) injectable solution; Bayer, cat. no. 816474)
- Buprenorphine SR (Zoopharm)
- Lacri-Lube eye ointment (2.5 g; Allergan, cat. no. 5089GB)
- Euthatal injectable solution (200 mg/mL; Rhone-Merieux, cat. no. 838093)
- Phosphate buffered saline (10%; 1 L; Crystalgen, cat. no. 221-133-10)
- Viruses
- Cholera Toxin Subunit B (Recombinant), Alexa Fluor 555 conjugate (Thermo Fischer Scientific, cat. no. C34776)
- Paraformaldehyde (20%, Electron Microscopy Sciences, cat. no. 15713-S)
- Ethanol (Sigma-Aldrich, cat. no. 459836)
- Tissue-Tek O.C.T. compound (Thermo Fisher Scientific, cat. no. 23-730-571)
- Sodium azide (Sigma-Aldrich, cat. no. S2002)
- Anti-RBPMS (rabbit IgG, Phosphosolutions, cat. no. 1830-RBPMS)
- Anti-rabbit IgG, Oregon Green conjugate (goat, Molecular Probes cat. no. O-6381)
- Normal goat serum (Thermo Fischer Scientific, cat. no. 16210072)
- Triton X-100 (Sigma-Aldrich, cat. no. X100)
- Sucrose (MP Biomedicals, cat. no. 152584)
- Distilled water
- Ice

EQUIPMENT

- Sterile operating bench
- Operating microscope (Zeiss OPMI CS-1 Varioskop)
- Dumont #5 straight forceps, Titanium straight tip (FST, cat. no. 11252-40)
- Dumont #5/45 curved forceps, Dumoxel standard tip (FST, cat. no. 11251-35)
- Vannas spring scissors, 2.5 mm blade, straight tip (FST, cat. no. 15000-08)
- PVA foam surgical spears, sterile (Network Medical Products, cat. no. 40-415-USA)

- Cover glasses, circular, 12 mm (Carolina, cat. no. 633029)

- 5 µL syringe, Model 65 (Hamilton, cat. no. 7633-01)

- 33-gauge removable needles, 0.375 in, point style = 2 (Hamilton, cat. no. 7803-05)

- 30-gauge Monoject needle, sterile (Thermo Fisher Scientific, cat. no. 22-557-172)

- Gelfoam (Pfizer, cat. no. 031508)

- Dissecting microscope (Nikon, cat. no. SMZ645)

- High intensity halogen illuminator (Chiu Technical Corporation, cat. no. F0-150)

- Operating scissors (Roboz, cat. no. RS-6751)

- Moloney curved forceps (Roboz, cat. no. RS-8254)

- Adson dressing forceps, 4.75 in. (V. Mueller, cat. no. NL1410)

- Extra narrow scissors, 23 mm edge, straight tip (FST, cat. no. 14088-10)

- Dumont #5 straight forceps, Titanium straight tip (FST, cat. no. 11252-40)

- Vannas spring scissors, 2.5 mm blade, straight tip (FST 15000-08)

- Small weigh boats (Heathrow Scientific, cat. no. 1420A)

- 20 µL pipette (Rainin, cat. no. 17014392)

- 20 µL pipette tips (Denville Scientific, cat. no. P1121)

- 24 well flat bottom polystyrene plate, sterile (Corning Incorporated, cat. no. 3524)

- 48 well flat bottom polystyrene plate, sterile (Corning Incorporated, cat. no. 3548)

- Mixed cellulose esters membrane, 0.80 µm pore size (EMD Millipore, cat. no. AABG01300)

- Liquid transfer pipettes (Samco, cat. no. #204)

- Cryostat (Leica Biosystems, cat. no. CM3050)

- Charged microscope slides (Globe Scientific, cat. no. 1354W)

- Cover glass (24 x 60 mm^2; Thermo Fisher Scientific, cat. no. 12-553-465)

- Fluoromount aqueous mounting medium (Sigma-Aldrich, cat. no. F4680)

- Confocal microscope (Zeiss, model no. LSM 780, inverted)

- Image analysis software (ImageJ, developed by Wayne Rasband, National Institutes of Health; http://rsb.info.nih.gov/ij/index.html)

REAGENT SETUP

PBS (1×) To make 0.1 M PBS, dilute 100 mL of 10× stock solution with 900 mL of distilled water. Make fresh on the day of the experiment.

PFA (4%)-PBS solution (0.1 M) (wt/vol, 1 L) To make 4% PFA, dilute 20 mL 20% PFA stock solution with 80 mL 1× PBS. Make sufficient volume for roughly 10 mL PFA per mouse. Note that PFA is highly toxic. Prepare in a fume hood.

EQUIPMENT SETUP

Preparation of operating microscope Turn on the operating microscope and arrange all surgical instruments on a sterile drape. All surgical procedures should be performed under sterile conditions using instruments treated by heat or gas sterilization and immersed in a bead sterilizer between animal subjects.

Microscope settings for image acquisition Our images are acquired using a Zeiss confocal microscope, but any similar microscope can be used with optimized settings. To acquire images of CTβ$^+$ regenerating axons in optic nerve sections, we used laser power of 5.0 and gain of 800. To acquire images of RBPMS$^+$ RGCs in retinal flatmounts, we used laser power of 8.0 and gain of 800.

3.3 | PROCEDURE

Intravitreal injection of virus (2 h)

1| Anesthetize 2-3 mice at a time by administering an intraperitoneal (i.p.) injection of ketamine (10 mg/kg) and xylazine (100 mg/kg) mixture. Confirm the depth of anesthetic with a paw pinch. Mice should be unresponsive with no withdrawal reflex, but maintain regular, unlabored breathing. All procedures involving animals should follow the relevant institutional regulatory board guidelines and regulations.

2| Place the mouse on a heating pad under the operating microscope and fix the head using a stereotaxic bite bar. Apply one drop of 0.5% tetracaine to the left eye for numbing, followed by 1 drop of 1.0% tropicamide to dilate the pupil. Wait ~60 seconds for the drops to take effect.

3| Draw 1 uL of AAV2 virus (stored on ice) into the Hamilton syringe. Grasp the conjunctiva at the limbus with forceps to steady the globe. Inject the solution through the superior nasal sclera at a 45° angle, avoiding the lens, external ocular muscle, and blood

vessels. The needle should be visible through the dilated pupil and its position can be monitored visually.

4| To relieve intraocular pressure and prevent backflow of the injected solution, puncture the anterior chamber with a sterile 30-gauge needle to drain the aqueous humor. After a few seconds, withdraw the syringe and rinse the injected eye with a few drops of sterile saline solution. Apply lubricating ointment (e.g., LacriLube) to both eyes.

5| Inject 1.0 mg/kg buprenorphine SR (e.g. 0.02 mL for a 20 g mouse) subcutaneously and place the mouse in a heated chamber with supplemental oxygen flow until it recovers from anesthesia and becomes mobile. Upon full recovery and resumption of normal exploratory behavior, typically 60-90 min., return the mouse to its cage. Rinse the syringe with ethanol followed by sterile PBS between injections. If different viruses are being used, it is advisable to switch needles as well.

6| Repeat steps #2-5 for each subsequent mouse. When surgeries are completed, clean and sterilize all instruments and return the mice to their housing facility. Monitor mice for signs of ocular inflammation over the following days, treating the cornea with lubricating ointment if it appears dry or irritated.

Optic nerve crush and implantation of gelfoam scaffold (4 h)

7| AAV2 takes ~2 weeks to achieve robust expression of the delivered gene in retinal neurons. On day 14 after the virus injection, anesthetize 2-3 mice at a time, as above.

8| Use a hemostat to clamp the skin above the upper eyelid, drawing it back to expose the globe. Prolapse the globe so it protrudes slightly. Ensure the sclera remains moist throughout the procedure. Apply sterile saline with a sterile cotton swab as needed. Drying of the eye can lead to cornea damage.

9| Make small incision in conjunctiva, moving from inferior-temporal to superior-temporal in an arc of about 45°. With micro-forceps, grasp the conjunctiva near the limbus and rotate the globe nasally to expose its posterior aspect. With the forceps tips closed to avoid puncturing the sclera, slide the curved forceps through the open incision in the conjunctiva and underneath the external ocular muscle. Carefully open the forceps to reveal the optic nerve, grasp the nerve 1 mm from the globe, and clamp down firmly for 10 seconds. It is essential to avoid puncturing the ophthalmic artery or damaging the external ocular muscle. If the artery bursts and severe bleeding occurs, surgery should be abandoned and the mouse should be euthanized and removed from the study. Mice should be monitored in the days following surgery to ensure no bleeding has occurred.

Mydriasis should be observed upon crush. Rinse a small circular cover glass with sterile PBS and hold it against the globe to flatten the cornea and visualize the fundus. Ensure that the retinal blood flow is undisturbed; retinal arteries should be visibly perfused. Ischemia caused by bleeding of retinal or ophthalmic blood vessels can compromise retinal neurons.

10| With curved forceps, remove the gelfoam scaffold from its sterile tube (stored on ice). Carefully insert the scaffold through the open incision in the conjunctiva until it is in contact with the lesioned optic nerve, approximately 1 mm behind the globe. Carefully remove the forceps and rotate the globe back into place. Apply lubricating ointment (e.g., LacriLube) to both eyes.

11| Inject 0.02 mL buprenorphine SR subcutaneously and place the mouse in a heated chamber with supplemental oxygen flow until it recovers from anesthesia and becomes mobile. Upon full recovery and resumption of normal exploratory behavior, typically 60-90 min., return the mouse to its cage. Rinse the syringe with ethanol followed by sterile PBS between injections. If different viruses are being used, it is advisable to switch needles as well.

12| Repeat steps #8-10 for each subsequent mouse. When surgeries are completed, clean and sterilize all instruments and return the mice to their housing facility. Monitor mice for signs of ocular inflammation or bleeding over the following days, treating the cornea with lubricating ointment if it appears dry or irritated.

Intravitreal injection of axon tracer (2 h)

13| On day 12 after optic nerve crush (2 days prior to tissue collection), anesthetize 2-3 mice at a time, as above.

14| Draw 1 µL of CTβ (stored on ice) into the Hamilton syringe. Grasp the limbus with forceps to steady the globe. Inject the solution through the superior nasal sclera at a 45° angle, avoiding the lens, external ocular muscle, and blood vessels. Puncture the anterior chamber with a sterile 30-gauge needle. Withdraw the syringe and rinse the eye with a few drops of saline. Apply ophthalmic ointment and recover animals as above.

Tissue collection (8 h)

15| *Transcardial perfusion.* On day 14 after optic nerve crush, administer a fatal dose of euthatal (sodium pentobarbitone; 1.5 mL per mouse, i.p.) and ensure the mouse is fully anesthetized by confirming lack of withdrawal reflex. Using operating scissors, open the

chest cavity, make two cuts on either side of the cavity to retract the ribs, and open the diaphragm to expose the heart. Pierce the left ventricle with a needle attached to an elevated PBS drip, and clamp the cardiac tissue around the needle with a hemostat to keep the needle in place. Make a small cut in the right atrium to open the circulation.

16| Perfuse the mouse with PBS (0.1 M, pH 7.4) for ~5 min or until the circulation is completely flushed and the fluid flowing from the right ventricle is clear.

17| Perfuse the mouse with 4% PFA in 0.1 M PBS for ~5 min. PFA is toxic. Perform perfusions in a fume hood and wear personal protective equipment, including gloves, goggles, and a face mask.

18| *Optic nerve dissection.* Isolate the head with large operating scissors. With small narrow scissors, make an incision in the skin, moving caudal-to-rostral from the base of the skull to the nose. Make a similar cut in the skull bone, followed by two lateral cuts from the base of the skull to just above the orbit on each side. With forceps, peel the bone forward to remove it, exposing the brain.

19| Cut the olfactory bulbs and lift the brain to expose the optic nerves and chiasm. With Vannas spring scissors, carefully cut the optic tract, leaving the optic chiasm intact. Remove and discard the brain.

20| Remove the orbital bone behind the globe, taking care not to disturb the optic nerve. With Vannas spring scissors, carefully remove the meninges from the optic nerve, cutting from the optic chiasm entry point to the optic nerve head. Separate the optic nerve from the globe. Repeat for both optic nerves, then carefully remove the intact optic pathway and lay it flat on a piece of filter paper. Transfer the filter paper to a labeled 24 well plate containing 1 mL of 4% PFA. Post-fix the nerves overnight at 4 °C. The optic nerve is extremely delicate, particularly at the lesion site. Any strain on the nerve may deform or disconnect the tissue. It is also essential to lay the nerve flat on the filter paper, as bending or twisting of the nerve may disrupt the ultrastructure of the axons.

21| *Globe dissection.* Isolate the globe away from the orbital cavity with a curved ophthalmic scissor. The globe can be more easily exposed by removing the eyelids. Transfer the intact globe to a labeled 48 well plate containing 1 mL of 4% PFA. Post-fix the globe for 60 min at room temperature.

22| *Retinal flatmount preparation.* Place the post-fixed globe in a small weigh boat filled with PBS. Use microscissors to make an incision at the limbus, then cut along the limbus to remove the cornea. Remove the lens and iris, taking care to prevent retinal detachment, as the lens may be connected to the retina via the vitreous body. While

grasping the sclera to stabilize it, insert closed forceps between the sclera and retina and gently nudge the retina free of the sclera. When the retina is fully detached from the limbus, pinch the optic disc with forceps to sever connecting axons. Carefully remove any strands of vitreous body still attached to the retina. Make four exterior cuts, roughly half the radius of the retina, dividing the retina into equal quadrants to create a "clover leaf" shape. Using a liquid transfer pipette, transfer the retina to a 48 well plate. Store in 0.05% sodium azide for up to 4 weeks prior to immunostaining.

Optic nerve processing (3 d)

23| After optic nerves have been post-fixed for 24 h in 4% PFA, replace the solution with 30% sucrose for cryoprotection.

24| Immediately before sectioning, immerse optic nerves in OCT compound for at least 5 min. Taking care not to touch the lesion site or damage the nerve, transfer the nerve to the surface of a glass SuperFrost slide, and place the slide on dry ice to snap-freeze the tissue, ensuring the nerve lies perfectly flat and straight. As the OCT begins to freeze, carefully add a small dollop of OCT on top of the nerve, avoiding the creation of any air bubbles.

25| Freeze OCT in a cubic embedding mold to create a uniform block with no air bubbles. Mount the block of OCT in the cryostat and arrange the cryostat blade such that the OCT block sectioned easily. Cut the block down to create a flat surface, then remove the detachable mounting stub with the block affixed. Mark the orientation of the block to ensure the cutting angle of the blade remains unchanged upon re-mounting. Cryostat blades are sharp and should be handled with care.

26| Using a razor blade, carefully detach the embedded optic nerve embedded from the glass slide, checking that the tissue is visible in the flat surface of the frozen OCT with no bubbles, chips or breaks. Place a dollop of OCT on the flat surface of the mounted block and quickly adhere the flat surface containing the embedded nerve directly to the block, ensuring that the nerve is flush and positioned along the vertical axis. After this "sandwich" has solidified, re-mount the stub in the cryostat.

Section the optic nerve at 14 um thickness onto glass superfrost slides. A flat nerve of roughly 300 um thickness should produce around 20 sections, which can be distributed across multiple slides. Dry the slides, wash at least three times with PBS, add 2-3 drops of mounting medium, and carefully lay cover glass over the slides, avoiding bubbles.

Store slides at 4 °C until they are ready for imaging. Slides can also be stored below -20 °C and immunostained prior to mounting and imaging.

Retinal flatmount processing (3 d)

27| Remove sodium azide solution and wash three times with 1 mL 0.5% Triton X-100 in PBS (PBST) at room temperature. The 48-well plate containing the floating retinas should be placed on a rocker at a slow speed for all washing and incubation steps. When removing solutions, take care to pipette from the corner of the well so as not to suck up or damage the delicate retinal tissue.

28| Add 500 µL blocking buffer (PBS, 2% BSA, 2% Triton, 10% NGS). Incubate for 1 h.

29| Add 350 µL primary antibody (rabbit anti-RBPMS, diluted 1:500 in blocking buffer). Incubate overnight at 4 °C.

30| Wash three times with PBST for 30 min each at room temperature.

31| Add 350 µL secondary antibody (Oregon green-conjugated goat anti-rabbit IgG, diluted 1:1,000 in PBST). Incubate for 2 h at room temperature. Wrap the 48 well plate with aluminum foil to prevent photobleaching of fluorophores.

32| Wash three times with PBS for 30 min each at room temperature. If desired, DAPI may be added (diluted 1:10,000 in PBS) in the second wash.

33| Using a fine paint brush, transfer the retina to a glass SuperFrost slide. Ensure the ganglion cell layer is facing up, and use the paint brush to remove any wrinkles. Use a dry wipe to remove excess PBS before adding mounting medium to the slide and carefully applying a glass cover slip. Handling retinal tissue with the paint brush may damage cells. Take care not to disrupt the ganglion cell layer.

34| Keep mounted slides in a dark container at 4 °C to preserve fluorescent signal until they are ready for imaging.

Image capture (12 h)

35| *Optic nerve imaging*. Use a Zeiss 780 confocal microscope with Zeiss imaging software. Using the 40× objective with immersion oil and the red channel, identify the optic nerve crush lesion site by locating the area of high density CTB-labeled axons. Perform a bounded grid tile scan by positioning the imaging field at the top and bottom of the lesion, store these positions, and then move to the distal end of the optic nerve and store the positions where the optic tracts exit the optic chiasm. Capture a tiled, z-stacked image (using a step size of < 1 µm) that contains the entire optic nerve and chiasm.

Repeat this step for each section to be imaged, at least four sections per mouse. It is straightforward to substitute alternative models of confocal microscopes and corresponding software without altering the protocol. All image capture and analysis should be performed by an experimenter blinded to the experimental groups and conditions.

36| *Retinal flatmount imaging*. Use the Zeiss 780 confocal microscope with Zeiss imaging software (a standard epifluorescence microscope is also acceptable). Focus on the ganglion cell layer, which will contain green RBPMS$^+$ and red CTB$^+$ RGCs. Using the 20× objective, capture three 500 μm × 500 μm regions of the retina from each quadrant: one from the central retina, one from the middle retina, and one from the peripheral retina. Each retina should yield 12 images.

Image analysis (4 h)

37| *Optic nerve image analysis.* Use ImageJ software to open each of the tiled, z-stacked images. In the Image menu, select Stacks, followed by Z Project to create a maximum intensity projection of the z-stack. Using the line tool, draw a horizontal line of 0.25 mm length extending distally from the lesion site. The lesion site can be identified by the bright line of severed axons. In samples with robust regeneration, it is useful to examine the DAPI channel to identify the lesion site, which contains substantially higher cellularity. Using the line tool, measure the radius of the optic nerve at the 0.25 mm point and record this number. Draw a vertical line at the 0.25 mm point, and use the microscope tool to zoom in so that CTB$^+$ axons are easily visible. Count the total number of CTB$^+$ axons transecting the vertical line and record this number. Repeat this step for successive distances in increments of 0.25 mm, proceeding from the lesion site to the optic chiasm (typically about 4-5 mm total, assuming a lesion located 1.0 mm from the eye). Count at least four sections from each optic nerve. When measuring distances in μm from saved images, it is essential to confirm that the metadata accurately converts pixels to μm. This can be done by opening the 'Image' menu and selecting 'Properties.'

38| *Retinal flatmount image analysis*. Use ImageJ software to open each of the 500 μm × 500 μm captured images. In the Image menu, select 'Channels tool' and convert to grayscale, then select 'Split channels' to isolate the green RBPMS channel. In the Image menu, select Adjust, then Threshold to apply a threshold to eliminate background noise. The threshold will be dependent on the brightness settings used during image acquisition, but as a general rule, the round, brightly stained RBPMS$^+$/CTB$^+$ RGCs

should be preserved while any faded RBPMS^{+}/CTB^{-} cells should be excluded. Select the multi-point tool and mark each cell in the image. Record the total number of cells per image.

Calculations (1 h)

39| *RGC axon regeneration*. The total number of regenerating CTB^{+} axons per nerve at each distance increment is calculated using a formula defined previously (Lim et al. 2016; Bei et al. 2016):

$$\sum axons = \frac{\pi r^2 n}{t}$$

Where r = the maximum measured radius of the optic nerve at the defined distance increment, in µm, n = the number of transecting axons, t = the thickness of the section, in µm, which in this protocol equals 14 µm.

40| *RGC survival*. Eight 20× images of each whole mount retina are acquired, one from the central retina of each quadrant and one from the peripheral retina of each quadrant. The total number of surviving RBPMS^{+} RGCs is calculated by using the average total number of counted RGCs per image to define the mean RGC density (cells/mm^2) in each sample. The total area of the retinal sample is obtained by acquiring a tiled image of the whole retina, defining the boundary in ImageJ, and measuring the area of the bounded region. Multiplying the mean RGC density by the total area of the retina yields the total number of surviving RBPMS^{+} cells. To determine percent survival, this value is compared with the number of RBPMS^{+} cells calculated in the non-lesioned contralateral control retina. All cell counting should be performed by an observer blinded to the experimental conditions.

TIMING

The timing information below corresponds to an experiment in which 18 animals are used:

Steps 1-6, intravitreal injection of virus: 2 h

Steps 7-12, optic nerve crush and implantation of gelfoam scaffold: 4 h

Steps 13-14, intravitreal injection of axon tracer: 2 h

Steps 15-22, tissue collection: 8 h

Steps 23-26, optic nerve processing: 3 d

Steps 27-34, retinal flatmount processing: 3 d

Steps 35-36, image capture: 12 h

Steps 37-38, image analysis: 4 h

Steps 39-40, calculations: 1 h

3.4 | TROUBLESHOOTING

Troubleshooting advice can be found in **Table 3.1**.

Table 3.1 | Troubleshooting table.

Step	Problem	Possible reason	Solution
1, 7, 13	Animals continue to exhibit withdrawal reflex.	Anesthetic dose is insufficient.	Wait at least 15 min, then administer an additional injection of ketamine (10 mg/kg). If the mouse still does not display proper depth of anesthesia, remove the subject from the study.
9	Bleeding occurs due to damage of the ophthalmic artery.	Surgical error.	Immediately euthanize the mouse and note the removal of the subject from the study.
26	Sections do not contain whole, intact optic pathway.	Tissue was deformed during the fixation or embedding step, or mounted at an angle.	Adjust the angle of the cryostat. If the optic pathway is not in a flat plane, section as much of the tissue as possible and evaluate sections during image acquisition. Images where the lesion site is not detectable should be discarded.
40	Survival of RGCs in lesioned, untreated control eyes does not match published data.	Surgical inconsistencies.	Perform a pilot experiment with lesioned, untreated controls and assess RGC survival at several time points. Ensure that the RGC death profile matches previously published time course to confirm that surgical technique is adequate.

3.5 | RESULTS

3.5.1 | Anticipated results from a generalized experiment

RGC axons undergo Wallerian degeneration immediately following ONC, and the cell bodies in the retina start dying within 5 to 6 days in the absence of treatment (Fischer &

Leibinger 2012). By 14 days, roughly 90% of RGCs have become unviable, and are therefore unable to contribute to the regeneration of axonal tracts (Fischer & Leibinger 2012). Intravitreal injection of AAV2 typically infects 80-90% of RGCs, with some off-target infection of Muller glia and other retinal neurons (Buch et al. 2008). In our laboratory, we have found that the enhancement of cell survival correlates with the quality of the injection, as reflux of injected virus can lead to lower infection efficiency. The RBPMS antibody reliably labels 94-97% of RGCs and does not label other retinal neurons (Kwong et al. 2010). This means that efficiency of injected AAV2 with a gene for a fluorescently tagged protein such as GFP can be easily quantified by co-labeling with RBPMS and calculating the number of GFP$^+$/RBPMS$^+$ cells in retinal flatmounts. Furthermore, cells that survive after injury can be identified as GFP$^+$ or GFP$^-$. Regenerating axons are easily visualized with CTβ, although care should be taken when analyzing tissue sections, as axons spared by an incomplete ONC will also be CTβ$^+$. Another advantage of CTβ is that it enables 3D visualization of regenerating axons via whole mounting and tissue clearing of nerve tissue, followed by confocal or light sheet fluorescence microscopy (Luo et al. 2013). Optic nerve sections should be examined for signs of spared axons, including uncharacteristically straight paths and groups of axons near the periphery of the nerve traveling long distances (**Figure 3.1**) (Fischer et al. 2017).
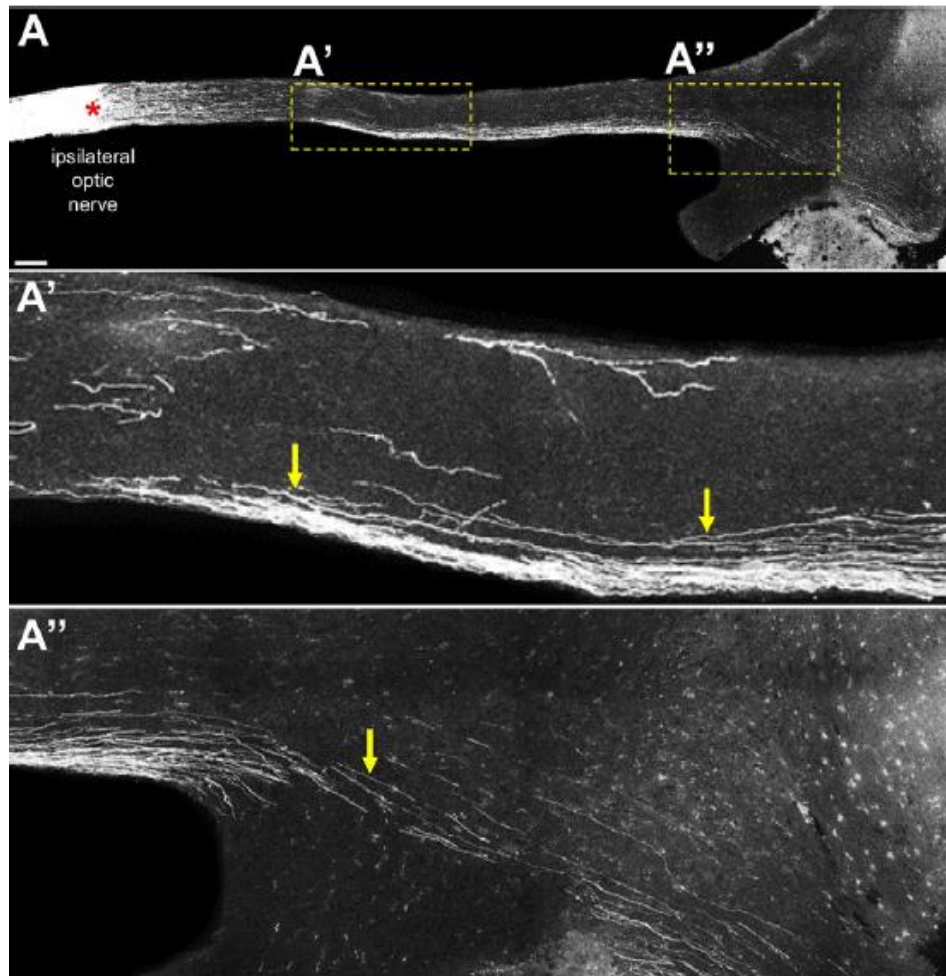
Figure 3.1. Identifying spared vs. regenerating axons. (a) Micrograph showing incomplete crush of a mouse optic nerve results in the presence of spared axons that are visualized by CTβ injected 3 weeks following the surgery. (a') Inset showing spared axons that appear uncharacteristically linear, often grouped near the periphery of the optic nerve. (a'') Inset showing spared axons traversing the optic chiasm into the contralateral optic tract, again with uncharacteristically linear morphology and close grouping. Asterisk indicates lesion site. Scale bar = 200 μm. Figure adapted from (Fischer et al. 2017).

Many pro-regenerative therapies are additive, meaning that their enhancement of axon regeneration is greater when delivered together than separately. This creates a necessity for rigorous control groups where individual components of a therapy are tested in isolation, to determine whether they are additive or redundant, and to what degree. Different treatments can also stimulate regeneration from different RGC subtypes, as was recently demonstrated (Norsworthy et al. 2017). It may be useful for future experiments to utilize transgenic mouse lines with labeled RGC subtypes to determine whether treatments preferentially enhance regeneration from specific subtypes. Optic nerve sections may also be probed with antibodies against specific cell markers and proteins, enabling studies of the interactions between regenerating axons and non-neuronal cells or extracellular matrix in the optic nerve. My

101

protocol describes the basic steps of an ONC experiment, but adaptations and additions such as these permit a wide range of flexibility for analysis of different mechanisms and outcomes. I have detailed an experiment using adult C57/Bl6 mice. It is known that the regenerative capacity of RGCs declines with age (Goldberg, Klassen, et al. 2002), and so the numbers given here do not reflect those likely to be found in much younger or older animals. Given the fact that many degenerative CNS conditions occur more frequently in older populations of patients, future studies may wish to examine more carefully the effects of age on RGC survival and axon regeneration, and the receptiveness to treatments such as those described here.

3.5.2 | Enzymatic modification of the extracellular matrix in the mouse optic nerve

To demonstrate the efficacy of applying CSPG-targeting enzymes directly to the optic nerve, I first assayed their activity over time *in vitro* and *in vivo*, and then measured the functional digestion of GAG chains by ChABC in optic nerve tissue. ChABC cleaves GAG chains at the linkage sites between disaccharides, releasing them from the proteoglycan core protein (**Figure 3.2a**). These disaccharide products possess an absorbance peak at 232 nm. Therefore, the activity of ChABC can be reliably measured by introducing a small volume of ChABC into a solution containing purified CSPG substrate, and then quantifying the change in absorbance at 232 nm. ARSB activity can be measured by introducing the enzyme to a solution containing 4-nitrocatechol sulfate, a 4-sulfated substrate whose absorbance peak shifts from yellow to red (510 nm) when the 4S group is removed (Roy 1987) (**Figure 3.3b**). I incubated ARSB and ChABC at physiological temperature (37 °C) for 4 d and found that while ARSB activity remains stable, ChABC loses as much as 50% of its activity within 4 d (**Figure 3.2c**).
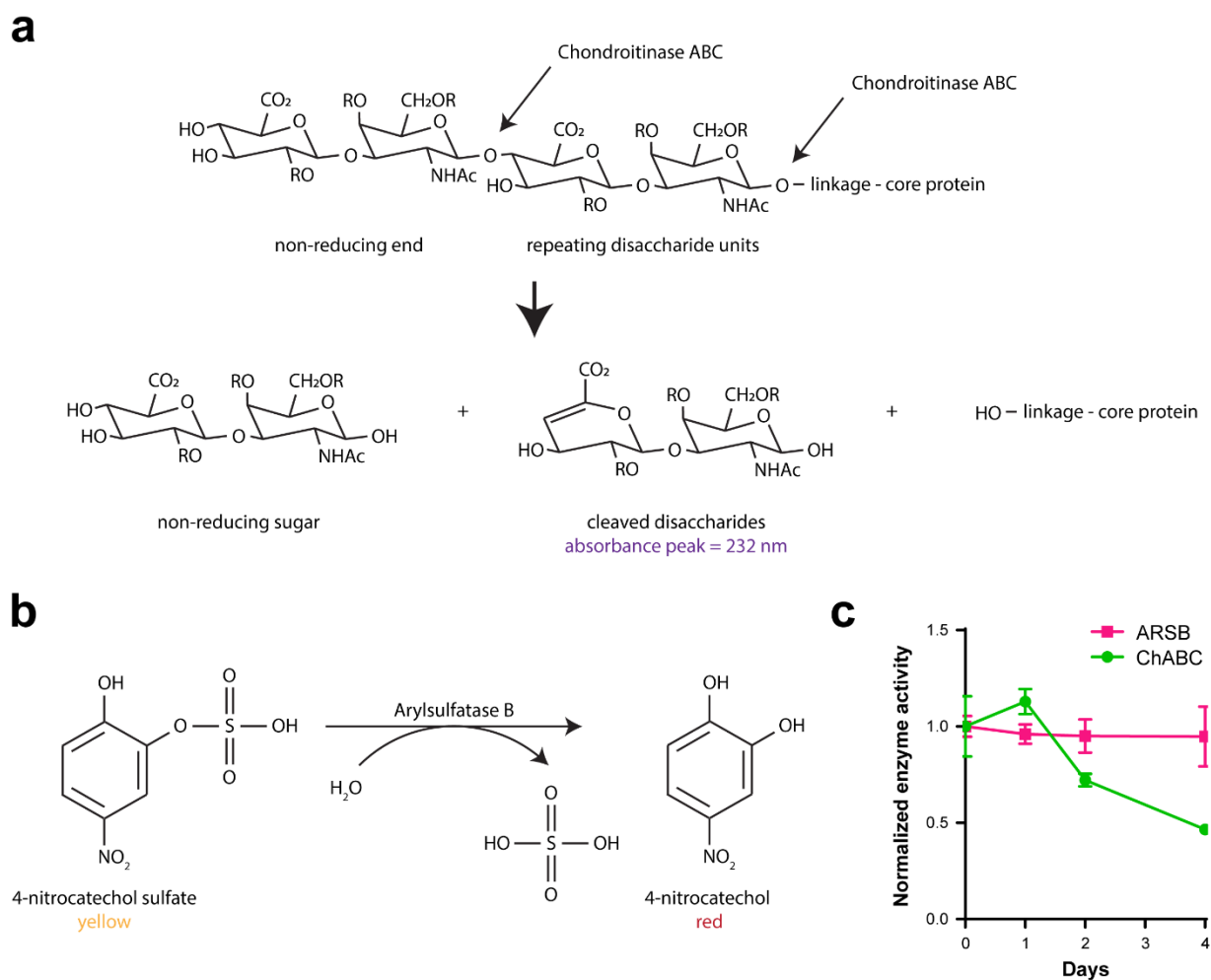
Figure 3.2. Maintenance of ChABC and ARSB activity *in vitro*. (a) Schematic diagram showing chondroitinase ABC digestion of the glycosaminoglycan chain and the reaction products. (b) Schematic diagram showing arylsulfatase B digestion of 4-nitrocatechol sulfate and the reaction products. (c) Graph showing changes in assayed activity of ChABC and ARSB after incubation at 37 °C.

I then evaluated the activity of ARSB and ChABC *in vivo*. Gelfoam scaffolds soaked with ARSB, ChABC, or a control buffer were implanted in direct contact with non-lesioned mouse optic nerves (**Figure 3.3a**). Mice were sacrificed at 1, 2, and 4 d post implantation (dpi), gelfoam scaffolds were recovered, and their contents were assayed for ARSB or ChABC activity. Activity detected from recovered scaffolds was then normalized against fresh stock solutions of the two enzymes. At 1 dpi, solutions from ARSB-loaded scaffolds showed significantly ($p < 0.05$) higher ARSB activity than buffer-loaded scaffolds (**Figure 3.3b**). The ChABC-loaded scaffolds showed no measurable difference in recovered ChABC activity at any time point when compared with buffer-loaded scaffolds (**Figure 3.3b**). Next, the ability of implanted enzymes to modify CSPGs within the optic nerve was tested. Because changes in terminal sulfation of GAG chains can only be detected by highly sensitive methods such as mass spectrometry, I relied on ChABC, whose digestion products are easily detected by immunohistochemistry, as representative of both enzymes. ChABC-loaded scaffolds were implanted in lesioned mouse optic nerves at 3 dpc, then recovered at 5 dpc (**Figure 3.3c**). Immunoreactivity of CS-56, which detects intact CSPGs, was significantly ($p < 0.05$) decreased in ChABC-treated samples when compared with buffer-treated samples (**Figure 3.3d-e**). Correspondingly, immunoreactivity of BE-123, which detects "stub" proteins stripped of their GAG chains, was significantly ($p < 0.05$) increased in ChABC-treated samples.
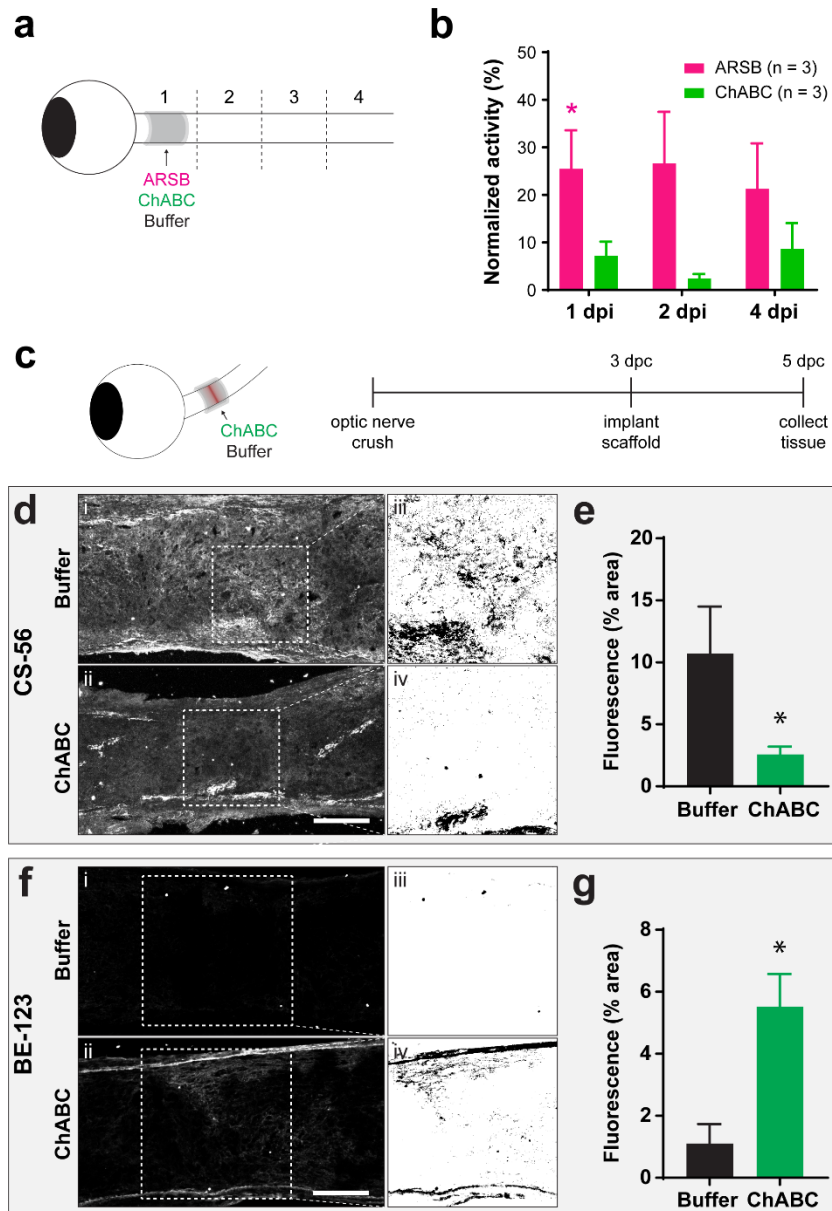
Figure 3.3. Maintenance of ChABC and ARSB activity *in vivo*. (a) Schematic diagram showing treatment of non-lesioned optic nerves with ARSB, ChABC, or buffer. (b) Graph showing activity of enzymes recovered from implanted gelfoam scaffolds, normalized to activity measurements from enzyme solutions prior to implantation. Statistical significance was determined by Student's t-test. * $p < 0.05$. (c) Schematic diagram and experiment timeline showing treatment of lesioned optic nerves with ChABC or buffer. (d) Micrographs showing CS-56 staining of ChABC-treated and control optic nerves. Scale bar = 100 µm. (e) Graph showing quantification of CS-56 fluorescence intensity of insets centered at the lesion site. Statistical significance was determined by Student's t-test. * $p < 0.05$. (f) Micrographs showing BE-123 staining of ChABC-treated and control optic nerves. Scale bar = 100 µm. (g) Graph showing quantification of BE-123 fluorescence intensity of insets centered at the lesion site. Statistical significance was determined by Student's t-test. * $p < 0.05$.

Quantitative analysis of protein or RNA from mouse optic nerve tissue is challenging due to the nerve's small size (~5 mm from eye to optic chiasm, with a diameter of ~250 μm). Isolating the site of a lesion, where astrogliosis takes place over the days and weeks following ONC, is even more difficult, as collecting too much tissue reduces the signal-to-noise ratio around the lesion site, whereas collecting too little yields insufficient amounts of protein or RNA. I developed a dissection protocol that enables successful Western blot analysis of tissue from the region directly behind the eye, containing the ONC lesion site, and measured the average protein yield. Optic nerves from non-lesioned mice were cut into four equal-sized segments of ~1 mm length and each placed in 30 μL of lysis buffer (cOmplete™ Lysis-M EDTA-free buffer, Sigma) (**Figure 3.4a**). Tissue was mechanically homogenized with a sterile pestle and centrifuged. The protein concentration of the supernatant was measured using a bicinchoninic acid (BCA) assay. The average protein amount of 1 mm optic nerve segments was 11.3±0.48 μg (mean±SE). To assess whether the BCA was precise and confirm that extracted proteins could be detected by immunoblotting, I loaded 2 μg protein from individual segments isolated from two optic nerves (left and right) of the same mouse, then performed gel electrophoresis and Western blot analysis using an anti-β actin antibody. Actin bands of comparable intensity were observed in the membrane (**Figure 3.4b**), confirming that protein extracted from 1 mm segments of mouse optic nerve can be semi-quantitatively analyzed using this technique.
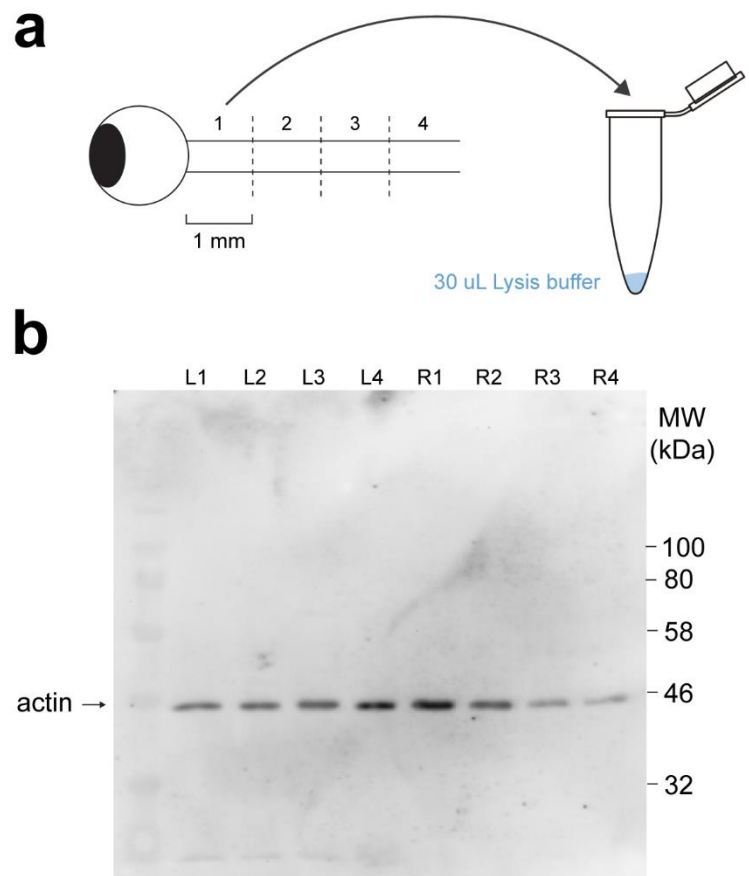
Figure 3.4. Extraction of protein from optic nerve segments. (a) Schematic diagram showing dissection of optic nerve tissue into ~1 mm segments and preparation of protein lysates. (b) Western blot image showing optic nerve protein extracts from two optic nerves (left [L] and right [R], #1-4) stained with actin.

3.6 | DISCUSSION

Few experimental therapies that seek to stimulate optic nerve regeneration target the extracellular matrix, due to the relative difficulty of accessing the optic nerve directly as opposed to introducing therapeutic substances into the eye. In rats, direct injection of enzymes or tracers into the optic nerve has been demonstrated, although such studies remain rare (Raykova et al. 2015; D'Onofrio et al. 2011). In mice, some studies have used gelfoam to deliver therapeutic substances, but the kinetics and efficiency of delivery were not reported (Brown et al. 2012). Here, I have outlined a complete protocol for a prototypical experiment involving intravitreal injection, optic nerve crush, application of gelfoam scaffolds to the optic nerve, collection of tissue, and analysis of RGC survival and axon regeneration. I present evidence that confirms the maintenance of activity and effectiveness of CSPG-targeting enzymes delivered to the optic nerve via an implanted scaffold, and I show that protein extracted from small segments of optic nerve tissue can be semi-quantitatively analyzed using Western blot. This detailed and rigorous protocol will facilitate the use of ECM-targeting therapies in future studies of optic nerve regeneration, a crucial consideration for combinatorial treatments that endeavor to stimulate long-distance regeneration of RGC axons.

An important finding was that ARSB maintains its activity over an appreciable timescale both *in vitro* and *in vivo*, whereas ChABC activity declines quickly under physiological conditions. It is important to note that most of the loaded enzyme in our gelfoam scaffold will have diffused away by the time the scaffold is recovered days after the implantation; therefore, the observance of significant trace amounts of ARSB activity in the scaffold is indicative of more robust activity, not adequately reflected by the low amplitude of the assay's absorbance change. Similarly, while my protein yield of 11.3 μg per 1 mm nerve segment is relatively small, I showed that this amount is sufficient for repeated Western blot analyses, making this strategy amenable to the detection of changes in protein expression at the site of an ONC lesion. In Chapter 4, I utilize the methods described here to evaluate changes in CSPG expression following injury and design a therapy that uses ARSB and ChABC to reduce CSPG-mediated inhibition of RGC axon extension through the glial scar.

CHAPTER 4: IDENTIFICATION OF A CRITICAL SULFATION IN CHONDROITIN THAT INHIBITS AXONAL REGENERATION

4.1 | INTRODUCTION

The deposition of inhibitory CSPGs at the site of CNS lesions is a major obstacle to regeneration of neurons in the brain, spinal cord, and optic nerve. While experimental therapies such as injections of ChABC to digest the GAG chains of CSPGs have been attempted in the spinal cord (Bradbury & Carter 2011), most treatments in the visual system prioritize intrinsic modifications to RGCs. These interventions have demonstrated substantial success in stimulating moderate levels of axonal regeneration, and in some cases, axons have been reported at central targets in the brain (de Lima et al. 2012; Kurimoto et al. 2010; Lim et al. 2016). Given these advances, addressing the extrinsic barriers to regeneration has emerged as a critical next step in promoting robust, long distance regeneration of visual neurons. As I noted in Section 1.6.6, evidence exists that CSPGs may be upregulated in the optic nerve (Brown et al. 2012; Sellés-Navarro et al. 2001; Sengottuvel et al. 2011; Qu & Jakobs 2013), but a comprehensive examination of this phenomenon has not been performed, and no studies have specifically analyzed changes in 4S GAGs following injury. Among the key challenges of modifying the extracellular matrix in the optic nerve are refining the methods of surgical intervention (addressed in Chapter 3) and selectively targeting inhibitory molecules without altering damage-restricting and/or growth-promoting features of the lesion microenvironment. In this chapter, I describe the importance of 4-sulfated CSPGs as inhibitors of neuronal growth and axonal regeneration, characterize the extracellular features of astrogliosis following acute injury to the optic nerve, and provide evidence that ARSB specifically cleaves 4S from the non-reducing ends of GAG chains and promotes regeneration after optic nerve crush.

4.1.1 | Reactive gliosis as a barrier to axon regeneration

In recent years, studies of astrogliosis have overturned the long-held notion that the astrocytic scar is unilaterally opposed to axon regeneration. A recent study discovered that reactive astrocytes can be divided into two genetically distinct subtypes, of which only one, A1 astrocytes, actively suppresses axon growth (Liddelow et al. 2017). The RNA expression profiles of A1 and A2 astrocytes were described, and it was discovered that A1 astrocytes are

activated by microglia-secreted cytokines. Upon activation, A1 astrocytes induce death of neurons and oligodendrocytes and contribute to the failure of CNS axons to regenerate following injury. The study showed evidence that specifically blocking A1 astrocyte formation enhances RGC survival after ONC. Whether A1 and A2 astrocytes produce CSPGs equally, or whether the CSPGs they produce might differ in their sulfation pattern or core proteins, was not explored and thus deserves further study. In a similar approach, another group characterized astrocyte responses to spinal cord injury over time (Hara et al. 2017). They described three phases of astrocyte reactivity based on morphological and genetic criteria: naïve astrocytes (NAs) populate the uninjured spinal cord; reactive astrocytes (RAs) were found at 7 days post injury (dpi) and expressed nestin and β-catenin; and scar-forming astrocytes (SAs) were found at 14 dpi and expressed N-cadherin and Sox9. Notably, RNA analysis revealed that SAs expressed elevated levels of several CSPG-related transcripts. Blocking the transformation of RAs to SAs reduced glial scar formation and GFAP expression, and increased the number of GAP-43$^+$ axons in spinal cord lesions. These findings imply that the emergence of SAs between 7 and 14 dpi is instrumental to the glial scar's inhibition of axon regeneration. The link between SAs and CSPG production is likely a primary driver of this effect, although the published study did not investigate this connection.

Additional evidence suggests that CSPGs, rather than astrocytes themselves, are responsible for the hostile effects of the glial scar on regenerating axons. It has been shown that preventing astrogliosis in the spinal cord by using transgenic mice engineered to kill proliferating scar-forming astrocytes successfully attenuates astrocytic scar formation but fails to promote axon regeneration (Anderson et al. 2016). Notably, even ablating chronic astrocytic scars 5 weeks after injury did not lead to spontaneous regeneration (Anderson et al. 2016). These transgenic mice did not show decreased CSPG levels within or around the lesion after astrocytic scar ablation, perhaps due to the fact that many non-astrocytic cells were found associated with CSPGs, implying that these non-astrocytic cells may produce CSPG after injury (Anderson et al. 2016). It is therefore likely that the persistence of CSPGs within the astrocytic scar, rather than the astrocytes themselves, is a primary source of extrinsic axon inhibition in CNS lesions, and that attenuating astrogliosis without reducing the deposition of axon-inhibitory CSPGs is insufficient to promote regeneration and functional recovery. The observation that regenerating axons associate with astrocyte processes (Davies et al. 1997) further supports the theory that astrocytes in the glial scar are not intrinsically inhibitory to axonal growth.

The mechanisms by which CSPGs inhibit axonal growth are not entirely understood. During neuronal development, as described previously, CSPGs play the role of repulsive guidance cues, inducing growth cone turning away from areas of high CSPG concentration to prevent growing axons from deviating from their proper paths (Erskine & Herrera 2007). This process appears to be largely mediated by the binding of surface receptors in neurons to domains in the GAG chains of CSPGs, initiating signaling cascades that lead to growth cone collapse. However, evidence also exists that argues for an attractive interaction between axons and CSPGs. Some have argued that growth cones become entrapped by CSPGs by showing cultured neurons with axons stalled in areas coated with CSPGs (Filous et al. 2014). Treating cultures with ChABC appears to "release" these trapped axons (Filous et al. 2014). The contact points between axons and CSPG occasionally express proteins associated with synapse formation (Filous et al. 2014). This aggressive "stabilization" of growth cones leads to the formation of dystrophic endbulbs at the axon terminal (Lang et al. 2014). Therefore, it could be argued that, in some contexts, CSPG-mediated inhibition of axon growth is a product of excessive adhesion as opposed to repulsion. Importantly, this specific observation appears to be predominantly related to the NG2 proteoglycan, which is expressed on the surface of OPCs (Filous et al. 2014). Whether this phenomenon also holds true for CSPGs produced by reactive astrocytes or activated microglia was not explored. Understanding the differences between the mechanisms of CSPG interactions with axons in development and following injury, as well as of different CSPG core proteins and GAG chains, is therefore essential for developing treatments that aim to stimulate axonal regeneration.

Despite their central role, CSPGs are by no means the only component of the glial scar that inhibits axonal regeneration. For instance, extensive research has demonstrated that activated macrophages can cause the retraction of axons through physical contact, ligand/receptor interactions, and secretion of proteases (Silver 2016; Horn et al. 2008; Busch et al. 2009; Busch et al. 2010; Hollis & Zou 2012; Gensel et al. 2015). Additionally, neurotoxic A1 astrocytes appear to play a key role in the spread of tissue damage and regeneration failure after injuries (Liddelow et al. 2017). While I have focused my experiments on modifying CSPGs, addressing the roles of these other cells, including how they interact with CSPGs and other ECM proteins, is vital for developing a comprehensive understanding of the glial scar and designing therapies that most effectively enable axons to navigate through it.

4.1.2 | Importance of GAG sulfation after CNS injury

Studies that link CSPGs to the failure of axon regeneration overwhelmingly fail to distinguish between differentially sulfated GAG chains, often showing instead that digestion of GAG chains with ChABC enhances neurite growth *in vitro* and axon regeneration *in vivo* (Bradbury & Carter 2011). The importance of sulfation in governing CSPG function has been demonstrated using sodium chlorate, which broadly eliminates GAG sulfation (Smith-Thomas et al. 1995). Recent studies have characterized the behaviors of specific sulfation motifs. For instance, axons grow readily over surfaces coated with 6S CSPGs (Wang et al. 2008), and deleting the enzyme that adds 6S to GAGs impairs axonal regeneration in mice (Lin et al. 2011). In contrast, axons avoid 4S GAGs, an effect abolished by treatment with 4-sulfatase (Wang et al. 2008). Elevation of 4S has been observed after traumatic brain injury (Yi et al. 2012). Notably, the area of CSPG immunoreactivity surrounding the lesion core overlapped with 4S, but not 6S, suggesting a differential expression of these sulfation motifs following injury (Yi et al. 2012). Production of 4S was not limited to a single cell type, but was associated with astrocytes, microglia, macrophages, OPCs, and fibroblasts, implying multicellular sources of 4S GAG, although direct evidence of production was not demonstrated in each case (Yi et al. 2012). In addition to the brain, another study showed elevation of 4S deposition after spinal cord injury, and found that treating the lesioned area with ARSB improved motor function (Yoo et al. 2013). Blocking 4,6S with a custom antibody enhanced regeneration of RGC axons after ONC (Brown et al. 2012). The case of 4,6S is particularly interesting, as it may be possible that GAG chains with terminal 4,6S could be converted to growth-permissive 6S motifs in the presence of ARSB. An age-related increase in the ratio of 4S to 6S was linked to declines in plasticity and memory (Foscarin et al. 2017; Miyata et al. 2012), indicating that sulfation-specific changes may be programmed to convert an environment that promotes growth and plasticity during development into a more inhibitory, stabilized environment in adulthood. Collectively, these observations suggest that reducing 4S while preserving 6S on intact GAG chains may be a viable strategy to enable growing axons to overcome CSPG-mediated inhibition, and that this may ultimately be more effective than indiscriminate reductions in sulfation or destruction of GAGs. I therefore sought to use ARSB to selectively remove 4S from the non-reducing ends of CSPGs expressed after optic nerve crush injury in mice.

4.1.3 | Arylsulfatase B

ARSB is an enzyme that cleaves 4S groups from GalNAc at the non-reducing ends of GAG chains (Litjens & Hopwood 2001). ARSB is generally localized in the lysosome, where it initiates a stepwise degradation of GAGs. In humans, several mutations of the gene encoding ARSB have been reported (Litjens & Hopwood 2001). The absence or dysfunction of lysosomal ARSB interferes with GAG degradation, leading to an accumulation of partially degraded GAGs in the lysosome. Because this pathology affects multiple cell types, many tissues and organs are affected, leading to an extensive pathological phenotype. In humans, this condition is known as mucopolysaccharidosis type VI (MPS VI) or Maroteaux-Lamy syndrome. Its symptoms include skeletal abnormalities such as short stature and facial dysmorphism, stiff joints, clouding of the cornea, cardiac abnormalities, and hepatosplenomegaly. Interestingly, the nervous system is generally not affected, and patients have normal intelligence and do not suffer cognitive deficits. The myriad effects elsewhere in the body mean that patients with MPS VI suffer enormous reductions in quality of life. They also have a dramatically reduced life expectancy, often dying within two decades of birth. MPS VI affects anywhere from 1 in 100,000 to 1 in 1,300,000 patients depending on the population studied (Harmatz et al. 2004). The severity of this illness has led to aggressive research aimed at replacing absent or defective ARSB. In recent years, an enzyme replacement therapy was developed using recombinant human ARSB and has shown remarkable success (Naglazyme®, Biomarin) (Muñoz-Rojas et al. 2010; Harmatz et al. 2004; Harmatz 2005). According to Biomarin, patients who undergo enzyme replacement therapy with Naglazyme experience a 23% improvement in a walking distance test and a 38% improvement in a stair-climbing test, indicative of reduced breathing difficulties and increased endurance. These beneficial effects were maintained over a period of ten years of regular treatments.

The application of ARSB in the nervous system is relatively new. As a lysosomal enzyme, ARSB exhibits peak activity at acidic pH. However, evidence from *in vitro* and *in vivo* studies (Yoo et al. 2013), as well as my own work, demonstrates that ARSB maintains moderate activity even at neutral pH, making therapeutic use in the extracellular matrix of the CNS a viable possibility. One study has shown that ARSB can be inhibited by ethanol, and that when exogenous ARSB was added to astrocyte cultures, the presence of ethanol led to increases in CSPGs, including 4S, and inhibited the growth of neurites from neurons cocultured with these astrocytes (Zhang et al. 2014). The study concluded that the presence of

ARSB supports neurite growth and may reduce total 4S levels, and that silencing ARSB reverses these effects. ARSB was also delivered to the site of a spinal cord injury in mice, leading to improvements in motor function (Yoo et al. 2013). The objective of my studies was to characterize the increase in 4S expression within the glial scar following an optic nerve crush lesion, and then to selectively target elevated 4S by directly administering ARSB to the injured area. I combined ARSB with an intrinsic stimulus known to stimulate the regeneration of RGC axons, and evaluated the effects of ARSB both on axonal regeneration and on the morphology and composition of the glial scar.

4.2 | RESULTS

4.2.1 | ARSB reverses the inhibition of neurite growth caused by 4-sulfated CSPGs

ARSB selectively cleaves sulfate groups from the C4 position of GalNAc at the non-reducing ends of GAG chains (**Figure 4.1a**). In work performed by Dr. Caitlin Mencio, we studied whether this reaction can alter the inhibitory properties of CSPGs. We used a previously established cell culture model of the glial scar (Wang et al. 2008), where monolayers of confluent mouse astrocytes were treated with TGF-β to stimulate elevated CSPG production (**Figure 4.1b**). To assess whether neurite inhibition by CSPGs could be reduced through ARSB treatment, cultures of dissociated mouse hippocampal neurons were exposed to 5 µg/ml CSPG with and without ARSB treatment for 48 h. Cultures were stained for βIII-tubulin, and the lengths of neurites were measured. Neurons grown in the presence of CSPGs were significantly shorter ($p < 0.0001$) than untreated neurons (neurite length [mean±SE]: 77.7±6.2 µm and 122.2±9.3 µm, respectively) (**Figure 4.1c-d**). Growth was unaffected by CSPGs that had been treated with ARSB, suggesting that ARSB treatment was sufficient to remove neurite outgrowth inhibiting characteristics of CSPGs (**Figure 4.1c-d**).

To test the actions of ARSB in a cellular model, monolayers of confluent mouse astrocytes were treated with TGF-β to stimulate elevated CSPG production (**Figure 4.1b**). Mouse cerebellar granule neurons (CGNs) were then seeded onto these astrocytes and allowed to grow for 24 h. Cultures were stained for GFAP and βIII-tubulin, and the lengths of CGN neurites were measured. Neurons growing on TGF-β-treated astrocytes exhibited significantly ($p = 0.0024$) lower neurite outgrowth than those plated on untreated control astrocytes (neurite length [mean±SE]: 67.4±4.4 µm and 89±7.6 µm, respectively) (**Figure**

4.1e-f). However, incubating TGF-β-treated co-cultures with ARSB restored average neurite length to the levels observed in untreated controls (**Figure 4.1e-f**), suggesting that cleaving 4S from the non-reducing ends of GAG chains is sufficient to neutralize the inhibitory effects of CSPGs on neurons.

To demonstrate that ARSB acts on extracellular CSPGs, rather than being internalized into astrocytes and interfering with CSPG production or secretion, conditioned medium (CM) was collected from TGF-β-treated astrocytes and left untreated, treated with ARSB or treated with ChABC. The isolated and treated CM was added to separately cultured CGNs. Application of CM from TGF-β-treated astrocytes significantly reduced neurite outgrowth while ARSB treatment reversed this effect to a degree equivalent to ChABC (**Figure 4.2**). Together, these findings demonstrate that the presence of CSPGs can inhibit neurite outgrowth, and that this inhibition is overcome by exposing the CSPGs to either ARSB or ChABC

To further validate that ARSB does not interfere with CSPG secretion, the level of CSPGs in CM was measured by immunoblotting with the antibody CS-56, which reacts with 4S and 6S groups on GAG chains (Avnur & Geiger 1984). The increase in CSPGs caused by TGF-β treatment (Wang et al. 2008) was not altered by treatment with ARSB, even after repeated additions (**Figure 4.1b**), indicating that its enhancement of neurite growth was derived from modifying the sulfation pattern rather than attenuating CSPG production or secretion. These data also demonstrate that CS-56 immunoreactivity is not altered by removal of 4S from the non-reducing end of CS GAG chains.

Figure 4.1. ARSB reverses neurite outgrowth inhibition caused by 4-sulfated CSPGs. (a) Schematic diagram showing actions of ARSB and ChABC on GAG chains. (b) Western blot showing CS-56 signal in conditioned medium. (c) Micrographs showing hippocampal neurons treated with no treatment, CSPG (5 µg/ml), or CSPG+ARSB. Scale bar = 25 µm. (d) Plot showing lengths of longest neurite measured from β-III-tubulin stained neurons. Statistical significance was determined by one-way ANOVA. (e) Micrographs showing co-cultures of CGNs grown on astrocytes and treated with TGF-β, TGF-β and ARSB, or no treatment. Scale bar = 25 µm. (f) Plot showing lengths of longest neurite measured from β-III-tubulin stained neurons. Statistical significance was determined by one-way ANOVA. * $p < 0.05$, ** $p < 0.005$, *** $p < 0.001$, **** $p < 0.0001$. Figure produced by Dr. Caitlin Mencio.
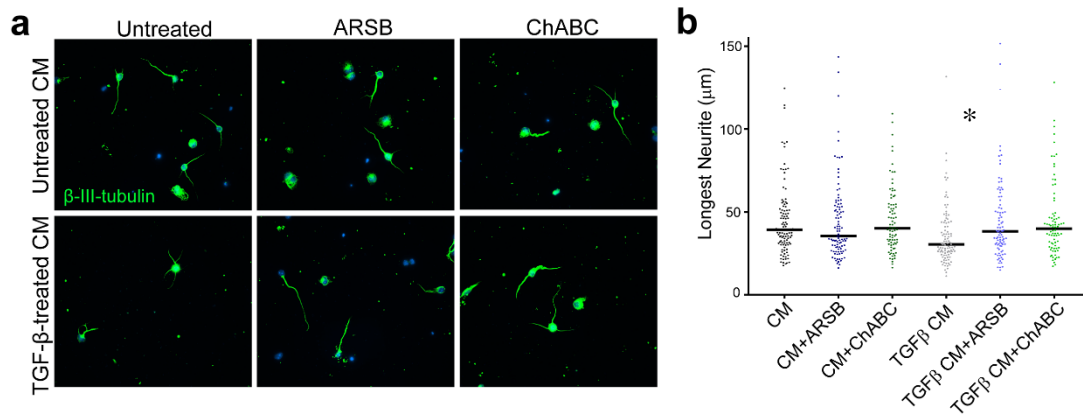
Figure 4.2. ARSB reverses neurite outgrowth inhibition caused by 4-sulfated CSPGs. (a) Micrographs showing CGNs treated with astrocyte conditioned medium containing TGF-β and either ARSB, ChABC, or no enzyme. Scale bar = 25 µm. (b) Plot showing length of longest neurite measured from β-III-tubulin stained neurons, displayed as median. Statistical significance was determined by two-way ANOVA with Tukey post-hoc test for multiple comparisons. * $p < 0.05$. Figure produced by Dr. Caitlin Mencio.

4.2.2 | 4-sulfated CSPGs are elevated following injuries to the optic nerve and spinal cord

To assess the time course and spatial distribution of CSPG and 4S GAG deposition after injury, optic nerve crush or dorsal column crush surgery was performed on cohorts of adult mice and rats, and tissue was collected 1, 3, 5, 7, 14, and 21 dpc (**Figure 4.3**, examples of mouse optic nerve crush and rat dorsal column crush). CSPG content in the lesion area was detected using CS-56 and 2H6, an antibody that reacts predominantly with 4S (Yamamoto et al. 1995), and to a lesser degree, with 6S (Sugiura et al. 2012) and 2,6S (Matsushita et al. 2018). CS-56 immunohistochemistry revealed an increase in CSPG deposition at the lesion during the scar-forming phase at 7 dpc in all conditions (**Figure 4.4a-c**). 4S was also visibly enhanced in both species and injury models (**Figure 4.4a-c**). In non-lesioned sham control tissue, CSPGs were evenly distributed within the tissue and meninges. In mouse ONC tissue, where CSPG was assessed over an extended time course and immunoreactivity was quantified from multiple replicate samples, levels of CSPG and 4S peaked at 7 dpc and remained high as late as 21 dpc (**Figure 4.5**). A specific increase in 4S expression was noted, with levels reaching 2.5-fold those in non-lesioned sham controls (fold change [mean±SE]: 2.53±0.15). The elevation of CSPGs was further confirmed by Western blot analysis of tissue segments collected from the optic nerve or spinal cord lesion in rats. Bands detected by CS-56 at 50 kB showed a reliable increase in lesioned vs. non-lesioned tissue (**Figure 4.4d-e**). Taken together, these results illustrate that optic nerve and spinal cord injuries in mice and

rats lead to astrogliosis and elevated expression of CSPGs, especially those with 4S GAGs, which is sustained for at least 21 days after ONC in mice.
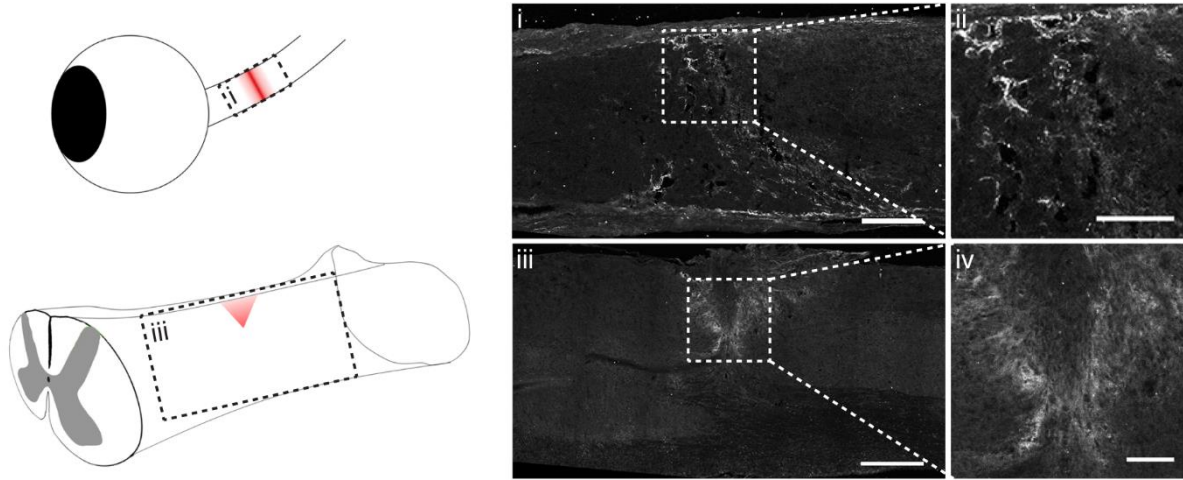
Figure 4.3. 4-sulfated CSPGs accumulate in the glial scar after injury. Schematic diagram depicting optic nerve crush and dorsal column crush surgeries. Micrographs showing injured tissue 7 days after injury analyzed by immunohistochemistry with CS-56 in (i, ii) mouse optic nerve and (iii, iv) rat spinal cord. Scale bar = (i) 100 µm, (ii) 50 µm, (iii) 400 µm, (iv) 100 µm.
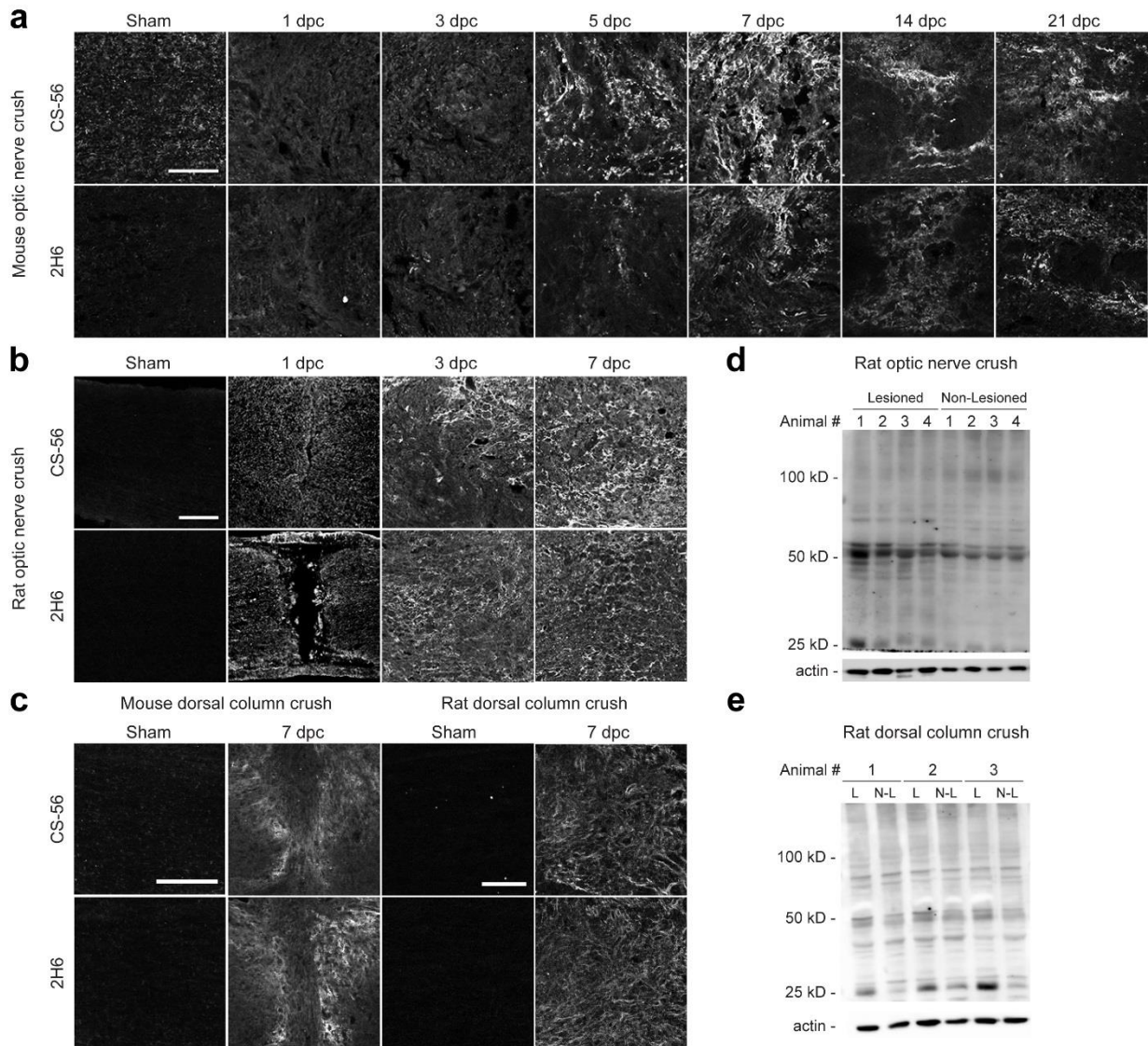
Figure 4.4. 4-sulfated CSPGs accumulate in the glial scar after injury. Micrographs showing (a) mouse optic nerve crush, (b) rat optic nerve crush, and (c) mouse and rat dorsal column crush tissue. Sections were analyzed by immunohistochemistry with antibodies detecting CSPGs (CS-56) and 4S (2H6). Scale bars = (a) 50 µm, (b) 100 µm, and (c) 200 µm. (d) Western blot analysis showing elevation of CS-56 signal within lesioned rat optic nerve tissue. (e) Western blot of CS-56 in rat spinal cord tissue. L = lesioned, N-L = non-lesioned.
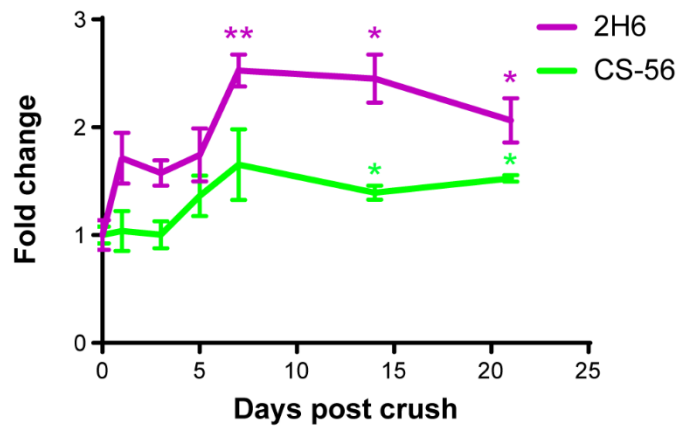
Figure 4.5. Optic nerve crush stimulates sustained elevation of chondroitin sulfate proteoglycans and inhibitory 4S epitopes. Fluorescence intensity of CS-56 and 2H6 immunostaining expressed as fold change vs. non-lesioned sham controls. Insets from n = 3 animals per condition were used. Statistical significance versus sham was determined by Student's t-test. * $p < 0.05$, ** $p < 0.005$. Colored asterisks indicate significance for different groups (CS-56 = green, 2H6 = magenta).

The axons of injured mouse RGCs were visualized with fluorescently-tagged CTβ. CTβ was injected intravitreally 1 d prior to tissue harvest. CTβ+ axons failed to traverse the injury site and instead formed dystrophic endbulbs that appeared to be associated with areas of high CSPG deposition (**Figure 4.6a-ii, arrows**), which included areas of high 4S immunostaining as detected by the 2H6 antibody (**Figure 4.6b-ii, arrows**). When CTβ+ axons did penetrate the lesion site, they appeared to do so through areas where CSPG signals were comparatively reduced (**Figure 4.6a-iii, iv, arrowheads**).
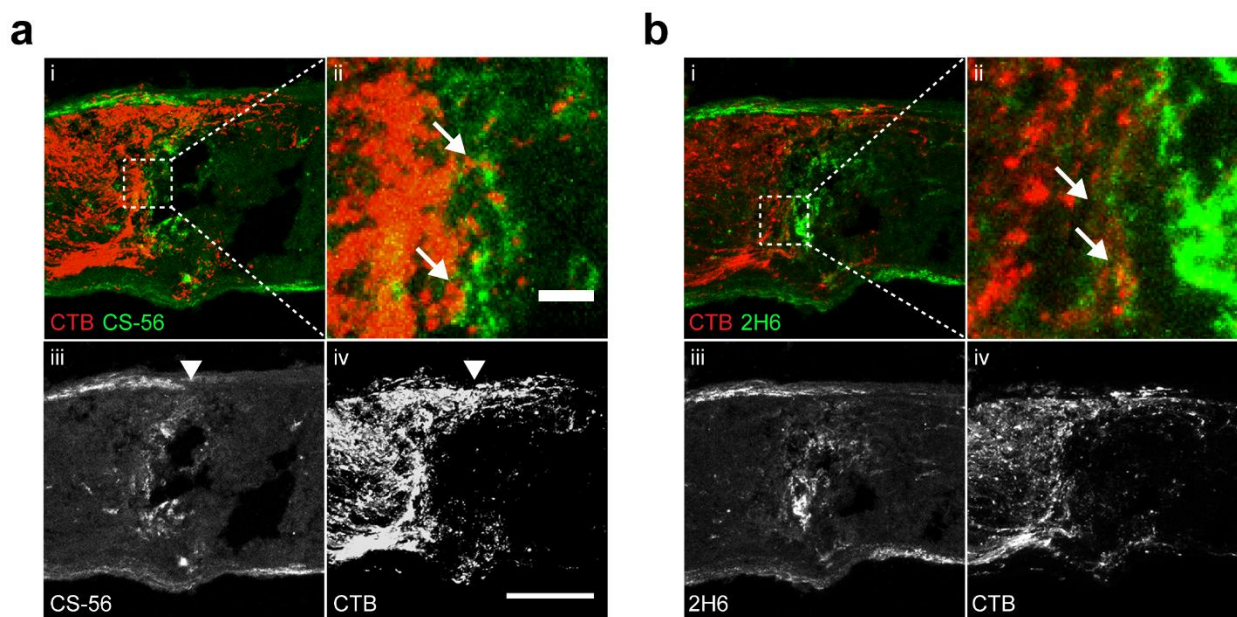
Figure 4.6. Retinal ganglion cell axon growth is blocked by 4-sulfated CSPGs in the glial scar. (a) Micrographs showing lesioned mouse optic nerve tissue at 7 dpc. Axons are visualized with CTβ and form dystrophic endbulbs in areas of high CSPG immunoreactivity. (i) Co-labeling of CTβ and CS-56 shows axons terminating in areas of high CSPG expression. (ii) Inset shows dystrophic endbulbs in CTβ+ axons. (iii) CS-56 channel shows pattern of CSPG expression. (iv) CTβ channel alone shows paths of axons. Scale bar = 100 μm, inset = 10 μm. (b) Micrographs showing CTβ+ axons blocked by 4S GAG.

4.2.3 | CSPGs associate with reactive astrocytes and activated microglia

The sources of CSPG deposition have been well characterized in other CNS tissues, where CSPGs have been observed to associate with astrocytes, OPCs, microglia, macrophages, and meningeal fibroblasts, implying that they may be produced by multiple cell types (Yi et al. 2012). Reactive gliosis is a multicellular process, and to understand how glial cells contribute to CSPG deposition in the optic nerve, I validated the time course of astrocyte reactivity and microglia activation by immunohistochemistry with GFAP (to detect astrocytes) and Iba1 (to detect microglia and macrophages) (**Figure 4.7, 4.8**). My results aligned with the observations of others who have assessed the responses of astrocytes and microglia to ONC injury (Qu & Jakobs 2013). At 7 dpc, GFAP immunoreactivity was enhanced, with reactive astrocytes withdrawing from the lesioned area to form a cavity that was filled with Iba1$^+$ activated microglia and macrophages (**Figure 4.7b-i**). Astrocyte morphology was visibly changed, with many GFAP$^+$ cells becoming hypertrophic and extending elongated processes that defined the lesion boundary (**Figure 4.7b-iii**). Some GFAP$^+$ cells were also found within the lesion core (**Figure 4.7b-vii, arrow**). Likewise, Iba1$^+$ cells displayed more intense immunoreactivity and were larger and rounder, with retracted processes (**Figure 4.7b-viii, arrow**), distinct from cells in the distal optic nerve or in the non-lesioned sham condition, which exhibited a striated morphology (**Figure 4.7a-viii**). By 21 dpc, astrocytes had begun to repopulate the cavity and form a chronic scar (**Figure 4.8**).
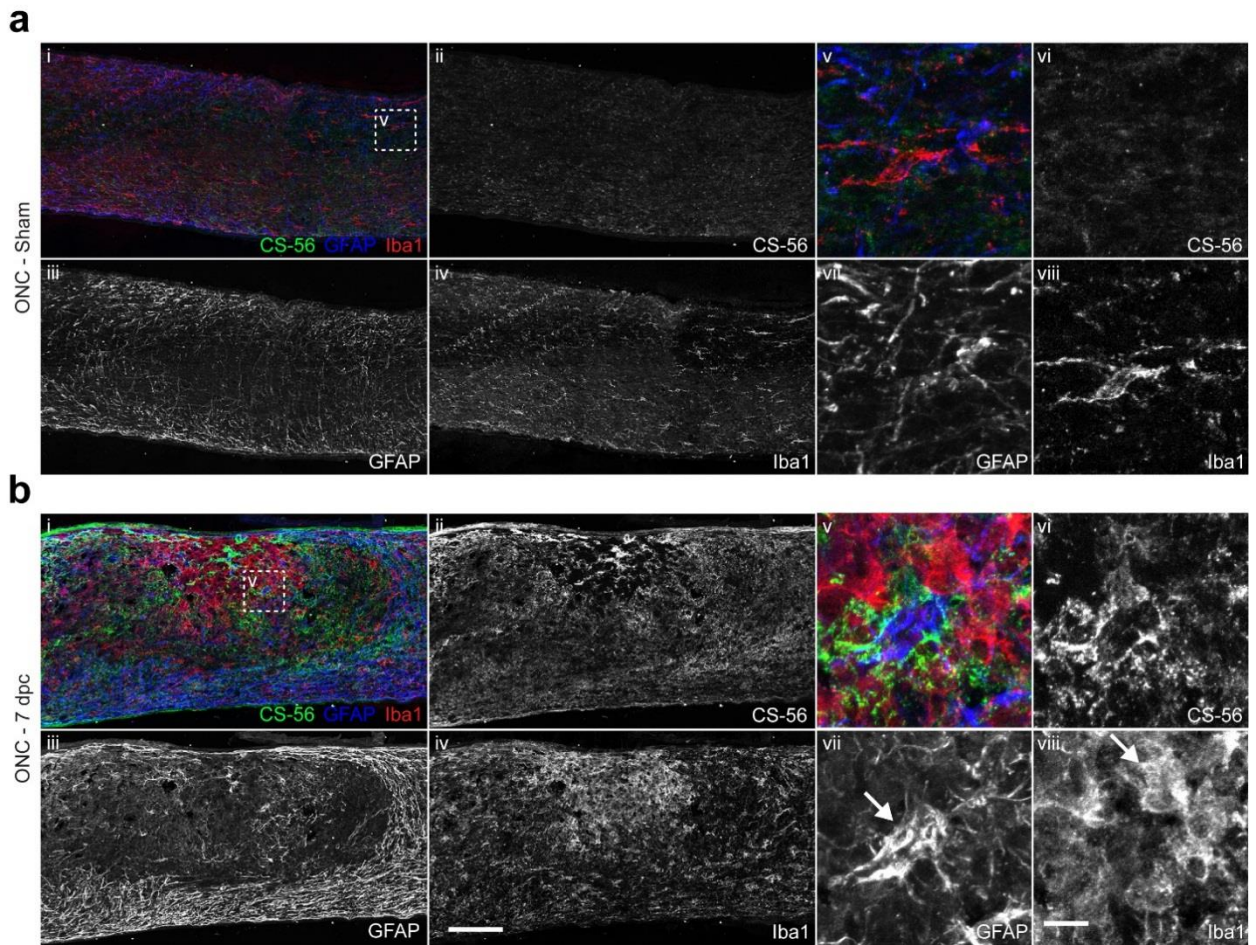
Figure 4.7. Elevation of CSPGs corresponds to peak of astrogliosis. Micrographs showing (a) sham or (b) 7 dpc mouse optic nerve tissue analyzed by immunohistochemistry with antibodies detecting reactive astrocytes (GFAP), activated microglia and macrophages (Iba1), and CSPGs (CS-56). Scale bar = 100 µm, insets = 10 µm.
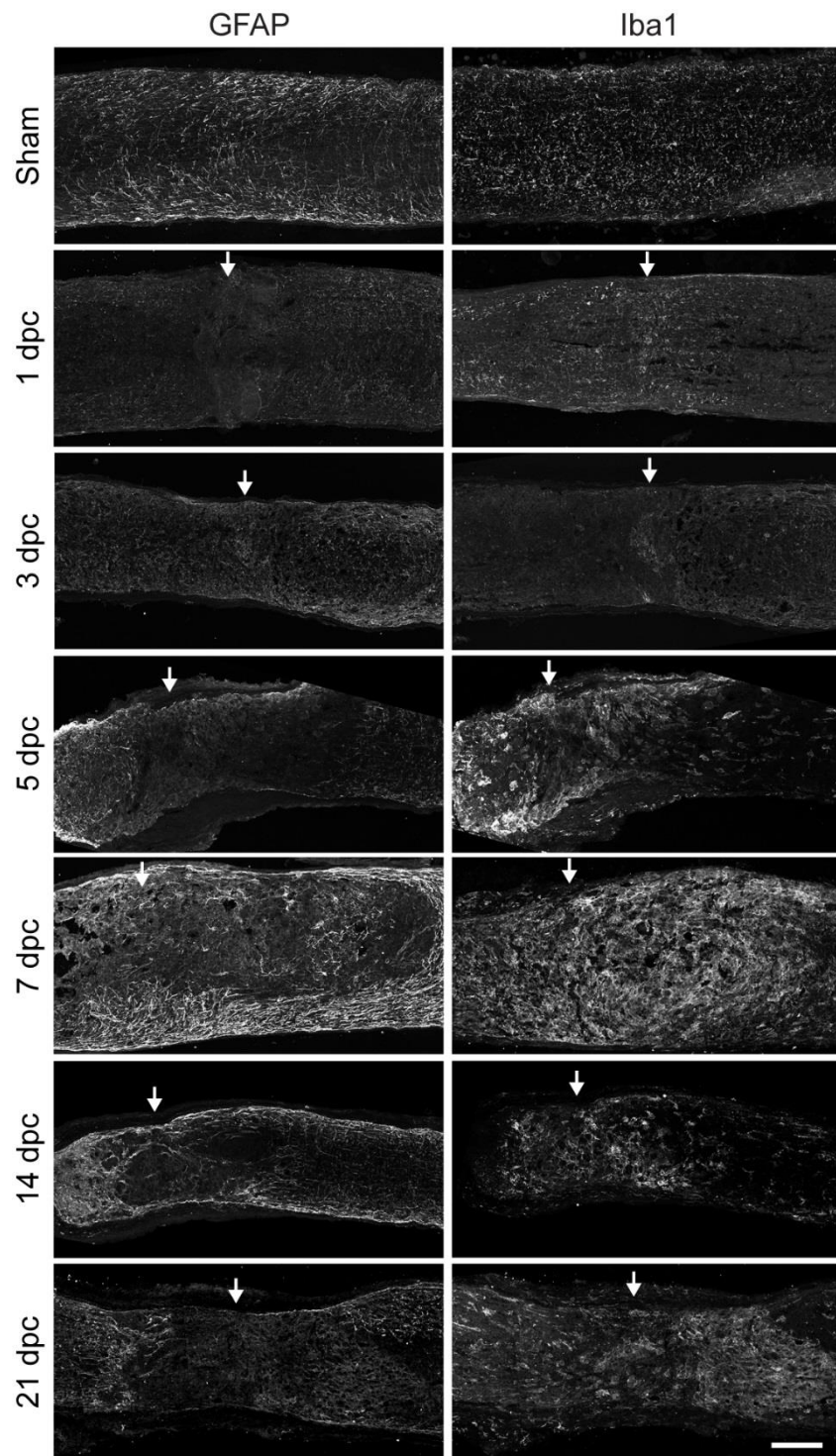
Figure 4.8. Reactive astrocytes and activated microglia form glial scar after optic nerve crush. Micrographs showing mouse optic nerve tissue analyzed by immunohistochemistry with GFAP and Iba1 at several time points. Arrows indicate lesion site. Scale bar = 100 µm.

High magnification images revealed that CSPGs were closely associated with both reactive astrocytes and microglia, both around the boundary of the lesion and within the lesion core (**Figure 4.7, 4.9**). This association was observed with both CS-56 and 2H6 immunostaining (**Figure 4.9**). Glial cells that were associated with elevated levels of CSPG typically displayed reactive or activated morphologies (**Figure 4.9-iii, iv, vi, viii**).
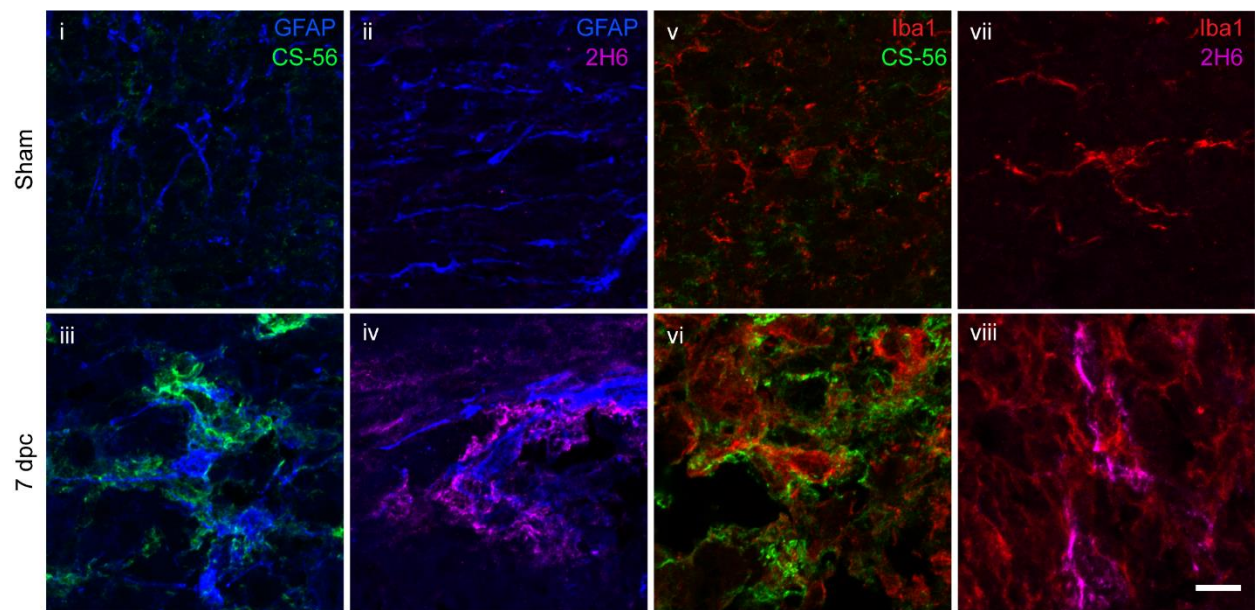
Figure 4.9. CSPGs associate with astrocytes and microglia at the lesion site. Micrographs showing mouse optic nerve tissue analyzed by immunohistochemistry with antibodies detecting reactive astrocytes (GFAP) and activated microglia and macrophages (Iba1), as well as CSPGs (CS-56) and 4S GAGs (2H6). (i-iv) CSPGs are elevated at 7 dpc and associate with GFAP$^+$ astrocytes. (v-viii) CSPGs associate with Iba1$^+$ microgila. Scale bar = 10 µm.

4.2.4 | Optic nerve crush elevates CSPG expression in the retina

ONC severs RGC axons in the optic nerve, which leads the distal axon segments to undergo Wallerian degeneration, leaving behind cellular debris including myelin, which can itself be highly inhibitory to the subsequent regeneration of the injured axons. This axonal damage, when left untreated, also contributes to the progressive death of most RGCs, with their cell bodies in the retina undergoing apoptosis in the days and weeks following the lesion. I sought to assess whether there are changes to CSPGs or reactive gliosis in the retina following ONC. Retinas were collected from mice at the time points described above, sectioned, and stained with antibodies against CSPGs, astrocytes, and microglia. I observed a robust gliotic response at 21 dpc in comparison with non-lesioned sham control retinas (**Figures 4.10, 4.11**). In control retinas, GFAP$^+$ astrocytes were largely restricted to the GCL, with no processes extending into the IPL, CS-56 immunoreactivity was essentially undetectable (**Figure 4.10-i, iii**). At 21 dpc, GFAP$^+$ astrocytes were visibly reactive, and several extended processes into the IPL and INL (**Figure 4.10-ii, iv**). Reactive astrocytes in the GCL were associated with regions of elevated CS-56 immunoreactivity, suggesting that they were producing CSPGs. Elevation of 4S GAGs was also observed (**Figure 4.11**). In non-lesioned sham control retinas, 2H6 immunoreactivity was low in the GCL (**Figure 4.11-iii**), and Iba1$^+$ microglia were distributed throughout the retina (**Figure 4.11-i**). Microglia had striated morphologies, suggesting they were not activated (**Figure 4.11-v**). At 21 dpc, Iba1$^+$ cells were rounder and many had withdrawn their processes, suggesting an activated state (**Figure 4.11-ii, iv, vi**). 4S GAGs were visibly elevated in the GCL (**Figure 4.11-iv**). Together, these observations suggest that the reactive gliosis and deposition of CSPGs observed in the optic nerve also occurs, at least to some extent, within the retina, including the GCL.

126
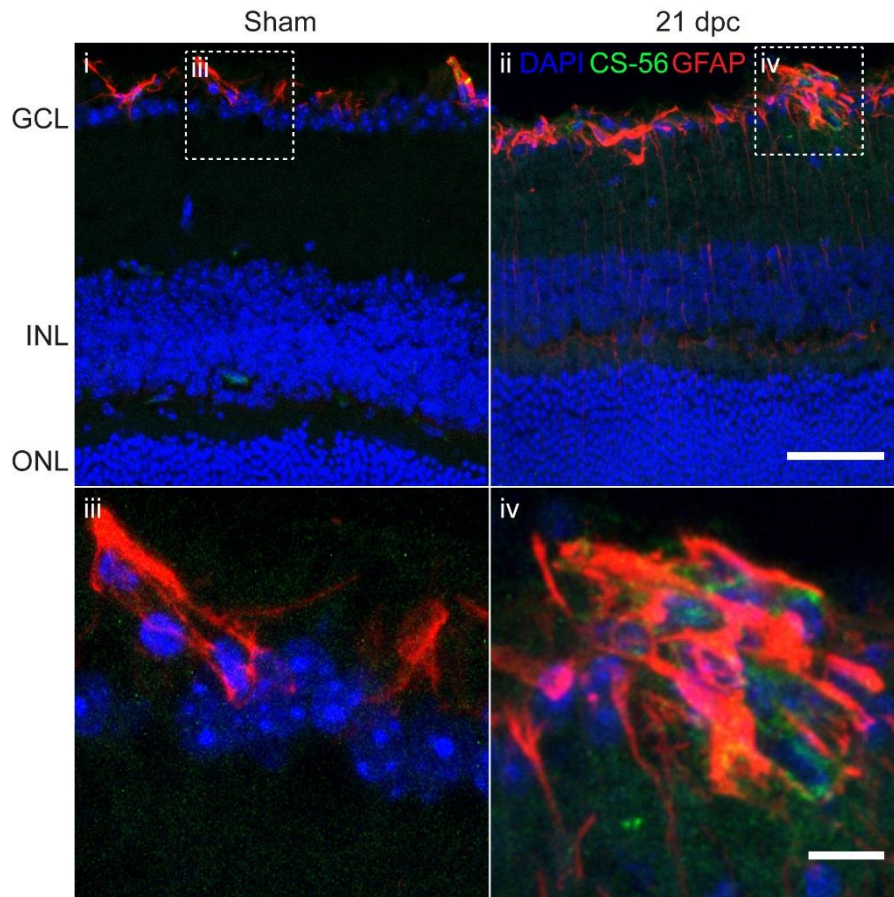
Figure 4.10. Optic nerve crush stimulates astrocyte reactivity and upregulates CSPGs in the retina. Micrographs showing mouse retina sections from (i) non-lesioned sham controls and (ii) 21 days post ONC, analyzed by immunohistochemistry with antibodies detecting CSPG (CS-56) and reactive astrocytes (GFAP). Insets (iii, iv) show elevation of CSPG in conjunction with reactive astrocytes in the GCL. Scale bar = 50 µm, inset = 10 µm.
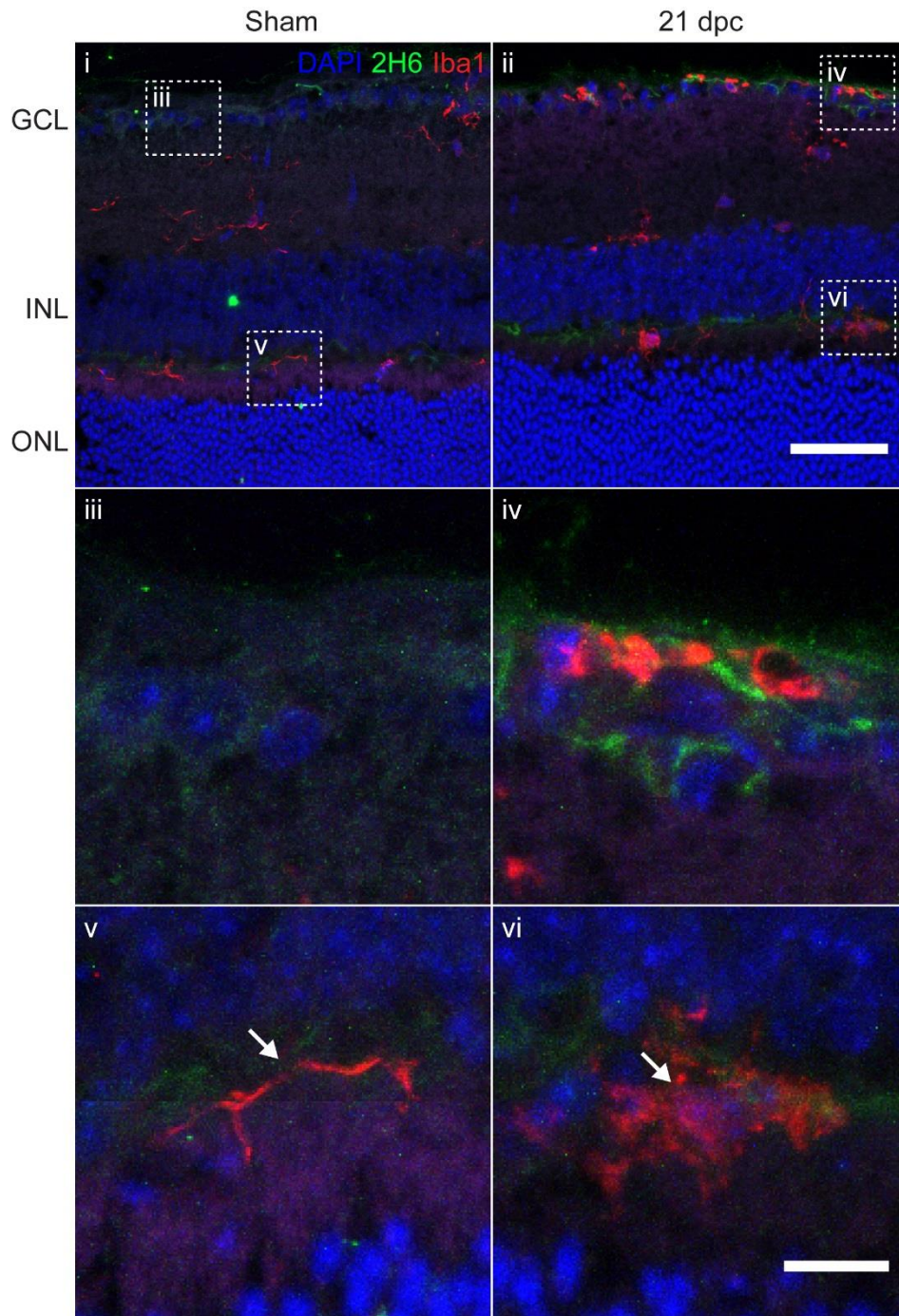
Figure 4.11. Optic nerve crush activates microglia and upregulates 4S GAG in the retina. Micrographs showing mouse retina sections from (i) non-lesioned sham controls and (ii) 21 days post ONC, analyzed by immunohistochemistry with antibodies detecting 4S GAG (2H6) and microglia (Iba1). Insets (iii, iv) show elevation of 4S GAG in conjunction with activated microglia in the GCL. Insets (v, vi) show activated microglia in the IPL. Scale bar = 50 µm, inset = 10 µm. Abbreviations: GCL = ganglion cell layer; INL = inner nuclear layer; ONL = outer nuclear layer.

4.2.5 | Modifying CSPG sulfation enhances retinal ganglion cell axon regeneration

Given the *in vitro* evidence presented above showing that 4S is critical to CSPG-mediated inhibition of neurite growth, and the observation that 4S is highly expressed within optic nerve lesions, I investigated whether cleaving 4S from the non-reducing ends of GAG chains at the ONC lesion site would enhance RGC axon regeneration in the mouse optic nerve. To accomplish this, an intrinsic pro-regenerative stimulus, Zymosan A and CPT-cAMP (Leon et al. 2000; Yin et al. 2003), was combined with direct application of ARSB to the lesioned nerve. ChABC was used as a control to evaluate the effects of digesting GAG chains entirely rather than selectively removing 4S groups.

Mice received ONC, followed 3 days later by an intravitreal injection of Zymosan A (12.5 µg/µL) supplemented with CPT-cAMP (50 mM), followed immediately by implantation of a gelfoam scaffold loaded with 5 µL of ARSB (1 mg/mL), ChABC (455 µg/mL), or control buffer. At 14 dpc, optic nerves were dissected, sectioned, and stained for GAP-43 to detect regenerating axons. In accordance with previous reports (Leaver et al. 2006), we found that GAP-43 selectively labels regenerating axons, as GAP-43 signal is absent from intact, non-lesioned optic nerves (data not shown). On its own, injection of Zymosan/CPT-cAMP induced significantly ($p = 0.0226$) higher RGC axon regeneration than PBS controls at 14 dpc (axons at 0.25 mm distal to the lesion [mean±SE]: 282±83.4 and 42.3±11.1, respectively) (**Figure 4.12a-c**). Zymosan did not alter CSPG expression at the lesion site (**Figure 4.12d-e**). When Zymosan was combined with enzyme delivery, both ARSB and ChABC significantly ($p = 0.0006$ and $p < 0.0001$, respectively) enhanced RGC axon regeneration compared with the buffer control (axons at 0.25 mm distal to the lesion [mean±SE]: 472±62, 535±123, and 217±53, respectively) (**Figure 4.13**). Interestingly, delivering ARSB or ChABC in the absence of Zymosan injection did not enhance RGC axon regeneration (**Figure 4.14**).
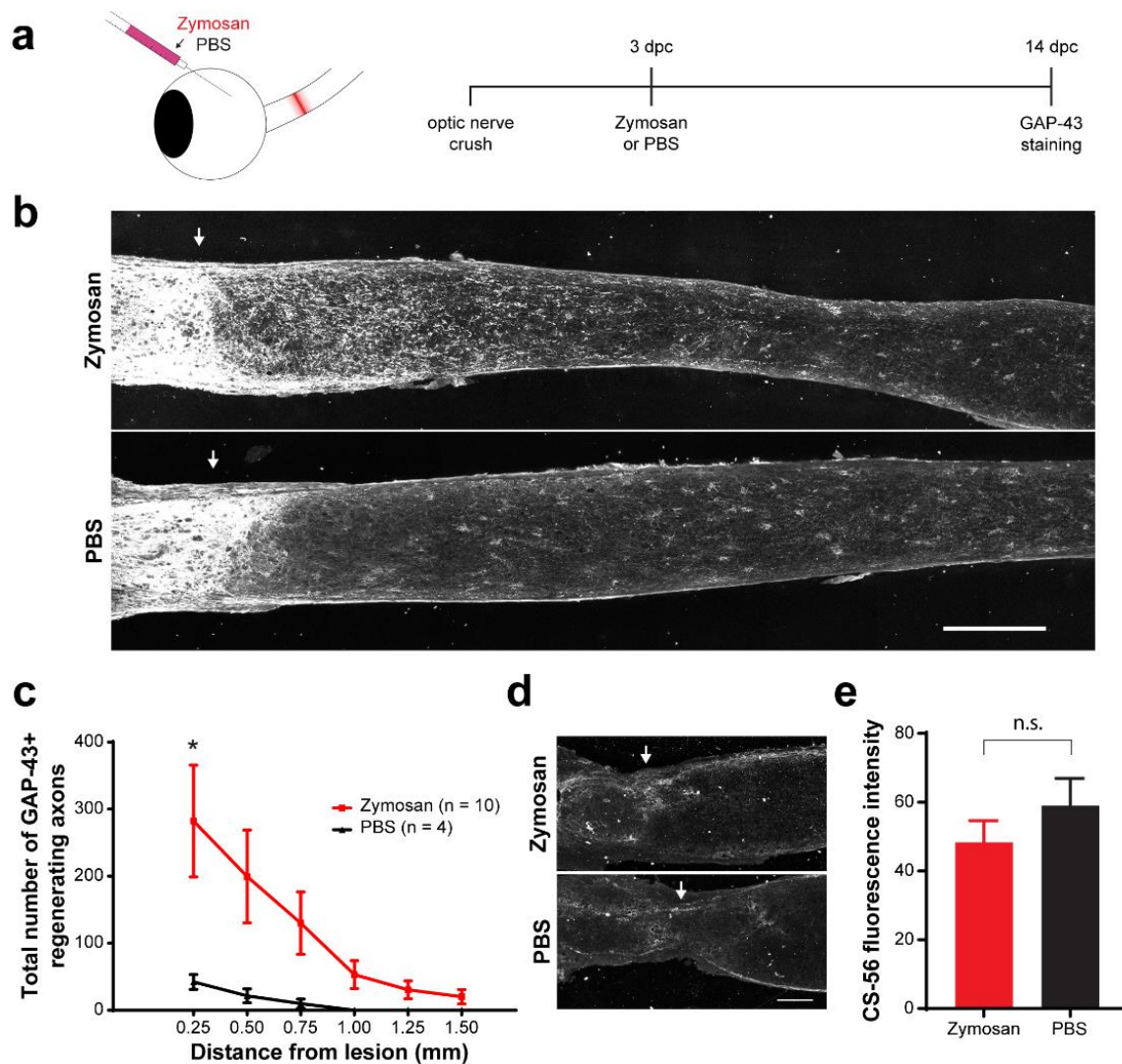
Figure 4.12. Zymosan and CPT-cAMP stimulate axon regeneration. (a) Experiment timeline and schematic diagram showing intravitreal injection of Zymosan/CPT-cAMP or PBS. (b) Micrographs showing GAP-43-labeled optic nerves from mice treated with Zymosan or PBS. Arrows indicate lesion site. Scale bar = 200 µm. (c) Graph showing the number of regenerating axons at distances distal to the lesion site, displayed as mean +/- SEM. Statistical significance was determined by two-way ANOVA with Bonferroni post-hoc test for multiple comparisons. * p < 0.05. (d) Micrographs showing CS-56 immunostaining at the lesion site of optic nerves from animals treated with Zymosan or PBS. Arrows indicate lesion site. Scale bar = 100 µm. (e) Graph showing quantification of CS-56 fluorescence intensity (arbitrary units) measured from 150×150 µm insets centered at ONC lesion site. Statistical significance was determined by Student's t-test. * p < 0.05.
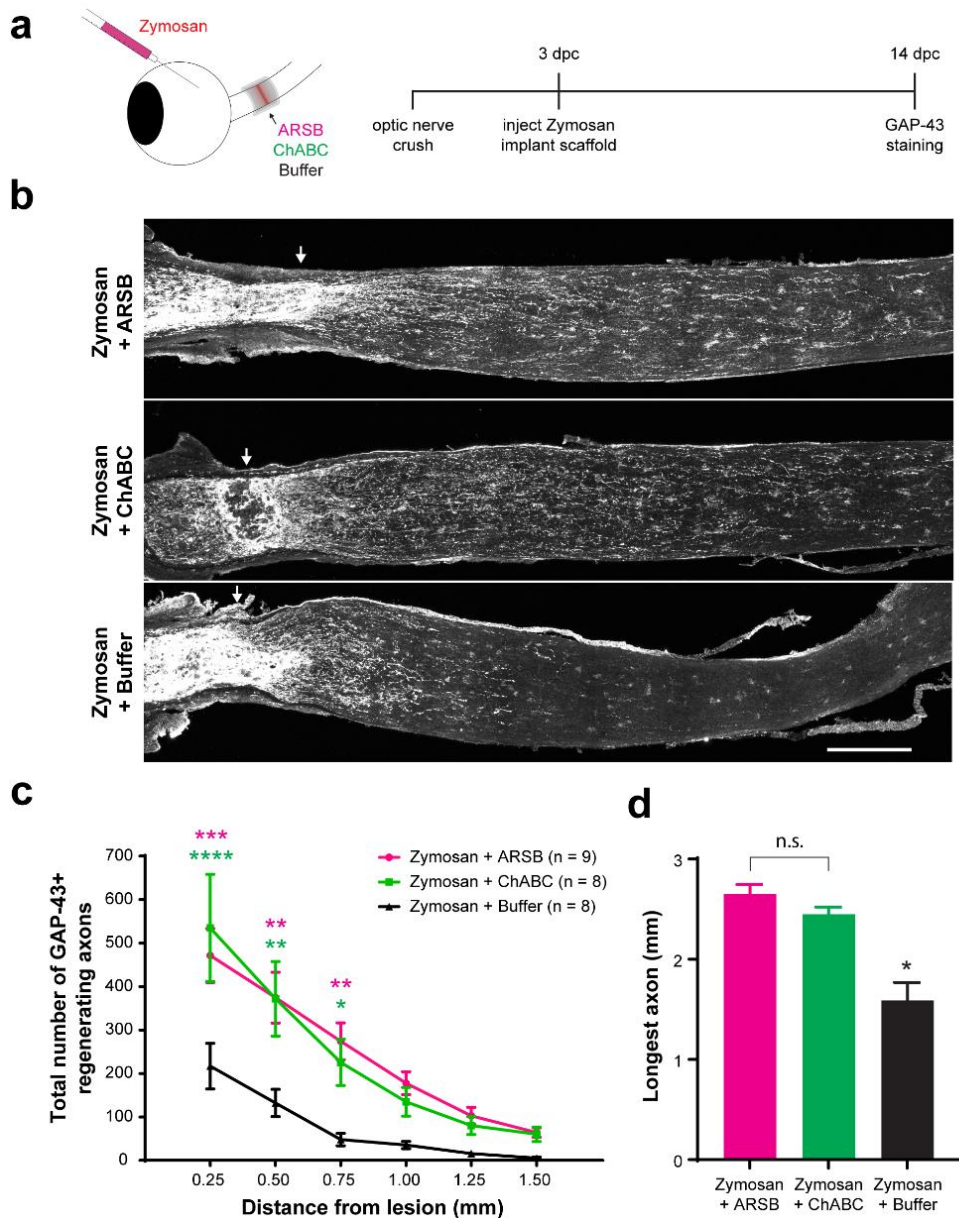
Figure 4.13. Selectively targeting inhibitory CSPGs enhances retinal ganglion cell axon regeneration. (a) Experiment timeline and schematic diagram showing intravitreal injection of Zymosan/CPT-cAMP and implantation of gelfoam scaffolds containing ARSB, ChABC, or control buffer. (b) Micrographs showing GAP-43-labeled optic nerves from mice treated with Zymosan/CPT-cAMP and gelfoam scaffolds loaded with ARSB, ChABC, or control buffer. Arrows indicate lesion site. Scale bar = 200 µm. (c) Graph showing the number of regenerating axons at distances distal to the lesion site, displayed as mean +/- SEM. Statistical significance was determined by two-way ANOVA with Bonferroni post-hoc test for multiple comparisons. * $p < 0.05$, ** $p < 0.005$, *** $p < 0.001$, **** $p < 0.0001$. Colored asterisks indicate statistical significance for different groups (ARSB = magenta, ChABC = green). (d) Graph showing average length of longest GAP-43^{+} regenerating axon. Statistical significance was determined by Student's t-test. * $p < 0.05$.
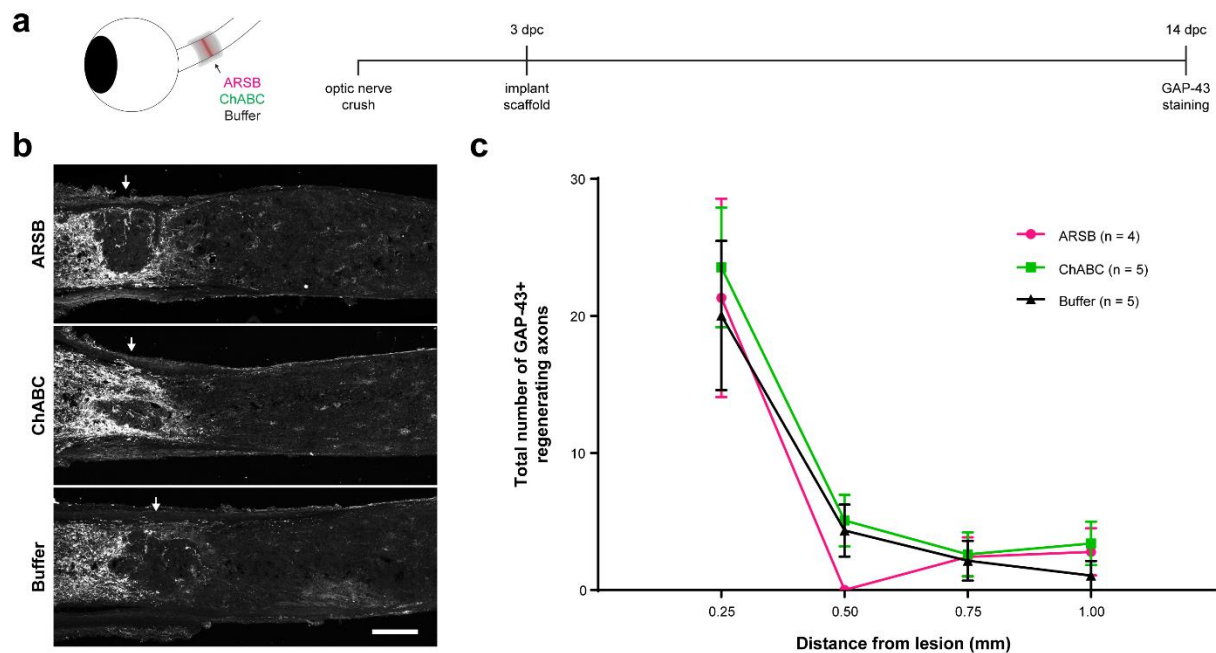
Figure 4.14. CSPG-targeting enzymes alone do not induce axon regeneration. (a) Experiment timeline and schematic diagram showing delivery of ARSB, ChABC, and control buffer to the lesioned optic nerve via implanted gelfoam scaffold. (b) Micrographs showing GAP-43-labeled optic nerves from mice treated with ARSB, ChABC, and control buffer. Arrows indicate lesion site. Scale bar = 100 µm. (c) Graph showing the number of regenerating axons at distances distal to the lesion site, displayed as mean +/- SEM.

The products of the reaction catalyzed by ARSB are not readily detectable by immunohistochemistry or Western blot; therefore, to specifically validate the penetration of ARSB into the optic nerve fibers, mice received ONC surgery, and gelfoam scaffolds soaked in 200 µg/mL His-Tagged ARSB or control buffer were implanted behind the eyes at the ONC lesion site (**Figure 4.15a**). Tissue collected at 1 dpc was analyzed by immunohistochemistry using anti-His antibody, and recovered scaffolds were tested for the presence of active ARSB. His-Tagged ARSB was detected in lesioned tissue using immunohistochemistry (**Figure 4.15b**), and active enzyme was detected from recovered scaffolds (**Figure 4.15c**). To further validate that the enzymes had successfully penetrated the optic nerve and modified CSPGs, I stained ChABC-treated samples with the antibody BE-123, which recognizes the "stubs" produced on proteoglycans by ChABC digestion of the GAG chains (**Figure 4.16a**). Immunohistochemistry analysis revealed significantly more BE-123 immunoreactivity in ChABC-treated nerves (**Figure 4.16a-b**), while Western blot analysis of non-lesioned sham control tissue treated with ChABC revealed BE-123 signal exclusively in nerve segments exposed to ChABC-loaded scaffolds (**Figure 4.16c**). Together, these observations establish that the enzymes released from the scaffold penetrate the tissue and digest GAG chains.
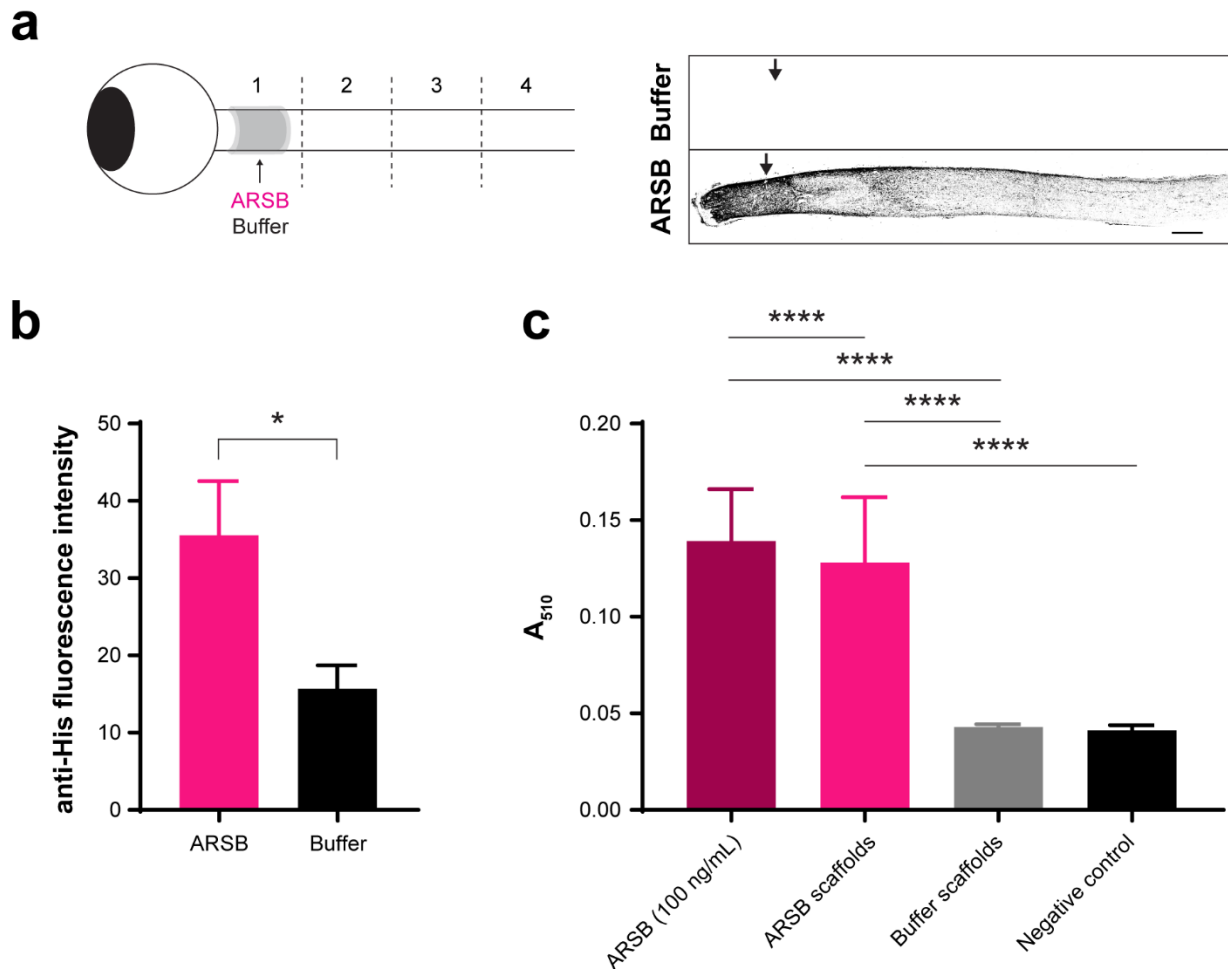
Figure 4.15. Tagged ARSB penetrates the optic nerve. (a) Schematic diagram showing delivery of ARSB or control buffer to lesioned optics nerve via implanted gelfoam scaffold. Optic nerves were dissected at 1 dpi and divided into four segments (#1-4). Micrographs showing thresholded images of lesioned optic nerves treated with ARSB-His or buffer and stained with anti-His antibody. Arrows indicate lesion site. Scale bar = 200 µm. (b) Graph showing quantification of anti-His fluorescence intensity measured from insets centered at the lesion site. Statistical significance was determined by Student's t-test. * $p < 0.05$. (c) Graph showing ARSB activity of recovered gelfoam scaffolds compared with 100 ng/mL stock control. Statistical significance was determined by Student's t-test. **** $p < 0.0001$.
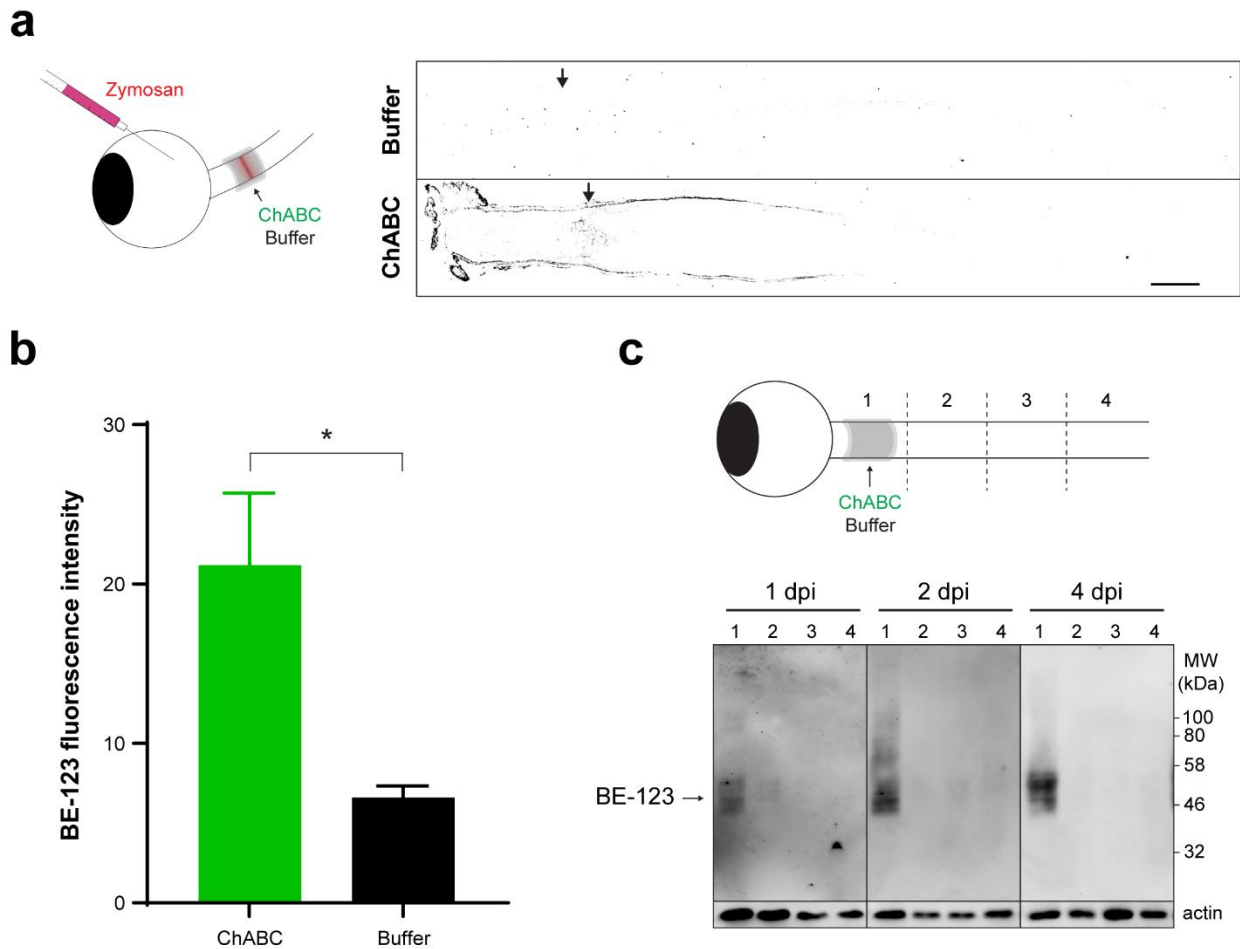
Figure 4.16. ChABC penetrates the optic nerve and modifies GAG chains. Zymosan was delivered to the retina via intravitreal injection and ARSB, ChABC, and control buffer were delivered to the lesioned optic nerve via implanted gelfoam scaffolds. (a) Schematic diagram showing delivery of ChABC or buffer to lesioned optic nerves via implanted gelfoam scaffold. Micrographs showing thresholded images of lesioned optic nerves treated with ChABC or buffer and stained with BE-123. Arrows indicate lesion site. Scale bar = 200 µm. (b) Graph showing quantification of BE-123 fluorescence intensity measured from insets centered at the lesion site. Statistical significance was determined by Student's t-test. * $p < 0.05$. (c) Schematic diagram showing delivery of ChABC to non-lesioned optics nerve via implanted gelfoam scaffold. Optic nerves were dissected at 1, 2, and 4 dpi and divided into four segments (#1-4). Western blot analysis showing enzyme-treated optic nerve segments stained with anti-BE-123 "stub" antibody.

4.2.6 | ARSB promotes axon regeneration with an extended therapeutic window

The duration of the regeneration enhancing effects of ARSB was assessed by measuring axon regeneration at early and late time points. At 7 dpc, only 4 days after implantation of the gelfoam scaffolds, a small but significant (p = 0.0149) increase in the number of axons navigating through the lesion site was already detectable in the ARSB-treated group compared with the buffer control (axons at 0.50 mm distal to the lesion [mean±SE]: 69.2±12.3 and 16.0±8.9, respectively) (**Figure 4.17a-d**). By 28 dpc, regenerating axons were found extending as far as 4.0 mm beyond the lesion site, to the optic chiasm entry point (**Figure 4.17e-g**). There was a significant (p = 0.0002) increase in the number of axons in ARSB-treated animals versus buffer-treated controls (axons at 0.25 mm distal to the lesion [mean±SE]: 568±96.3 and 273±63.0, respectively). The enhancing effect of ARSB treatment appeared to be concentrated at distances proximal to the lesion site (0.25-1.50 mm). At distances beyond 1.50 mm, there was relatively little difference between the ARSB-treated and buffer-treated groups (**Figure 4.18a-b**). I isolated this effect by subtracting the number of regenerating axons in the Zymosan/buffer groups from those in the Zymosan/ARSB groups (**Figure 4.18c**). ARSB strongly increased the number of axons regenerating through the lesion site but did not appear to substantially extend the distances of axons that were already regenerating.
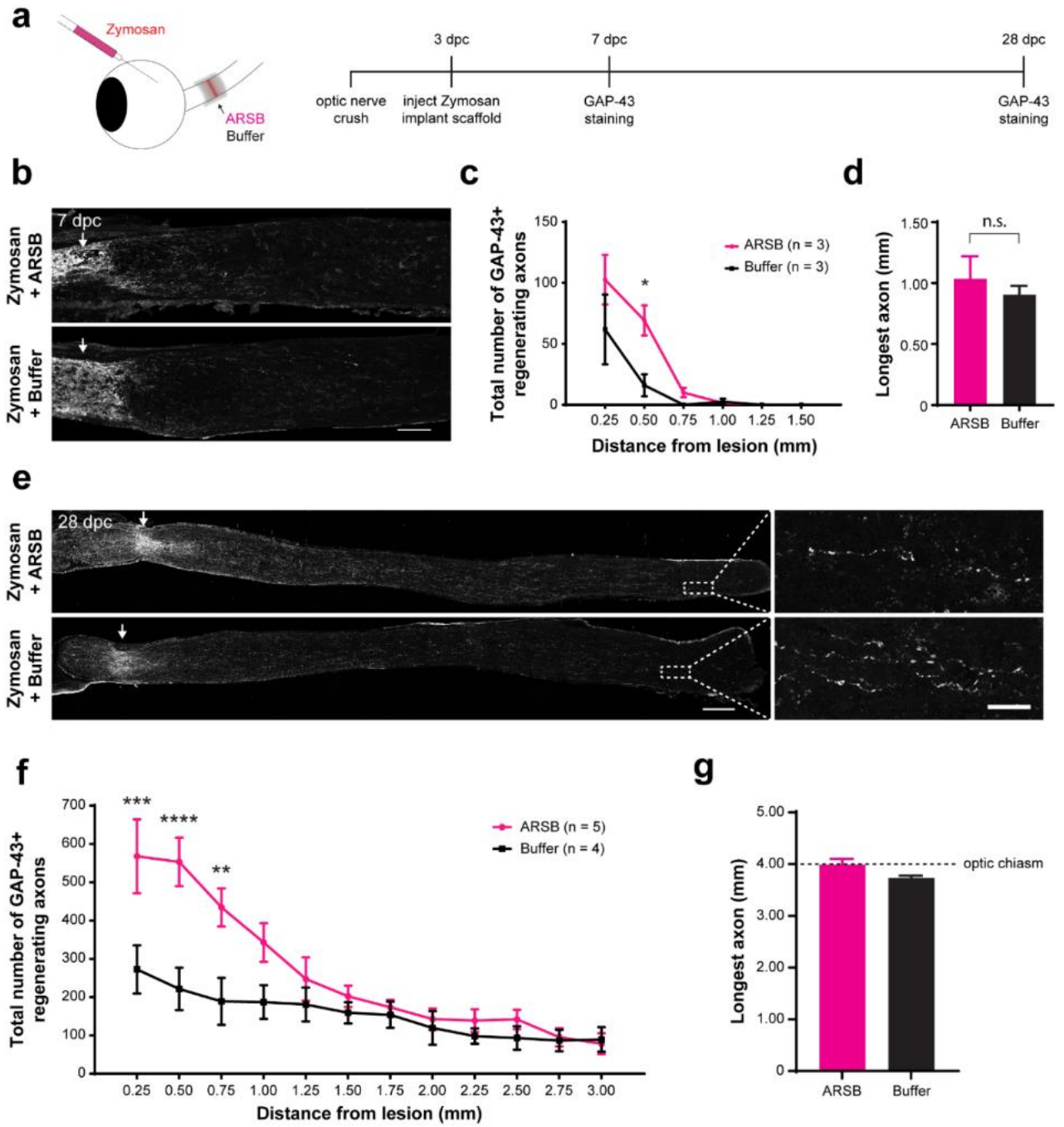
Figure 4.17. ARSB enhances axon regeneration over an extended therapeutic window.
(a) Experiment timeline and schematic diagram showing intravitreal injection of Zymosan and CPT-cAMP and delivery of ARSB and control buffer to the lesioned optic nerve via implanted gelfoam scaffold. (b) Micrographs showing GAP-43-labeled optic nerves from mice treated with Zymosan/CPT-cAMP and gelfoam scaffolds loaded with ARSB or a control buffer. Arrows indicate lesion site. Scale bar = 200 µm. (c) Graph showing the number of regenerating axons at distances distal to the lesion site, displayed as mean +/- SEM. Statistical significance was determined by two-way ANOVA with Bonferroni post-hoc test for multiple comparisons. * $p < 0.05$. (d) Graph showing length of the longest regenerating axon, displayed as mean +/- SEM. Statistical significance was determined by Student's t-test. (e) Micrographs showing GAP-43-labeled optic nerves from mice treated with intravitreal injections of Zymosan and gelfoam scaffold loaded with ARSB or a control buffer. Arrows indicate lesion site. Scale bar = 200 µm. (f) Graph showing the number of regenerating axons at distances distal to the lesion site, displayed as mean +/- SEM. Statistical significance was determined by two-way ANOVA with Bonferroni post-hoc test for multiple comparisons. ** $p < 0.005$, *** $p < 0.001$, **** $p < 0.0001$. (g) Graph showing length of the longest regenerating axon, displayed as mean +/- SEM. Statistical significance was determined by Student's t-test.
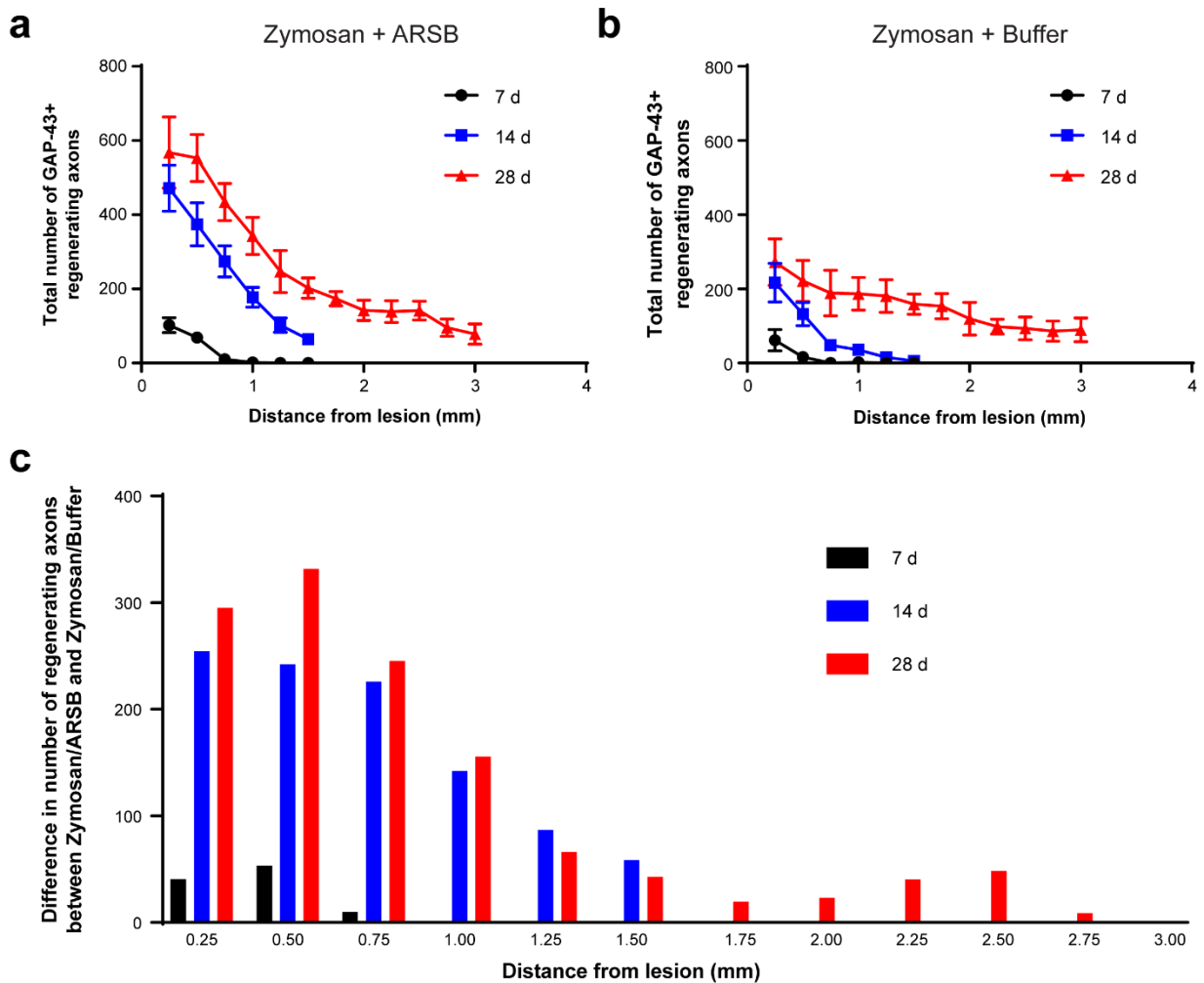
Figure 4.18. ARSB strongly enhances axon regeneration proximal to the lesion site. (a-b) Graphs showing the number of regenerating axons at distances distal to the lesion site, displayed as mean +/- SEM. Data were collected from separate cohorts of mice where regeneration was quantified at 7, 14, and 28 days following ONC. (c) Graph showing the average increase in regenerating axons for each measured distance and time point, calculated by subtracting the number of axons in the buffer-treated group from the number of axons in the ARSB-treated group.

4.2.7 | ARSB does not alter the astrocytic scar or perineuronal nets

To determine whether treatment with ARSB alters glial cells at the lesion site, tissue from enzyme-treated nerves was stained with GFAP and Iba1. Neither ARSB nor ChABC treatment disrupted formation of the astrocytic scar. The area delineated by GFAP$^+$ astrocytes decreased over time but was not significantly different between treatment groups at any time point (**Figure 4.19c-d**). Correspondingly, the total GFAP immunoreactivity increased from 7 to 28 dpc as astrocytes repopulated the glial scar region, but no differences were observed between treatment groups (**Figure 4.19e**). Both ChABC and ARSB increased Iba1 immunoreactivity relative to the buffer control (fluorescence intensity [mean±SE]: 21.7±2.95, 12.9±1.71, and 6.96±1.79, respectively), but ChABC elicited significantly ($p < 0.05$) higher Iba1 immunoreactivity than ARSB (**Figure 4.19a-b**).

In addition to their deposition in the glial scar, CSPGs are a major component of PNNs, structures that limit synaptic plasticity in the brain and spinal cord but are not present in the optic nerve. ChABC is known to disturb PNNs and alter plasticity in the visual cortex (Pizzorusso et al. 2002). To evaluate whether ARSB alters CSPG structure beyond the selective cleavage of 4S groups, we incubated post-fixed mouse brain tissue sections with ARSB (1 mg/mL), ChABC (≥ 20 µg/mL), or buffer control, and detected PNNs with *Wisteria floribunda* agglutinin (WFA). ChABC completely eliminated WFA-stained PNNs (**Figure 4.20**). However, incubation with ARSB left PNNs intact, with no observable differences from PNNs in buffer-treated brain tissue (**Figure 4.20**).
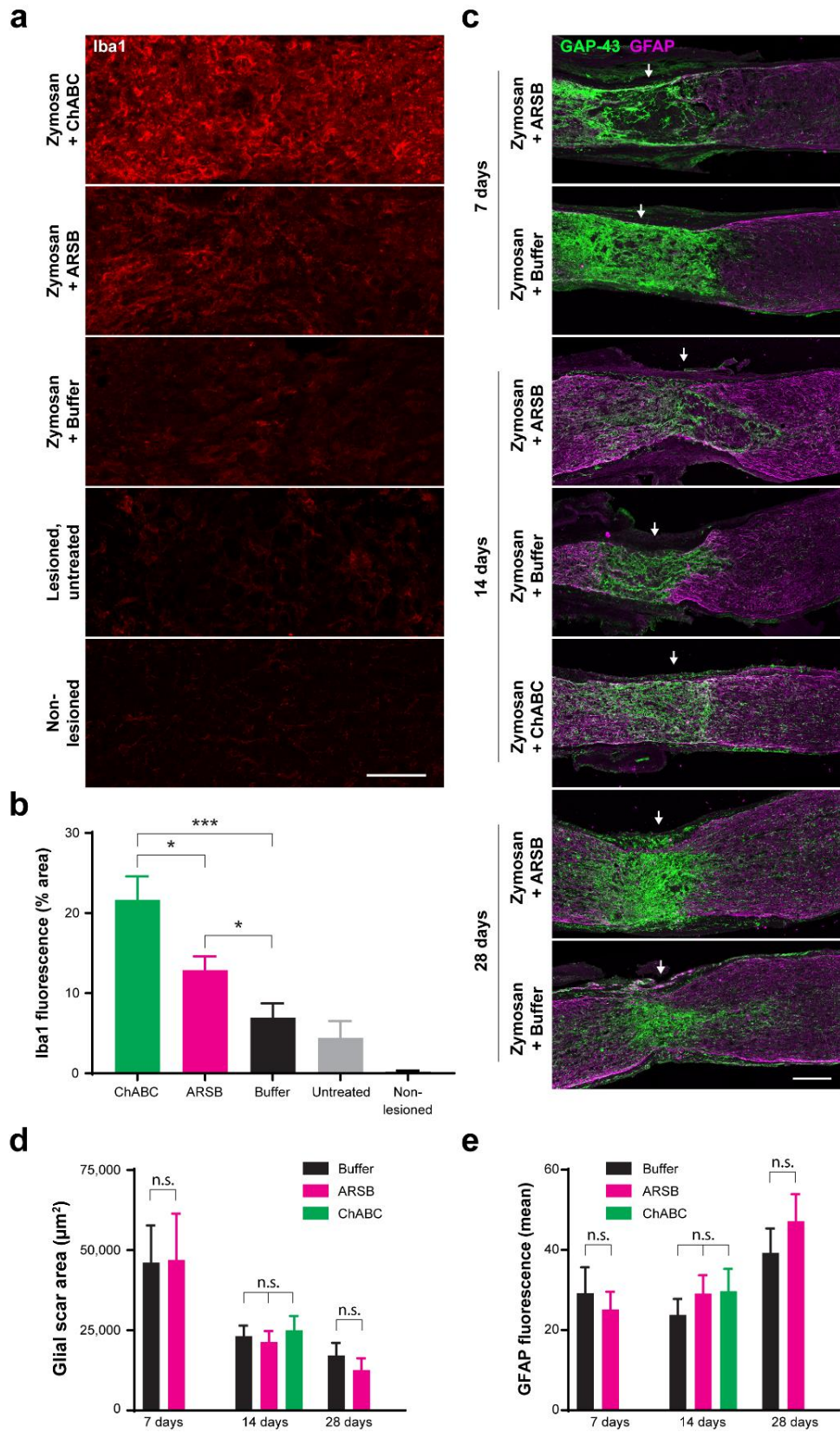
Figure 4.19. ARSB provokes muted immune response but does not alter astrocyte reactivity, glial scar size, or association of regenerating axons with astrocyte processes. (a) Micrographs showing Iba1 immunostaining at the optic nerve crush site for samples treated with Zymosan/CPT-cAMP and ChABC, Zymosan/CPT-cAMP and ARSB, Zymosan/CPT-cAMP and a control buffer, no treatment, and non-lesioned controls. Scale bar = 50 µm. (b) Graph showing quantification of Iba1 fluorescence intensity measured as % area of thresholded insets centered at the lesion site. Statistical significance was determined by Student's t-test. * $p < 0.05$, *** $p < 0.001$. (c) Micrographs showing GFAP and GAP-43 immunostaining at the optic nerve crush site for samples treated with Zymosan/CPT-cAMP and either ARSB, ChABC, or a control buffer and analyzed at 7, 14, and 28 dpc. Arrows indicate lesion site. Scale bar = 100 µm. (d) Graph showing quantification of glial scar size measured as the area delineated by GFAP$^+$ astrocytes at the optic nerve crush site. Statistical significance was determined by Student's t-test. (e) Graph showing quantification of GFAP immunoreactivity at the optic nerve crush site. Statistical significance was determined by Student's t-test.
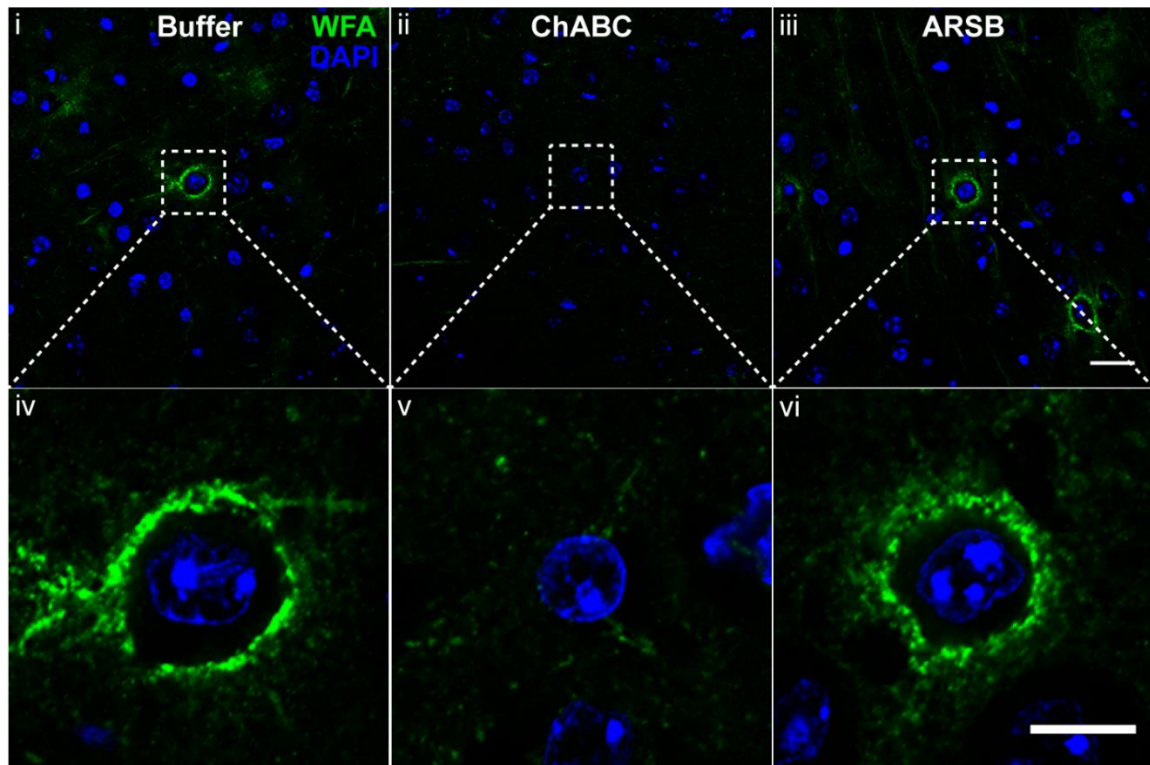
Figure 4.20. ARSB preserves CSPG-rich perineuronal net structure. Micrographs showing mouse cortex from tissue incubated with control buffer, ChABC, or ARSB for 8 h at 37°C and stained with WFA to detect perineuronal nets. Images (iv), (v), and (vi) are insets of (i), (ii), and (iii), respectively. Scale bar = 25 µm, insets 10 µm.

4.3 | DISCUSSION

The glial scar is considered a major impediment to axonal regeneration in the optic nerve and elsewhere in the CNS. Here, I have shown that the injured optic nerve develops a glial scar rich in CSPGs, including the 4S motif, and that these CSPGs inhibit the extension of regenerating RGC axons. I show evidence that the human enzyme ARSB promotes neurite growth in culture without altering production or secretion of GAG chains. I then demonstrate that ARSB enhances the regeneration of RGC axons following optic nerve injury. The treatment is robustly effective even when administered 3 days after injury, an important consideration for translational therapies. Enhanced regeneration was evident as early as 7 days post ONC and remained significant at 28 days, illustrating an extended therapeutic window from a single treatment. ARSB is active *in vivo*, provokes less Iba1 immunoreactivity than ChABC, and preserves perineuronal structures that depend on intact GAG chains. Taken together, these findings demonstrate that the 4S motif at the non-reducing end of CS GAG chains plays a critical role in mediating the inhibitory actions of CSPGs. Given the clinical approval for ARSB as an enzyme replacement therapy in human patients, my evidence that ARSB enhances axon regeneration in the optic nerve means that future treatments could readily combine ARSB with intrinsic approaches to achieve robust regeneration of damaged or degenerated axons in the CNS.

4.3.1 | CSPG deposition is a key source of axon growth inhibition in the glial scar

The formation of a glial scar, including deposition of sulfated proteoglycans, is well documented in the brain and spinal cord (Bradbury et al. 2002; Bradbury & Carter 2011; Yi et al. 2012; Burnside & Bradbury 2014; Galtrey & Fawcett 2007). Studies that have suggested that CSPGs are upregulated after ONC have not quantified this phenomenon or explored its time course (Brown et al. 2012; Sengottuvel et al. 2011; Sellés-Navarro et al. 2001). Others have sought to circumvent CSPG-mediated inhibition by inactivating key signaling pathways that are initiated when CSPG ligands interact with their RPTP receptors on neurons. For instance, evidence shows that suppressing the Rho/ROCK pathway, which is activated by exposure to CSPGs, enhances regeneration of RGC axons after ONC (Fischer et al. 2004; Lingor et al. 2007). Likewise, inhibiting EGFR, another downstream effector of CSPGs, promotes RGC axonal regeneration (Koprivica et al. 2005). However, there is a dearth of comprehensive, quantitative evidence of CSPG deposition within the lesion area

following ONC. Similarly, the evidence that exists fails to discriminate between different sulfation patterns. Therefore, I sought to identify whether and to what extent 4S is expressed among the CSPGs in the glial scar. I analyzed not only the mouse optic nerve, but also rat optic nerve and mouse and rat spinal cord, to ensure that my findings were generally translatable between rodent species and across different types of CNS injury.

I found that CSPGs, and 4S GAGs in particular, were significantly elevated after mouse ONC, reaching peak levels at 7 dpc. This was similarly true of samples from injured rat optic nerve, mouse spinal cord, and rat spinal cord. The precise timing of CSPG deposition appears to differ slightly between species: elevated levels of CS-56 and 2H6 immunoreactivity were first evident at earlier time points in the rat optic nerve than in the mouse. The association of CSPGs with astrocytes and microglia was similar across conditions, suggesting that the multicellular sources of these inhibitory proteins are mostly conserved. The sustained elevation of CSPGs at 21 dpc suggests that the optic nerve environment remains hostile to axon growth for extended periods after injury. I observed that RGC axons appeared to terminate in areas of high CSPG expression in optic nerve lesions. Axonal growth cones exhibited dystrophic morphology, forming the characteristic endbulbs indicative of stalled growth. Notably, sites at which axons terminated in association with CSPG deposition contained visibly high levels of 4S immunoreactivity.

Cleaving 4S from the non-reducing ends of GAG chains with ARSB, or completely digesting GAG chains with ChABC, both enhanced axon regeneration without disrupting formation of the astrocytic scar. This supports a critical role for CSPG deposition, rather than scar formation *per se*, as a primary cause of axon growth inhibition. This is consistent with findings that ablating astrocytic scar formation without reducing CSPG levels does not lead to spontaneous regeneration of axons (Anderson et al. 2016; Silver 2016). Conversely, blocking the formation of neurotoxic A1 astrocytes (Liddelow et al. 2017), or the transformation of reactive astrocytes into scar-forming astrocytes, which express elevated levels of CSPG-related transcripts (Hara et al. 2017), were found to significantly enhance cell survival and axon regeneration, respectively. My findings support the notion that many aspects of astrogliosis are in fact essential to preserving tissue integrity and promoting survival of injured neurons, and that it is a specific component of this response—namely, the deposition and sustained expression of inhibitory 4S GAGs—that opposes axonal regeneration.

Accumulating evidence that sulfation is a primary determinant of CSPG behavior raises questions of which of the putative CSPG receptors bind to different sulfated motifs, and

145

whether these interactions trigger different or overlapping signaling cascades. Of the vertebrate type-IIa RPTP receptors—LAR, RPTPσ and RPTPδ—RPTPσ and LAR are known to bind CSPGs with high affinity. This binding appears to be dependent on interactions with GAG chains, as it can be disrupted by treatment with ChABC (Shen et al. 2009; Fisher et al. 2011). In mice where RPTPσ or LAR receptors were knocked out, isolated dorsal root ganglion neurons were less sensitive to a mixture of CSPGs *in vitro*, and axon regeneration after a spinal cord injury was improved *in vivo* (Fisher et al. 2011; Lang et al. 2014). Sulfation appears to be an integral component of these ligand-receptor interactions. Neurons from RPTPσ$^{-/-}$ mice fail to bind to 4S or 6S CSPGs, but will still bind DS, 4,6S, and 2,6S (Dickendesher et al. 2012). The dynamic flexibility in the interaction between receptors and their proteoglycan ligands has already been demonstrated in one context: it is known that the receptor RPTPσ interacts with both CSPGs and HSPGs, possibly via different binding sites, and that binding of RPTPσ to CSPGs impedes axonal growth, whereas binding to HSPGs is growth-permissive. This flexibility may extend to sulfation patterns as well, although substantial future work will be required to investigate this possibility.

4.3.2 | Delayed application of ARSB promotes regeneration

Most experimental therapies that stimulate RGC axon regeneration involve interventions at the time of injury or, in the case of many gene therapies, several weeks prior to injury (Buch et al. 2008). While such studies are immensely valuable for identifying therapeutic targets and elucidating mechanisms of RGC axon regeneration, they are not readily translatable to human patients. In humans, CNS tracts are often damaged by acute trauma, such as spinal cord injury, traumatic brain injury, and stroke, or by progressive neurodegenerations, as in the case of glaucoma and multiple sclerosis. In such cases, intervening before or even immediately following the injury is often not possible. Therefore, identifying therapies that effectively promote regeneration even after a delay is a top priority for clinically translatable research. I found that delivery of ARSB in conjunction with Zymosan/CPT-cAMP significantly enhanced RGC axon regeneration when administered 3 days after ONC, making a strong case for its future clinical viability.

Delaying ARSB treatment may confer additional advantages beyond clinical considerations such as time of treatment. The mechanisms of CSPG expression and inhibition of neurons have been shown, in some contexts, to be time-sensitive, with intervention more

effective after a delay than immediately following an insult. One study has argued that CSPG synthesis in the acute phase (0-2 dpi) may actually promote, rather than inhibit, recovery. Rolls et al. (2008) blocked CSPG synthesis immediately after spinal cord injury in mice and found that axon regeneration and functional recovery were impaired, whereas blocking synthesis in the subacute phase (2-7 dpi) enhanced regeneration and recovery. This argues for a potential role of CSPGs in the lesion area for reducing damage and/or promoting growth. Some possible explanations for such a role are described below.

4.3.3 | ARSB preserves perineuronal structures

Some studies have proposed a role for CSPGs as regulators of microglia and macrophage localization and phenotype. After injuries to the mature CNS, CSPGs have been shown to recruit blood-borne monocytes and bias macrophages toward a resolving phenotype (Shechter et al. 2011), and to regulate the spatial organization of microglia and macrophages and promote neurotrophic factor production by resident microglia after spinal cord injury (Rolls et al. 2008; Shechter et al. 2009). Stripping CSPGs of their GAG chains, e.g. by treatment with ChABC, may impede these repair functions. The presence of CSPGs during the acute phase of injury also alters monocyte phenotype and is linked to the production of the matrix metalloprotease MMP-13, which degrades CSPGs, suggesting a potential feedback loop wherein CSPGs regulate immune cells before indirectly catalyzing their own destruction (Rolls et al. 2008). Taken together, this evidence argues for the usefulness of an intervention that renders CSPGs more permissive to axon extension without degrading GAG chains. Selectively modifying sulfation with ARSB could reduce GAG-mediated inhibition of neurons without disrupting their interactions with other cells.

To demonstrate that ARSB preserves perineuronal structures composed of CSPGs, I analyzed the effects of ARSB treatment on PNNs in the mouse cortex. It has been known since the work of Hubel and Wiesel that the visual cortex requires input from retinal neurons in order to achieve functional organization (Wiesel & Hubel 1963). The discovery of critical periods, during which cortical networks reorganize according to the intensity and selective patterns of neural activity, arose from Hubel and Wiesel's observations in the visual system and has since been expanded to many other domains of nervous system development. The visual cortex remains an essential system for studying the role of the ECM in regulating neural plasticity. In the early postnatal period, networks in the visual cortex respond to and

organize themselves around the inputs of retinal neurons (Berardi et al. 2003). As development continues, the expression of CSPGs in the retina and optic pathways progressively declines, and in the thalamus, CSPGs drop to barely detectable levels within the third postnatal week in rats (Vitellaro-Zuccarello et al. 2001). The subsequent emergence of CSPGs in the cortex signals the end of the critical period (Hockfield et al. 1990). At this stage, CSPGs become restricted to PNNs, which cluster around the soma and dendrites of GABAergic interneurons (Wang & Fawcett 2012). The formation of PNNs coincides with a sustained suppression of cortical plasticity. Repeated injections of ChABC into the visual cortex of adult rats caused reductions in PNNs and led to a pronounced increase in ocular dominance plasticity (Pizzorusso et al. 2002). ChABC injection alleviated other impairments associated with monocular deprivation in rats, including reduced receptive field size, low visual acuity, and loss of dendritic spine density (Pizzorusso et al. 2006). A similar phenomenon was observed in the superior colliculus, where ChABC injection degraded GAG chains and increased the sprouting of intact retinal axons (Tropea et al. 2003). Intriguingly, the sulfation pattern of brain CSPGs appears to play an important role in visual cortex plasticity. Transgenic mice engineered to overexpress human C6ST-1, the enzyme that catalyzes addition of 6S to CS GAG chains, exhibited a decreased ratio of 4S to 6S GAGs (Miyata et al. 2012). These mice underwent normal visual development, but showed a reduced number of PNNs during and after the critical period, despite no observed reductions in the total amount of CSPG core proteins, as well as lower levels of Otx2 (Miyata et al. 2012). C6ST-1 overexpressing neurons failed to undergo spike shortening at levels comparable to those in neurons in wildtype mice, indicating that elevated 6S in the visual cortex may prolong mechanisms linked to synaptic plasticity (Miyata et al. 2012). These observations provide a strong incentive for studying the differential effects of ARSB and ChABC on PNNs.

When I treated mouse cortical tissue with ARSB and ChABC, I found that ChABC eliminated PNNs, whereas ARSB left PNNs intact. The fact that ARSB preserved PNN structures supports the argument that ARSB might be used to modify CSPGs in the glial scar while leaving their GAG chains intact, potentially freeing them to continue to regulate microglia and macrophage recruitment, although additional studies will be required to prove this definitively. My evidence also supports the idea that ARSB might be useful beyond studies of axon regeneration and in areas other than the optic nerve, with potential applications to investigations of neural plasticity, memory formation, and other processes dependent on PNNs or other CSPG microstructures. The ubiquity of CSPGs in the CNS

provides myriad opportunities for using ARSB, with its selective action on axon-growth-inhibiting C4S motifs, to alter the extracellular matrix and influence axonal growth and connectivity. I am currently collaborating with Dr. Panpan Yu, at Jinan University in China, to design *in vivo* experiments that will test the effects of ARSB injections in the mouse brain following controlled cortical injury. Our preliminary results show that injections of ChABC into the mouse cortex eliminate WFA[+] PNNs within the injection radius, whereas ARSB injections appear to preserve PNNs. Future studies will assess whether and how these enzymes alter plasticity and memory in mice by comparing the animals' performance on a set of behavioral assays.

4.3.4 | ARSB activity and mechanism

The precise mechanism of how ARSB modifies the inhibitory actions of GAG chains is unknown. ARSB did not reduce the total amount of sulfated GAG in the culture medium as detected by the anti-CS antibodies, suggesting that its effects are mediated by altering GAG chain sulfation. ARSB, a lysosomal enzyme, maintains its highest activity at acidic pH, raising the question of whether it can cleave sulfate groups from secreted CSPGs, or whether lysosomal uptake is required. Others in my laboratory have observed that ARSB cleaves 4S from extracellular GAG chains in culture medium, suggesting that its activity at neutral pH is sufficient to perform its sulfatase function. This was validated by my discovery that ARSB promotes regeneration of optic nerve axons when administered exogenously.

The advantages of ARSB over ChABC, while they exert equivalent pro-regenerative effects when administered at the site of an optic nerve lesion, are compelling. ARSB has relatively lower immunogenicity than ChABC *in vitro* (Yoo et al. 2013). ARSB has also been shown to maintain its activity longer *in vitro* than ChABC, implying a more extended therapeutic window (Yoo et al. 2013). While the durability of ARSB *in vivo* has not been characterized, studies have shown that ChABC injected directly into rat brains maintains detectable activity levels for at least 10 days (Lin et al. 2007), and that even low levels of ChABC activity can suppress CSPG levels *in vivo* for periods of weeks (Chau et al. 2004; Hyatt et al. 2010), suggesting that ARSB may potentially last even longer. Unlike ChABC, ARSB is highly stable at physiological temperature and pH (Yoo et al. 2013). Crucially, ARSB is a human enzyme with approval for clinical use, meaning its transition from animal

models to human therapies will face fewer obstacles (Muñoz-Rojas et al. 2010; Harmatz et al. 2004; Harmatz 2005).

Another important distinction between ChABC and ARSB is that their enzymatic activity produces different byproducts. It has been observed that cleavage of inhibitory GAG chains by ChABC generates disaccharide byproducts that, intriguingly, seem to promote axon regeneration independently: administering CSPG disaccharide after spinal cord injury led to significant improvements in motor recovery (Rolls et al. 2008). This calls into question the assumption that ChABC promotes regeneration exclusively by reducing GAG-mediated axon growth inhibition. Instead, some of its effect may derive from the presence of these growth-promoting disaccharide products.

One challenge of studying ARSB *in vivo* is the lack of a straightforward readout for its enzymatic activity. I used the production of CSPG "stubs" stripped of their GAG chains by ChABC, which are detectable by antibodies such as BE-123, as an indicator for the delivery of active enzyme from implanted gelfoam scaffolds and penetration into the optic nerve fibers. The fact that ARSB and ChABC enhanced RGC axon regeneration equally implies that ARSB was present and active within the optic nerve, but future studies will be required to characterize the efficiency and thoroughness of its actions *in vivo*.

4.3.5 | Combining extrinsic and intrinsic stimuli enhances axon regeneration

Treating lesioned optic nerves with ARSB or ChABC alone failed to enhance regeneration, but combining them with Zymosan/CPT-cAMP promoted significantly greater regeneration than the intrinsic treatment alone. Most studies demonstrating long distance regeneration of RGC axons achieve their effects by modifying the intrinsic state of RGCs: knocking out the tumor suppressor PTEN (Park et al. 2008), delivering growth factors (Sieving et al. 2006), stimulating inflammatory pathways (Yin et al. 2003), enhancing the endogenous activity of RGCs (Lim et al. 2016), chelating neurotoxic ions in the retina (Li et al. 2017), and various combinations thereof. In Chapter 5, I describe my efforts to combine multiple intrinsic therapies with delivery of ARSB to the optic nerve crush lesion site to stimulate long-distance regeneration of RGC axons.

Despite these advances, however, knowledge of how regenerating axons traverse the glial scar and navigate the growth-inhibitory microenvironment is incomplete. Studies that have examined the three-dimensional growth patterns of regenerating RGC axons consistently find that axons induced to regenerate via intrinsic manipulations display highly

irregular and aberrant growth patterns (Luo et al. 2013; Bray et al. 2017; Fischer et al. 2017). Understanding how axons respond to their extrinsic microenvironment, particularly the sulfated GAG chains within the glial scar, will be vital to future efforts to stimulate robust long-distance regeneration of retinal neurons and successful innervation of visual targets in the brain.

4.3.6 | Summary

I analyzed optic nerve and spinal cord lesions in mice and rats and observed a common response to injury, where reactive astrocytes, activated microglia, and macrophages begin to form a glial scar at the lesion site, depositing elevated levels of CSPGs, including the highly inhibitory 4S motif. The presence of 4S in the lesioned tissue blocked RGC axons from regenerating beyond the crush site and led to growth cone collapse and the formation of dystrophic endbulbs. Directly targeting 4S at the non-reducing ends of GAG chains with ARSB, and digesting GAG chains entirely with ChABC, significantly enhanced the extension of RGCs induced to regenerate by intravitreal injection of Zymosan and CPT-cAMP. This enhancement was notable for several reasons:

1) The therapy was administered at a delay, 3 days post injury. The effects of the intervention were visible across a wide therapeutic window, from 7 d to as late as 28 d of continued growth.

2) ARSB, a human enzyme, produced less immunoreactivity for Iba1, a marker of activated microglia and macrophages, implying that it may be less immunogenic than ChABC, a bacterial enzyme.

3) ARSB did not directly modify astrocytes or alter the formation of the astrocytic scar in the optic nerve, and preserved the structure of PNNs in the cortex, indicating its specificity to the inhibitory 4S epitope rather than global changes to CSPGs more broadly.

Together, these findings point to a potential therapeutic strategy that selectively targets 4S GAGs in CNS lesions, reversing the inhibitory actions of CSPGs without preventing them from engaging in other regulatory or potentially growth-promoting functions. Future studies will need to address the need for ARSB to be paired with an intrinsic stimulus, as Zymosan and many other experimental pro-regenerative stimuli are unsuitable for clinical use. Despite these challenges, this work lays a foundation for translational research on the ability of a

clinically approved human enzyme to facilitate regeneration and functional recovery of CNS pathways.

CHAPTER 5: COMBINING INTRINSIC AND EXTRINSIC STIMULATION TO ACHIEVE LONG-DISTANCE RGC AXON REGENERATION

5.1 | INTRODUCTION

Early evidence that adult mammalian CNS neurons are capable of regenerating their axons was obtained when researchers found that axons extended into peripheral nerve grafts implanted at sites of injured CNS tissue, including the brain (Benfey & Aguayo 1982), spinal cord (Richardson et al. 1980; David & Aguayo 1981), and optic nerve (So & Aguayo 1985). Over the following decades, it was discovered that intrinsic manipulations of neurons, such as inactivation of Rho, a GTPase that participates in the signaling cascade activated by axon-inhibiting CSPGs, also stimulate low levels of axon regeneration (Lehmann et al. 1999). In recent years, a multitude of experimental therapies have been developed that either modify the intrinsic state of CNS neurons or remove growth-inhibiting obstacles from their environment. Many of these interventions activate or suppress discrete molecular pathways, contributing to a body of evidence that suggests axon growth depends on many overlapping signaling systems (He & Jin 2016). Achieving robust regeneration of CNS tracts is therefore likely to require combinatorial treatments that address a host of both intrinsic and extrinsic factors. Of the treatments that have purported to achieve successful long-distance axon regeneration in the optic nerve, essentially all have utilized multiple intrinsic stimuli (de Lima et al. 2012; Lim et al. 2016; Kurimoto et al. 2010). None, however, have combined intrinsic manipulations with direct modification of the extrinsic microenvironment, such as targeting the growth-inhibiting glial scar. In this chapter, I sought to develop a therapy that activates multiple intrinsic growth pathways in combination with using ARSB to reduce CSPG-mediated inhibition of axon extension through the glial scar, with the goal of stimulating regeneration of retinal neurons through the optic chiasm to reach central visual targets in the brain.

5.1.1 | Zymosan and CPT-cAMP promote regeneration by activating inflammatory pathways

One of the early intrinsic mechanisms that successfully stimulated regeneration of RGC axons was the use of lens injury to provoke an inflammatory response in the retinas of

rats (Leon et al. 2000; Fischer et al. 2001). Creating a small puncture wound in the lens with an injecting needle enhanced RGC survival in the retina and promoted mild levels of axon regeneration in the optic nerve. These early studies confirmed that inflammatory pathways were responsible for this effect by injecting Zymosan, a bacterial cell wall protein known to stimulate inflammation, into the vitreous. Zymosan injection was sufficient to promote RGC survival and axon regeneration even in the absence of lens injury (Leon et al. 2000). Successive studies further clarified the role of inflammation in promoting RGC axon regeneration. Zymosan activates macrophages in the rat retina, and it was discovered that macrophage-secreted factors are at least partially responsible for Zymosan's enhancement of axon regeneration (Yin et al. 2003). The protein oncomodulin (Ocm) was identified as a macrophage-derived factor that promotes RGC survival and axon regeneration in rats, even in the absence of other treatments (Yin et al. 2006). The binding of Ocm to rat RGCs requires cyclic adenosine monophosphate (cAMP), and Ocm activates a signaling cascade that includes Ca^{2+}/calmodulin kinase, suggesting that cAMP and calcium are required for its pro-regenerative effect (Yin et al. 2006). Injecting both Ocm and cAMP led to higher sustained levels of Ocm in the mouse retina and doubled the number of regenerating RGC axons in the optic nerve (Kurimoto et al. 2010). A subsequent study confirmed that intraocular inflammation stimulates release of Ocm from activated macrophages in both mice and rats, and that blocking the binding of Ocm to its receptor abolishes its positive effects on RGCs (Yin et al. 2009). It was later shown that specific downstream signaling pathways are required for inflammation-induced regeneration. Injection of lipopolysaccharide (LPS), an inflammatory agent, failed to stimulate regeneration of RGC axons (Baldwin et al. 2015). Intravitreal injection of curdlan, a form of β(1, 3)-glucan that is considered the active ingredient of Zymosan, stimulated regeneration via dectin-1 signaling, and knockout mice lacking dectin-1 failed to exhibit axon regeneration following Zymosan injection (Baldwin et al. 2015). Together, these findings describe an inflammation-induced pathway for stimulating the regeneration of injured RGC axons. Because Zymosan is one of the earliest, most widely used, and most reliably effective regenerative stimuli in the visual system, and because obtaining and administering Zymosan and CPT-cAMP is straightforward and relatively low-cost, I used Zymosan as the primary intrinsic stimulus for the majority of my optic nerve regeneration experiments (see Chapter 4).

5.1.2 | The hM3Dq DREADD receptor enhances the endogenous activity of RGCs

Evidence from developmental studies suggests that visual experience is required to establish sophisticated visual processing networks in the brain (Wiesel & Hubel 1963). A similar phenomenon has been observed with somatosensory stimulation, with experience-dependent synaptic plasticity observed in the mouse barrel cortex (Trachtenberg et al. 2002). It follows that the stimulated activity of RGCs may therefore play a critical role in their growth, navigation, formation of synapses with central targets, and strengthening of synaptic connections. Cultured RGCs do not spontaneously extend axons, but will do so when exposed to electrical stimulation that mimics physiological levels of activity (Goldberg, Espinosa, et al. 2002). Conversely, blocking electrical activity with tetrodotoxin leads to RGC death *in vitro* (Lipton 1986). The retina contains a subpopulation of ipRGCs that express melanopsin, allowing them to respond directly to light stimulation (Provencio et al. 2000; Foster et al. 1991). Infection of mouse RGCs with a virus carrying melanopsin resulted in an enhancement of axon regeneration after ONC (Li et al. 2016). Melanopsin overexpression enhanced the responsiveness of RGCs to light stimulation. Elevated levels of mTOR complex 1 (mTORC1) were observed in these cells, suggesting that electrical stimulation promotes RGC axon regeneration in an mTOR-dependent manner (Li et al. 2016). This appears to suggest that artificially overexpressing melanopsin might promote regeneration of RGC axons in a manner similar to direct stimulation of mTOR pathways. However, it remains unknown whether other subtypes, rather than just ipRGCs, have the capacity to process opsin proteins. It is possible, for instance, that only ipRGCs possess the biomachinery required to recycle opsin photopigments, and that introducing melanopsin to other RGC subtypes would have a muted effect, if any, thereby limiting the long-term usefulness of an intervention that ultimately provides benefit to only a small fraction of the total RGC population. The study does, however, convincingly emphasize the potential link between elevating endogenous activity levels in RGCs and improving their capacity for regenerating their axons following injury.

RGC activity can be chemogenetically increased by expressing designer receptors exclusively activated by designer drugs (DREADDs) such as hM3Dq (human M3 muscarinic DREADD receptor coupled to Gq) (Urban & Roth 2015). In the presence of the ligand clozapine-N-oxide (CNO), hM3Dq enhances the basal activity of neurons (Urban & Roth 2015). Overexpression of virally-delivered hM3Dq in RGCs in conjunction with systemic delivery of CNO led to significant increases in axon regeneration after ONC (Lim et al.

2016). Intriguingly, exposing mice to high-contrast visual stimulation following ONC in the optic nerve of one eye and enucleation of the contralateral eye also promoted axon regeneration (Lim et al. 2016). These findings suggest that biased visual stimulation may be a useful non-invasive intervention to elevate RGC activity levels and promote axonal growth. Electrical stimulation therapy has already been applied to several ophthalmic diseases, including optic neuropathy and Best Vitelliform Macular Dystrophy, with improvements in visual acuity reported in several case studies (Fu et al. 2015). Transcorneal electrical stimulation also enhanced regeneration of RGC axons after ONC in rats (Miyake et al. 2007). In human patients with retinitis pigmentosa, a progressive neurodegenerative condition, RGCs in the central retina survive better than those in the periphery, possibly due to higher endogenous activity levels in the central retina (Santos et al. 1997). With these observations in mind, I chose to incorporate elevation of basal RGC activity via hM3Dq into my combinatorial therapy.

5.1.3 | shRNA against PTEN elevates mTOR activity

One of the most common targets of CNS regeneration therapies is the phosphatase and tensin homolog (PTEN) gene. PTEN is an upstream inhibitor of mammalian target of rapamycin (mTOR), the hub of a signaling pathway that controls cell growth and protein synthesis (Lipton & Sahin 2014) (**Figure 5.1**). PTEN, acting through the phosphoinositide 3-kinase (PI3K)-Akt-mTOR pathway, plays a central role in cell survival and proliferation (M. S. Song et al. 2012). Knocking down or suppressing PTEN activates the mTOR pathway, thereby promoting cell growth. Deletion of PTEN in a transgenic floxed mouse line led to enhanced survival and robust regeneration of RGC axons after optic nerve injury (Park et al. 2008). PTEN deletion and elevation of mTOR activity have since been incorporated into many combinatorial therapies that successfully stimulated robust, long-distance RGC axon regeneration (Sun et al. 2011; de Lima et al. 2012; Kurimoto et al. 2010; Bei et al. 2016; Lim et al. 2016). However, many of these therapies use transgenic mice, which can require substantial investment of time and resources, and may ultimately be less clinically translatable. I chose to use a short hairpin RNA (shRNA) that silences PTEN, developed by Dr. Amanda Barber using constructs from Dr. Zhigang He, in my therapy.
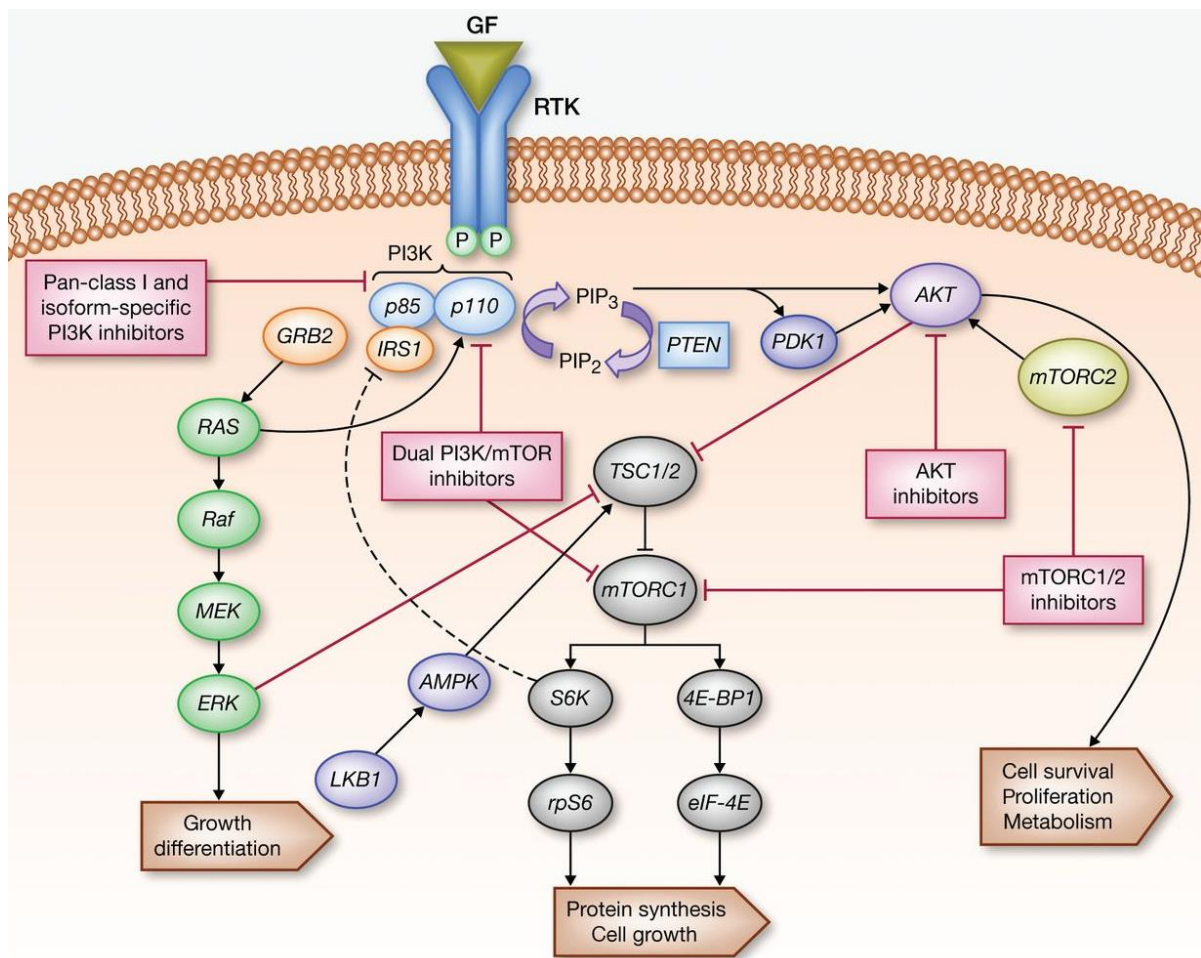
Figure 5.1. The PI3K-Akt-mTOR pathway leads to cell survival and proliferation.
Activation of PI3K catalyzes the conversion of PIP_2 to PIP_3. PIP_3 then prompts
phosphorylation of Akt, which leads to enhanced cell survival, growth, and proliferation via
mTOR activation. The reverse reaction is catalyzed by PTEN, which converts PIP_3 to PIP_2.
Feeding into the mTOR pathway, by activating PI3K or its subunits, or by suppressing
PTEN, leads to greater survival and growth of the targeted cells. Figure adapted from
(Dienstmann et al. 2014).

5.1.4 | The p110α subunit of PI3K elevates mTOR activity

PTEN dephosphorylates phosphatidylinositol-3,4,5-trisphosphate (PIP_3), thereby
reducing activation of PIP_3's downstream effectors 3-phosphoinositide-dependent kinase
(PDK) and Akt (Maehama & Dixon 1998). PI3K catalyzes the reverse reaction (M. S. Song
et al. 2012). Class IA PI3Ks consist of a p110 catalytic subunit that associates with a p85
regulatory subunit (M. S. Song et al. 2012) (**Figure 5.1**). Among Class IA PI3Ks (p110α,
p110β, and p110δ), those containing the p110α catalytic subunit are the most widely
expressed. Extensive work conducted by Dr. Richard Eva demonstrates that inhibitors of
p110α inhibit regeneration of axons in cultured mouse cortical neurons. With assistance from

Dr. Eva and Dr. Patrice Smith, I developed transgenic mice containing a cre-inducible hyperactive mutant (H1047K) form of the p110α subunit of PI3K. Preliminary studies performed by Dr. Patrice Smith using mice heterozygous for the p110α mutant suggested that hyperactive p110α may enhance RGC survival and axon regeneration. Therefore, I chose to evaluate the regenerative potential of homozygous p110α mutant mice. I also treated p110α mice with ChABC applied directly to the optic nerve lesion site to reduce the CSPG-mediated inhibition of axon growth within the glial scar. These studies, conducted with some assistance in dissections and data analysis from Dr. Joshua Cave and Dr. Amanda Barber, were designed to provide critical pilot data examining the effects of combined intrinsic and extrinsic therapies to promote axon regeneration in the optic nerve.

5.1.5 | Combining intrinsic and extrinsic stimuli

Experimental therapies that promote robust, long-distance axon regeneration in the optic nerve remain rare (de Lima et al. 2012; Lim et al. 2016; Kurimoto et al. 2010). I sought to integrate several of the intrinsic interventions described above with modification of glial scar CSPGs by ARSB (see Chapter 4). This combinatorial treatment included viral expression of hM3Dq and shPTEN in RGCs, as well as treatment with Zymosan, CPT-cAMP, and ARSB following ONC.

5.2 | RESULTS

5.2.1 | Zymosan and CPT-cAMP promote axon regeneration

The pro-regenerative effects of Zymosan and CPT-cAMP were quantified previously (**Figure 4.12**). Intravitreal injection of Zymosan (12.5 µg/µL) and CPT-cAMP (50 mM) at 3 d after ONC resulted in significantly (p = 0.0226) higher RGC axon regeneration at 14 dpc than injection of PBS (axons at 0.25 mm distal to the lesion [mean±SE]: 282±83.4 and 42.3±11.1, respectively) (**Figure 4.12**).

5.2.2 | Enhancing electrical activity of RGCs with hM3Dq promotes axon regeneration

Endogenous levels of electrical activity in RGCs were elevated by viral expression of hM3Dq. In a pilot experiment, mouse eyes were injected intravitreally with 1 µL of AAV2-

hSyn-HA-hM3Dq-mCherry (3.48×10^{12} genome copies (GC)/mL), and whole mount retinas were harvested at 14 days post injection. Expression of the hM3Dq-mCherry fusion protein was observed throughout the retina, indicating successful infection of RGCs (**Figure 5.2a**). To determine the effects of enhanced activity on RGC survival and axon regeneration, mice received either AAV2-hM3Dq or PBS control injection, followed by ONC at 14 d (**Figure 5.3a**). The hM3Dq ligand CNO was injected intraperitoneally twice daily from 14 d to 28 d, at which point retinas and optic nerves were collected for analysis. Surviving RGCs were immunolabeled with the RBPMS antibody, which colocalized with mCherry (**Figure 5.2c**). RGC survival in hM3Dq-treated mice showed an increase vs. PBS controls that failed to reach statistical significance (p = 0.0532) (RGC survival as % of non-lesioned controls [mean±SE]: 17.2±1.73 and 9.11±1.78, respectively) (**Figure 5.3b-c**). Axon regeneration was significantly (p = 0.0164) enhanced in hM3Dq-treated mice (axons at 0.25 mm distal to the lesion [mean±SE]: 67.3±26.2 and 16.1±5.64, respectively) (**Figure 5.3d-e**).

5.2.3 | Stimulation of the mTOR pathway with PTEN shRNA promotes axon regeneration

Activation of the mTOR pathway was enhanced by intravitreal injection of a virus carrying shRNA against PTEN. Successful infection of RGCs in non-lesioned retinas was observed 14 days post injection of AAV2-shPTEN-GFP (1 µL, 6.52×10^{12} GC/mL) (**Figure 5.2b**). To assess the ability of shPTEN to promote RGC survival and axon regeneration, intravitreal injection of AAV2-shPTEN or PBS was administered, followed by ONC at 14 d and collection of retinas and optic nerves at 28 d (**Figure 5.3a**). Surviving RBPMS[+] RGCs colocalized with GFP (**Figure 5.2d**). RGC survival in shPTEN-treated mice was not significantly different (p = 0.8680) from PBS controls (RGC survival as % of non-lesioned controls [mean±SE]: 9.81±2.83 and 9.11±1.78, respectively) (**Figure 5.3b-c**). Axon regeneration was also slightly but not significantly (p = 0.1006) elevated (axons at 0.25 mm distal to the lesion [mean±SE]: 104±93.2 and 16.1±5.64, respectively) (**Figure 5.3d-e**).
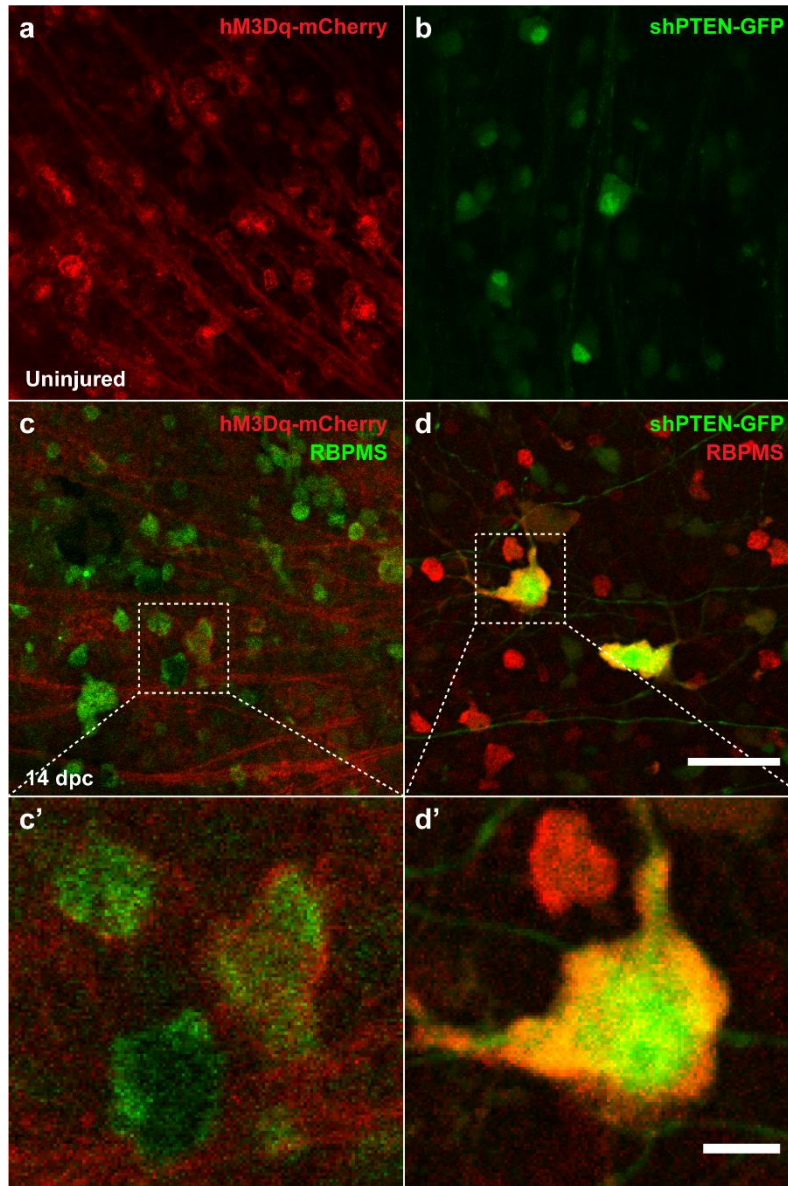
Figure 5.2. shPTEN and hM3Dq are expressed in virally infected retinal ganglion cells.
(a, b) Micrographs showing the expression of shPTEN-GFP (green) and hM3Dq-mCherry
(red) fusion proteins in the retinas of non-lesioned mice 14 d after intravitreal virus injection.
(c, d) In lesioned mice, retinas collected at 14 dpc were immunolabeled with RBPMS, which
colocalized with GFP and mCherry in surviving cells. (c', d') Insets showing co-labeled
RGCs from (c) and (d). Scale bar = 50 µm, insets = 10 µm.
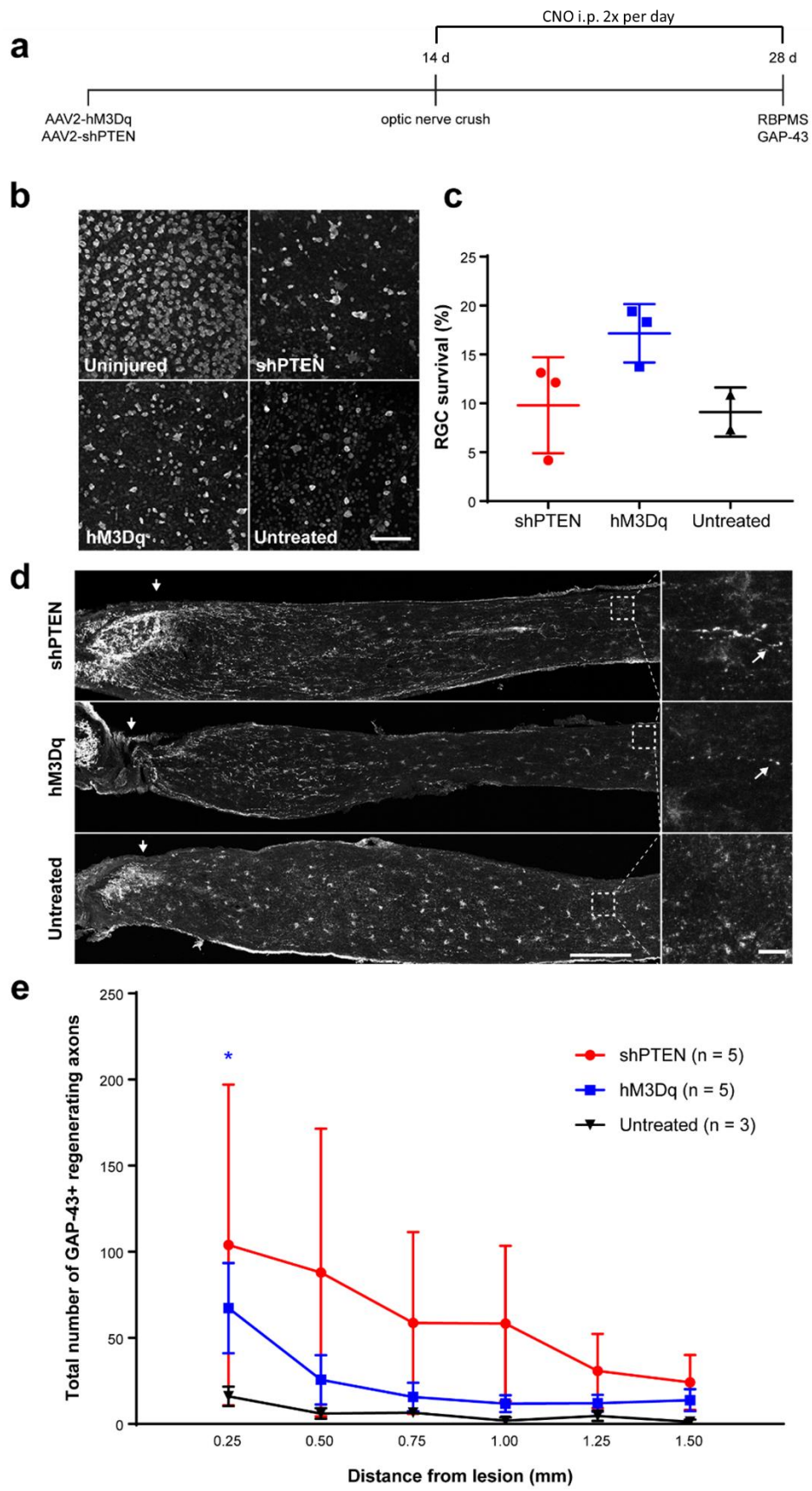
Figure 5.3 hM3Dq and shPTEN promote RGC survival and axon regeneration. (a) Experiment timeline. (b) Micrographs showing RBPMS$^+$ immunolabeled RGCs from retinal whole mounts collected 14 d after ONC. Scale bar = 100 µm. (c) Graph showing quantification of RGC survival in hM3Dq- and shPTEN-treated and untreated mice expressed as % of cells versus non-lesioned control retinas. Statistical significance was determined by Student's t-test. (d) Micrographs showing GAP-43-labeled optic nerves from mice injected with hM3Dq, shPTEN, or PBS. Arrows indicate lesion site. Scale bar = 200 µm, insets = 15 µm. (e) Graph showing the number of regenerating axons at distances distal to the lesion site, displayed as mean±SEM. Statistical significance was determined by two-way ANOVA with Bonferroni post-hoc test for multiple comparisons. * p < 0.05. Blue asterisk indicates significance for hM3Dq vs. untreated comparison.

5.2.4 | Hyperactive p110α promotes RGC survival and regeneration

The genotypes of wildtype mice and transgenic mice homozygous for the mutant hyperactive p110α subunit were confirmed by PCR. Genomic DNA was extracted from transgenic p110α mice and WT mice, and PCR was performed with the following primer pair: GGCTCAGTTGGGCTGTTTTG, forward; TCTGTGGGAAGTCTTGTCCC, reverse. The expected band (359 bp) was observed only in p110α mice (**Figure 5.4**). To determine the effects of enhancing mTOR pathway activation via hyperactive p110α, transgenic and wildtype mice were injected with AAV2-cre to induce expression of mutant p110α in the transgenic mice (**Figure 5.5a**). Both young (6-8 weeks) and aged (9-12 months) mice were included in each group, to evaluate whether age affects RGC survival or axon regeneration under these conditions. ONC was performed at 14 d, and retinas and optic nerves were collected at 42 d. RGC survival was significantly enhanced by p110α in both young mice (p = 0.0139) (RGC survival as % of non-lesioned controls [mean±SE]: 10.7±0.67 in p110α vs. 5.59±0.55 in WT) and old (p = 0.0075) mice (RGC survival as % of non-lesioned controls [mean±SE]: 12.8±1.10 in p110α vs. 4.53±0.67 in WT) (**Figure 5.5b-c**). Axon regeneration was significantly (p = 0.0234) elevated in young p110α mice vs. young WT controls (axons at 0.50 mm distal to the lesion [mean±SE]: 71.6±13.5 and 19.0±6.11, respectively) (**Figure 5.5d-e**). However, aged p110α mice failed to show a significant increase versus WT controls (p = 0.0796) (48.9±21.1 axons).

After validating the efficacy of several intrinsic pro-regenerative stimuli, the effectiveness of a combined stimulus was assessed. mTOR pathway activity was elevated with hyperactive p110α, and an implant loaded with 5 μL ChABC (50 U/mL) was applied directly to the optic nerve lesion site to reduce extrinsic inhibition of axon regeneration. Transgenic p110α mice received intravitreal AAV2-cre or AAV2-eGFP, followed by ONC at 14 d and either ChABC or PBS implant at 17 d. Nerves were collected at 42 d and stained with GAP-43 to detect regenerating axons (**Figure 5.6a**). As shown previously, p110α mice that received cre showed higher levels of axon regeneration than controls that did not receive cre (axons at 0.50 mm distal to the lesion [mean±SE]: 119±56.3 and 10.7±8.92, respectively) (**Figure 5.6b-c**). Axon regeneration in mice that received both cre and ChABC was higher than that of mice that received cre and PBS (axons at 0.50 mm distal to the lesion [mean±SE]: 217±119 and 119±56.3, respectively), although the difference was not statistically significant (p < 0.05) (**Figure 5.6b-c**).
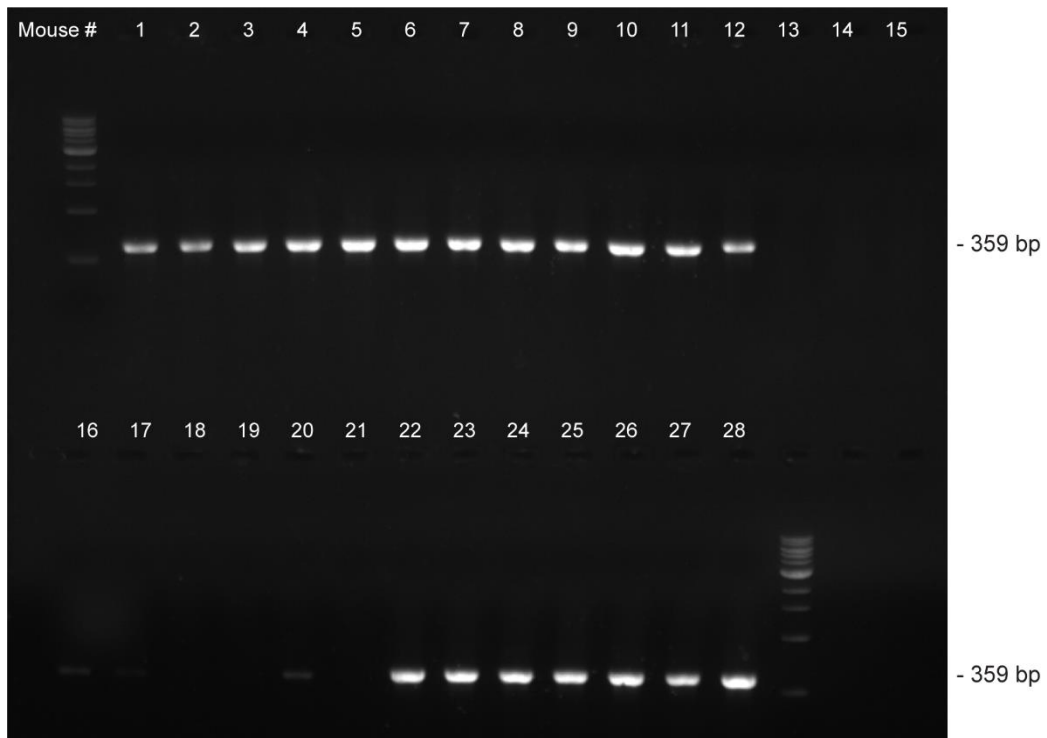
Figure 5.4 Validation of hyperactive p110α genotype. DNA gel showing the products of a PCR reaction designed to isolate a sequence from the p110α mutant gene from transgenic p110α mice (#1-12, 22-28) and WT mice (#13-21).

Figure 5.5 Expression of hyperactive p110α promotes RGC survival and axon regeneration. (a) Experiment timeline. (b) Micrographs showing Brn3a immunolabeled RGCs in retinal whole mounts. Scale bar = 100 µm. (c) Graph showing quantification of RGC survival in young and aged p110α and wildtype mice expressed as % of cells versus non-lesioned control retinas. Statistical significance was determined by Student's t-test. * p < 0.05, ** p < 0.01. (d) Micrographs showing CTβ-labeled optic nerves from young p110α and wildtype mice. Arrows indicate lesion site. Scale bar = 100 µm. (e) Graph showing the number of regenerating axons at 0.5 mm distal to the lesion site, displayed as mean±SEM. Statistical significance was determined by Student's t-test. *** p < 0.001.

Figure 5.6 ChABC enhances regeneration stimulated by hyperactive p110α. (a) Experiment timeline. (b) Micrographs showing GAP-43-labeled optic nerves from p110α mice injected with (i, iii) AAV2-cre or (v) AAV2-eGFP and treated with either (i) ChABC or (iii) PBS. Arrows indicate lesion site. Scale bar = 200 µm. Insets (ii, iv, vi) show GAP-43+ regenerating axons. Scale bar = 25 µm. (c) Graph showing the number of regenerating axons at 0.5 mm distal to the lesion site, displayed as mean±SEM. Statistical significance was determined by Student's t-test. * $p < 0.05$, ** $p < 0.01$.

5.2.5 | Combination of intrinsic and extrinsic stimuli yields robust long-distance regeneration

I observed that combining intrinsic and extrinsic regenerative stimuli promotes RGC axon regeneration to a greater degree than either stimulus alone (**Figure 4.13**). The intrinsic stimuli characterized above activate distinctive, though occasionally overlapping, pathways. It was therefore hypothesized that combining several intrinsic stimuli in addition to reducing CSPG-mediated inhibition with ARSB might have an additive effect, leading to long-distance axon regeneration into and even beyond the optic chiasm. To test this, a combinatorial treatment was devised. Viruses containing hM3Dq and shPTEN were injected intravitreally, followed by ONC at 14 d, and intravitreal injection of Zymosan/CTP-cAMP and implantation of ARSB scaffolds at 17 d (**Figure 5.7a**). CNO was administered by intraperitoneal injection twice daily from 14 d to 42 d to activate the hM3Dq receptor. At 42 d, whole optic pathways were collected and stained with GAP-43. Robust regeneration of RGC axons was observed in mice receiving the combinatorial treatment (**Figure 5.7b**). GAP-43 axons were found entering the optic chiasm (**Figure 5.7b-iii**), and GFP$^+$ axons were observed distally in the contralateral optic tract (**Figure 5.7b-iv**). GFP$^+$ axons expressed GAP-43, indicating that GFP$^+$ axons were genuinely regenerating axons rather than axons spared by an incomplete crush injury (**Figure 5.8**). When GAP-43$^+$ labeled axons were compared to data from previous experiments (**Figures 4.14, 4.17, 5.3**), the combinatorial treatment revealed an enhancement of the number and distance of regenerating axons in comparison with individual treatments (**Figure 5.7c**). During development in mice, nearly all RGC axons cross at the optic chiasm into the contralateral optic tract. In the mice treated with the combinatorial therapy, however, misrouting of regenerating axons was observed at the optic chiasm (**Figure 5.9a-ii, b-ii**), with GFP$^+$ axons traveling not only into the contralateral optic tract (**Figure 5.9a-iii, b-iii**), but also into the ipsilateral optic tract in large numbers (**Figure 5.9a-iv, b-iv**).
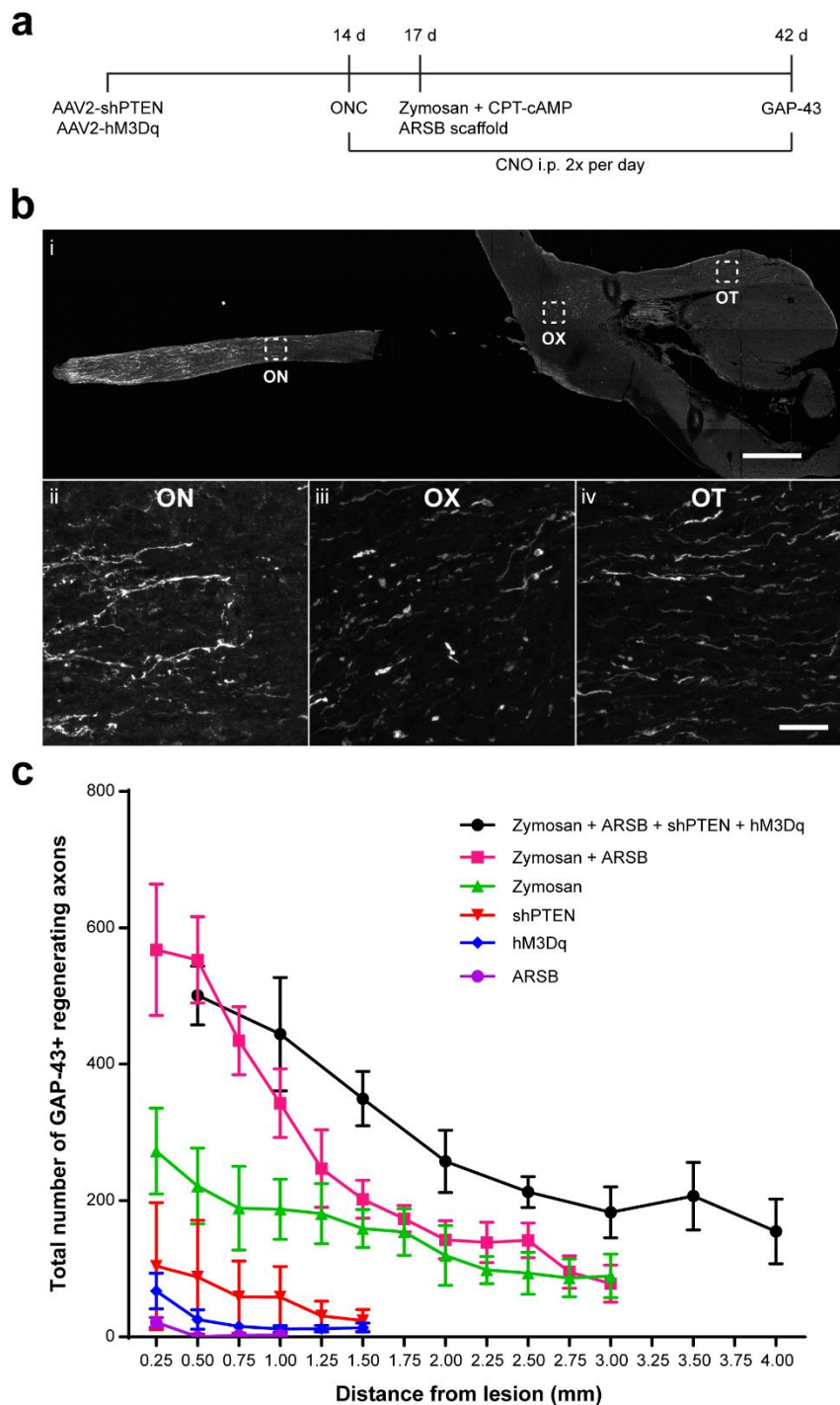
Figure 5.7. Combining intrinsic and extrinsic stimuli promotes axon regeneration into the optic tract. (a) Experiment timeline. (b) Micrographs showing a representative optic pathway treated with the combined stimulus. (i) GFP$^+$ axons in the optic pathway. Scale bar = 500 µm. Insets show GFP$^+$ axons in the (ii) optic nerve, (iii) optic chiasm, and (iv) contralateral optic tract. Scale bar = 25 µm. (c) Graph showing the number of GAP-43$^+$ regenerating axons at distances distal to the lesion site, displayed as mean +/- SEM. Graph includes reference data from previous experiments (**Figures 4.14, 4.17, 5.3**).
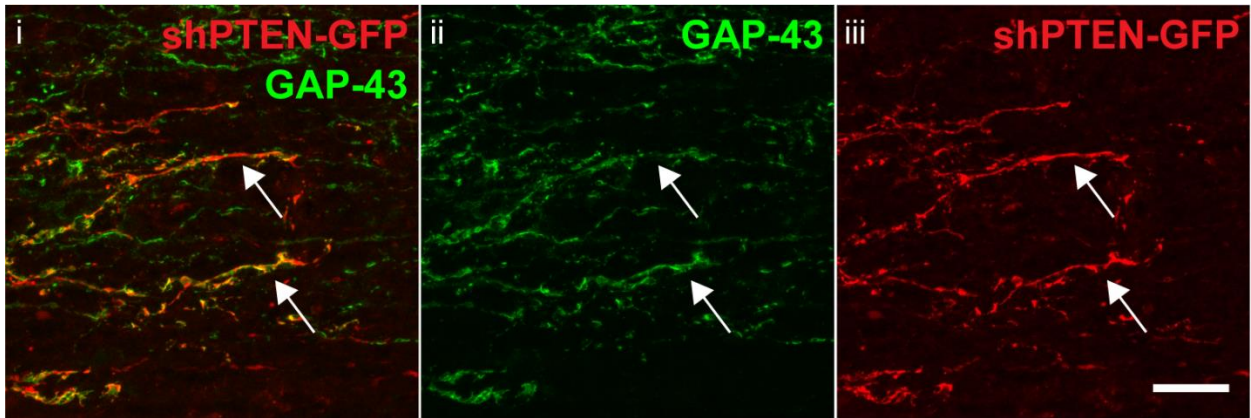
Figure 5.8. GFP+ regenerating axons express GAP-43. Micrographs show (i) co-localization of shPTEN-GFP and GAP-43, (ii) GAP-43 alone, and (iii) shPTEN-GFP alone. Arrows indicate GFP+/GAP-43+ regenerating axons. Scale bar = 25 µm.
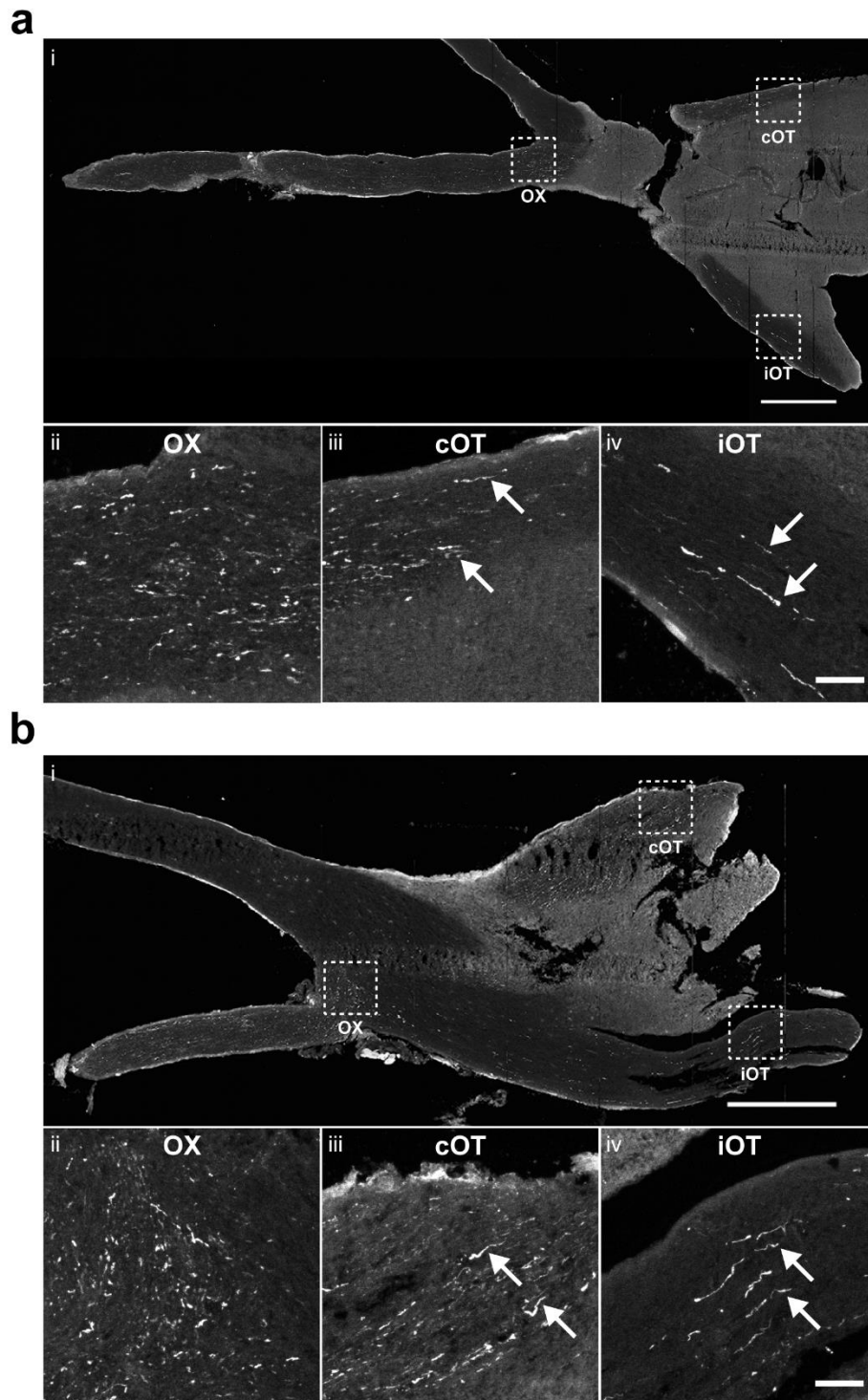
Figure 5.9. Regenerating axons fail to navigate correctly at the optic chiasm.
Micrographs showing GFP$^+$ regenerating axons in the optic pathways (i) of two mice (a) and (b). In the optic chiasm (ii), axons lose their linearity and appear to navigate in multiple directions without a uniform path. Many axons correctly navigate to the contralateral optic tract (iii), but several aberrantly navigate to the ipsilateral optic tract (iv). Arrows indicate GFP$^+$ regenerating axons. Scale bar = 500 µm, insets = 50 µm.

5.3 | DISCUSSION

I characterized the effects of several intrinsic stimuli on RGC survival and axonal regeneration and found that combining these stimuli and simultaneously targeting CSPGs in the glial scar with ARSB led to a significant, additive enhancement of axonal regeneration. Regenerating axons were observed traversing the optic chiasm and entering the optic tract. These findings demonstrate the additive effects of activating discrete molecular pathways that support cell survival and regeneration.

5.3.1 | Intrinsic modifications of RGCs stimulate axonal regeneration

I showed that three classes of intrinsic manipulation—stimulation of inflammatory pathways, elevation of neuronal activity levels, and enhancement of mTOR pathway activation via PTEN suppression or PI3K hyperactivation—function both independently and in combination to enhance the regeneration of RGC axons after an ONC lesion. Of these, intravitreal injection of Zymosan and CPT-cAMP proved the most robust and reliable, although variation in experimental technique and the fact that studies were not run in parallel makes direct comparison inadvisable. My inclusion of Zymosan injection in a combined intrinsic/extrinsic therapy is described in Chapter 4. Here, I show that expanding this therapy to include hM3Dq and shPTEN viruses dramatically increases the number and length of regenerating RGC axons, resulting in robust, long-distance growth, with axons found deep in both the contralateral and ipsilateral optic tracts.

Stimulation of inflammatory pathways

The discovery that lens injury stimulates axonal regeneration was among the earliest indicators that modulating factors intrinsic to RGCs could promote their survival and growth (Leon et al. 2000). Since then, numerous studies have sought to elucidate the underlying mechanisms by which ocular inflammation promotes the survival and axonal regeneration of RGCs. One important variable is timing. In rats, when Zymosan was injected at several time points following ONC, the 3 dpc time point showed the strongest pro-regenerative effect, with more than 1,000 GAP-43^{+} regenerating axons observed at 0.50 mm distal from the lesion site at 14 dpc, in comparison with ~750 axons when Zymsoan was injected at 0 dpc

and almost none when it was injected at 7 dpc (Yin et al. 2003). A study in mice found ~250 axons at 0.50 mm at 14 dpc when Zymosan was injected at 0 dpc (Baldwin et al. 2015). My experiments in mice generally showed ~150-200 regenerating axons at 0.50 mm at 14 dpc when Zymosan was injected at 3 dpc. While direct comparisons with these other studies are not possible—due not only to the difference in species and injection time, respectively, but also to the fact that manual counting of axons often varies between observers, and therefore absolute values may be appreciably different in separate laboratories and even between studies from the same group—the regeneration I observed is of a similar order to that reported by others.

The macrophage-secreted factor Ocm has been identified as a critical element of the inflammatory response that stimulates RGC growth (Yin et al. 2006; Yin et al. 2009). However, the precise signaling pathways within RGCs that control inflammation-induced regeneration remain under debate. It was reported that activation of the JAK/STAT3 pathway via repeated intravitreal injections of Pam(3)Cys, an agonist of toll-like receptor 2 (TLR2), transforms RGCs into a regenerative state and promotes axonal regeneration to an even greater degree than lens injury (Hauk et al. 2010). Pam(3)Cys stimulated higher levels of ciliary neurotrophic factor (CNTF) and GFAP expression in retinal glia, a phenomenon also observed after lens injury. In response to Pam(3)Cys administration, cultured RGCs exhibited elevated GAP-43 expression and extended longer neurites (Hauk et al. 2010). However, subsequent work demonstrated that administering a form of Zymosan specifically depleted of its ability to stimulate TLR2 while preserving stimulation of dectin-1 signaling (Ikeda et al. 2008) nonetheless stimulated robust RGC axon regeneration (Baldwin et al. 2015). A similar phenomenon was observed in knockout mice that lacked MyD88, the downstream effector through which most TLR family members signal. Administering Zymosan in MyD88$^{-/-}$ mice promoted comparable regeneration to that observed in wildtype mice (Baldwin et al. 2015). This group then argued that TLR2 acts in a complementary manner with dectin-1, but that dectin-1 signaling is required for Zymosan-induced regeneration whereas TLR2 is not. This was demonstrated by administering intravitreal injections of curdlan, a form of β(1, 3)-glucan that signals through dectin-1, and observing that curdlan enhances axon regeneration via the dectin-1 downstream effector CARD9 (Baldwin et al. 2015). Precisely how dectin-1 or other signaling pathways transform RGCs into a regenerative state remains unknown.

The clinical relevance of inflammatory signaling to support neuronal growth and regeneration is ambiguous. On the one hand, Zymosan injection is most effective at a delay of 3 d after the initial ONC injury, suggesting that robust regeneration is possible even when

treatment is delayed (Yin et al. 2003). This observation was confirmed by my own findings. Similarly, it was observed that administering β-glucan 2 d after ONC was equally effective as administering it at the time of ONC, suggesting an extended therapeutic window (Baldwin et al. 2015). In clinical situations where axonal regeneration is desired, such as acute spinal cord injury or neurodegenerative diseases like glaucoma, interventions are rarely available immediately after an injury. Therefore, therapies that can be delivered after a significant delay are highly attractive. However, stimulating ocular inflammation to promote regeneration naturally produces a set of side effects, many of which are potentially damaging. For instance, intraspinal injections of Zymosan promoted regeneration of DRG axons, but the concurrent activation of macrophages also leads to toxicity that destroyed proximate axons (Gensel et al. 2009). Toxicity was similarly observed after Zymosan injections into the eye, generating symptoms reminiscent of experimental autoimmune uveitis (Baldwin et al. 2015). In my experiments, mouse eyes injected with Zymosan were visibly inflamed, with retinal folding and detachment, similar to the results reported by others (Baldwin et al. 2015). To maximize clinical relevance, therefore, future studies will likely need to expand our understanding of the specific signaling pathways downstream of inflammatory stimuli that modify RGCs and enable them to regenerate their axons, and target these pathways directly.

Elevation of neuronal activity levels

I used an AAV2 vector carrying hM3Dq to elevate endogenous activity levels in RGCs and promote axonal regeneration. My pilot results showed a significant enhancement of regeneration, but not a significant enhancement of cell survival. The absence of a robust effect similar to that observed in previously published work (Lim et al. 2016)—which found >150 regenerating axons at 0.50 mm in comparison to my findings of <50 axons at this distance—likely derives from the small number of animals used (n = 5) and a failure to fully optimize all experimental conditions. Additionally, it must be acknowledged that electrophysiology was not performed to validate that hM3Dq was enhancing action potentials in RGCs. However, the fact that axon regeneration was improved suggests that hM3Dq was indeed elevating RGC activity and modifying the cells' intrinsic state. Another possible explanation for the difference in magnitude in comparison with the previous study is the viruses used. I administered injections of AAV2-hSyn-HA-hM3Dq-mCherry, which generates a fusion protein, hM3Dq-mCherry, whereas Lim et al. used AAV2-hSyn-HA-

hM3Dq-IRES-mCitrine. The internal ribosome entry site (IRES) element facilitates translation of two distinct proteins, meaning hM3Dq and mCitrine will be expressed independently in infected RGCs. In my case, the fusion of mCherry to the hM3Dq receptor is not expected to dramatically affect its function; however, it is impossible to rule out this possibility.

The mechanisms by which neural activity stimulates RGC growth and regeneration are not entirely characterized, but several key signaling pathways have been identified. Cultured RGCs exposed to physiological levels of electrical stimulation were observed to be more responsive to BDNF and other trophic factors (Goldberg, Espinosa, et al. 2002). When RGCs are depolarized or subjected to cAMP elevation, levels of the TrkB receptor, which binds BDNF, undergo an abrupt increase at the cell surface, indicating recruitment of TrkB from the intracellular space to the plasma membrane (Meyer-Franke et al. 1998). cAMP elevation also increases TrkB receptor gene expression (Deogracias et al. 2004). cAMP appears to be critical for activity-dependent enhancement of neuronal growth, as blocking adenylate cyclase, which lies upstream of cAMP, abolishes the positive effect of electrical stimulation (Goldberg, Espinosa, et al. 2002). Blocking cAMP's downstream partner PKA has a similar effect (Meyer-Franke et al. 1995). cAMP has been shown to influence the functioning of NMDA receptors in RGCs (Dong et al. 2008). It is worth noting that cAMP potentiates the pro-regenerative effects of Zymosan and facilitates Ocm binding to the inner retina (Yin et al. 2006). This implies that elevated activity and inflammatory stimulation may function through partially overlapping pathways. In melanopsin-expressing ipRGCs, light activates a signaling pathway mediated by the GPCR Gq/11, which feeds into the mTOR pathway (Li et al. 2016). Silencing ipRGCs suppressed activation of mTOR and abolished the growth-enhancing effects of light stimulation (Li et al. 2016), suggesting that mTOR also overlaps with activity dependent signaling in RGCs. Future studies will need to determine whether different types of electrical activity stimulate different molecular pathways. It has already been demonstrated that the pattern of stimulation is critical (Corredor & Goldberg 2009). Retinal prostheses have been designed to replace damaged or degenerated photoreceptors, and it seems clear that the patterns of activity produced by these devices strongly influence their effectiveness (Corredor & Goldberg 2009).

Enhancement of mTOR pathway activation

I utilized two distinct stimuli to enhance mTOR activity in RGCs: suppression of PTEN with shRNA and activation of PI3K with transgenic mice expressing a hyperactive p110α subunit. In previously published studies, transgenic floxed PTEN$^{-/-}$ mice demonstrated significant increases in axon regeneration following cre injection (Park et al. 2008). The magnitude of these increases was enormous, with ~1,500 CTβ$^+$ regenerating axons estimated at 0.50 mm distal from the lesion site at 14 dpc. There are several reasons why the levels of regeneration observed in our cohort of mice treated with shPTEN (~100 axons at 0.50 mm at 14 dpc) did not match the magnitude of the effect seen previously. Firstly, as mentioned previously, comparison of absolute axon counts is generally unreliable due to differences in counting technique between observers; it is possible that my counts underestimate the magnitude of the effect, or that published reports overestimate theirs, or both. Secondly, my low animal number reduced the statistical power of the study. Any errors in the injection would thus be magnified; indeed, shPTEN-GFP expression did not appear equally robust in all animals. Retinas where shPTEN-GFP expression was high correlated with those that exhibited the strongest effect on axon regeneration, indicating that variable injection efficiency may underlie the somewhat diminished effect of the cohort overall. Additionally, cre-induced knockdown of PTEN in transgenic mice is likely to be more efficient and affect more RGCs than injections of shPTEN. Nonetheless, my shPTEN did appear to enhance regeneration, with a very strong effect observed in some of the experimental animals.

PTEN suppression elevates activation of the mTOR pathway, which has been repeatedly linked to gains in cell growth and proliferation. In species that naturally regenerate their axons, mTOR signaling has been shown to play an important role (Barber et al. 2017). These include *Drosophila* (Y. Song et al. 2012), *C. elegans* (Byrne et al. 2014), and zebrafish (Abe et al. 2010; Hirose et al. 2014). It has been suggested that suppressing PTEN may be less effective than directly activating its counterpart PI3K. I found that introducing a hyperactive mutant of p110α significantly enhanced the regeneration of severed RGC axons, and that this effect was enhanced by the application of ChABC to the lesion site. Ongoing work by Dr. Richard Eva aims to explore the complex role of PI3K and its product PIP$_3$ in stimulating the mTOR pathway and boosting axonal growth and regeneration. Future studies will address this pathway in greater depth, evaluating the differences between p110α, which is expressed at low levels in adult RGCs, and p110δ, which is absent in adult RGCs but has been shown to play a pivotal role in the regeneration of sensory axons (Eickholt et al. 2007).

mTOR activation seems to preferentially preserve α-RGCs (Duan et al. 2015). Even in the absence of intervention, α-RGCs are more likely than other RGCs to survive following an ONC injury (Duan et al. 2015). When mice were treated with AAV2-shPTEN, nearly all regenerating axons were from α-RGCs (Duan et al. 2015). α-RGCs selectively express the protein osteopontin (OPN) and receptors for insulin-like growth factor 1 (IGF-1). The same study found that administering OPN and IGF-1 yielded a regenerative effect comparable to that of shPTEN, indicating that directly targeting α-RGCs may be equivalent to enhancing mTOR activation by suppressing PTEN (Duan et al. 2015).

5.3.2 | Other factors affecting RGC axon regeneration

RGC subtype

RGCs can be classified into more than 30 subtypes by features such as morphology, gene expression, and physiology (Sanes & Masland 2015). With the increasing availability of molecular markers and transgenic mice with labeled subpopulations of RGCs, new findings are emerging that suggest different RGC subtypes respond to separate stimuli and exhibit differential survival and regeneration depending on the type of intervention used (Dhande & Huberman 2014). As described above, suppressing PTEN overwhelmingly favors survival of α-RGCs, which comprise roughly 6% of the total RGC population in healthy retinas, but account for more than 90% of regenerating cells after treatment with shPTEN (Duan et al. 2015). However, in a related study, it was discovered that overexpressing the transcription factor Sox11 promoted RGC axon regeneration but simultaneously killed nearly all α-RGCs, providing evidence that α-RGCs are not the only regeneration competent subtype of RGCs (Norsworthy et al. 2017). Fascinatingly, mice with double knockout for PTEN and Sox11 had fewer total numbers of regenerating axons that PTEN knockout alone, and yet the axons that did regenerate grew longer distances than those in the PTEN-only control (Norsworthy et al. 2017). These findings illustrate the complexity and diversity of RGCs and underline the urgent need for future studies to address which subpopulations of RGCs respond to different stimuli.

In my comparison of p110α and WT mice, I found that p110α mice exhibited enhanced cell survival after ONC when compared with WT controls, but that only young (6-8 weeks) p110α mice showed a significant elevation of axon regeneration, while aged (9-12 months) p110α mice did not. This study emphasizes the widely observed phenomenon that the regenerative capacity of CNS neurons declines with age. In a similar study, PTEN deletion in aged mice failed to promote regeneration of injured spinal cord axons to the same degree as it did in young mice (Geoffroy et al. 2016). In cultured rat RGCs isolated from animals at different stages of development, embryo-derived cells exhibit substantially better growth potential than do cells from neonates (Goldberg, Espinosa, et al. 2002). Dramatic changes in gene expression occur after birth, and it has been proposed that neurons transform from an "axon outgrowth mode" to a "synapse formation and stabilization mode" at this time (He & Jin 2016). For instance, mTOR expression progressively declines over the course of development, rendering more advanced axons less capable of regeneration (Park et al. 2008; Belin et al. 2015). Intriguingly, PNS neurons do not show this age-related reduction of mTOR expression, perhaps explaining their sustained regenerative capacity in adulthood (Belin et al. 2015). Expression levels of kruppel-like factors (KLFs), which modulate the intrinsic growth potential of neurons, also drop in RGCs around birth (Moore et al. 2009). It has therefore been proposed that modifying epigenetic regulators, such as histone acetyltransferases, may enable neurons to more easily return to an active growth state similar to that observed during development (He & Jin 2016).

It has been proposed that age affects not only the intrinsic state of neurons, but also their environment. In the brain, advancing age correlates with an increase in the ratio of 4S to 6S GAG chains in endogenously expressed CSPGs (Foscarin et al. 2017). A similar shift was observed over the course of early development (Miyata et al. 2012). Future studies might evaluate whether injury-induced deposition of CSPGs follows a similar pattern.

5.3.3 | Barriers to long-distance axon regeneration

Navigation errors

As I observed in my mice treated with the combinatorial therapy, strong pro-regenerative stimuli can induce extensive axonal growth, but many of the regenerating axons

exhibit unusual growth paths and aberrant navigation at the optic chiasm. This phenomenon has been reported by other groups. One study used light sheet fluorescence microscopy (LSFM) to generate three-dimensional images of whole cleared optic nerves demonstrating that the regenerating axons of PTEN/SOCS3 knockout mice as well as PTEN knockout mice treated with Zymosan and CPT-cAMP both displayed highly irregular growth paths, often failing to decussate and enter the contralateral optic tract, instead traveling into the ipsilateral optic tract, contralateral optic nerve, or even back into the lesioned nerve from which they had originally extended (Luo et al. 2013). Some axons were found innervating the SCN, although the identity of these RGCs was unclear (Luo et al. 2013). A related study used the CNTFRα "super-agonist" DH-CNTF to stimulate long-distance regeneration of RGC axons, and observed axonal branching and misguidance at the optic chiasm (Pernet et al. 2013). Three-dimensional reconstructions of individual Thy1-YFP$^+$ axons revealed that many RGC axons extend their axons over long distances even in the absence of a stimulus, undertaking tortuous, looping paths that fail to penetrate the lesion site (Bray et al. 2017). Axons that did cross the lesion following treatment with CNTF also exhibited complex branching and turning (Bray et al. 2017). These mixed results have led to an intense focus on defining rigorous methods for determining whether axons extending beyond the site of an optic nerve lesion are in fact evidence of regeneration, or if they may be surviving axons spared by an incomplete lesion (Fischer et al. 2017). More research is required to understand whether different stimuli lead to more or less efficient pathfinding in RGCs, and whether altering the microenvironment might reduce navigational errors.

Remyelination failure

Even in cases where RGC axons regenerate long distances, it remains debated whether they have the capacity to form functional synapses and restore visual behavior. In one study, an optic tract transection was performed to limit the distance necessary for axons to travel from the lesion to their targets in the brain (Bei et al. 2016). Axons stimulated by co-deletion of PTEN and SOCS3, or by overexpression of OPN, IGF-1, and CNTF, were observed forming functional synapses in the SC; however, this innervation did not result in restoration of visual behaviors (Bei et al. 2016). It was hypothesized that this failure was due to lack of remyelination of regenerated axons, rendering them unable to conduct action potentials. Correspondingly, administering voltage-gated potassium channel blockers restored

conduction in regenerated axons and led to a significant enhancement of visual acuity, suggesting that remyelination is a critical barrier for RGCs to restore visual function (Bei et al. 2016). Curiously, another study found that axons stimulated to regenerate by PTEN deletion and administration of Zymosan and CPT-cAMP displayed signs of spontaneous remyelination and reassembly of nodes of Ranvier, even in axonal regions distal from the lesion (Marin et al. 2016). Additional studies will be required to validate these findings and expand our understanding of whether and how regenerated axons remyelinate and form functional synapses in the brain.

5.3.4 | Summary

In this chapter, I have demonstrated the pro-regenerative effects of a diverse set of intrinsic stimuli, including inflammatory signaling, neural activity levels, and activation of the mTOR pathway. I combined these interventions with ARSB administered at the ONC lesion site and observed robust long-distance regeneration of RGC axons. I found, in agreement with the findings produced by other groups, persistent errors in pathfinding of regenerating axons, with growth cones entering the ipsilateral optic tract or contralateral optic nerve rather than decussating at the optic chiasm and extending into the contralateral optic tract. However, by demonstrating the effectiveness of a combinatorial stimulus that incorporates direct modification of the inhibitory extracellular matrix at the glial scar using a clinically safe enzyme, I have advanced the tools available for promoting RGC growth with more translatable methods. Future studies will need to examine the extent to which ARSB can be combined with intrinsic stimuli that do not produce high-risk side effects, and whether modifying CSPGs in the matrix has any effects on axonal navigation and pathfinding during regeneration.

CHAPTER 6: CONCLUSIONS AND PERSPECTIVES

The objective of this thesis was to examine the dynamics of CSPG expression in the glial scar, and to investigate the potential of modifying CSPGs to enhance the regeneration of RGC axons after optic nerve injury. I found that selectively altering the sulfation pattern of GAG chains with the enzyme ARSB results in a robust and reliable increase in the number and distance of regenerating axons following optic nerve crush. ARSB is a human enzyme that has been approved for clinical use, making it a promising candidate for future combinatorial therapies that seek to promote regeneration of damaged CNS neurons in multiple contexts.

6.1 | OVERVIEW OF FINDINGS

In Chapter 3, I described a surgical technique for delivering therapeutic enzymes to the mouse optic nerve. I demonstrated that the enzymes ARSB and ChABC remain active *in vivo* and successfully penetrate into the axon fibers of the optic nerve, and quantified the digestion products of ChABC to show that the enzyme was actively modifying CSPGs. This protocol should prove useful for future studies that seek to modify the ECM in the optic nerve, an approach often ignored in regeneration studies due to its technical difficulty.

In Chapter 4, I showed comprehensive evidence that CSPGs, including the highly growth-inhibitory 4S GAGs, are upregulated within optic nerve and spinal cord lesions in mice and rats. I found that these changes were associated with reactive astrogliosis, and that injuring the optic nerve stimulates gliosis not only at the site of the lesion, but also in the ganglion cell layer of the retina. RGC axons fail to regenerate beyond the lesion site, a phenomenon that appears to be at least partially due to CSPGs, as I observed dystrophic axon endbulbs localized in proximity with high areas of CSPG deposition. I then used two CSPG-targeting enzymes, ARSB and ChABC, to modify CSPGs in the lesioned optic nerve, and showed a significant enhancement of axon regeneration when enzymes were administered in conjunction with Zymosan/CPT-cAMP, a growth-promoting inflammatory stimulus (**Figure 6.1**). Neither ARSB nor ChABC altered the formation of an astrocytic scar, although ChABC caused an elevation of Iba1 expression at the lesion site. ChABC also destroyed PNNs in the cortex, whereas ARSB left these structures intact. Together, these findings provide strong

evidence that modifying GAG chain sulfation with ARSB could be combined with existing or novel intrinsic pro-regenerative therapies to enhance their effectiveness without posing significant clinical risks.

In Chapter 5, I assessed several potential intrinsic stimuli and characterized their effects on RGC survival and axon regeneration. These included inducing a sterile inflammatory response in the retina (Zymosan), elevating endogenous activity levels in RGCs (hM3Dq), and activating the PI3K-mTOR pathway (shPTEN and hyperactive p110α). I observed that these stimuli are mutually enhancing when combined, and found that a combinatorial treatment which included Zymosan/CPT-cAMP, shPTEN, hM3Dq, and ARSB stimulated robust, long-distance regeneration of RGC axons, with many axons crossing the optic chiasm and entering the contralateral optic tract. I noted that, unlike during development when extracellular guidance cues populate the optic pathway to facilitate axonal navigation, many regenerating axons in the adult mice exhibited aberrant pathfinding, with axons diverging at the optic chiasm and entering the ipsilateral optic tract. Modifying the extracellular matrix at the ONC lesion site significantly improved axonal regeneration, but the environment at the optic chiasm remains a key obstacle for regenerating axons before robust repair can be achieved.

As of yet, no therapies aimed at stimulating repair of CNS axons have entered clinical trials. Several critical challenges remain before true translational treatments can be developed. These include limitations on the number of axons that regenerate even when long-distance growth is observed, impaired navigation and pathfinding of regenerating axons, and the existence of risks and side effects from gene therapies and therapeutic agents introduced into the visual system. Resolving these issues will be vital before viable translational treatments can be developed for use in humans.
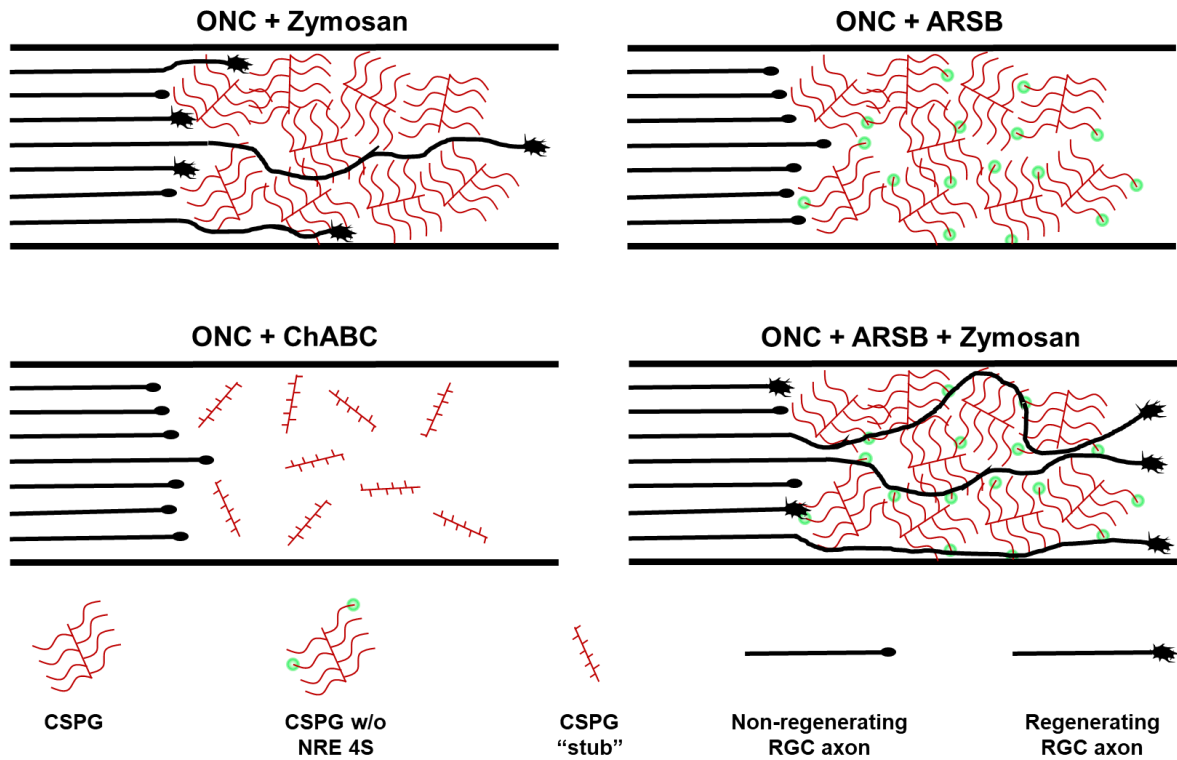
Figure 6.1. Summary of findings. Removing 4S groups from the non-reducing end of CS GAG chains with ARSB enhanced RGC axon regeneration in the presence of an intrinsic pro-regenerative stimulus. Modification of the ECM alone, with ARSB or ChABC, was insufficient to stimulate regeneration. Intrinsic modification of RGCs with Zymosan and other stimuli combined in an additive fashion to collectively promote axon regeneration, especially in combination with ARSB.

6.2 | LONG-DISTANCE RGC AXON REGENERATION AND RECOVERY OF FUNCTIONAL VISION

During development, RGC axons extend from the retina through the optic nerve, where most decussate at the optic chiasm before traveling up the optic tract and synapsing at central targets including the SCN and the LGN in the thalamus. Recapitulating this growth pathway is the primary objective of regenerative therapies in the visual system. As strategies for inducing and sustaining RGC axon regeneration have improved, more studies have demonstrated long-distance growth of axons, including, in some cases, the establishment of connections in the brain and the recovery of functional visual behaviors.

In mice subjected to co-deletion of PTEN and SOCS3, regenerating axons were observed traversing the optic chiasm (Sun et al. 2011). A combinatorial treatment that included PTEN deletion and two injections of Zymosan and CPT-cAMP, many axons crossed

the chiasm into the optic tract and some, visualized with CTβ, were found in the ventral LGN (Kurimoto et al. 2010). The same treatment was later shown to promote regeneration of axons into the SCN, LGN, superior colliculus (SC), and medial terminal nucleus (MTN), and to restore some visual behaviors, although gains in visual function were not sustained (de Lima et al. 2012). It should be noted that the degree of innervation was very low, with just a handful (< 10) of axon terminals detected in some regions (de Lima et al. 2012), and yet these numbers were reported to be sufficient for restoring behaviors such as the optokinetic reflex (OKR), which relies on the innervation of dsRGCs into multiple brain regions, including the LGN, SC, and accessory optic system (AOS). It must also be noted that while observers in this study were blinded to the experimental conditions, they were not blinded to the direction of the rotating drum, providing an opportunity for false positive detection of the OKR, which the authors acknowledge (de Lima et al. 2012). They also report that mice from their treatment group that did not show histological reinnervation of target regions were excluded from the statistical analysis of the OKR. These caveats make the assertion that visual behaviors were rescued by PTEN/SOCS3 deletion somewhat problematic, and robust, unequivocal evidence of recovered visual function remains to be seen in virtually all of the treatments described here.

In another study, a combination of mTOR stimulation using constitutively active ras homolog enriched in brain 1 (cRheb1) alongside biased visual stimulation yielded regeneration of axons into the SCN, LGN, SC, MTN, pretectum, and olivary pretectal nucleus (OPN) (Lim et al. 2016). Using a transgenic mouse line that express GFP in cochlin[+] RGCs, where most labeled RGCs are of the α-RGC subtype, the same group showed that α-RGCs appear to navigate to appropriate target regions and avoid non-target regions, suggesting that subtype-specific pathfinding behavior is preserved in adult regenerating axons under these experimental conditions (Lim et al. 2016). The presence of regenerating axons in the ipsilateral optic tract was not quantified, as I and others have consistently observed, and images were not provided, making it difficult to definitively argue that misguidance did not occur. These mice also showed improvements in some behavioral measures of visual function, including the OKR and looming response, but not others, such as direct pupil response, consensual pupil response, and the visual cliff assay (Lim et al. 2016). It is worth noting, again, that the observer of the OKR was not blinded to the direction of rotation, allowing for possible false positive detection; additionally, in this study, while it is stated that the observer was blind to the experimental conditions when counting the number of regenerating axons, it is not stated that they were blinded to the experimental conditions

when performing behavioral studies. If this is indeed the case, it could undermine the reported findings, given the high degree of subjectivity in measuring the OKR.

6.3 | NAVIGATION OF REGENERATING AXONS

While many experimental treatments, such as those mentioned above, have shown success in regenerating RGC axons, it remains the case that even in the best therapies, only a fraction of RGCs project their axons as far as the optic chiasm, with most stalling at various points along the optic nerve. Numerous groups have reported that regenerating RGC axons are prone to misguidance, turning back on themselves, forming branches, and/or demonstrating inadequate pathfinding at the optic chiasm (**Figure 6.2**), a key decision point in both development and regeneration states (Luo et al. 2013; Pernet et al. 2013; Berry et al. 1999). The failure of axons to regenerate beyond the chiasm may be due in part to inhibitory cues in the microenvironment, including CSPGs (Wang et al. 2012; Burnside & Bradbury 2014; Rodriguez-Grande et al. 2014; Deguchi et al. 2005). Pathfinding errors likely also arise from the lack of guidance cues in the adult visual pathway and/or from changes in the expression of their respective receptors on RGCs (Springer et al. 1990; Burnside & Bradbury 2014). Some experiments have generated data implying that the chiasm itself is inherently inhibitory to retinal axons, or at least promotes their divergence. For instance, co-culture of retinal neurites with optic chiasm explants led to a reduction in neurite outgrowth (Wang et al. 1996). It is known that RGC axon bundles defasciculate at the optic nerve-chiasm junction and fasciculate at the optic chiasm-tract junction (Jeffery 2001; Plas et al. 2005). In my own data, I observed that regenerating axons which appeared more or less linear, or at least were traveling unidirectionally, within the optic nerve were far more disorganized upon entering the optic chiasm. Notably, cells near these junctions have been observed to express CSPGs (Reese et al. 1997; Leung et al. 2003), although I did not specifically observe that in my studies. Whether CSPGs or other inhibitory ECM proteins may prompt axon rearrangement at both ends of the optic chiasm remains to be seen. Regardless, improving our understanding of how the extracellular environment changes at these key transition points will prove increasingly important for studies of axonal regeneration in the optic pathway.
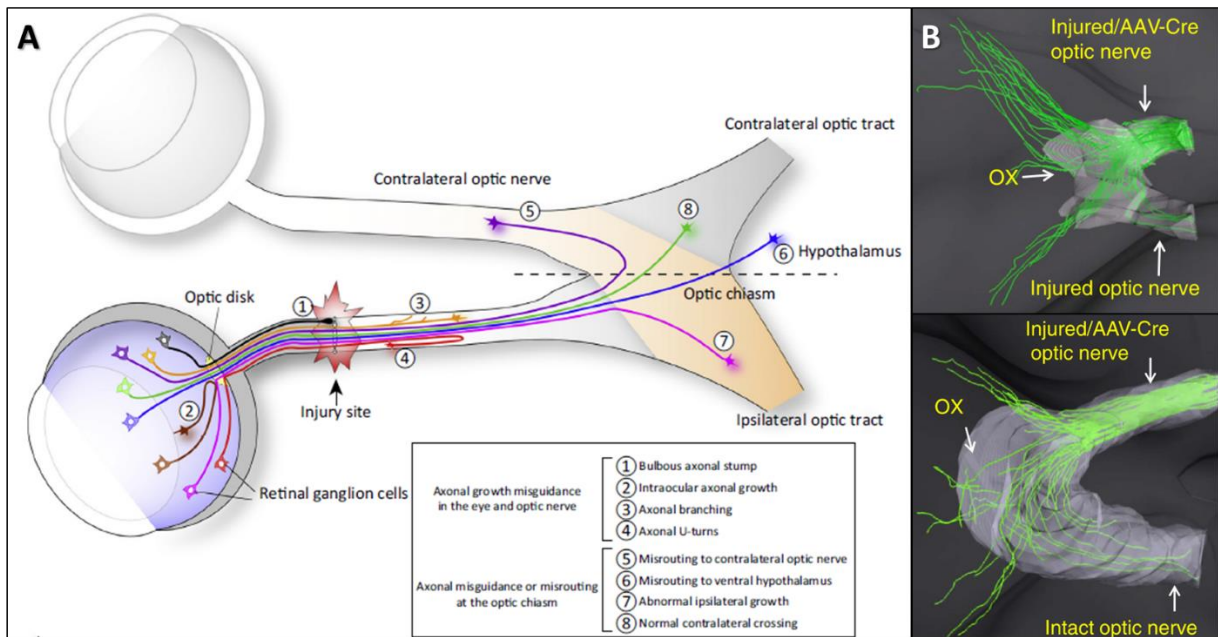
Figure 6.2. RGC axon misguidance at the optic chiasm. (A) After optic nerve injury, regenerating RGC axons are prone to misguidance at various points along the optic pathway. Panel adapted from (Pernet & Schwab 2014). (B) Three-dimensional reconstruction of regenerating axon tracts at the optic chiasm using light sheet fluorescence microscopy shows irregular pathfinding of individual axons, with some crossing ipsilaterally, others contralaterally, and others migrating into the contralateral optic nerve or back into the nerve through which they originally grew. Panel adapted from (Luo et al. 2013).

Navigational challenges also affect how cells ultimately find their terminals in the brain, where RGCs must connect with one of several target regions (**Figure 6.3**). If RGC axons regenerate long distances but fail to synapse at the proper targets, it is possible—and indeed likely—that few beneficial outcomes will be observed. It should be acknowledged, however, that even a low number of functional synapses may provide meaningful therapeutic benefit in some cases. Studies have suggested that as little as 5-10% of the original population of axonal connections may be required for meaningful recovery of some visual functions (Bregman et al. 1995). Increased sensitivity to light/dark boundaries could improve quality of life for patients even if higher order visual functioning remains impaired. Additionally, different RGC subtypes appear to have different capacities to regenerate, and, as noted in previous chapters, certain stimuli promote preferential growth from some subpopulations over others. As the functions of these different subtypes become more well established, prioritizing the regeneration of certain cells to their proper targets will be an increasingly important priority. The navigational aptitude of different RGC subtypes has not yet been studied, but this will almost certainly be a topic of interest for future research.
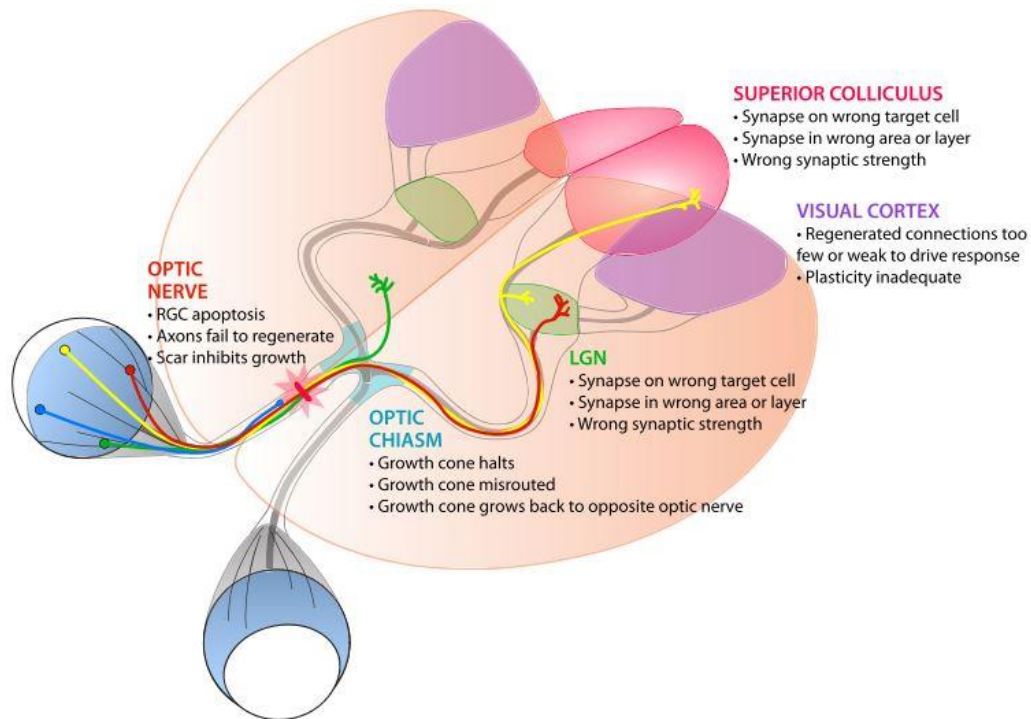
Figure 6.3. Summary of barriers to regeneration of visual pathways. Before translational regenerative therapies can migrate into the clinic, several prominent challenges must be overcome. These include barriers to cell survival in the retina and regeneration through the optic nerve, navigation of growing axons, reinnervation of accurate targets in the brain, and restoration of functional visual circuits. Figure adapted from (Crair & Mason 2016).

Many of the most successful pro-regenerative stimuli activate oncogenic pathways or knock out tumor suppressor genes such as PTEN. Some have warned that these strategies may be clinically unviable, given the potential risks to human health (Barber et al. 2017). Discovering ways to mediate these risks may be one path forward; investing in therapies that draw from more clinically plausible solutions is another. So far, the experimental therapies that produce robust regeneration tend to combine multiple stimuli to achieve long-distance regeneration, potentially compounding these risk factors. Future research should prioritize therapies with lower barriers to use in human patients.

6.4 | TRANSLATIONAL POTENTIAL OF PRO-REGENERATIVE THERAPIES

The extent to which experimental therapies that promote RGC survival and axon regeneration in animal models will translate to human patients remains unknown. As noted above, the severity of many forms of blindness and visual impairment and the sensitivity of RGCs mean that even a small number of functional connections has the potential to provide

substantial gains in function and improvements in quality of life. However, many of the most successful interventions in animals are unlikely to be suitable for clinical use. Activating inflammatory pathways causes retinal folding and detachment (Baldwin et al. 2015). The role of PTEN in cell growth was first identified as a common mutation in cancers, including glioblastoma (Li et al. 1997). Forced expression of c-myc, another cancer-related gene, was also found to promote regeneration (Belin et al. 2015). Given the oncogenic risks associated with knocking out a tumor suppressor gene such as PTEN or overexpressing an oncogene such as Myc, their use in experimental therapies has been questioned (Barber et al. 2017). Future strategies will need to prioritize clinically safe treatments that promote regeneration without risking severe side effects.

My discovery that ARSB enhances the regeneration of RGC axons is an encouraging one for precisely this reason. ARSB, a human enzyme, is currently approved for clinical use and has been utilized as an enzyme replacement therapy for MPS VI for more than a decade. However, there are caveats. Firstly, delivering ARSB to the optic nerve in humans will naturally be far more challenging than doing so in mice or other animals. One of the benefits of many existing therapies for visual system pathologies is the ability to inject agents such as viruses or small molecules directly into the eye, where they diffuse through the vitreous humor and eventually reach the retina. Directly targeting the optic nerve would require surgery, which carries many risks. Similarly, it should be noted that the type of injury I used in my studies, optic nerve crush, is rarely seen in humans. Far more common in the visual system are neurodegenerative conditions such as glaucoma, which, while they are known to be associated with CSPG elevation, occur over a much longer time course and lack a specific lesion site. It is possible, then, that ARSB may be more applicable to acute injuries of the brain or spinal cord, where the glial scarring and focal CSPG expression are far more common. This is a promising direction for future research. Still, it remains possible that ARSB might improve outcomes in glaucoma or other related visual system pathologies, whether by alleviating 4S GAG deposition in the ganglion cell layer of the retina, or even by using gene therapy to engineer expression of ARSB by glial cells or by RGCs themselves. Regardless of the approach, it will be crucial to address features of the extracellular environment when designing therapies to stimulate regeneration of axons in the visual system or elsewhere in the CNS. As this thesis demonstrates, inhibitory features of the extracellular matrix are critical obstacles that prevent the effective extension of new axons, and therefore modifying these features may prove essential to successful translational therapies in the future.

REFERENCES

Abe, N., Borson, S.H., Gambello, M.J., Wang, F. & Cavalli, V., 2010. Mammalian Target of Rapamycin (mTOR) activation increases axonal growth capacity of injured peripheral nerves. J. Biol. Chem., 285(36), 28034–28043.

Acott, T.S., Kelley, M.J., Keller, K.E., Vranka, J. a., Abu-Hassan, D.W., Li, X., Aga, M. & Bradley, J.M., 2014. Intraocular Pressure Homeostasis: Maintaining Balance in a High-Pressure Environment. J. Ocul. Pharmacol. Ther., 30(2–3), 94–101.

Acott, T.S. & Kelley, M.J., 2008. Extracellular matrix in the trabecular meshwork. Exp. Eye Res., 86(4), 543–561.

Ahmed, Z., Dent, R.G., Leadbeater, W.E., Smith, C., Berry, M. & Logan, A., 2005. Matrix metalloproteases: Degradation of the inhibitory environment of the transected optic nerve and the scar by regenerating axons. Mol. Cell. Neurosci., 28(1), 64–78.

Alvarado, J., Murphy, C., Polansky, J. & Juster, R., 1981. Age-related changes in trabecular meshwork cellularity. Investig. Ophthalmol. Vis. Sci., 21(5), 714–727.

Anderson, M.A., Burda, J.E., Ren, Y., Ao, Y., O'Shea, T.M., Kawaguchi, R., Coppola, G., Khakh, B.S., Deming, T.J. & Sofroniew, M. V., 2016. Astrocyte scar formation aids central nervous system axon regeneration. Nature.

Andrews, M.R., Czvitkovich, S., Dassie, E., Vogelaar, C.F., Faissner, a., Blits, B., Gage, F.H., ffrench-Constant, C. & Fawcett, J.W., 2009. 9 Integrin Promotes Neurite Outgrowth on Tenascin-C and Enhances Sensory Axon Regeneration. J. Neurosci., 29(17), 5546–5557.

Asher, R.A., Morgenstern, D.A., Shearer, M.C., Adcock, K.H., Pesheva, P. & Fawcett, J.W., 2002. Versican is upregulated in CNS injury and is a product of oligodendrocyte lineage cells. J. Neurosci., 22(6), 2225–36.

Avnur, Z. & Geiger, B., 1984. Immunocytochemical localization of native chondroitin-sulfate in tissues and cultured cells using specific monoclonal antibody. Cell, 38(3), 811–822.

Azuma, N., Tajima, S., Konomi, H., Hida, T., Akiya, S. & Uemura, Y., 1998. Glycosaminoglycan and collagen distribution in the developing human vitreous. Graefe's Arch. Clin. Exp. Ophthalmol., 236(9), 679–687.

Badea, T.C., Cahill, H., Ecker, J., Hattar, S. & Nathans, J., 2009. Distinct Roles of Transcription Factors Brn3a and Brn3b in Controlling the Development, Morphology, and Function of Retinal Ganglion Cells. Neuron, 61(6), 852–864.

Baldwin, K.T., Carbajal, K.S., Segal, B.M. & Giger, R.J., 2015. Neuroinflammation triggered

by β-glucan/dectin-1 signaling enables CNS axon regeneration. Proc. Natl. Acad. Sci. U. S. A., 112(8), 2581–6.

Bao, X., Nishimura, S., Mikami, T., Yamada, S., Itoh, N. & Sugahara, K., 2004. Chondroitin Sulfate/Dermatan Sulfate Hybrid Chains from Embryonic Pig Brain, Which Contain a Higher Proportion of L-Iduronic Acid than Those from Adult Pig Brain, Exhibit Neuritogenic and Growth Factor Binding Activities. J. Biol. Chem., 279(11), 9765–9776.

Barber, A., Farmer, K., Martin, K.R. & Smith, P.D., 2017. Retinal regeneration mechanisms linked to multiple cancer molecules: A therapeutic conundrum. Prog. Retin. Eye Res., 56, 19–31.

Barber, A.C., Hippert, C., Duran, Y., West, E.L., Bainbridge, J.W.B., Warre-cornish, K., Luhmann, U.F.O., Lakowski, J. & Sowden, J.C., 2013. Repair of the degenerate retina by photoreceptor transplantation. Proc. Natl. Acad. Sci., 110(1), 354–359.

Barnabé-Heider, F., Göritz, C., Sabelström, H., Takebayashi, H., Pfrieger, F.W., Meletis, K. & Frisén, J., 2010. Origin of New Glial Cells in Intact and Injured Adult Spinal Cord. Cell Stem Cell, 7(4), 470–482.

Battisti, W.P., Shinar, Y., Schwartz, M., Levitt, P. & Murray, M., 1992. Temporal and spatial patterns of expression of laminin, chondroitin sulfate proteoglycan and HNK-1 immunoreactivity during regeneration in the goldfish optic-nerve. J Neurocytol, 21(8), 557–573.

Bei, F., Lee, H.H.C., Liu, X., Gunner, G., Jin, H., Ma, L., Wang, C., Hou, L., Hensch, T.K., Frank, E., Sanes, J.R., Chen, C., Fagiolini, M. & He, Z., 2016. Restoration of Visual Function by Enhancing Conduction in Regenerated Axons. Cell, 164(1–2), 219–232.

Beirowski, B., Babetto, E., Coleman, M.P. & Martin, K.R., 2008. The WldS gene delays axonal but not somatic degeneration in a rat glaucoma model. Eur. J. Neurosci., 28(6), 1166–1179.

Belin, S., Nawabi, H., Wang, C., Tang, S., Latremoliere, A., Warren, P., Schorle, H., Uncu, C., Woolf, C.J., He, Z. & Steen, J. a., 2015. Injury-Induced Decline of Intrinsic Regenerative Ability Revealed by Quantitative Proteomics. Neuron, 86(4), 1000–1014.

Benfey, M. & Aguayo, A.J., 1982. Extensive elongation of axons from rat brain into peripheral nerve grafts. Nature, 296(11), 150–152.

Benowitz, L.I. & Popovich, P.G., 2011. Inflammation and axon regeneration. Curr. Opin. Neurol., 24(6), 577–583.

Berardi, N., Pizzorusso, T., Ratto, G.M. & Maffei, L., 2003. Molecular basis of plasticity in

the visual cortex. Trends Neurosci., 26(7), 369–378.

Berry, M., Carlile, J., Hunter, A., Tsang, W., Rosenstiel, P., Rosustrel, P. & Sievers, J., 1999. Optic nerve regeneration after intravitreal peripheral nerve implants: trajectories of axons regrowing through the optic chiasm into the optic tracts. J. Neurocytol., 28(9), 721–41.

Berson, D.M., Dunn, F.A. & Takao, M., 2002. Phototransduction By Retinal Ganglion Cells That Set the Circadian Clock. Science (80-.)., 295(February), 1070–1074.

Bertrand, J., Winton, M.J., Rodriguez-Hernandez, N., Campenot, R.B. & McKerracher, L., 2005. Application of Rho Antagonist to Neuronal Cell Bodies Promotes Neurite Growth in Compartmented Cultures and Regeneration of Retinal Ganglion Cell Axons in the Optic Nerve of Adult Rats. J. Neurosci., 25(5), 1113–1121.

Bicknese, A.R., Sheppard, a M., O'Leary, D.D. & Pearlman, a L., 1994. Thalamocortical axons extend along a chondroitin sulfate proteoglycan-enriched pathway coincident with the neocortical subplate and distinct from the efferent path. J. Neurosci., 14(6), 3500–3510.

Bignami, a. & Dahl, D., 1974. Astrocyte-specific protein and neuroglial differentiation. An immunofluorescence study with antibodies to the glial fibrillary acidic protein. J. Comp. Neurol., 153(1), 27–37.

Borisoff, J.F., Chan, C.C.M., Hiebert, G.W., Oschipok, L., Robertson, G.S., Zamboni, R., Steeves, J.D. & Tetzlaff, W., 2003. Suppression of Rho-kinase activity promotes axonal growth on inhibitory CNS substrates. Mol. Cell. Neurosci., 22(3), 405–416.

Bovolenta, P. & Mason, C., 1987. Growth cone morphology varies with position in the developing mouse visual pathway from retina to first targets. J. Neurosci., 7(May), 1447–1460.

Bradbury, E.J., Moon, L.D.F., Popat, R.J., King, V.R., Bennett, G.S., Patel, P.N., Fawcett, J.W. & McMahon, S.B., 2002. Chondroitinase ABC promotes functional recovery after spinal cord injury. Nature, 416(6881), 636–640.

Bradbury, E.J. & Carter, L.M., 2011. Manipulating the glial scar: chondroitinase ABC as a therapy for spinal cord injury. Brain Res. Bull., 84(4–5), 306–16.

Bray, E.R., Noga, M., Thakor, K., Wang, Y.-F., Lemmon, V.P., Park, K.K. & Tsoulfas, P., 2017. 3D Visualization of Individual Regenerating Retinal Ganglion Cell Axons Reveals Surprisingly Complex Growth Paths. eNeuro, 4(August), 1–15.

Bregman, B.S., Kunkel-Bagden, E., Schnell, L., Dai, H.N., Gao, D. & Schwab, M.E., 1995. Recovery from spinal cord injury mediated by antibodies to neurite growth inhibitors.

Nature, 378(6556), 498–501.

Brittis, P.A., Canning, D.R. & Silver, J., 1992. Chondroitin Sulfate As a Ergulator of Neuronal Patterning in the Retina. Science (80-.)., 255(16), 733–736.

Brittis, P.A. & Silver, J., 1995. Multiple Factors Govern Intraretinal Axon Guidance - a Time-Lapse Study. Mol. Cell. Neurosci., 6(5), 413–432.

Brown, J.M., Xia, J., Zhuang, B., Cho, K.-S., Rogers, C.J., Gama, C.I., Rawat, M., Tully, S.E., Uetani, N., Mason, D.E., Tremblay, M.L., Peters, E.C., Habuchi, O., Chen, D.F. & Hsieh-Wilson, L.C., 2012. A sulfated carbohydrate epitope inhibits axon regeneration after injury. Proc. Natl. Acad. Sci., 109(13), 4768–4773.

Brown, N.L., Patel, S., Brzezinski, J. & Glaser, T., 2001. Math5 is required for retinal ganglion cell and optic nerve formation. Development, 128, 2497–2508.

Buch, P.K., Bainbridge, J.W. & Ali, R.R., 2008. AAV-mediated gene therapy for retinal disorders: from mouse to man. Gene Ther., 15(11), 849–857.

Buller, C., Johnson, D.H. & Tschumper, R.C., 1990. Human trabecular meshwork phagocytosis: Observations in an organ culture system. Investig. Ophthalmol. Vis. Sci., 31(10), 2156–2163.

Burnside, E.R., De Winter, F., Didangelos, A., James, N.D., Andreica, E.-C., Layard-Horsfall, H., Muir, E.M., Verhaagen, J. & Bradbury, E.J., 2018. Immune-evasive gene switch enables regulated delivery of chondroitinase after spinal cord injury. Brain, (June), 1–20.

Burnside, E.R. & Bradbury, E.J., 2014. Review: Manipulating the extracellular matrix and its role in brain and spinal cord plasticity and repair. Neuropathol. Appl. Neurobiol., 40(1), 26–59.

Busch, S.A., Horn, K.P., Cuascut, F.X., Hawthorne, A.L., Bai, L., Miller, R.H. & Silver, J., 2010. Adult NG2+ Cells Are Permissive to Neurite Outgrowth and Stabilize Sensory Axons during Macrophage-Induced Axonal Dieback after Spinal Cord Injury. J. Neurosci., 30(1), 255–265.

Busch, S.A., Horn, K.P., Silver, D.J. & Silver, J., 2009. Overcoming Macrophage-Mediated Axonal Dieback Following CNS Injury. J. Neurosci., 29(32), 9967–9976.

Butterfield, K.C., Conovaloff, A., Caplan, M. & Panitch, A., 2010. Chondroitin sulfate-binding peptides block chondroitin 6-sulfate inhibition of cortical neurite growth. Neurosci. Lett., 478(2), 82–87.

Byrne, A.B., Walradt, T., Gardner, K.E., Hubbert, A., Reinke, V. & Hammarlund, M., 2014. Insulin/IGF1 Signaling Inhibits Age-Dependent Axon Regeneration. Neuron, 81(3),

561–573.

Cammisa, M., Correra, A., Andreotti, G. & Cubellis, M.V., 2013. Identification and analysis of conserved pockets on protein surfaces. BMC Bioinformatics, 14(SUPPL7), 1–9.

Carbonetto, S., Gruver, M.M. & Turner, D.C., 1983. Nerve fiber growth in culture on fibronectin, collagen, and glycosaminoglycan substrates. J. Neurosci., 3(11), 2324–35.

Challacombe, J.F. & Elam, J.S., 1997. Chondroitin 4-Sulfate Stimulates Regeneration of Goldfish Retinal Axons. Exp. Neurol., 143(1), 10–17.

Challacombe, J.F., Snow, D.M. & Letourneau, P.C., 1996. Actin filament bundles are required for microtubule reorientation during growth cone turning to avoid an inhibitory guidance cue. J. Cell Sci., 109 (Pt 8, 2031–40.

Chan, C.C.M., Roberts, C.R., Steeves, J.D. & Tetzlaff, W., 2008. Aggrecan Components Differentially Modulate Nerve Growth Factor– Responsive and Neurotrophin-3- Responsive Dorsal Root Ganglion Neurite Growth. J. Neurosci. Res., 86, 581–592.

Chau, C.H., Shum, D.K., Li, H., Pei, J., Lui, Y.Y., Wirthlin, L., Chan, Y.S. & Xu, X.M., 2004. Chondroitinase ABC enhances axonal regrowth through Schwann cell-seeded guidance channels after spinal cord injury. FASEB, 18(1), 194–196.

Cheah, M., Andrews, M.R., Chew, D.J., Moloney, E.B., Verhaagen, J., Fassler, R. & Fawcett, J.W., 2016. Expression of an Activated Integrin Promotes Long-Distance Sensory Axon Regeneration in the Spinal Cord. J. Neurosci., 36(27), 7283–7297.

Chung, K.-Y., Shum, D.K.-Y. & Chan, S.-O., 2000. Expression of chondroitin sulfate proteoglycans in the chiasm of mouse embryos. J. Comp. Neurol., 417(2), 153–163.

Chung, K.Y., Taylor, J.S., Shum, D.K. & Chan, S.O., 2000. Axon routing at the optic chiasm after enzymatic removal of chondroitin sulfate in mouse embryos. Development, 127(12), 2673–2683.

Clement, A.M., Nadanaka, S., Masayama, K., Mandl, C., Sugahara, K. & Faissner, A., 1998. The DSD-1 carbohydrate epitope depends on sulfation, correlates with chondroitin sulfate D motifs, and is sufficient to promote neurite outgrowth. J. Biol. Chem., 273(43), 28444–28453.

Clement, A.M., Sugahara, K. & Faissner, A., 1999. Chondroitin sulfate E promotes neurite outgrowth of rat embryonic day 18 hippocampal neurons. Neurosci. Lett., 269(3), 125–128.

Compston, A. & Coles, A., 2008. Multiple sclerosis. Lancet, 372(9648), 1502–1517.

Condic, M.L., 2001. Adult neuronal regeneration induced by transgenic integrin expression. J. Neurosci., 21(13), 4782–4788.

Corredor, R.G. & Goldberg, J.L., 2009. Electrical activity enhances neuronal survival and regeneration. J. Neural Eng., 6(5), 055001.

Crair, M.C. & Mason, C.A., 2016. Reconnecting Eye to Brain. J. Neurosci., 36(42), 10707–10722.

D'Onofrio, P.M., Magharious, M.M. & Koeberle, P.D., 2011. Methods for experimental manipulations after optic nerve transection in the Mammalian CNS. J. Vis. Exp., (51), 2–5.

David, S. & Aguayo, A.J., 1981. Axonal Elongation into Peripheral Nervous System "Bridges" after Central Nervous System Injury in Adult Rats. Science (80-.)., 214(4523), 931–933.

Davies, S.J., Fitch, M.T., Memberg, S.P., Hall, a K., Raisman, G. & Silver, J., 1997. Regeneration of adult axons in white matter tracts of the central nervous system. Nature, 390(6661), 680–3.

Deepa, S.S., Yamada, S., Zako, M., Goldberger, O. & Sugahara, K., 2004. Chondroitin sulfate chains on syndecan-1 and syndecan-4 from normal murine mammary gland epithelial cells are structurally and functionally distinct and cooperate with heparan sulfate chains to bind growth factors: A novel function to control binding of m. J. Biol. Chem., 279(36), 37368–37376.

Deepa, S.S., Umehara, Y., Higashiyama, S., Itoh, N. & Sugahara, K., 2002. Specific molecular interactions of oversulfated chondroitin sulfate E with various heparin-binding growth factors: Implications as a physiological binding partner in the brain and other tissues. J. Biol. Chem., 277(46), 43707–43716.

Deguchi, K., Takaishi, M., Hayashi, T., Oohira, A., Nagotani, S., Li, F., Jin, G., Nagano, I., Shoji, M., Miyazaki, M., Abe, K. & Huh, N., 2005. Expression of neurocan after transient middle cerebral artery occlusion in adult rat brain. Brain Res., 1037(1–2), 194–199.

Deiner, M.S., Kennedy, T.E., Fazeli, A., Serafini, T., Tessier-Lavigne, M. & Sretavan, D.W., 1997. Netrin-1 and DCC mediate axon guidance locally at the optic disc: Loss of function leads to optic nerve hypoplasia. Neuron, 19(3), 575–589.

Deogracias, R., Espliguero, G., Iglesias, T. & Rodríguez-Peña, A., 2004. Expression of the neurotrophin receptor trkB is regulated by the cAMP/CREB pathway in neurons. Mol. Cell. Neurosci., 26(3), 470–480.

Dhande, O.S., Stafford, B.K., Lim, J.-H.A. & Huberman, A.D., 2015. Contributions of Retinal Ganglion Cells to Subcortical Visual Processing and Behaviors. Annu. Rev. Vis.

Sci., 1(1), 291–328.

Dhande, O.S. & Huberman, A.D., 2014. Retinal ganglion cell maps in the brain: Implications for visual processing. Curr. Opin. Neurobiol., 24(1), 133–142.

Dick, G., Liktan, C., Alves, J.N., Ehlert, E.M.E., Miller, G.M., Hsieh-Wilson, L.C., Sugahara, K., Oosterhof, A., Van Kuppevelt, T.H., Verhaagen, J., Fawcett, J.W. & Kwok, J.C.F., 2013. Semaphorin 3A binds to the perineuronal nets via chondroitin sulfate type E motifs in rodent brains. J. Biol. Chem., 288(38), 27384–27395.

Dickendesher, T.L., Baldwin, K.T., Mironova, Y. a, Koriyama, Y., Raiker, S.J., Askew, K.L., Wood, A., Geoffroy, C.G., Zheng, B., Liepmann, C.D., Katagiri, Y., Benowitz, L.I., Geller, H.M. & Giger, R.J., 2012. NgR1 and NgR3 are receptors for chondroitin sulfate proteoglycans. Nat. Neurosci., 15(5), 703–712.

Dienstmann, R., Rodon, J., Serra, V. & Tabernero, J., 2014. Picking the Point of Inhibition: A Comparative Review of PI3K/AKT/mTOR Pathway Inhibitors. Mol. Cancer Ther., 13(5), 1021–1031.

Dill, J., Wang, H., Zhou, F. & Li, S., 2008. Inactivation of glycogen synthase kinase 3 promotes axonal growth and recovery in the CNS. J. Neurosci., 28(36), 8914–8928.

Dong, C.J., Guo, Y., Agey, P., Wheeler, L. & Hare, W.A., 2008. α2 adrenergic modulation of NMDA receptor function as a major mechanism of RGC protection in experimental glaucoma and retinal excitotoxicity. Investig. Ophthalmol. Vis. Sci., 49(10), 4515–4522.

Duan, X., Qiao, M., Bei, F., Kim, I.-J., He, Z. & Sanes, J.R., 2015. Subtype-Specific Regeneration of Retinal Ganglion Cells following Axotomy: Effects of Osteopontin and mTOR Signaling. Neuron, 85(6), 1244–1256.

Eickholt, B.J., Ahmed, A.I., Davies, M., Papakonstanti, E.A., Pearce, W., Starkey, M.L., Bilancio, A., Need, A.C., Smith, A.J.H., Hall, S.M., Hamers, F.P., Giese, K.P., Bradbury, E.J. & Vanhaesebroeck, B., 2007. Control of axonal growth and regeneration of sensory neurons by the p110δ PI 3-kinase. PLoS One, 2(9), 1–9.

Elkington, A.R., Inman, C.B.E., Steart, P. V. & Weller, R.O., 1990. The structure of the lamina cribrosa of the human eye: An immunocytochemical and electron microscopical study. Eye, 4(1), 42–57.

Emerling, D.E. & Lander, A.D., 1996. Inhibitors and promoters of thalamic neuron adhesion and outgrowth in embryonic neocortex: Functional association with chondroitin sulfate. Neuron, 17(6), 1089–1100.

Engel, M., Meyer-Puttlitz, B., Junker, E., Margolis, R.U. & Margolis, R.K., 1996. Chondroitin sulfate proteoglycans in the developing central nervous system .2.

Immunocytochemical localization of neurocan and phosphacan. J Comp Neurol, 366(1), 44–54.

Erskine, L. & Herrera, E., 2007. The retinal ganglion cell axon's journey: Insights into molecular mechanisms of axon guidance. Dev. Biol., 308(1), 1–14.

Faulkner, J.R., 2004. Reactive Astrocytes Protect Tissue and Preserve Function after Spinal Cord Injury. J. Neurosci., 24(9), 2143–2155.

Fernaud-Espinosa, I., Nieto-Sampedro, M. & Bovolenta, P., 1994. Differential effects of glycosaminoglycans on neurite outgrowth from hippocampal and thalamic neurones. J. Cell Sci., 107 (Pt 6, 1437–48.

Filous, A.R., Tran, A., Howell, C.J., Busch, S. a, Evans, T. a, Stallcup, W.B., Kang, S.H., Bergles, D.E., Lee, S.-I., Levine, J.M. & Silver, J., 2014. Entrapment via Synaptic-Like Connections between NG2 Proteoglycan+ Cells and Dystrophic Axons in the Lesion Plays a Role in Regeneration Failure after Spinal Cord Injury. J. Neurosci., 34(49), 16369–84.

Fischer, D., Harvey, A.R., Pernet, V., Lemmon, V.P. & Park, K.K., 2017. Optic nerve regeneration in mammals: Regenerated or spared axons? Exp. Neurol., 296, 83–88.

Fischer, D., Petkova, V., Thanos, S. & Benowitz, L.I., 2004. Switching Mature Retinal Ganglion Cells to a Robust Growth State In Vivo: Gene Expression and Synergy with RhoA Inactivation. J. Neurosci., 24(40), 8726–8740.

Fischer, D., Heiduschka, P. & Thanos, S., 2001. Lens-Injury-Stimulated Axonal Regeneration throughout the Optic Pathway of Adult Rats. Exp. Neurol., 172(2), 257–272.

Fischer, D. & Leibinger, M., 2012. Promoting optic nerve regeneration. Prog. Retin. Eye Res., 31(6), 688–701.

Fisher, D., Xing, B., Dill, J., Li, H., Hoang, H.H., Zhao, Z., Yang, X.-L., Bachoo, R., Cannon, S., Longo, F.M., Sheng, M., Silver, J. & Li, S., 2011. Leukocyte common antigen-related phosphatase is a functional receptor for chondroitin sulfate proteoglycan axon growth inhibitors. J. Neurosci., 31(40), 14051–66.

Foscarin, S., Raha-Chowdhury, R., Fawcett, J.W. & Kwok, J.C.F., 2017. Brain ageing changes proteoglycan sulfation, rendering perineuronal nets more inhibitory. Aging (Albany. NY)., 9(6).

Foster, R.G., Provencio, I., Hudson, D., Fiske, S., De Grip, W. & Menaker, M., 1991. Circadian photoreception in the retinally degenerate mouse (rd/rd). J. Comp. Physiol. A, 169(1), 39–50.

Franklin, R.J.M., 2002. Why does remyelination fail in multiple sclerosis? Nat. Rev. Neurosci., 3(9), 705–714.

Fu, L., Lo, A.C.Y., Lai, J.S.M. & Shih, K.C., 2015. The role of electrical stimulation therapy in ophthalmic diseases. Graefe's Arch. Clin. Exp. Ophthalmol., 253(2), 171–176.

Fukuda, T., Kawano, H., Ohyama, K., Li, H.P., Takeda, Y., Oohira, A. & Kawamura, K., 1997. Immunohistochemical localization of neurocan and L1 in the formation of thalamocortical pathway of developing rats. J. Comp. Neurol., 382(2), 141–152.

Galtrey, C.M. & Fawcett, J.W., 2007. The role of chondroitin sulfate proteoglycans in regeneration and plasticity in the central nervous system. Brain Res. Rev., 54(1), 1–18.

Garcia-Valenzuela, E., Shareef, S., Walsh, J. & Sharma, S.C., 1995. Programmed cell death of retinal ganglion cells during experimental glaucoma. Exp. Eye Res., 61(1), 33–44.

Gensel, J.C., Nakamura, S., Guan, Z., van Rooijen, N., Ankeny, D.P. & Popovich, P.G., 2009. Macrophages promote axon regeneration with concurrent neurotoxicity. J Neurosci, 29(12), 3956–3968.

Gensel, J.C., Wang, Y., Guan, Z., Beckwith, K.A., Braun, K.J., Wei, P., McTigue, D.M. & Popovich, P.G., 2015. Toll-Like Receptors and Dectin-1, a C-Type Lectin Receptor, Trigger Divergent Functions in CNS Macrophages. J. Neurosci., 35(27), 9966–9976.

Geoffroy, C.G., Hilton, B.J., Tetzlaff, W. & Zheng, B., 2016. Evidence for an Age-Dependent Decline in Axon Regeneration in the Adult Mammalian Central Nervous System Cell Reports Report Evidence for an Age-Dependent Decline in Axon Regeneration in the Adult Mammalian Central Nervous System. Cell Rep., 15, 238–246.

Goel, M., 2010. Aqueous Humor Dynamics: A Review~!2010-03-03~!2010-06-17~!2010-09-02~! Open Ophthalmol. J., 4(1), 52–59.

Gold, E., Gussler, D. & Schwartz, E., 1976. Enzymes from human articular cartilage: isolation of arylsulfatase B and its comparison with arylsulfatase A. Connect. Tissue Res., 4(4), 237–245.

Goldberg, J.L., Klassen, M.P., Hua, Y. & Barres, B.A., 2002. Amacrine-signaled loss of intrinsic axon growth ability by retinal ganglion cells. Science (80-.)., 296(5574), 1860–1864.

Goldberg, J.L., Espinosa, J.S., Xu, Y., Davidson, N., Kovacs, G.T. a. & Barres, B. a., 2002. Retinal Ganglion Cells Do Not Extend Axons by Default. Neuron, 33(5), 689–702.

Gomez, T.M. & Spitzer, N.C., 2000. Regulation of growth cone behavior by calcium: New dynamics to earlier perspectives. J. Neurobiol., 44(2), 174–183.

Gopalakrishnan, S.M., Teusch, N., Imhof, C., Bakker, M.H.M., Schurdak, M., Burns, D.J. &

Warrior, U., 2008. Role of Rho kinase pathway in chondroitin sulfate proteoglycan-mediated inhibition of neurite outgrowth in PC12 cells. J. Neurosci. Res., 86(10), 2214–2226.

Göz, D., Studholme, K., Lappi, D.A., Rollag, M.D., Provencio, I. & Morin, L.P., 2008. Targeted destruction of photosensitive retinal ganglion cells with a saporin conjugate alters the effects of light on mouse circadian rhythms. PLoS One, 3(9).

Grierson, I. & Howes, R.C., 1987. Age-related depletion of the cell population in the human trabecular meshwork. Eye, 1(2), 204–210.

Gu, W.-L., Fu, S.-L., Wang, Y.-X., Li, Y., Lü, H.-Z., Xu, X.-M. & Lu, P.-H., 2009. Chondroitin sulfate proteoglycans regulate the growth, differentiation and migration of multipotent neural precursor cells through the integrin signaling pathway. BMC Neurosci., 10, 128–143.

Güler, A.D., Ecker, J.L., Lall, G.S., Haq, S., Altimus, C.M., Liao, H.W., Barnard, A.R., Cahill, H., Badea, T.C., Zhao, H., Hankins, M.W., Berson, D.M., Lucas, R.J., Yau, K.W. & Hattar, S., 2008. Melanopsin cells are the principal conduits for rod-cone input to non-image-forming vision. Nature, 453(7191), 102–105.

Habuchi, O., 1967. Purification and Properties and Chondrosulfatases " of Bacterial Chondroitinases. J. Biol. Chem., 243(7), 1523–1535.

Hara, M., Kobayakawa, K., Ohkawa, Y., Kumamaru, H., Yokota, K., Saito, T., Kijima, K., Yoshizaki, S., Harimaya, K., Nakashima, Y. & Okada, S., 2017. Interaction of reactive astrocytes with type I collagen induces astrocytic scar formation through the integrin–N-cadherin pathway after spinal cord injury. Nat. Med., 23(7), 818–828.

Harmatz, P., 2005. Direct Comparison of Measures of Endurance, Mobility, and Joint Function During Enzyme-Replacement Therapy of Mucopolysaccharidosis VI (Maroteaux-Lamy Syndrome): Results After 48 Weeks in a Phase 2 Open-Label Clinical Study of Recombinant Human N-Acetylga. Pediatrics, 115(6), e681–e689.

Harmatz, P., Whitley, C.B., Waber, L., Pais, R., Steiner, R., Plecko, B., Kaplan, P., Simon, J., Butensky, E. & Hopwood, J.J., 2004. Enzyme replacement therapy in mucopolysaccharidosis VI (Maroteaux-Lamy syndrome). J. Pediatr., 144(5), 574–580.

Hashiguchi, T., Mizumoto, S., Yamada, S. & Sugahara, K., 2010. Analysis of the structure and neuritogenic activity of chondroitin sulfate/dermatan sulfate hybrid chains from porcine fetal membranes. Glycoconj. J., 27(1), 49–60.

Hatori, M., Le, H., Vollmers, C., Keding, S.R., Tanaka, N., Schmedt, C., Jegla, T. & Panda, S., 2008. Inducible ablation of melanopsin-expressing retinal ganglion cells reveals their

central role in non-image forming visual responses. PLoS One, 3(6).

Hauk, T.G., Leibinger, M., Müller, A., Andreadaki, A., Knippschild, U. & Fischer, D., 2010. Stimulation of axon regeneration in the mature optic nerve by intravitreal application of the toll-like receptor 2 agonist Pam3Cys. Investig. Ophthalmol. Vis. Sci., 51(1), 459–464.

He, Z. & Jin, Y., 2016. Intrinsic control of axon regeneration. Neuron, 90, 437–451.

Hikino, M., Mikami, T., Faissner, A., Vilela-Silva, A.C.E.S., Pavão, M.S.G. & Sugahara, K., 2003. Oversulfated Dermatan Sulfate Exhibits Neurite Outgrowth-promoting Activity toward Embryonic Mouse Hippocampal Neurons: Implications of dermatan sulfate in neuritogenesis in the brain. J. Biol. Chem., 278(44), 43744–43754.

Hirose, K., Shiomi, T., Hozumi, S. & Kikuchi, Y., 2014. Mechanistic target of rapamycin complex 1 signaling regulates cell proliferation, cell survival, and differentiation in regenerating zebrafish fins. BMC Dev. Biol., 14, 1–15.

Hockfield, S., Kalb, R.G., Zaremba, S. & Fryer, H., 1990. Expression of neural proteoglycans correlates with the acquisition of mature neuronal properties in the mammalian brain. Cold Spring Harb. Symp. Quant. Biol., 55, 505–14.

Hollis, E.R. & Zou, Y., 2012. Reinduced Wnt signaling limits regenerative potential of sensory axons in the spinal cord following conditioning lesion. Proc. Natl. Acad. Sci., 109(36), 14663–14668.

Holt, C.E., 1989. A single-cell analysis of early retinal ganglion cell differentiation in Xenopus: from soma to axon tip. J. Neurosci., 9(9), 3123–3145.

Horn, K.P., Busch, S. a., Hawthorne, a. L., van Rooijen, N. & Silver, J., 2008. Another Barrier to Regeneration in the CNS: Activated Macrophages Induce Extensive Retraction of Dystrophic Axons through Direct Physical Interactions. J. Neurosci., 28(38), 9330–9341.

Hur, E.-M., Yang, I.H., Kim, D.-H., Byun, J., Xu, W.-L., Nicovich, P.R., Cheong, R., Levchenko, A., Thakor, N. & Zhou, F.-Q., 2011. Engineering neuronal growth cones to promote axon regeneration over inhibitory molecules. Proc. Natl. Acad. Sci., 108(12), 5057–5062.

Hyatt, A.J.T., Wang, D., Kwok, J.C., Fawcett, J.W. & Martin, K.R., 2010. Controlled release of chondroitinase ABC from fibrin gel reduces the level of inhibitory glycosaminoglycan chains in lesioned spinal cord. J. Control. Release, 147(1), 24–29.

Ichijo, H. & Kawabata, I., 2001. Roles of the Telencephalic Cells and their Chondroitin Sulfate Proteoglycans in Delimiting an Anterior Border of the Retinal Pathway. J.

Neurosci., 21(23), 9304–9314.

Iida, J., Meijne, A.M., Oegema Jr., T.R., Yednock, T.A., Kovach, N.L., Furcht, L.T. & McCarthy, J.B., 1998. A role of chondroitin sulfate glycosaminoglycan binding site in a4b1 integrin-mediated melanoma cell adhesion. J. Biol. Chem., 273(10), 5955–5962.

Ikeda, Y., Adachi, Y., Ishii, T., Miura, N., Tamura, H. & Ohno, N., 2008. Dissociation of Toll-like receptor 2-mediated innate immune response to zymosan by organic solvent-treatment without loss of Dectin-1 reactivity. Biol. Pharm. Bull., 31(1), 13–8.

Inatani, M., Tanihara, H., Honjo, M., Hangai, M., Kresse, H. & Honda, Y., 1999. Expression of proteoglycan decorin in neural retina. Investig. Ophthalmol. Vis. Sci., 40(8), 1783–1791.

Inatani, M., Tanihara, H., Oohira, A., Honjo, M. & Honda, Y., 1999. Identification of a nervous tissue-specific chondroitin sulfate proteoglycan, neurocan, in developing rat retina. Investig. Ophthalmol. Vis. Sci., 40(10), 2350–2359.

Inatani, M., Honjo, M., Otori, Y., Oohira, A., Kido, N., Tano, Y., Honda, Y. & Tanihara, H., 2001. Inhibitory effects of neurocan and phosphacan on neurite outgrowth from retinal ganglion cells in culture. Invest. Ophthalmol. Vis. Sci., 42(8), 1930–8.

Inatani, M., Tanihara, H., Oohira, a., Honjo, M., Kido, N. & Honda, Y., 2000. Upregulated expression of neurocan, a nervous tissue specific proteoglycan, in transient retinal ischemia. Investig. Ophthalmol. Vis. Sci., 41(9), 2748–2754.

Ishii, M. & Maeda, N., 2008a. Oversulfated chondroitin sulfate plays critical roles in the neuronal migration in the cerebral cortex. J. Biol. Chem., 283(47), 32610–32620.

Ishii, M. & Maeda, N., 2008b. Spatiotemporal expression of chondroitin sulfate sulfotransferases in the postnatal developing mouse cerebellum. Glycobiology, 18(8), 602–614.

Jain, A., Brady-Kalnay, S.M. & Bellamkonda, R. V., 2004. Modulation of Rho GTPase activity alleviates chondroitin sulfate proteoglycan-dependent inhibition of neurite extension. J. Neurosci. Res., 77(2), 299–307.

Jeffery, G., 2001. Architecture of the optic chiasm and the mechanisms that sculpt its development. Physiol. Rev., 81(4), 1393–1414.

Jones, L.L., Margolis, R.U. & Tuszynski, M.H., 2003. The chondroitin sulfate proteoglycans neurocan, brevican, phosphacan, and versican are differentially regulated following spinal cord injury. Exp. Neurol., 182(2), 399–411.

Kaneko, M., Kubo, T., Hata, K., Yamaguchi, A. & Yamashita, T., 2007. Repulsion of cerebellar granule neurons by chondroitin sulfate proteoglycans is mediated by MAPK

pathway. Neurosci. Lett., 423(1), 62–67.

Kantor, D.B., Chivatakarn, O., Peer, K.L., Oster, S.F., Inatani, M., Hansen, M.J., Flanagan, J.G., Yamaguchi, Y., Sretavan, D.W., Giger, R.J. & Kolodkin, A.L., 2004. Semaphorin 5A is a bifunctional axon guidance cue regulated by heparan and chondroitin sulfate proteoglycans. Neuron, 44(6), 961–975.

Karumbaiah, L., Anand, S., Thazhath, R., Zhong, Y., Mckeon, R.J. & Bellamkonda, R. V., 2011. Targeted downregulation of N-acetylgalactosamine 4-sulfate 6-O-sulfotransferase significantly mitigates chondroitin sulfate proteoglycan-mediated inhibition. Glia, 59(6), 981–996.

Keller, K.E., Aga, M., Bradley, J.M., Kelley, M.J. & Acott, T.S., 2009. Extracellular matrix turnover and outflow resistance. Exp. Eye Res., 88(4), 676–682.

Knaust, A., Schmidt, B., Dierks, T., Von B??low, R. & Von Figura, K., 1998. Residues critical for formylglycine formation and/or catalytic activity of arylsulfatase A. Biochemistry, 37(40), 13941–13946.

Köppe, G., Brückner, G., Härtig, W., Delpech, B. & Bigl, V., 1997. Characterization of proteoglycan-containing perineuronal nets by enzymatic treatments of rat brain sections. Histochem. J., 29(1), 11–20.

Koprivica, V., Cho, K.-S., Park, J.B., Yiu, G., Atwal, J., Gore, B., Kim, J. a, Lin, E., Tessier-Lavigne, M., Chen, D.F. & He, Z., 2005. EGFR Activation Mediates Inhibition of Axon Regeneration by Myelin and Chondroitin Sulfate Proteoglycans. Science (80-.)., 310(5745), 106–110.

Kurimoto, T., Yin, Y., Omura, K., Gilbert, H.Y., Kim, D., Cen, L.P., Moko, L., Kugler, S. & Benowitz, L.I., 2010. Long-Distance Axon Regeneration in the Mature Optic Nerve: Contributions of Oncomodulin, cAMP, and pten Gene Deletion. J. Neurosci., 30(46), 15654–15663.

Kwok, J.C.F., Carulli, D. & Fawcett, J.W., 2010. In vitro modeling of perineuronal nets: hyaluronan synthase and link protein are necessary for their formation and integrity. J. Neurochem., 114(5), no-no.

Kwong, J.M.K., Caprioli, J. & Piri, N., 2010. RNA binding protein with multiple splicing: A new marker for retinal ganglion cells. Investig. Ophthalmol. Vis. Sci., 51(2), 1052–1058.

Lafuente, M.P., Villegas-Pérez, M.P., Mayor, S., Aguilera, M.E., Miralles de Imperial, J. & Vidal-Sanz, M., 2002. Neuroprotective effects of brimonidine against transient ischemia-induced retinal ganglion cell death: A dose response in vivo study. Exp. Eye

Res., 74(2), 181–189.

Lang, B.T., Cregg, J.M., DePaul, M.A., Tran, A.P., Xu, K., Dyck, S.M., Madalena, K.M., Brown, B.P., Weng, Y.-L., Li, S., Karimi-Abdolrezaee, S., Busch, S. a., Shen, Y. & Silver, J., 2014. Modulation of the proteoglycan receptor PTPσ promotes recovery after spinal cord injury. Nature, 518(7539), 404–408.

Lau, L.W., Keough, M.B., Haylock-Jacobs, S., Cua, R., Döring, A., Sloka, S., Stirling, D.P., Rivest, S. & Yong, V.W., 2012. Chondroitin sulfate proteoglycans in demyelinated lesions impair remyelination. Ann. Neurol., 72(3), 419–432.

Leaver, S.G., Cui, Q., Plant, G.W., Arulpragasam, A., Hisheh, S., Verhaagen, J. & Harvey, A.R., 2006. AAV-mediated expression of CNTF promotes long-term survival and regeneration of adult rat retinal ganglion cells. Gene Ther., 13(18), 1328–1341.

Lee, H., McKeon, R.J. & Bellamkonda, R. V, 2010. Sustained delivery of thermostabilized chABC enhances axonal sprouting and functional recovery after spinal cord injury. Proc. Natl. Acad. Sci. U. S. A., 107(8), 3340–5.

Lehmann, M., Fournier, A., Selles-Navarro, I., Dergham, P., Sebok, A., Leclerc, N., Tigyi, G. & McKerracher, L., 1999. Inactivation of Rho signaling pathway promotes CNS axon regeneration. J. Neurosci., 19(17), 7537–7547.

Lemons, M.L., Barua, S., Abanto, M., Halfter, W. & Condic, M., 2005. Adaptation of Sensory Neurons to Hyalectin and Decorin Proteoglycans. J. Neurosci., 25(20), 4964–4973.

Lemons, M.L., Sandy, J.D., Anderson, D.K. & Howland, D.R., 2001. Intact aggrecan and fragments generated by both aggrecanse and metalloproteinase-like activities are present in the developing and adult rat spinal cord and their relative abundance is altered by injury. J. Neurosci., 21(13), 4772–81.

Leon, S., Yin, Y., Nguyen, J., Irwin, N. & Benowitz, L.I., 2000. Lens injury stimulates axon regeneration in the mature rat optic nerve. J. Neurosci., 20(12), 4615–4626.

Leung, K.-M., Taylor, J.S.H. & Chan, S.-O., 2003. Enzymatic removal of chondroitin sulphates abolishes the age-related axon order in the optic tract of mouse embryos. Eur. J. Neurosci., 17(9), 1755–1767.

Levin, L. a, Beck, R.W., Joseph, M.P., Seiff, S. & Kraker, R., 1999. The treatment of traumatic optic neuropathy: the International Optic Nerve Trauma Study. Ophthalmology, 106(7), 1268–77.

Levkovitch-Verbin, H., Quigley, H. a., Martin, K.R.G., Valenta, D., Baumrind, L. a. & Pease, M.E., 2002. Translimbal laser photocoagulation to the trabecular meshwork as a model

of glaucoma in rats. Investig. Ophthalmol. Vis. Sci., 43(2), 402–410.

Li, H., Leung, T.C., Hoffman, S., Balsamo, J. & Lilien, J., 2000. Coordinate regulation of cadherin and integrin function by the chondroitin sulfate proteoglycan neurocan. J. Cell Biol., 149(6), 1275–1288.

Li, J., Yen, C., Liaw, D., Podsypanina, K., Bose, S., Wang, S.I., Puc, J., Miliaresis, C., Rodgers, L., McCombie, R., Bigner, S.H., Giovanella, B.C., Ittmann, M., Tycko, B., Hibshoosh, H., Wigler, M.H. & Parsons, R., 1997. PTEN, a putative protein tyrosine phosphatase gene mutated in human brain, breast, and prostate cancer. Science (80-.)., 275(5308), 1943–7.

Li, S., Yang, C., Zhang, L., Gao, X., Wang, X., Liu, W., Wang, Y., Jiang, S., Wong, Y.H., Zhang, Y. & Liu, K., 2016. Promoting axon regeneration in the adult CNS by modulation of the melanopsin/GPCR signaling. Proc. Natl. Acad. Sci., 113(7), 1937–1942.

Li, Y., Anderggen, L., Yuki, K., Omura, K., Yin, Y., Gilbert, H.-Y., Erdogan, B., Asdourian, M.S., Shrock, C., de Lima, S., Apfel, U.-P., Zhuo, Y., Hershfinkel, M., Lippard, S.J., Rosenberg, P.A. & Benowitz, L., 2017. Mobile zinc increases rapidly in the retina after optic nerve injury and regulates ganglion cell survival and optic nerve regeneration. Proc. Natl. Acad. Sci., 201616811.

Liddelow, S.A. et al., 2017. Neurotoxic reactive astrocytes are induced by activated microglia. Nature.

Lim, J.-H.A., Stafford, B.K., Nguyen, P.L., Lien, B. V, Wang, C., Zukor, K., He, Z. & Huberman, A.D., 2016. Neural activity promotes long-distance, target-specific regeneration of adult retinal axons. Nat. Neurosci., (July), 1–14.

de Lima, S., Koriyama, Y., Kurimoto, T., Oliveira, J.T., Yin, Y., Li, Y., Gilbert, H.-Y., Fagiolini, M., Martinez, A.M.B. & Benowitz, L., 2012. Full-length axon regeneration in the adult mouse optic nerve and partial recovery of simple visual behaviors. Proc. Natl. Acad. Sci. U. S. A., 109(23), 9149–54.

Lin, R., Rosahl, T.W., Whiting, P.J., Fawcett, J.W. & Kwok, J.C.F., 2011. 6-Sulphated Chondroitins Have a Positive Influence on Axonal Regeneration. PLoS One, 6(7), e21499.

Lin, R., Kwok, J.C.F., Crespo, D. & Fawcett, J.W., 2007. Chondroitinase ABC has a long-lasting effect on chondroitin sulphate glycosaminoglycan content in the injured rat brain. J. Neurochem., 0(0), 071116233414006–???

Lingor, P., Teusch, N., Schwarz, K., Mueller, R., Mack, H., Bähr, M. & Mueller, B.K., 2007.

Inhibition of Rho kinase (ROCK) increases neurite outgrowth on chondroitin sulphate proteoglycan in vitro and axonal regeneration in the adult optic nerve in vivo. J. Neurochem., 103, 181–189.

Lipton, J.O. & Sahin, M., 2014. The Neurology of mTOR. Neuron, 84(2), 275–291.

Lipton, S.A., 1986. Blockade of electrical activity promotes death of mammalian retinal ganglion cells in culture. Proc.Natl.Acad.Sci.USA, 83(December), 9774–9778.

Litjens, T. & Hopwood, J.J., 2001. Mucopolysaccharidosis type VI: Structural and clinical implications of mutations in N-acetylgalactosamine-4-sulfatase. Hum. Mutat., 18(4), 282–295.

Liton, P.B., Challa, P., Stinnett, S., Luna, C., Epstein, D.L. & Gonzalez, P., 2005. Cellular senescence in the glaucomatous outflow pathway. Exp. Gerontol., 40(8–9), 745–748.

Liu, K., Tedeschi, A., Park, K.K. & He, Z., 2011. Neuronal Intrinsic Mechanisms of Axon Regeneration. Annu. Rev. Neurosci., 34(1), 131–152.

Lorber, B., Berry, M., Hendriks, W., Den Hertog, J., Pulido, R. & Logan, A., 2004. Stimulated regeneration of the crushed adult rat optic nerve correlates with attenuated expression of the protein tyrosine phosphatases RPTPα, STEP, and LAR. Mol. Cell. Neurosci., 27(4), 404–416.

Luo, X., Salgueiro, Y., Beckerman, S.R., Lemmon, V.P., Tsoulfas, P. & Park, K.K., 2013. Three-dimensional evaluation of retinal ganglion cell axon regeneration and pathfinding in whole mouse tissue after injury. Exp. Neurol., 247, 653–62.

Maehama, T. & Dixon, J.E., 1998. The Tumor Suppressor, PTEN/MMAC1, Dephosphorylates the Lipid Second Messenger, Phosphatidylinositol 3,4,5-Trisphosphate. J. Biol. Chem., 273(22), 13375–13379.

Marcus, R.C. & Mason, C. a, 1995. The first retinal axon growth in the mouse optic chiasm: axon patterning and the cellular environment. J. Neurosci., 15(10), 6389–402.

Marin, M. a, de Lima, S., Gilbert, H.-Y., Giger, R.J., Benowitz, L. & Rasband, M.N., 2016. Reassembly of Excitable Domains after CNS Axon Regeneration. J. Neurosci., 36(35), 9148–60.

Maroto, M., Fern??ndez-Morales, J.C., Pad??n, J.F., Gonz??lez, J.C., Hern??ndez-Guijo, J.M., Montell, E., Verg??s, J., De Diego, A.M.G. & Garc??a, A.G., 2013. Chondroitin sulfate, a major component of the perineuronal net, elicits inward currents, cell depolarization, and calcium transients by acting on AMPA and kainate receptors of hippocampal neurons. J. Neurochem., 125(2), 205–213.

Mason, C. a & Wang, L.C., 1997. Growth cone form is behavior-specific and, consequently,

position-specific along the retinal axon pathway. J. Neurosci., 17(3), 1086–100.

Matsushita, K., Nakata, T., Takeda-Okuda, N., Nadanaka, S., Kitagawa, H. & Tamura, J. ichi, 2018. Synthesis of chondroitin sulfate CC and DD tetrasaccharides and interactions with 2H6 and LY111. Bioorganic Med. Chem., 26(5), 1016–1025.

McAdams, B.D. & McLoon, S.C., 1995. Expression of chondroitin sulfate and keratan sulfate proteoglycans in the path of growing retinal axons in the developing chick. J. Comp. Neurol., 352(4), 594–606.

McGeer, P.L. & McGeer, E.G., 1995. The inflammatory response system of brain: implications for therapy of Alzheimer and other neurodegenerative diseases. Brain Res. Rev., 21(2), 195–218.

Mckeon, R., 1995. Injury-Induced Proteoglycans Inhibit the Potential for Laminin-Mediated Axon Growth on Astrocytic Scars. Exp. Neurol., 136(1), 32–43.

McLoon, S.C. & Barnes, R.B., 1989. Early differentiation of retinal ganglion cells: an axonal protein expressed by premigratory and migrating retinal ganglion cells. J. Neurosci., 9(4), 1424–32.

Meletis, K., Barnabé-Heider, F., Carlén, M., Evergren, E., Tomilin, N., Shupliakov, O. & Frisén, J., 2008. Spinal Cord Injury Reveals Multilineage Differentiation of Ependymal Cells. PLoS Biol., 6(7), e182.

Meyer-Franke, A., Kaplan, M.R., Pfieger, F.W. & Barres, B.A., 1995. Characterization of the signaling interactions that promote the survival and growth of developing retinal ganglion cells in culture. Neuron, 15(4), 805–819.

Meyer-Franke, A., Wilkinson, G.A., Kruttgen, A., Hu, M., Munro, E., Hanson, M.G., Reichardt, L.F. & Barres, B.A., 1998. Depolarization and cAMP elevation rapidly recruit TrkB to the plasma membrane of CNS neurons. Neuron, 21(4), 681–693.

Mikami, T., Yasunaga, D. & Kitagawa, H., 2009. Contactin-1 is a functional receptor for neuroregulatory chondroitin sulfate-E. J. Biol. Chem., 284(7), 4494–4499.

Miller, G.M. & Hsieh-Wilson, L.C., 2015. Sugar-dependent modulation of neuronal development, regeneration, and plasticity by chondroitin sulfate proteoglycans. Exp. Neurol., 274, 115–125.

Mitsunaga-Nakatsubo, K., Kusunoki, S., Kawakami, H., Akasaka, K. & Akimoto, Y., 2009. Cell-surface arylsulfatase A and B on sinusoidal endothelial cells, hepatocytes, and Kupffer cells in mammalian livers. Med. Mol. Morphol., 42(2), 63–69.

Miyake, K., Yoshida, M., Inoue, Y. & Hata, Y., 2007. Neuroprotective Effect of Transcorneal Electrical Stimulation on the Acute Phase of Optic Nerve Injury. Investig.

Opthalmology Vis. Sci., 48(5), 2356.

Miyata, S., Komatsu, Y., Yoshimura, Y., Taya, C. & Kitagawa, H., 2012. Persistent cortical plasticity by upregulation of chondroitin 6-sulfation. Nat. Neurosci., 15(3), 414–422.

Monnier, P.P., Sierra, A., Schwab, J.M., Henke-Fahle, S. & Mueller, B.K., 2003. The Rho/ROCK pathway mediates neurite growth-inhibitory activity associated with the chondroitin sulfate proteoglycans of the CNS glial scar. Mol. Cell. Neurosci., 22(3), 319–330.

Moore, D.L., Blackmore, M.G., Hu, Y., Kaestner, K.H., Bixby, J.L., Lemmon, V.P. & Goldberg, J.L., 2009. KLF Family Members Regulate Intrinsic Axon Regeneration Ability. Science (80-.)., 326(5950), 298–301.

Morgan, J.L., Berger, D.R., Wetzel, A.W. & Lichtman, J.W., 2016. The Fuzzy Logic of Network Connectivity in Mouse Visual Thalamus. Cell, 165(1), 192–206.

Morgenstern, D.A., Asher, R.A. & Fawcett, J.W., 2002. Chondroitin sulphate proteoglycans in the CNS injury response. Prog. Brain Res., 137, 313–332.

Morin, L.P. & Studholme, K.M., 2014. Retinofugal projections in the mouse. J. Comp. Neurol., 522(16), 3733–3753.

Morrison, J.C., Moore, C.G., Deppmeier, L.M., Gold, B.G., Meshul, C.K. & Johnson, E.C., 1997. A rat model of chronic pressure-induced optic nerve damage. Exp. Eye Res., 64, 85–96.

Muir, E.M., Fyfe, I., Gardiner, S., Li, L., Warren, P., Fawcett, J.W., Keynes, R.J. & Rogers, J.H., 2010. Modification of N-glycosylation sites allows secretion of bacterial chondroitinase ABC from mammalian cells. J. Biotechnol., 145(2), 103–110.

Muñoz-Rojas, M.V., Horovitz, D.D.G., Jardim, L.B., Raymundo, M., Llerena, J.C., de Magalhães, T.D.S.C.P., Vieira, T.A., Costa, R., Kakkis, E. & Giugliani, R., 2010. Intrathecal administration of recombinant human N-acetylgalactosamine 4-sulfatase to a MPS VI patient with pachymeningitis cervicalis. Mol. Genet. Metab., 99(4), 346–350.

Niederöst, B.P., Zimmermann, D.R., Schwab, M.E. & Bandtlow, C.E., 1999. Bovine CNS myelin contains neurite growth-inhibitory activity associated with chondroitin sulfate proteoglycans. J. Neurosci., 19(20), 8979–89.

Norsworthy, M.W., Bei, F., Kawaguchi, R., Wang, Q., Tran, N.M., Li, Y., Brommer, B., Zhang, Y., Wang, C., Sanes, J.R., Coppola, G. & He, Z., 2017. Sox11 Expression Promotes Regeneration of Some Retinal Ganglion Cell Types but Kills Others. Neuron, 94(6), 1112–1120.e4.

Novak, U. & Kaye, A.H., 2000. Extracellular matrix and the brain: Components and function.

J. Clin. Neurosci., 7(4), 280–290.

Novozhilova, E., Englund-Johansson, U., Kale, A., Jiao, Y. & Olivius, P., 2015. Effects of ROCK inhibitor Y27632 and EGFR inhibitor PD168393 on human neural precursors co-cultured with rat auditory brainstem explant. Neuroscience, 287, 43–54.

O'Brien, J.F., Cantz, M. & Spranger, J., 1974. Maroteaux-Lamy Disease (Mucopolysaccharidosis VI), Subtype A: Deficiency of a N-Acetylgalactossamine-4-sulfatase. Biochem. Biophys. Res. Commun., 60(3), 1170–1177.

Ohtake, Y., Wong, D., Abdul-Muneer, P.M., Selzer, M.E. & Li, S., 2016. Two PTP receptors mediate CSPG inhibition by convergent and divergent signaling pathways in neurons. Sci. Rep., 6(October), 37152.

Okamoto, M., Sakiyama, J., Mori, S., Kurazono, S., Usui, S., Hasegawa, M. & Oohira, A., 2003. Kainic acid-induced convulsions cause prolonged changes in the chondroitin sulfate proteoglycans neurocan and phosphacan in the limbic structures. Exp. Neurol., 184(1), 179–195.

Oohira, A., Matsui, F., Tokita, Y., Yamauchi, S. & Aono, S., 2000. Molecular interactions of neural chondroitin sulfate proteoglycans in the brain development. Arch. Biochem. Biophys., 374(1), 24–34.

Oster, S.F., 2003. Invariant Sema5A inhibition serves an ensheathing function during optic nerve development. Development, 130(4), 775–784.

Park, K.K., Liu, K., Hu, Y., Smith, P.D., Wang, C., Cai, B., Xu, B., Connolly, L., Kramvis, I., Sahin, M. & He, Z., 2008. Promoting Axon Regeneration in the Adult CNS by Modulation of the PTEN/mTOR Pathway. Science (80-.)., 322(5903), 963–966.

Pernet, V., Joly, S., Dalkara, D., Jordi, N., Schwarz, O., Christ, F., Schaffer, D. V, Flannery, J.G. & Schwab, M.E., 2013. Long-distance axonal regeneration induced by CNTF gene transfer is impaired by axonal misguidance in the injured adult optic nerve. Neurobiol. Dis., 51, 202–13.

Pernet, V. & Schwab, M.E., 2014. Lost in the jungle: new hurdles for optic nerve axon regeneration. Trends Neurosci., 37(7), 381–387.

Peterson, P.E., Pow, C.S., Wilson, D.B. & Hendrickx, a G., 1995. Localisation of glycoproteins and glycosaminoglycans during early eye development in the macaque. J. Anat., 186 (Pt 1, 31–42.

Petros, T.J., Rebsam, A. & Mason, C. a, 2008. Retinal axon growth at the optic chiasm: to cross or not to cross. Annu. Rev. Neurosci., 31, 295–315.

Pizzorusso, T., Medini, P., Berardi, N., Chierzi, S., Fawcett, J.W. & Maffei, L., 2002.

Reactivation of Ocular Dominance Plasticity in the Adult Visual Cortex. Science (80-.)., 298(5596), 1248–1251.

Pizzorusso, T., Medini, P., Landi, S., Baldini, S., Berardi, N. & Maffei, L., 2006. Structural and functional recovery from early monocular deprivation in adult rats. Proc. Natl. Acad. Sci. U. S. A., 103(22), 8517–8522.

Plas, D.T., Lopez, J.E. & Crair, M.C., 2005. Pretarget sorting of retinocollicular axons in the mouse. J. Comp. Neurol., 491(4), 305–319.

Porter, M.T., Fluharty, a L. & Kihara, H., 1969. Metachromatic leukodystrophy: arylsulfatase-A deficiency in skin fibroblast cultures. Proc. Natl. Acad. Sci. U. S. A., 62(3), 887–891.

Powell, E.M., Mercado, M.L.T., Calle-Patino, Y. & Geller, H.M., 2001. Protein kinase C mediates neurite guidance at an astrocyte boundary. Glia, 33(4), 288–297.

Preston, E., Webster, J. & Small, D., 2001. Characteristics of Sustained Blood-Brain Barrier Opening and Tissue Injury in a Model for Focal Trauma in the Rat. J. Neurotrauma, 18(1), 83–92.

Properzi, F., Carulli, D., Asher, R. a, Muir, E., Camargo, L.M., van Kuppevelt, T.H., ten Dam, G.B., Furukawa, Y., Mikami, T., Sugahara, K., Toida, T., Geller, H.M. & Fawcett, J.W., 2005. Chondroitin 6-sulphate synthesis is up-regulated in injured CNS, induced by injury-related cytokines and enhanced in axon-growth inhibitory glia. Eur. J. Neurosci., 21(2), 378–90.

Provencio, I., Rodriguez, I.R., Jiang, G., Hayes, W.P., Moreira, E.F. & Rollag, M.D., 2000. A Novel Human Opsin in the Inner Retina. J. Neurosci., 20(2), 600–605.

Pyka, M., Wetzel, C., Aguado, A., Geissler, M., Hatt, H. & Faissner, A., 2011. Chondroitin sulfate proteoglycans regulate astrocyte-dependent synaptogenesis and modulate synaptic activity in primary embryonic hippocampal neurons. Eur. J. Neurosci., 33(12), 2187–2202.

Qu, J. & Jakobs, T.C., 2013. The Time Course of Gene Expression during Reactive Gliosis in the Optic Nerve. PLoS One, 8(6), e67094.

Rapp, A., Brandl, N., Volpi, N. & Huettinger, M., 2005. Evaluation of chondroitin sulfate bioactivity in hippocampal neurones and the astrocyte cell line U373: Influence of position of sulfate groups and charge density. Basic Clin. Pharmacol. Toxicol., 96(1), 37–43.

Rawat, M., Gama, C.I., Matson, J.B. & Hsieh-Wilson, L.C., 2008. Neuroactive chondroitin sulfate glycomimetics. J. Am. Chem. Soc., 130(10), 2959–2961.

Raykova, K., Jones, M. V., Huang, H., Hoffman, P.F. & Levy, M., 2015. Minimally-invasive Technique for Injection into Rat Optic Nerve. J. Vis. Exp., (99), e52249.

Reese, B.E., Johnson, P.T., Hocking, D.R. & Bolles, a. B., 1997. Chronotopic fiber reordering and the distribution of cell adhesion and extracellular matrix molecules in the optic pathway of fetal ferrets. J. Comp. Neurol., 380(3), 355–372.

Reese, B.E., 2011. Development of the retina and optic pathway. Vision Res., 51(7), 613–632.

Reese, B.E., 1988. "Hidden lamination" in the dorsal lateral geniculate nucleus: the functional organization of this thalamic region in the rat. Brain Res. Rev., 13(2), 119–137.

Richardson, P.M., McGuinness, U.M. & Aguayo, A.J., 1980. Axons from CNS neurons regenerate into PNS grafts. Nature, 284(5753), 264–5.

Ring, C., Lemmon, V. & Halfter, W., 1995. Two Chondroitin Sulfate Proteoglycans Differentially Expressed in the Developing Chick Visual System. Dev. Biol., 168, 11–27.

Rodriguez-Grande, B., Swana, M., Nguyen, L., Englezou, P., Maysami, S., Allan, S.M., Rothwell, N.J., Garlanda, C., Denes, A. & Pinteaux, E., 2014. The acute-phase protein PTX3 is an essential mediator of glial scar formation and resolution of brain edema after ischemic injury. J. Cereb. Blood Flow Metab., 34(3), 480–488.

Rolls, A., Shechter, R., London, A., Segev, Y., Jacob-Hirsch, J., Amariglio, N., Rechavi, G. & Schwartz, M., 2008. Two Faces of Chondroitin Sulfate Proteoglycan in Spinal Cord Repair: A Role in Microglia/Macrophage Activation. PLoS Med., 5(8), e171.

Roy, A., 1987. Arylsulfatases: Colorimetry and Fluorometry. Methods Enzymol., 143(1953), 207–17.

Sabelstrom, H., Stenudd, M., Reu, P., Dias, D.O., Elfineh, M., Zdunek, S., Damberg, P., Goritz, C. & Frisen, J., 2013. Resident Neural Stem Cells Restrict Tissue Damage and Neuronal Loss After Spinal Cord Injury in Mice. Science (80-.)., 342(6158), 637–640.

Sadun, A.A. & Bassi, C.J., 1990. Optic Nerve Damage in Alzheimer's Disease. Ophthalmology, 97(1), 9–17.

Sagawa, H., Terasaki, H., Nakamura, M., Ichikawa, M., Yata, T., Tokita, Y. & Watanabe, M., 2007. A novel ROCK inhibitor, Y-39983, promotes regeneration of crushed axons of retinal ganglion cells into the optic nerve of adult cats. Exp. Neurol., 205(1), 230–240.

Sanes, J.R. & Masland, R.H., 2015. The Types of Retinal Ganglion Cells: Current Status and Implications for Neuronal Classification. Annu. Rev. Neurosci., 38(1), 221–246.

Santos, A., Humayun, M.S., Juan, E. De, Marsh, M.J., Klock, I.B. & Milam, A.H., 1997. Preservation of the inner retina in retinitis pigmentosa. Arch Ophthalmol, 115.

Sapieha, P.S., Duplan, L., Uetani, N., Joly, S., Tremblay, M.L., Kennedy, T.E. & Di Polo, A., 2005. Receptor protein tyrosine phosphatase sigma inhibits axon regrowth in the adult injured CNS. Mol. Cell. Neurosci., 28(4), 625–635.

Schwend, T., Deaton, R.J., Zhang, Y., Caterson, B. & Conrad, G.W., 2012. Corneal sulfated glycosaminoglycans and their effects on trigeminal nerve growth cone behavior in vitro: Roles for ECM in cornea innervation. Investig. Ophthalmol. Vis. Sci., 53(13), 8118–8137.

Sellés-Navarro, I., Ellezam, B., Fajardo, R., Latour, M. & McKerracher, L., 2001. Retinal Ganglion Cell and Nonneuronal Cell Responses to a Microcrush Lesion of Adult Rat Optic Nerve. Exp. Neurol., 167(2), 282–289.

Sellés-Navarro, I., Villegas-Perez, M.P., Salvador-Silva, M., Ruiz-Gómez, J.M. & Vidal-Sanz, M., 1996. Retinal ganglion cell death after different transient periods of pressure-induced ischemia and survival intervals: A quantitative in vivo study. Investig. Ophthalmol. Vis. Sci., 37(10), 2002–2014.

Sengottuvel, V., Leibinger, M., Pfreimer, M., Andreadaki, A. & Fischer, D., 2011. Taxol Facilitates Axon Regeneration in the Mature CNS. J. Neurosci., 31(7), 2688–2699.

Shapira, E., DeGregorio, R.R., Matalon, R. & Nadler, H.L., 1975. Reduced arylsulfatase B activity of the mutant enzyme protein in Maroteaux-Lamy syndrome. Biochem. Biophys. Res. Commun., 62(2), 448–455.

Shechter, R., London, A., Varol, C., Raposo, C., Cusimano, M., Yovel, G., Rolls, A., Mack, M., Pluchino, S., Martino, G., Jung, S. & Schwartz, M., 2009. Infiltrating blood-derived macrophages are vital cells playing an anti-inflammatory role in recovery from spinal cord injury in mice. PLoS Med., 6(7).

Shechter, R., Raposo, C., London, A., Sagi, I. & Schwartz, M., 2011. The glial scar-monocyte interplay: A pivotal resolution phase in spinal cord repair. PLoS One, 6(12).

Shen, Y., Tenney, a. P., Busch, S. a., Horn, K.P., Cuascut, F.X., Liu, K., He, Z., Silver, J. & Flanagan, J.G., 2009. PTP Is a Receptor for Chondroitin Sulfate Proteoglycan, an Inhibitor of Neural Regeneration. Science (80-.)., 326(5952), 592–596.

Shimbo, M., Ando, S., Sugiura, N., Kimata, K. & Ichijo, H., 2013. Moderate repulsive effects of E-unit-containing chondroitin sulfate (CSE) on behavior of retinal growth cones. Brain Res., 1491, 34–43.

Siebert, J.R., Conta Steencken, A. & Osterhout, D.J., 2014. Chondroitin sulfate proteoglycans

in the nervous system: inhibitors to repair. Biomed Res. Int., 2014, 845323.

Siebert, J.R. & Osterhout, D.J., 2011. The inhibitory effects of chondroitin sulfate proteoglycans on oligodendrocytes. J. Neurochem., 119(1), 176–188.

Sieving, P. a., Caruso, R.C., Tao, W., Coleman, H.R., Thompson, D.J.S., Fullmer, K.R. & Bush, R. a., 2006. Ciliary neurotrophic factor (CNTF) for human retinal degeneration: Phase I trial of CNTF delivered by encapsulated cell intraocular implants. Proc. Natl. Acad. Sci., 103(10), 3896–3901.

Silver, D.J. & Silver, J., 2014. Contributions of chondroitin sulfate proteoglycans to neurodevelopment, injury, and cancer. Curr. Opin. Neurobiol., 27, 171–178.

Silver, J., 2016. The glial scar is more than just astrocytes. Exp. Neurol., 286, 147–149.

Silver, J. & Miller, J.H., 2004. Regeneration beyond the glial scar. Nat. Rev. Neurosci., 5(2), 146–156.

Silver, J., Schwab, M.E. & Popovich, P.G., 2015. Central Nervous System Regenerative Failure: Role of Oligodendrocytes, Astrocytes, and Microglia. Cold Spring Harb Perspect Biol, 7, a020602.

Sivasankaran, R., Pei, J., Wang, K.C., Zhang, Y.P., Shields, C.B., Xu, X.-M. & He, Z., 2004. PKC mediates inhibitory effects of myelin and chondroitin sulfate proteoglycans on axonal regeneration. Nat. Neurosci., 7(3), 261–268.

Smith-Thomas, L.C., Stevens, J., Fok-Seang, J., Faissner, A., Rogers, J.H. & Fawcett, J.W., 1995. Increased axon regeneration in astrocytes grown in the presence of proteoglycan synthesis inhibitors. J. Cell Sci., 108 (Pt 3, 1307–1315.

Snow, D.M., Watanabe, M., Letourneau, P.C. & Silver, J., 1991. A chondroitin sulfate proteoglycan may influence the direction of retinal ganglion cell outgrowth. Development, 113(4), 1473–85.

Snow, D.M., Atkinson, P.B., Hassinger, T.D., Letourneau, P.C. & Kater, S.B., 1994. Chondroitin sulfate proteoglycan elevates cytoplasmic calcium in DRG neurons. Dev Biol, 166(1), 87–100.

So, K.F. & Aguayo, A.J., 1985. Lengthy regrowth of cut axons from ganglion cells after peripheral nerve transplantation into the retina of adult rats. Brain Res., 328(2), 349–354.

Sobel, R.A. & Ahmed, A.S., 2001. White matter extracellular matrix chondroitin sulfate/dermatan sulfate proteoglycans in multiple sclerosis. J. Neuropathol. Exp. Neurol., 60(12), 1198–1207.

Soderblom, C., Luo, X., Blumenthal, E., Bray, E., Lyapichev, K., Ramos, J., Krishnan, V.,

Lai-Hsu, C., Park, K.K., Tsoulfas, P. & Lee, J.K., 2013. Perivascular Fibroblasts Form the Fibrotic Scar after Contusive Spinal Cord Injury. J. Neurosci., 33(34), 13882–13887.

Song, M.S., Salmena, L. & Pandolfi, P.P., 2012. The functions and regulation of the PTEN tumour suppressor. Nat Rev Mol Cell Biol, 13(5), 283–296.

Song, Y., Ori-McKenney, K.M., Zheng, Y., Han, C., Jan, L.Y. & Jan, Y.N., 2012. Regeneration of Drosophila sensory neuron axons and dendrites is regulated by the Akt pathway involving Pten and microRNA bantam. Genes Dev., 26(14), 1612–1625.

Springer, A.D., Morel, K.D. & Wilson, B.R., 1990. Topographic disorganization of the optic tracts following long-term optic nerve regeneration: A quantitative image analysis study. J. Comp. Neurol., 298(4), 458–471.

Sugiura, N., Shioiri, T., Chiba, M., Sato, T., Narimatsu, H., Kimata, K. & Watanabe, H., 2012. Construction of a Chondroitin Sulfate Library with Defined Structures and Analysis of Molecular Interactions. J. Biol. Chem., 287(52), 43390–43400.

Sun, F., Park, K.K., Belin, S., Wang, D., Lu, T., Chen, G., Zhang, K., Yeung, C., Feng, G., Yankner, B. a. & He, Z., 2011. Sustained axon regeneration induced by co-deletion of PTEN and SOCS3. Nature, 480(7377), 372–375.

Suzuki, S., Saito, H., Yamagata, T., Anno, K., Seno, N., Kawai, Y. & Furuhashi, T., 1968. Formation of Three Types Sulfates of Disulfated by Chondroitinase Disaccharides from Chondroitin Digestion. J. Biol. Chem., 243(7), 1543–1550.

Tan, C.L., Kwok, J.C.F., Patani, R., Ffrench-Constant, C., Chandran, S. & Fawcett, J.W., 2011. Integrin Activation Promotes Axon Growth on Inhibitory Chondroitin Sulfate Proteoglycans by Enhancing Integrin Signaling. J Neurosci, 31(17), 6289–6295.

Tan, H., Zhong, Y., Shen, X., Cheng, Y., Jiao, Q. & Deng, L., 2012. Erythropoietin promotes axonal regeneration after optic nerve crush in vivo by inhibition of RhoA/ROCK signaling pathway. Neuropharmacology, 63(6), 1182–1190.

Tedeschi, A. & Bradke, F., 2017. Spatial and temporal arrangement of neuronal intrinsic and extrinsic mechanisms controlling axon regeneration. Curr. Opin. Neurobiol., 42, 118–127.

Tester, N.J., Plaas, A.H. & Howland, D.R., 2007. Effect of Body Temperature on Chondroitinase ABC's Ability To Cleave Chondroitin Sulfate Glycosaminoglycans Nicole. J. Neurosci. Res., 85, 1110–1118.

Tham, M., Ramasamy, S., Gan, H.T., Ramachandran, A., Poonepalli, A., Yu, Y.H. & Ahmed, S., 2010. CSPG is a secreted factor that stimulates neural stem cell survival possibly by enhanced EGFR signaling. PLoS One, 5(12).

Tham, Y.-C., Li, X., Wong, T.Y., Quigley, H.A., Aung, T. & Cheng, C.-Y., 2014. Global Prevalence of Glaucoma and Projections of Glaucoma Burden through 2040. Ophthalmology, 121(11), 2081–2090.

Titze, I.R., Svec, J.G. & Popolo, P.S., 2003. Vocal dose measures: quantifying accumulated vibration exposure in vocal fold tissues. J. Speech. Lang. Hear. Res., 46(4), 919–32.

Trachtenberg, J.T., Chen, B.E., Knott, G.W., Feng, G., Sanes, J.R., Welker, E. & Svoboda, K., 2002. Long-term in-vivo imaging of experience-dependent synaptic plasticity in adult cortex. Nature, 420(December), 788–94.

Tropea, D., Caleo, M. & Maffei, L., 2003. Synergistic effects of brain-derived neurotrophic factor and chondroitinase ABC on retinal fiber sprouting after denervation of the superior colliculus in adult rats. J. Neurosci., 23(18), 7034–7044.

Tully, S.E., Mabon, R., Gama, C.I., Tsai, S.M., Liu, X. & Hsieh-Wilson, L.C., 2004. A chondroitin sulfate small molecule that stimulates neuronal growth. J. Am. Chem. Soc., 126(25), 7736–7737.

Tuttle, R., Braisted, J.E., Richards, L.J. & O'Leary, D.D., 1998. Retinal axon guidance by region-specific cues in diencephalon. Development, 125(5), 791–801.

Urban, D.J. & Roth, B.L., 2015. DREADDs (Designer Receptors Exclusively Activated by Designer Drugs): Chemogenetic Tools with Therapeutic Utility. Annu. Rev. Pharmacol. Toxicol., 55(1), 399–417.

Varner, H.H., Rayborn, M.E., Osterfeld, A.M. & Hollyfield, J.G., 1987. Localization of proteoglycan within the extracellular matrix sheath of cone photoreceptors. Exp. Eye Res., 44(5), 633–642.

Verna, J.M., Fichard, A. & Saxod, R., 1989. Influence of glycosaminoglycans on neurite morphology and outgrowth patterns in vitro. Int. J. Dev. Neurosci., 7(4), 389–399.

Vidal-Sanz, M., Bray, G.M., Villegas-Pérez, M.P., Thanos, S. & Aguayo, a J., 1987. Axonal regeneration and synapse formation in the superior colliculus by retinal ganglion cells in the adult rat. J. Neurosci., 7(9), 2894–909.

Vidal-Sanz, M., Salinas-Navarro, M., Nadal-Nicolás, F.M., Alarcón-Martínez, L., Valiente-Soriano, F.J., Miralles de Imperial, J., Avilés-Trigueros, M., Agudo-Barriuso, M. & Villegas-Pérez, M.P., 2012. Understanding glaucomatous damage: Anatomical and functional data from ocular hypertensive rodent retinas. Prog. Retin. Eye Res., 31(1), 1–27.

Vitellaro-Zuccarello, L., Meroni, A., Amadeo, A. & De Biasi, S., 2001. Chondroitin sulfate proteoglycans in the rat thalamus: Expression during postnatal development and

correlation with calcium-binding proteins in adults. Cell Tissue Res., 306(1), 15–26.

Walker, B. a., Ji, S.-J. & Jaffrey, S.R., 2012. Intra-Axonal Translation of RhoA Promotes Axon Growth Inhibition by CSPG. J. Neurosci., 32(41), 14442–14447.

Wang, D. & Fawcett, J., 2012. The perineuronal net and the control of CNS plasticity. Cell Tissue Res., 349(1), 147–160.

Wang, H., Katagiri, Y., Mccann, T.E., Unsworth, E., Yu, Z., Tan, F., Santiago, L., Mills, E.M., Wang, Y., Aviva, J. & Geller, H.M., 2008. Chondroitin-4-sulfation negatively regulates axonal guidance and growth. J Cell Sci, 121(18), 3083–3091.

Wang, L.C., Rachel, R. a, Marcus, R.C. & Mason, C. a, 1996. Chemosuppression of retinal axon growth by the mouse optic chiasm. Neuron, 17(5), 849–62.

Wang, R., Seifert, P. & Jakobs, T.C., 2017. Astrocytes in the optic nerve head of glaucomatous mice display a characteristic reactive phenotype. Investig. Ophthalmol. Vis. Sci., 58(2), 924–932.

Wang, X., Hasan, O., Arzeno, A., Benowitz, L.I., Cafferty, W.B.J. & Strittmatter, S.M., 2012. Axonal regeneration induced by blockade of glial inhibitors coupled with activation of intrinsic neuronal growth pathways. Exp. Neurol., 237(1), 55–69.

Weinreb, R.N., Aung, T. & Medeiros, F. a., 2014. The Pathophysiology and Treatment of Glaucoma. Jama, 311(18), 1901.

Wiesel, T.N. & Hubel, D.H., 1963. Effects of visual deprivation on morphology and physiology of cells in the cat's lateral geniculate body. J. Physiol., 26, 978–993.

Williams, C., Villegas, M., Atkinson, R. & Miller, C.A., 1998. Chondroitin sulfate proteoglycan specific to retinal horizontal neurons. J. Comp. Neurol., 390(2), 268–277.

Wong, R.O.L., 1999. Retinal Waves and Visual System Development. Annu. Rev. Neurosci., 22(1), 29–47.

Wu, K.Y., Hengst, U., Cox, L.J., Macosko, E.Z., Jeromin, A., Urquhart, E.R. & Jaffrey, S.R., 2005. Local translation of RhoA regulates growth cone collapse. Nature, 436(7053), 1020–1024.

Yamamoto, Y., Atoji, Y., Oohira, A. & Suzuki, Y., 1995. Immunohistochemical localization of chondroitin sulfate in the forestomach of the sheep. Eur J Histochem, 39(4), 265–272.

Yang, S., Hilton, S., Alves, J.N., Saksida, L.M., Bussey, T., Matthews, R.T., Kitagawa, H., Spillantini, M.G., Kwok, J.C.F. & Fawcett, J.W., 2017. Antibody recognizing 4-sulfated chondroitin sulfate proteoglycans restores memory in tauopathy-induced neurodegeneration. Neurobiol. Aging, 59, 197–209.

Yi, J.-H., Katagiri, Y., Susarla, B., Figge, D., Symes, A.J. & Geller, H.M., 2012. Alterations

in sulfated chondroitin glycosaminoglycans following controlled cortical impact injury in mice. J. Comp. Neurol., 520(15), 3295–3313.

Yin, Y., Cui, Q., Li, Y., Irwin, N., Fischer, D., Harvey, A.R. & Benowitz, L.I., 2003. Macrophage-derived factors stimulate optic nerve regeneration. J. Neurosci., 23(6), 2284–2293.

Yin, Y., Henzl, M.T., Lorber, B., Nakazawa, T., Thomas, T.T., Jiang, F., Langer, R. & Benowitz, L.I., 2006. Oncomodulin is a macrophage-derived signal for axon regeneration in retinal ganglion cells. Nat. Neurosci., 9(6), 843–52.

Yin, Y., Cui, Q., Gilbert, H. -y., Yang, Y., Yang, Z., Berlinicke, C., Li, Z., Zaverucha-do-Valle, C., He, H., Petkova, V., Zack, D.J. & Benowitz, L.I., 2009. Oncomodulin links inflammation to optic nerve regeneration. Proc. Natl. Acad. Sci., 106(46), 19587–19592.

Yiu, G. & He, Z., 2006. Glial inhibition of CNS axon regeneration. Nat. Rev. Neurosci., 7(8), 617–627.

Yoo, M., Khaled, M., Gibbs, K.M., Kim, J., Kowalewski, B., Dierks, T. & Schachner, M., 2013. Arylsulfatase B Improves Locomotor Function after Mouse Spinal Cord Injury. PLoS One, 8(3), e57415.

Yu, P., Santiago, L.Y., Katagiri, Y. & Geller, H.M., 2012. Myosin II activity regulates neurite outgrowth and guidance in response to chondroitin sulfate proteoglycans. J. Neurochem., 120(6), no-no.

Yu, P., Pearson, C.S. & Geller, H.M., 2017. Flexible Roles for Proteoglycan Sulfation and Receptor Signaling. Trends Neurosci., 0(0), 1–15.

Yutsudo, N. & Kitagawa, H., 2015. Involvement of chondroitin 6-sulfation in temporal lobe epilepsy. Exp. Neurol., 274, 126–133.

Zako, M., Shinomura, T., Miyaishi, O., Iwaki, M. & Kimata, K., 1997. Transient expression of PG-M/versican, a large chondroitin sulfate proteoglycan in developing chicken retina. J. Neurochem., 69(5), 2155–2161.

Zhang, X., Bhattacharyya, S., Kusumo, H., Goodlett, C.R., Tobacman, J.K. & Guizzetti, M., 2014. Arylsulfatase B modulates neurite outgrowth via astrocyte chondroitin-4-sulfate: Dysregulation by ethanol. Glia, 62(2), 259–271.

Zhang, X., Ognibene, C.M., Clark, A.F. & Yorio, T., 2007. Dexamethasone inhibition of trabecular meshwork cell phagocytosis and its modulation by glucocorticoid receptor β. Exp. Eye Res., 84(2), 275–284.

Zhao, R.-R. & Fawcett, J.W., 2013. Combination treatment with chondroitinase ABC in spinal cord injury--breaking the barrier. Neurosci. Bull., 29(4), 477–83.

Zhao, R.R., Muir, E.M., Alves, J.N., Rickman, H., Allan, A.Y., Kwok, J.C., Roet, K.C.D., Verhaagen, J., Schneider, B.L., Bensadoun, J.C., Ahmed, S.G., Yáñez-Muñoz, R.J., Keynes, R.J., Fawcett, J.W. & Rogers, J.H., 2011. Lentiviral vectors express chondroitinase ABC in cortical projections and promote sprouting of injured corticospinal axons. J. Neurosci. Methods, 201(1), 228–238.

Zukor, K., Belin, S., Wang, C., Keelan, N., Wang, X. & He, Z., 2013. Short Hairpin RNA against PTEN Enhances Regenerative Growth of Corticospinal Tract Axons after Spinal Cord Injury. J. Neurosci., 33(39), 15350–15361.